JAERI-M
89-100

ANNUAL REPORT OF THE NAKA FUSION RESEARCH ESTABLISHMENT FOR THE PERIOD OF APRIL 1 1988 TO MARCH 31 1989

August 1989

Naka Fusion Research Establishment

日本原子力研究所
Japan Atomic Energy Research Institute

JAERI-Mレポートは，日本原子力研究所が不定期に公刊している研究報告書です。
入手の問合わせは，日本原子力研究所技術情報部情報資料課（〒319-11茨城県那珂郡東海村）あて，お申しこしください。なお，このほかに財団法人原子力弘済会資料センター（〒319-11 茨城県那珂郡東海村日本原子力研究所内）で複写による実費頒布をおこなっております。

JAERI-M reports are issued irregularly.
Inquiries about availability of the reports should be addressed to Information Division Department of Technical Information, Japan Atomic Energy Research Institute, Tokai-mura, Naka-gun, Ibaraki-ken 319-11, Japan.

編集兼発行　日本原子力研究所
印　　刷　いばらき印刷㈱

JAERI-M 89-100

Annual Report of the Naka Fusion Research Establishment for the period of April 1 1988 to March 31 1989

Naka Fusion Research Establishment
Japan Atomic Energy Research Institute
Naka-machi, Naka-gun, Ibaraki-ken

(Received July 10, 1989)

The experiment on JT-60 was resumed in May 1988 after the modification of the divertor configuration into a lower single-null type. An improved confinement associated with significant remote radiative cooling at the divertor region was obtained. Good energy confinement was also observed in discharges with peaked density profile produced by pellet injection. A newly-developed multi-junction LH wave launcher showed the current drive efficiency of 3.4×10^{19} A·m^{-2}/W, well approaching to the value necessary for the steady state operation of a next generation tokamak reactor.

In the confinement experiment on JFT-2M, an improved L mode was also obtained, in which density profile is peaked without edge pedestal in contrast to the H-mode confinement. High beta experiments in Doublet III-D have shown marked progress to achieve the average plasma beta value of 8%. Theoretical and computational studies were made in close connection with the JT-60/JFT-2M experiments on transport, heating and MHD activities. Analyses of plasma beta, loss of alpha particles, disruption, bootstrap current and other critical physics issues related to ITER/FER conceptual design were also made extensively.

A system test of a turbo molecular pump with a gas turbine-driven ceramic rotor successfully demonstrated a pumping speed of greater than 500 ℓ/sec as expected.

A 400 kW electron beam irradiation system was constructed for development of high heat flux components. The development of negative ion sources progressed to demonstrate the extraction of hydrogen beams as high as 3 A at 50 keV. In the high power gyrotron development, a pulsed power of 520 kW at 120 GHz was achieved by a test tube gyrotron.

The Large Coil Task, a ten-year long international collaboration

under the auspices of the IEA, was successfully completed in January 1989 to produce vital contribution to establish basic technologies of large superconducting coils for a tokamak fusion reactor. The fabrication of two NbTi coils in the Demo Poloidal Coil program was completed and a preliminary test was started.

Experiments on the fuel clean-up and the cryogenic distillation were initiated as hot tests of the tritium processing technology.

The International Thermonuclear Experimental Reactor (ITER) Conceptual Design Activity was initiated under the auspices of the IAEA. Significant contribution was made by JAERI participants to define the concept of ITER. In parallel with the ITER activity, JAERI has also developed its own program of the Fusion Experimental Reactor (FER) and nearly completed its design concept.

Keywords: Annual Report, Fusion Research, JAERI, JT-60, NBI, RF, Heating, Confinement, Current Drive, H-mode, JFT-2M, Doublet III-D, Theory, Vacuum, Negative Ion Source, Gyrotron, Demo Poloidal Coil, Tritium Processing, TSTA, FER, ITER

JAERI－M 89－100

那珂研究所年報（昭和63年度）

日本原子力研究所
那珂研究所

（1989年7月10日受理）

JT－60は，下側ダイバータ配位への改造を行ない，1988年5月から実験を再開した。本年度の実験では，閉込めに関しては，ダイバータ部での放射冷却を伴う改善モードの発見，ペレット入射を用いた中心ピーク形の密度分布における閉込めの向上などを得ると共に，新たに開発した多分岐型LHランチャーにより電流駆動効率3.8×10^{19} A・m^2／Wを達成し，実験炉の定常運転に向けて成果を得た。

JFT－2Mにおける閉込め実験では，Hモードと異なり周辺に肩をもたない中心ピーク形の密度分布をもつ改良型Lモード放電を見い出した。DⅢ－Dにおける高ベータ化研究では，平均ベータ値8％を記録した。プラズマの理論については，輸送，加熱及びMHD安定性に関して実験と密着して研究が進められ，特に，ベータ値，α粒子損失及びディスラプションなどITER／FERの課題が検討された。

タービン駆動型セラミックターボ分子ポンプの試験では，予定通り500 ℓ／秒を超える排気速度を得た。

今年度，耐高熱負荷材料開発のための400 KW電子ビーム照射装置の製作が完了した。負イオン源の開発では，50 KV，3 Aと云うビームの引出しを実証するとともに，ジャイラトロン開発においても120 GHzで520 KWのパルス発振に成功した。

大型コイル事業は，89年1月に予定通り10年の協力計画を完了し，トカマク炉に必要な超電導コイル技術の基盤を確立した。また実証ポロイダルコイル計画として，NbTiコイルを製作し予備実験を開始した。

トリチウムについては，燃料精製及び深冷蒸留などのトリチウム実負荷試験を開始した。

国際熱核融合実験炉（ITER）の概念設計がIAEAの下で開始され，原研は多大の寄与をなしている。又これと併行して，原研独自の計画としての核融合実験炉（FER）についても設計概念を固めた。

那珂研究所：〒311－01 茨城県那珂郡那珂町大字向山 801－1

Contents

目　　次

I. PLASMA THEORY AND COMPUTATION

1. Introduction

During the period from April 1, 1988 to March 31, 1989, emphases of the theoretical and computational works were put on the studies of (1) analyses of the ICRF (Ion Cyclotron Range of Frequency) wave heating and relating phenomena, (2) MHD stability analyses, especially, in relation with the design studies of the next generation tokamaks, and (3) analyses of the burning plasma physics and the steady-state operation of a tokamak plasma.

As for the analyses of the ICRF wave heating, suppression of the fish-bone instability by the wave, the heating process combined with NBI (Neutral Beam Injection), and effect of spatial diffusion on the heating were studied. Analysis of FEL (Free Electron Laser) was continued in relation to the ECH (Electron Cycrotron Heating) of a tokamak plasma as that of the MTX (Microwave Tokamak Experiment) project. Effect of resistive liner on the locked mode was analyzed in the context of the confinement analyses of a tokamak plasma. MHD studies were carried out concerning the beta optimization of a large tokamak, nonlinear analyses of the finite beta plasma, and self-consistent calculation of the MHD equilibrium with the neoclassical current. Both basic processes such as the alpha particle behavior and global natures relating engineering problems of a tokamak fusion reactor were studied extensively as for the analyses of the burning plasma. Especially, studies of problems closely related with the fusion reactor design were commenced. Physics codes developed in this period were added to the TRITON-II system. Development and improvement of the supporting codes in the TRITON-II system were also continued. In order to facilitate establishment of necessary database for the next generation tokamaks design study of a plasma simulator was started on the basis of the parallel computer technology. Installation of the US-JAERI Data Link was carried out successfully.

2. Analyses of Confinement and Heating Process

2.1 Destabilizing effects of resistive liner

Stabilizing effect of a resistive liner was reexamined analytically for a uniform current model of a cylindrical plasma. The reduced set of MHD equations and the pseudo-vacuum model were used to analyze

I. PLASMA THEORY AND COMPUTATION

1. Introduction

During the period from April 1, 1988 to March 31, 1989, emphases of the theoretical and computational works were put on the studies of (1) analyses of the ICRF (Ion Cyclotron Range of Frequency) wave heating and relating phenomena, (2) MHD stability analyses, especially, in relation with the design studies of the next generation tokamaks, and (3) analyses of the burning plasma physics and the steady-state operation of a tokamak plasma.

As for the analyses of the ICRF wave heating, suppression of the fish-bone instability by the wave, the heating process combined with NBI (Neutral Beam Injection), and effect of spatial diffusion on the heating were studied. Analysis of FEL (Free Electron Laser) was continued in relation to the ECH (Electron Cycrotron Heating) of a tokamak plasma as that of the MTX (Microwave Tokamak Experiment) project. Effect of resistive liner on the locked mode was analyzed in the context of the confinement analyses of a tokamak plasma. MHD studies were carried out concerning the beta optimization of a large tokamak, nonlinear analyses of the finite beta plasma, and self-consistent calculation of the MHD equilibrium with the neoclassical current. Both basic processes such as the alpha particle behavior and global natures relating engineering problems of a tokamak fusion reactor were studied extensively as for the analyses of the burning plasma. Especially, studies of problems closely related with the fusion reactor design were commenced. Physics codes developed in this period were added to the TRITON-II system. Development and improvement of the supporting codes in the TRITON-II system were also continued. In order to facilitate establishment of necessary database for the next generation tokamaks design study of a plasma simulator was started on the basis of the parallel computer technology. Installation of the US-JAERI Data Link was carried out successfully.

2. Analyses of Confinement and Heating Process

2.1 Destabilizing effects of resistive liner

Stabilizing effect of a resistive liner was reexamined analytically for a uniform current model of a cylindrical plasma. The reduced set of MHD equations and the pseudo-vacuum model were used to analyze

the stability of the kink mode for a tokamak plasma. Stabilizing effect of resistive liner is enhanced significantly when the rotation speed of plasma column exceeds the resistive skin time of the liner.

$$v_p > \eta/d$$

where v_p is the poloidal rotation velocity of the plasma column, η and d are the resistivity and thickness of the liner, respectively. In this case, resistive liner works as a perfect conducting shell for the kink mode.

However, the rotation of the plasma column induces another kind of instability even in a stable region of the kink mode. In this region, cylindrical plasma column has two branches of the surface-Alfvén wave. One propagates along positive toroidal direction and the other propagates oppositely. One of the branches becomes unstable if the rotation speed exceeds its phase velocity. This instability has its maximum growth rate for $v_p \sim \eta/d$.

2.2 Effect of energetic trapped particles induced by ICRF wave heating on MHD mode

In order to investigate the effect of high energy trapped particles on the fish-bone instability[1] a radial profile of the ion distribution function during the intense ICRF wave heating was calculated by use of the bounce averaged Fokker-Planck code. It was found that the bounce averaged toroidal precession frequency ($<\omega_d>$) as well as the beta value of the trapped particles $<\beta_t>$, for the high field side resonance (HFSR) heating stays in an order of magnitude lower level than the one for the low field side resonance (LFSR) case. The result indicates that the HFSR heating is more advantageous than the LFSR one in the strong heating regime in order to reduce the growth rate of the fish-bone instability.

2.3 Effect of spatial diffusion of fast ions on high power ICRF wave heating

The effect of spatial diffusion of high energy particles generated by the ICRF wave on the absorption profile and the fusion reaction rate was investigated by solving the two-dimensional (2D) Fokker-Planck equation with one spatial dimension. Some specific results which are not explained in the local analysis[2] were obtained. The absorption profile becomes broad with increasing D_s (spatial diffusion coefficient), which indicates the nonlocal power deposition. It was also found that

in the strong heating regime the fusion multiplication factor, $Q_{rf} = P_f/P_{rf}$ (fusion power/RF power), increases in comparison with the ideal case ($D_s = 0$), because of the slowing down of the high energy tail ion in the off-center region irrelevant to the fusion reaction in the plasma center.

2.4 Study of beam- and RF-induced ion tail by bounce averaged Fokker-Planck code

Ion tail formation by combined NBI and ICRF heating was investigated with a bounce average Fokker-Planck code. The distribution function in the two dimensional velocity space, (θ_0: pitch angle, v_0: speed), was analyzed at the equatorial midplane of the torus. Emphasis was placed on the tangent resonance phenomena at

$$\theta_0 \approx \theta_{tang} \equiv \sin^{-1}\sqrt{\frac{n\omega_c(0)}{\omega(1+\varepsilon)}} ,$$

where the remarkable energy diffusion is induced (n: the cyclotron harmonic number, $\omega_c(0)$: the cyclotron frequency at the plasma center, ω: the wave frequency, and ε the inverse aspect ratio).

The ions in the beam induced tail couple efficiently with the ICRF wave by choosing the injection angle within the window around θ_{tang}, which results in enhancement of the extended-tail temperature and of the fusion reactivity. The effect of magnetically trapped particles on beam driven current was also examined and found to reduce the current drive efficiency in comparison with the case of the uniform magnetic field.

2.5 Current drive due to RF-helicity injection

A magnetic helicity injection is controlled by a boundary condition at a plasma surface. Recently Ohkawa[3] suggested that a transverse wave with finite helicity can drive a current by transferring its helicity to the plasma. The relation between a wave-particle interaction and a transport of helicity and/or momentum is not analyzed sufficiently. We solved the linear wave propagation equation as a stationary boundary value problem. In this study, the cold plasma model was employed as a first step. The current profile and drive efficiency was obtained. When the radiated power spectrum is optimized, the current drive efficiency is proportional to the inverse square root of the plasma density.

2.6 Effect of electrostatic field on high current Raman regime FEL[4]

The effect of the longitudinal electrostatic field on the efficiency for the saturation amplitude was investigated by use of the 1-D FEL amplification code[5] in the high current Raman regime. It was found that the repulsive electrostatic field prevents periodic electron bounce motion in ponderomotive potential well and trapped particles are changed into untrapped ones, obtaining the kinetic energy from the radiation field. Resultantly, the energy conversion efficiency averaged over the long wiggler distance after saturation stays in a lower level than that predicted by the trapping argument.

References

[1] Chen L., et al., Phys. Rev. Lett. 52 (1984) 1122.
[2] Itoh, K.*11, et al., Nucl. Fusion 28 (1988) 779.
[3] Ohkawa T.*1, General Atomic Report GA-A19379 (1988).
[4] Kishimoto Y., et al., to be published in JAERI-M.
[5] Kishimoto Y., et al., JAERI-M, 89-061(1989).

3. MHD Equilibrium and Stability Analysis

3.1 Self-consistent calculation of neoclassical current effect on MHD equilibrium[1,2]

MHD equilibria of tokamak plasmas with neoclassical current effects (neoclassical conductivity and bootstrap current) were calculated self-consistently. Neoclassical effects on JFT-2M tokamak plasmas, sustained by ohmic currents, were studied. Bootstrap currents flow little for L-mode type equilibria because of low attainable values of poloidal beta, β_J. H-mode type equilibria give bootstrap currents of 30% of ohmic currents for β_J attained by JFT-2M and 100% for $\beta_J \geq 1.5$, both of which are sufficient to change the current profiles and the resultant MHD equilibria. Neoclassical conductivity which has roughly half value of the classical Spitzer conductivity brings peaked ohmic current profiles to yield low safety factor at the magnetic axis.

3.2 Non-linear analysis of finite beta tokamak plasma

Non-linear calculations of resistive ballooning mode in a finite beta tokamak were carried out. The reduced set of resistive MHD equations was used. The equilibrium current profile was chosen as relatively

2.6 Effect of electrostatic field on high current Raman regime FEL[4]

The effect of the longitudinal electrostatic field on the efficiency for the saturation amplitude was investigated by use of the 1-D FEL amplification code[5] in the high current Raman regime. It was found that the repulsive electrostatic field prevents periodic electron bounce motion in ponderomotive potential well and trapped particles are changed into untrapped ones, obtaining the kinetic energy from the radiation field. Resultantly, the energy conversion efficiency averaged over the long wiggler distance after saturation stays in a lower level than that predicted by the trapping argument.

References

[1] Chen L., et al., Phys. Rev. Lett. 52 (1984) 1122.
[2] Itoh, K.*11, et al., Nucl. Fusion 28 (1988) 779.
[3] Ohkawa T.*1, General Atomic Report GA-A19379 (1988).
[4] Kishimoto Y., et al., to be published in JAERI-M.
[5] Kishimoto Y., et al., JAERI-M, 89-061(1989).

3. MHD Equilibrium and Stability Analysis

3.1 Self-consistent calculation of neoclassical current effect on MHD equilibrium[1,2]

MHD equilibria of tokamak plasmas with neoclassical current effects (neoclassical conductivity and bootstrap current) were calculated self-consistently. Neoclassical effects on JFT-2M tokamak plasmas, sustained by ohmic currents, were studied. Bootstrap currents flow little for L-mode type equilibria because of low attainable values of poloidal beta, β_J. H-mode type equilibria give bootstrap currents of 30% of ohmic currents for β_J attained by JFT-2M and 100% for $\beta_J \geq 1.5$, both of which are sufficient to change the current profiles and the resultant MHD equilibria. Neoclassical conductivity which has roughly half value of the classical Spitzer conductivity brings peaked ohmic current profiles to yield low safety factor at the magnetic axis.

3.2 Non-linear analysis of finite beta tokamak plasma

Non-linear calculations of resistive ballooning mode in a finite beta tokamak were carried out. The reduced set of resistive MHD equations was used. The equilibrium current profile was chosen as relatively

flat one, $q_o/q_a = 1.8/2.8$, and only terms of first order of ε (ε=a/R is inverse aspect ratio) was considered. The values of inverse aspect ratio, ε, poloidal beta, β_p, and magnetic Reynolds number, S, are chosen as $\varepsilon = 0.1$, $\beta_p = 1.0$ and $S = 10^6$, respectively. The time evolution of magnetic island is shown in Fig. I.3-1, where the evolution of the island with helicity of m/n = 2/1 exhibits much different behavior from that of usual tearing mode. The position of the island with the region of q = 2 surface moves towards the magnetic axis. For higher values of poloidal beta, the region of q = 2 surface in the radial direction becomes larger. Detailed mechanism of flattening of q profile is not known yet. For sufficient large value of beta poloidal, the q = 2 region is expected to extend to the magnetic axis like the case of m = 1 tearing mode evolution, and so the q = 2 sawtooth can be induced.

3.3 Pressure profile effects on ideal MHD stability of ITER[3]

The dependence of the ideal MHD beta limit on the pressure profile was investigated for different current density profile or internal inductance, l_i. When the safety factor (or current density) at the magnetic axis was fixed ($q_0 \sim 1.1$), the beta limit due to kink modes ($n \leq 4$) and ballooning modes was larger for smaller l_i. A strong mode coupling between low-m and high-m components (m: poloidal mode number) was observed in the structure of unstable kink modes for a divertor configuration of ITER. The low-m component became large and ballooning mode was unstable near the magnetic axis for large l_i due to lack of the central magnetic shear.

3.4 Access to the second stability regime near the plasma surface[4]

The accessibility to the second stability regime of ballooning modes near the plasma surface was confirmed in a nearly circular cross section of a tokamak plasma. It was shown that in an equilibrium with high safety factor and low shear near the plasma surface the second stability regime is accessible even for low q_0 (q_0: the safety factor at the magnetic axis). The accessibility was shown to be more easily realizable in a lower aspect ratio ($A < 3$) and a positive triangularity of the plasma cross section. It was also shown that the accessibility became higher by introducing pedestal to the current density profile near the plasma edge.

References

[1] Tokuda S., et al., JAERI-M 88-216 (1988).

[2] Tokuda S., et al., J. Phys. Soc. Japan 58 (1989) 871.

[3] Tsunematsu T., et al., Japanese Contribution to ITER Joint Work (Feb. - March, 1989, Garching) ITER-IL-Ph-11-9-J-01.

[4] Ozeki T., et al., submitted to Nucl. Fusion.

4. Analyses of Burning Plasma in a Tokamak

4.1 Fusion output power [1]

The simple computational form for the DT fusion output power from a toroidal plasma was presented, which is very useful in course of the zero-dimensional analysis on a fusion reactor plasma. The power is given as a function of plasma volume V_p, averaged density $\langle n \rangle$, averaged temperature $\langle T \rangle$, and profile parameters α_n and α_T (profiles are assumed to be $(1 - \rho^2)^{\alpha}$). The output power is maximized at the optimum averaged temperature under the condition of constant pressure. This maximum power is given by $P_f = 4FV_p\langle n_D \rangle\langle n_T \rangle\langle\langle T \rangle\rangle^2$, where $\langle\langle T \rangle\rangle$ denotes the density weighted averaged temperature. The "maximum fusion output power coefficient" F is approximated as a linear function of α_T and α_n, as $F = 0.01 \times (0.7 + 0.335\alpha_T + 0.405\alpha_n)$ MW.10^{-40}m^3.keV^{-2}.

4.2 Steady-state operation of tokamak reactor plasma [2]

Consistency of physics constraints imposed on a core plasma in a tokamak reactor was investigated. The parameter ranges, in which the conditions for the stationary operation of the ITER-grade plasma are simultaneously satisfied, were searched for by employing the L-mode confinement scaling. The Q-value (Q: the fusion power multiplication factor) and the size dependence were studied. The self-consistent working region of the stationary operation was found. If the offset-linear scaling is applied, the minimum and necessary input power is about 130 MW, which enables the full current-drive and stationary operation with $I_p = 20$ MA. When the input power is increased up to 200 MW, the Q-value of 5 is possible.

4.3 ICRF wave absorption by alpha particles [3]

The possibility of attainment of an effectively-high-Q plasma by the ICRF-enhanced power transfer from alpha particles to a D-T burning plasma was investigated. The effective Q-value, Q_{eff}, which is defined

References

[1] Tokuda S., et al., JAERI-M 88-216 (1988).

[2] Tokuda S., et al., J. Phys. Soc. Japan 58 (1989) 871.

[3] Tsunematsu T., et al., Japanese Contribution to ITER Joint Work (Feb. - March, 1989, Garching) ITER-IL-Ph-11-9-J-01.

[4] Ozeki T., et al., submitted to Nucl. Fusion.

4. Analyses of Burning Plasma in a Tokamak

4.1 Fusion output power [1]

The simple computational form for the DT fusion output power from a toroidal plasma was presented, which is very useful in course of the zero-dimensional analysis on a fusion reactor plasma. The power is given as a function of plasma volume V_p, averaged density $\langle n \rangle$, averaged temperature $\langle T \rangle$, and profile parameters α_n and α_T (profiles are assumed to be $(1 - \rho^2)^{\alpha}$). The output power is maximized at the optimum averaged temperature under the condition of constant pressure. This maximum power is given by $P_f = 4FV_p\langle n_D \rangle\langle n_T \rangle\langle\langle T \rangle\rangle^2$, where $\langle\langle T \rangle\rangle$ denotes the density weighted averaged temperature. The "maximum fusion output power coefficient" F is approximated as a linear function of α_T and α_n, as $F = 0.01 \times (0.7 + 0.335\alpha_T + 0.405\alpha_n)$ MW.10^{-40}m^3.keV^{-2}.

4.2 Steady-state operation of tokamak reactor plasma [2]

Consistency of physics constraints imposed on a core plasma in a tokamak reactor was investigated. The parameter ranges, in which the conditions for the stationary operation of the ITER-grade plasma are simultaneously satisfied, were searched for by employing the L-mode confinement scaling. The Q-value (Q: the fusion power multiplication factor) and the size dependence were studied. The self-consistent working region of the stationary operation was found. If the offset-linear scaling is applied, the minimum and necessary input power is about 130 MW, which enables the full current-drive and stationary operation with I_p = 20 MA. When the input power is increased up to 200 MW, the Q-value of 5 is possible.

4.3 ICRF wave absorption by alpha particles [3]

The possibility of attainment of an effectively-high-Q plasma by the ICRF-enhanced power transfer from alpha particles to a D-T burning plasma was investigated. The effective Q-value, Q_{eff}, which is defined

as the ratio of the indirect plasma heating power transferred from alphas to the direct heating power, was evaluated on the basis of the energy moments of the quasi-linear RF diffusion operator. The value of Q_{eff} increases with the cyclotron harmonic number and the toroidal magnetic field. The fourth harmonic alpha cyclotron wave, which is absorbed mainly by the alphas, is promising for attainment of the high-Q_{eff} plasma, and the third harmonic wave can also enhance Q_{eff} fairly well in the high magnetic field.

4.4 Heat load on the first wall due to ripple loss of alpha particles in ITER

The peak load on the first wall and the divertor plates due to ripple loss of alpha particles is one of the critical issues in the design of tokamak reactors. Accordingly, we investigated the two-dimensional (2D) heat load distribution by using an three-dimensional (3D) orbit-following Monte-Carlo (OFMC) code. Figure I.4-1 shows the 2D heat load distribution by the ripple loss of alpha particles in the ITER plasma with I_p = 20 MA and maximum ripple of 1.5%. Though the heat load by ripple-trapped loss particles is strongly localized as shown in Fig. I.4-1(a), the peak value is only of the order of 0.1 MW/m^2 because of very small loss fraction of ~0.5%. This level of heat load is low enough for the design of the first wall. The 2-D head load distribution by ripple-untrapped loss particles is shown in Fig. I.4-1(b). In spite of the Monte-Carlo noise due to very small number of loss test particles, the toroidal-angle localization seems to be weak and the peak value on the first wall is also of the order of 0.1 MW/m^2.

4.5 Burn control of tokamak plasma by toroidal field ripple [4]

It has been found from calculations by an orbit-following Monte-Carlo (OFMC) code, that ripple loss of suprathermal alpha particles in a non-circular, small aspect-ratio and high current plasma is much smaller than that in a circular, large aspect-ratio and low current plasma. It was also found that ripple induced loss of alpha power amount to 20 ~ 30% of the total power. Alpha power loss of this order is effective for the burn temperature control. By applying field ripple with additional coils, more than 30% of alpha power can be removed with the edge ripple of the order of 3% in a large aspect ratio tokamak. The alpha power deposition profiles altered by the ripple as well as the

temperature dependence of ripple losses were estimated by the OFMC code. These results were applied to a 1.5D tokamak transport code. The transport simulation shows that the burn control by the ripple-degraded fast-alpha confinement is feasible and effective.

References

[1] Takizuka T., et al., JAERI-M 88-234 (1988).
[2] Itoh K.*11, et al., JAERI-M 88-171 (1988).
[3] Yamagiwa M., et al., JAERI-M 88-259 (1988).
[4] Tani K., et al., IAEA-CN-50/D-2-5, 12th int. conf. on plasma physics and controlled nuclear fusion research, Nice, 1988.

5. TRITON System

5.1 Compressible MHD code[1]

The 3-dimensional non-linear resistive MHD code was developed. The code solves the full set of the resistive MHD equations directly by means of semi-implicit method in cylindrical geometry without reducing it on the assumption of the tokamak ordering and incompressibility. Efficient MHD computation was able to be performed and macroscopic phenomena in tokamak plasma that cannot be expressed by the reduced-set code was successfully simulated. Non-linear analysis of $m/n = 2/1$ and $m/n = 1/1$ resistive modes was carried out as a test calculation and by the reasonable results the validity of the code was concluded.

5.2 MHD equilibrium code with neoclassical current effects[2]

An MHD equilibrium code in which current sources are specified instead of toroidal field function or safety factor was developed. This code is appropriate to self-consistent analysis of neoclassical current effects (bootstrap current and neoclassical conductivity) in the plasma sustained by the ohmic current. The code can also be applied to equilibrium and stability analysis of tokamak plasmas with non-ohmic currents driven by external sources (NBI/RF-wave) and with neoclassical current effects.

5.3 One-dimensional single-mode nonlinear code for calculation of FEL amplification[3]

The one-dimensional (1D) single mode nonlinear FEL amplification code was developed. This code is useful for the basic design of an FEL

temperature dependence of ripple losses were estimated by the OFMC code. These results were applied to a 1.5D tokamak transport code. The transport simulation shows that the burn control by the ripple-degraded fast-alpha confinement is feasible and effective.

References

[1] Takizuka T., et al., JAERI-M 88-234 (1988).
[2] Itoh K.*11, et al., JAERI-M 88-171 (1988).
[3] Yamagiwa M., et al., JAERI-M 88-259 (1988).
[4] Tani K., et al., IAEA-CN-50/D-2-5, 12th int. conf. on plasma physics and controlled nuclear fusion research, Nice, 1988.

5. TRITON System

5.1 Compressible MHD code[1]

The 3-dimensional non-linear resistive MHD code was developed. The code solves the full set of the resistive MHD equations directly by means of semi-implicit method in cylindrical geometry without reducing it on the assumption of the tokamak ordering and incompressibility. Efficient MHD computation was able to be performed and macroscopic phenomena in tokamak plasma that cannot be expressed by the reduced-set code was successfully simulated. Non-linear analysis of $m/n = 2/1$ and $m/n = 1/1$ resistive modes was carried out as a test calculation and by the reasonable results the validity of the code was concluded.

5.2 MHD equilibrium code with neoclassical current effects[2]

An MHD equilibrium code in which current sources are specified instead of toroidal field function or safety factor was developed. This code is appropriate to self-consistent analysis of neoclassical current effects (bootstrap current and neoclassical conductivity) in the plasma sustained by the ohmic current. The code can also be applied to equilibrium and stability analysis of tokamak plasmas with non-ohmic currents driven by external sources (NBI/RF-wave) and with neoclassical current effects.

5.3 One-dimensional single-mode nonlinear code for calculation of FEL amplification[3]

The one-dimensional (1D) single mode nonlinear FEL amplification code was developed. This code is useful for the basic design of an FEL

machine, where the wiggler field is given by the helical configuration. The guiding magnetic field for the stable beam propagation and the axial beam energy spread are taken into account. The tapered-wiggler with arbitrary configuration was also considered. The nonlinear FEL characteristics in the wide range from the Compton to the Raman regimes can be analyzed since the basic equations of the code include the electrostatic interaction terms. The FEL code developed here is vectorized by about 95%. And the large amount of parameter study for optimization of machine design can be carried out efficiently.

5.4 FORTRAN77 version of ARGUS-V4

The graphic subroutine package, ARGUS-V4 was rewritten in the FORTRAN77 language. In this new version character sets are handled in CHARACTER variables and files are managed by OPEN and CLOSE statements. The size of the screen and the unit of length are defined by PARAMETER statement. These improvement makes the implementation to other computer system easier. This version is now being used for the ITER joint work.

5.5 Improvement of database system GAEA

Two new functions were added to the database system GAEA. By this improvement the GAEA system now supports the interactive graphical display for data which are not stored in the system. Users can also plot graphs of data generated by simple operations (arithmetic or integral) of the original data.

References

[1] Yamaguchi Y., et al., JAERI-M 89-021 (1989).
[2] Tokuda S., et al., JAERI-M 88-207 (1988).
[3] Kishimoto Y., et al., JAERI-M 89-061 (1989).

6. Others

6.1 Plasma simulator

Conceptual design work of a plasma simulator was carried out for attaining efficient analyses of plasma behavior on the basis of the Monte Carlo type particle model and the nonlinear time evolution of the fluid model. An alpha particle analysis code, SLWALF, and a nonlinear MHD simulation code, AEOLUS, were chosen as examples of the application softwares and these codes were analyzed from the viewpoints of numerical

machine, where the wiggler field is given by the helical configuration. The guiding magnetic field for the stable beam propagation and the axial beam energy spread are taken into account. The tapered-wiggler with arbitrary configuration was also considered. The nonlinear FEL characteristics in the wide range from the Compton to the Raman regimes can be analyzed since the basic equations of the code include the electrostatic interaction terms. The FEL code developed here is vectorized by about 95%. And the large amount of parameter study for optimization of machine design can be carried out efficiently.

5.4 FORTRAN77 version of ARGUS-V4

The graphic subroutine package, ARGUS-V4 was rewritten in the FORTRAN77 language. In this new version character sets are handled in CHARACTER variables and files are managed by OPEN and CLOSE statements. The size of the screen and the unit of length are defined by PARAMETER statement. These improvement makes the implementation to other computer system easier. This version is now being used for the ITER joint work.

5.5 Improvement of database system GAEA

Two new functions were added to the database system GAEA. By this improvement the GAEA system now supports the interactive graphical display for data which are not stored in the system. Users can also plot graphs of data generated by simple operations (arithmetic or integral) of the original data.

References

[1] Yamaguchi Y., et al., JAERI-M 89-021 (1989).
[2] Tokuda S., et al., JAERI-M 88-207 (1988).
[3] Kishimoto Y., et al., JAERI-M 89-061 (1989).

6. Others

6.1 Plasma simulator

Conceptual design work of a plasma simulator was carried out for attaining efficient analyses of plasma behavior on the basis of the Monte Carlo type particle model and the nonlinear time evolution of the fluid model. An alpha particle analysis code, SLWALF, and a nonlinear MHD simulation code, AEOLUS, were chosen as examples of the application softwares and these codes were analyzed from the viewpoints of numerical

algorithms and logical structures of the flows of calculation.

In SLWALF one thousand particles are used as a standard case and banana orbits are traced by using Runge-Kutta integration method. Collisions are simulated by the Monte Carlo method. In AEOLUS a set of the nonlinear differential equations (MHD equations) are solved by using the finite difference method for the radial direction and Fourier expansions for the poloidal and the toroidal directions. An implicit method is used for the time integration of the magnetic diffusion equation.

Detailed analysis showed that a plasma simulator with effective performance of about 1 GFLOPS in terms of a computer could be designed without difficulty.

6.2 Data link

Necessary devices and softwares for the US-Japan Data Link system was installed at Naka Fusion Research Establishment and test work was being carried out. In this system the VAX 8350 computer is connected to terminals and CAD system via Ethernet LAN, and to other VAX computers via PSI (Packet Switching Interface). The VAX 8350 computer is connected to the FACOM M780 host computer via INTERLINK system. By using this system the terminals accessible to the VAX computers can be used as character-display terminals of the FACOM M780 host computer.

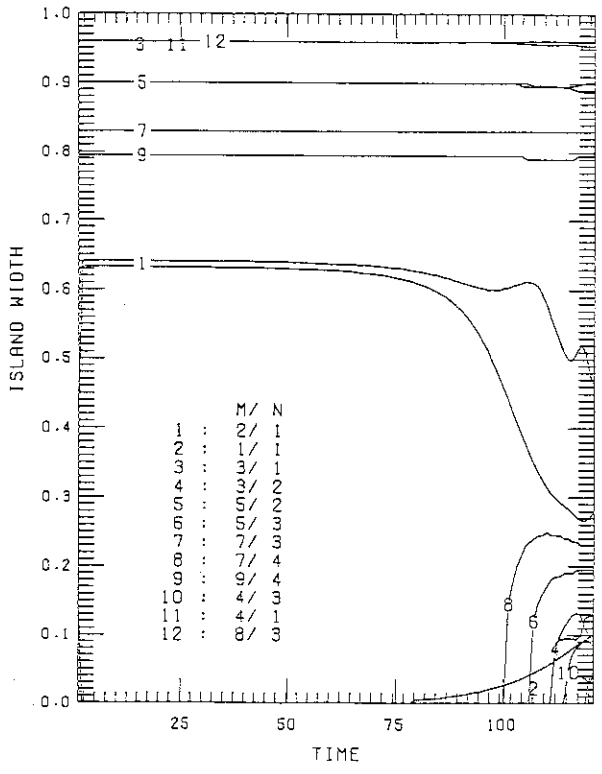

Fig.I.3-1 Island evolution of the resistive ballooning mode. M/N denotes helicity of the island, where M and N are poloidal and toroidal mode numbers, respectively.

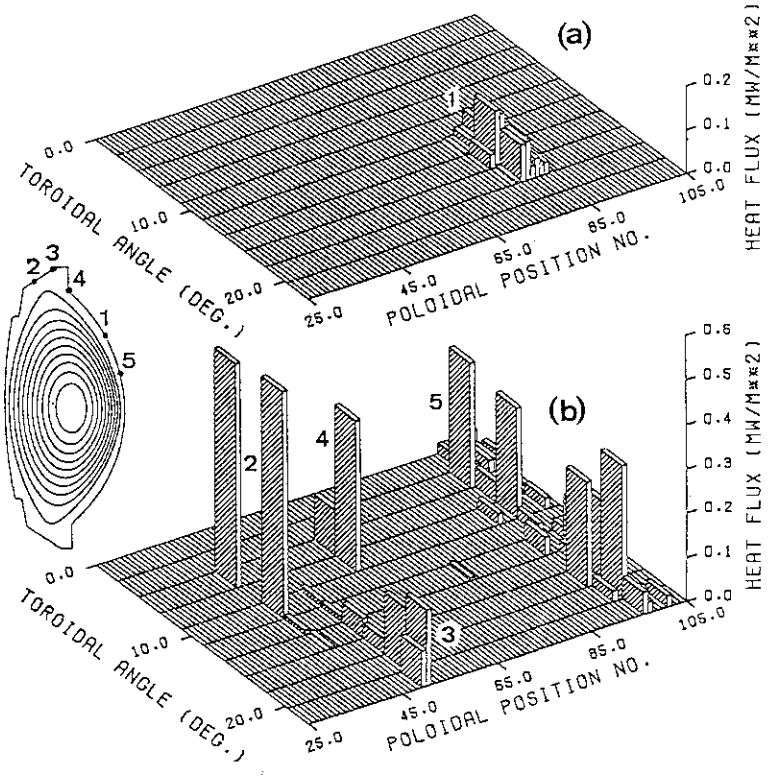

Fig.I.4-1 Two-dimensional heat load distribution on the first wall for (a) ripple-trapped loss alpha particles and for (b) ripple-untrapped loss.

II. JFT-2M PROGRAM

1. Toroidal Confinement Experiment

1.1 Introduction

Our activities on JFT-2M for FY88 (April 1988 to March 1989) are described. In the reporting period, the power supply for increasing plasma current by 30% in divertor configurations has been constructed and ergodic limiter coils have been installed as a part of the JFT-2M upgrade program. Pellet injection method has been under development on JFT-2M and for this fiscal year 10-pellets injector has been constructed.

1.2 Confinement studies

1.2.1 Studies of improved confinement

(a) Parameter dependence of H-mode confinement

The L-H transition occurs abruptly when the input power and the electron density exceed their respective threshold values. An increase in the stored energy, W_{dia}, follows, along with the formation of the so-called "pedestals", T_{ped} and N_{ped}, on the electron temperature and electron density profiles, respectively. During this fiscal year, we have continued our investigation of the conditions required for H-mode formation. The ten major factors and their effects on H-mode formation are presented in Table II.1-1.

As the neutral beam power, P_{NB}, is raised, the H-transition occurs just when $P_{NB} = P_{th}$, and W_{dia} jumps from its L-mode value to its H-mode value. This increment in W_{dia} clearly comes from the formation of pedestals on the $T_e(r)$ and $n_e(r)$ profiles. The H-mode with ELM's appears only near P_{th} and N_{th}, and W_{dia} stays at a slightly lower value as compared to the H-mode without ELM's. In the ELM-free case, W_{dia} increases linearly with increasing P_{NB}, and the incremental W_{dia} has offset-linear features, as is also the case in the L-mode. The τ_{inc} values for the H-mode are only slightly larger (10-20%) than for the L-mode[1]. It should be noted, however, that the density regimes for which the τ_{inc} values were determined are different in the two modes, and the W_{dia} values in the low-density regime inevitably include a beam component. The gross energy confinement time, τ_E, for the H-mode phase increases abruptly at P_{th}, but then decreases with increasing P_{NB}.

The τ_{inc} value increases linearly with I_p for both H^+ and D^+ plasmas,

but saturates near a surface safety factor, q_s, of 3. The increment in W_{dia} at the L-H transition (ΔW_{dia}) also increases with increasing I_p. Here, T_{ped} remains almost constant and N_{ped} increases with increasing I_p, so that the observed ΔW_{dia} dependence is probably due to an increase in the electron density.

One serious problem to be solved is that of impurity accumulation during the latter phase of the H-mode. Efforts to reduce metal impurities through the use of carbon wall tiles has resulted in H-modes with duration times of up to 300 ms, but we were unable to obtain stationary values of W_{dia}. The slow decay of W_{dia} seems to come from the decrease in the ion energy component, W_i, since it accompanies a decrease in the ion density due to the accumulation of light impurities. Thus, a clean plasma free of all impurities is required for improved H-mode performance, or a method for exhausting impurities from the plasma core must be developed.

(b) Analysis of the B_{theta} probe data[2]

MHD analysis of H-mode discharges

During the ohmic phase, an m = 2 mode is observed to rotate in the electron diamagnetic direction at a frequency of 4.7 kHz. The mode rotation frequency remains constant to within 0.1 kHz at the onset of beam (co-) injection. This result suggests that the toroidal rotation velocity of the surface where this fluctuation originates changes by less than 800 m/s when 1MW of neutral beam power is injected into the plasma. Core rotation speeds of 5×10^4 m/s are to be expected from velocity measurements on other discharges. This m = 2 activity must therefore originate near the plasma surface. Figure II.1-1 shows a contour plot from 732 to 734.5 ms. At the H-mode transition, which takes place at around 734 ms, the m = 2 mode suddenly reverses its direction of rotation, after which the amplitude of the oscillation dies down. This could be due to a sudden change of toroidal rotation speed at the plasma edge, or to a sudden change in the poloidal rotation speed, and corresponds to a change (towards more negative values) in the radial electric field associated with motion perpendicular to B.

MHD analysis of ELM/ERP activity

ELM/ERP activity takes place just before 756 ms, and the ECE signal and $\bar{n}_e$ at the plasma periphery (time resolution = 0.2 ms) dip at that instant. A peak in the H_α/D_α signal is also seen at about that time,

although the time resolution of only 1 ms for this signal does not permit a precise determination of the timing of this peak with respect to the onset of ELM/ERP activity. ELM/ERP activity onset is accompanied by the appearance of a strong m = 1 mode fluctuation in the magnetic probe signals. About 1 ms later, the m = 2 mode appears, with a rotation in the ion diamagnetic direction. This mode is fairly strongly localized in the region of bad curvature.

(c) Divertor plasma characteristics during the H-mode

Electron temperature, density, flux, and potential were measured as a function of poloidal angle using 17 Langmuir probes set into the divertor neutralizer plates[3,4].

The ion saturation current, which is proportional to particle flux, decreases quickly at the L- to H-mode transition, suggesting improved particle confinement in the main plasma. The width of the heat flux region at the neutralizer plates is about 5 cm when the distance between the null-point and the divertor plate is a maximum (9 cm). Asymmetries in the electron temperature and density between the inner and outer divertors were observed during both the ohmic and additional heating phases. They are caused by asymmetries of the heat and particle fluxes and are altered by changing the toroidal magnetic field direction. The flux of particles reaching the scrape-off layer by crossing the separatrix goes preferentially to the ion drift side, rather than to the electron drift side.

When the additional heating power is held constant, the electron density at the neutralizer plate is proportional to the main plasma density in the low density region, and saturates in the high-density region (Fig. II.1-2). The electron temperature does not vary so much. When the plasma density is held constant, the ion saturation current (proportional to particle flux) varies linearly with additional heating power. The electron density at the divertor thus varies linearly with heating power (the proportionality factor on the ion side being larger than that on the electron side) but the electron temperature is independent of heating power.

(d) Improved L-mode confinement

Improved confinement has been obtained after the H-L transition in both divertor and limiter discharges[5]. Edge phenomena are similar to those in the L-mode, rather than the H-mode, and the density profile is

strongly peaked. We therefore call this mode the Improved L-mode (IL-mode).

Density and electron temperature profiles

Helium neutral beam power (24 kV, 320 kW, co-injection) has been injected into deuterium plasmas in the single null divertor configuration (B_T = 1.3 T, I_p = 260 kA, R = 1.28 m, a = 0.27 m, κ = 1.4). The edge density decreases at the H-L transition, and the central density increases in the IL-mode. The density profile thus becomes more strongly peaked. Although a temperature pedestal at the plasma edge is seen in the H-mode, it is absent in the IL-mode. The central electron temperature is higher in the IL-mode than in the H-mode (Fig. II.1-3). These observations indicate that both particle and energy confinement at the plasma edge are worse in the IL-mode than in the H-mode. In spite of this deterioration in edge confinement properties, the confinement in the core region improved.

Power dependence

The power dependence of the stored energy in the IL-mode is similar to that in the ELM-free H-mode, as shown in Fig. II.1-4. This figure clearly shows that the confinement is improved in the IL-mode, as compared to the L-mode. Roughly speaking, the stored energy increases offset-linearly, and the incremental energy confinement time is the same as that of the L-mode.

Conditions for achieving the IL-mode

Wall conditioning seems to be of critical importance for obtaining the IL-mode, since the day-by-day reproducibility is not very good. The plasma current and toroidal field also affect this mode. Gas puffing is another important parameter for controlling the onset of this mode. Without gas puffing, the density decreases to a very low level. As well, the stored energy decreases to the level of the L-mode and does not recover. In such cases, strong sawteeth frequently occur. With adequate gas puffing, the density decrease can be minimized the L-phase which follows the H-phase, and the stored energy recovers. Under such conditions, sawteeth are reduced or suppressed. Thus, a high density without sawtooth activity seems to be important for obtaining improved confinement properties without the edge H-mode phenomena. A sawtooth crash in the IL-phase, as is sometimes observed after the H-L transition, induces the L-H transition once more, thus limiting the duration of the IL-mode. The values of the safety factor, q_s, is important for obtaining

the IL-mode, since activity is affected by the q_s value. A q_s value of about 3 is required for IL-mode production.

1.2.2 Ion Bernstein wave heating

In contrast to the behavior of conventional fast wave launchers, the coupling efficiency for launching ion Bernstein waves is expected to remain constant as the plasma edge density decreases. This feature is advantageous for H-mode plasmas. In addition, efficient ion heating has been observed in previous experiments. In order to clarify certain aspects of plasma coupling and heating, we have launched ion Bernstein waves (IBW) into plasma of various confinements in JFT-2M[6].

The heating regime corresponds to the 3/2 harmonic ion cyclotron resonance of hydrogen (3/2 ω_H), or the third harmonic resonance of deuterium (3 ω_D). Figure II.1-5 shows the dependence of the plasma loading impedance on the distance between the launcher and the separatrix. The loading impedance increases as the plasma approaches the launcher. This tendency contradicts the theoretical predictions. At the moment of the mode transition, the loading impedance for the H-mode plasma falls rapidly to about 40% of that for the L-mode plasma.

Enhanced radiation loss is observed during the IBW-phase. The radiation loss increase exceeds the launched IBW power by more than a factor of two. A slight increase in stored energy is observed, due mainly to density build-up, and the stored energy contribution from net heating by IBW is quite small. IBW power is launched into the H-mode plasma produced in the upper single null divertor configuration with the aid of neutral beam heating. As shown in Fig. II.1-6, the H-mode terminates at the onset of the IBW pulse. This phenomena is observed whenever the launched IBW power exceeds 20 kW. The electron temperature in the scrape-off plasma, T_e^{so}, increases suddenly at the onset of the IBW pulse, showing that some IBW power is deposited in the scrape-off layer.

References

[1] N. Suzuki, et al., in Plasma Physics and Controlled Nuclear Fusion Research (Proc. 12th Int. Conf. Nice, 1988) IAEA-CN-50/A-3-5, Vienna (1988).

[2] H. Matsumoto, et al., JAERI-M 89-020 (1989).

[3] T. Shoji, et al., IAEA Technical Committee Meeting on Impurity

Control, Naka, Japan (February, 1989).
[4] I. Nakazawa, et al., in Controlled Fusion and Plasma Physics (Proc. 16th Europ. Conf. Venice, 1989) Vol. 13B, Part III. 887.
[5] M. Mori, et al., Nucl. Fusion 28 (1988) 433.
[6] H. Tamai, et al., JAERI-M 89-036 (1989).

1.3 Current drive and electron cyclotron heating experiments

1.3.1 Current drive with fast wave and ECH

The loading resistance of the 4-loop antenna array increases with the density and strongly depends on the gap between the antenna and the plasma edge as well as ICRF loop antennas. The antenna loading has a peak at $\Delta\phi = 0$ and has a minimum value at $\Delta\phi = \pi$ because the evanescent depth increases with the parallel refractive index (N_z). An improvement of the antenna loading during ECH is related with a broadening of the density profile. The coupling of the excited fast wave with electron is studied[1]. Time evolution of typical plasma parameters is shown in Fig. II.1-7. The antenna phasing is $\Delta\phi = \pi$. The cold lower hybrid layer is located at the plasma edge ($r/a = 0.9$) in this case. When the fast wave is applied, a remarkable increase of the electron temperature at the plasma center and a slight decrease of the loop voltage, which are good indications of the coupling of the fast wave with electron, are observed. The spatial profile of the electron temperature from ECE and Thomson scattering shows a peaked profile at the center. An increment of T_e is proportional to the rf power at $n_e\Delta T_e/P_{rf} = 1.5 \times 10^{19}$ eVm^{-3}/kW. The heating efficiency strongly depends on the antenna phasing. As the phase velocity of the excited fast wave retarded, the absorption of the fast wave increases drastically. At $\Delta\phi = \pi$ the ratio of the wave phase velocity to the electron thermal velocity is about 3. In contrast to the electron heating, the phase dependence of the intensity of the radiation loss has a peak at $\Delta\phi = 0$. In the ohmic plasma with $T_e = 1$ keV, the single pass absorption of the fast wave at $\Delta\phi = \pi$ is estimated about 15-20%. The absorption efficiency is improved by retarding the phase velocity since the number of the resonant electrons increases. The same effect is expected when T_e goes up with keeping the phase velocity constant. The experimental results obtained are consistent with the theoretical predictions.

The 2nd harmonic ECH is applied to improve the absorption efficiency of the fast wave[2,3]. When the electron is heated by 180 kW ECH up to

1.5 keV, an additional loop voltage drop of about 0.1 V is observed as well as the increase of ECE emissions. On the other hand, applied fast wave does not increase ECE signals strongly in the ohmic plasma with T_e of 1 keV below the density of $1 \times 10^{19} m^{-3}$. The ECH pre-heating improves the fast wave absorption efficiency at low density region below 1.5×10^{19} m^{-3}.

Present FWCD experiment in JFT-2M tokamak is summarized as follows;

(1) Phase dependence of the loading resistance of the antenna and heating efficiency shows that the control of the wave number spectrum of the excited fast waves can be done effectively by a phased 4-loop antenna array.

(2) Excited fast wave with relatively large N_z is absorbed by electron effectively. The absorption efficiency is improved with increasing the electron temperature.

(3) The absorption of the fast wave is explained by simple linear theory. The problem of so-called "SPECTRAL GAP" in LHCD is not seemed to exist in FWCD.

1.3.2 H-mode transition by the ECH

H-mode transition occurred by the edge heating[4,5] solely by ECH [6]. The launched wave has frequency of 60 GHz and extraordinary mode polarization. The threshold power for the H-mode transition is as low as 120 kW, which is the least threshold power observed in the JFT-2M tokamak. The H transition by the edge electron heating occurs not only in the lower single null divertor configuration but also in the D-shape limiter configuration. These results show that no additional power in the core plasma region is required to obtain the H-mode, and that the increase of the peripheral electron temperature is closely related to the trigger of the H-mode.

It is observed that the H-mode occurs by the edge ECH when the second harmonic electron cyclotron resonance (ECR) layer is located at 0.85a, where a denotes the minor radius of the separatrix. A clear drop in the intensity of the D_α line with bursts is observed. The average density increases at the H-mode transition, and saturates when bursts appear in the D_α signal. Figure II.1-8 shows the density region where the H-mode transition occurs when the ECR layer is located at 0.85a. It shows the power threshold of the minimum 120 kW for the H-mode transition. The broken line shows the threshold power for the H

transition solely by the neutral beam injection (NBI) heating which was taken at the same experimental condition. Comparison of the data point with the broken line shows that the threshold power for the edge ECH is smaller than the threshold power of NBI heating (core heating) at around $\bar{n}_e = 3.0 \times 10^{19}$ m^{-3} in spite of the edge power deposition of the ECH. Further, we found that a short ECH pulse of the pulse length of 20 ms can induce the H transition. A burst free H-mode lasts as long as 50 ms after the ECH pulse is off. The density increases continuously after the ECH is off, and the high edge temperature is maintained throughout the H-mode.

In conclusion, the H-mode is shown to be closely related to the increase in the electron temperature of the plasma periphery.

References

[1] Y. Uesugi, et al., in Controlled Fusion and Plasma Physics (Proc. of 16th Europ. Conf., Venice, 1989) Vol.13B, Part IV, European Physical Society (1989) 1259.

[2] T. Yamamoto, et al., in Plasma Physics and Controlled Nuclear Fusion (Proc. of 12th Int. Conf., Nice, 1988) IAEA-CN-50/E-4-6 (1988).

[3] H. Kawashima, et al., in Radio Frequency Power in Plasmas (Proc. of 8th Topical Conf., Irvine, 1989).

[4] K. Hoshino, et al., Nucl. Fusion 28 (1988) 301.

[5] K. Hoshino, et al., Phys. Letters A130 (1988) 26.

[6] K. Hoshino, et al., JAERI-M 89-038 (1989).

1.4 Particle control

1.4.1 Fueling by pellet injection

The JFT-2M pellet injector is an ORNL type gas propellant 4 pellets injector[1]. The injection experiment is done during ohmic, NBI and ICRF heated divertor or D-shape limiter configuration.

In the case of ohmic heating at D-shape limiter configuration (I_p = 0.4 MA), the line averaged density, $\bar{n}_e$ is effectively increased by pellets of about 50 ms interval. The peaking of the density profile $[\bar{n}_e(r = 0.2)/\bar{n}_e(r = 0.7)]$ is increased after pellets even in the case of shallow penetration. At high density ($\bar{n}_e > 3 - 4 \times 10^{19}$ m^{-3}) the energy confinement is improved but less than 20%. Large improvement of the confinement like ALCATOR or ASDEX is not observed in JFT-2M. At low

density ALCATOR regime, the confinement is not different from the gas puffing case even in the case of highly peaked density profile.

In the case of NBI heating, 4 pellets are injected into the single null divertor plasma at the same time. The line averaged density increased about $3-7\times10^{19}$ m^{-3} (this scatter is due to the injected pellet size). And even the plasma cooled by pellets the L-H transition, which is characterized by the decrease of H_α/D_α signal, the decrease of Mirnov signal $|\dot{B}_\theta|$ and the increase of the edge density, occurs after 20 - 30 ms from beam-on. For the improved case, pellets are injected between the co and ctr beam, but the other case two beams are fired at the same time. Then for the later case, the H transition has occurred before pellets, The behavior of the two cords of the density is the key parameter for the improvement. The improvement is observed when the particles are fueled effectively around the center[2]. In Fig. II.1-9, the peak diamagnetic energy is plotted against the $\Delta\bar{n}_e$ ($r = 0.2a$) - $\Delta\bar{n}_e$ ($r = 0.7a$) just after pellets injection. The clear dependence of the improvement due to the fueling can be seen in this figure. The improvement is about 30% compared to the gas puffing H-mode case and this is about 10 kJ of the diamagnetic energy. Another shots are not improved but are the same as the gas puffing H-mode. The ablation monitor also indicates the central fueling for the improved shot. The pellets which are injected into the H-mode ablate very rapidly around edge. This result may come from the pedestal of high edge electron temperature and density. Therefore, the deep penetration cannot be realized during H-mode, then the condition to get this improvement is to inject pellets before H transition. the discharge shows the very good confinement for impurities. The radiation loss increases very fast and shows the highly peaked profile. The peak stored energy does not continue for a long time. After the radiation loss shows the peaked profile, the stored energy decreases faster compared to a gas puffing H-mode.

1.4.2 Peripheral plasma control with pump limiter[3]

In this fiscal year, a pump limiter is employed aiming to prevent the neutral back flow in JFT-2M open divertor operation.

The pump limiter[4] is located close to the divertor null-point outside the separatrix. One of the gas-puff outlet is located between the separatrices intersecting the divertor plate. The peripheral neutral pressure P_{D_2} (measured by RGA) is considerably decreased by the

pump limiter (PL) with gas puff from the divertor region. The electron temperature at the plasma edge T_e^{edge} is relatively high with the pump limiter at higher density.

In ohmic phase, the dense and cold divertor plasma was not observed up to the maximum gas-feed rate. The electron density at the divertor plate, n_e, does not build up during the gas puffing. After the reduction or termination of the gas-puff, the T_e^{edge} increases, the $\bar{n}_e$ builds up from 0.6×10^{19} m^{-3} to 2×10^{19} m^{-3} and the electron temperature at the divertor plate T_e cools down from 17 eV to 10 eV. This implies that the ionization mean-free-path (0.2 m) is too long due to low T_e^{edge} during the gas-puffing compared to the length of divertor channel (~0.07 m).

In a beam-heating phase, T_e^{edge} is two times higher than that of ohmic phase even though a gas-puff Q_H is introduced. The power flow to the divertor channel is supposed to be large in this case. The Q_H up to 20 Torr·l/s is compatible for switching on an H-mode by using the pump limiter. The build-up or n_e^d is very strong and T_e^d is below 10 eV with the power of 1.7 MW as shown in Fig. II.1-10 for the case with the bottom gas-puff ($\bar{n}_e \sim 6 \times 10^{19}$ m^{-3} at $t = 0.8$ sec). The discharge becomes L-mode when $Q_H = 30$ Torr·l/s.

In conclusion, the combination of a pump limiter and divertor is examined. A dense and cold divertor plasma is obtained by using a pump limiter in JFT-2M tokamak. In an ohmic phase, the divertor plasma density builds up only when a gas-puff is terminated. It is shown, however, that a very dense and cold divertor plasma ($\sim 4 \times 10^{19}$ m^{-3}, ≤ 10 eV) is compatible with a beam heated H-mode discharge.

References

[1] Annual Report of the Naka Fusion Research Establishment, JAERI-M 88-231 (1988).

[2] N. Suzuki, et al., in Plasma Physics and Controlled Nuclear Fusion Research (Proc. 12th Int. Conf. Nice, 1988) IAEA-CN-50/A-3-5, Vienna, (1988).

[3] S. Sengoku, et al., in Controlled Fusion and Plasma Physics (Proc. 16th Europ. Conf. Venice, 1989) Vol.13B, Part III, (1989) 959.

[4] S. Sengoku, et al., presented at the 8th Int. Conf. on Plasma Surface Interactions in Fusion Devices, Jülich, May 1988, paper 192.

1.5 Diagnostics

1.5.1 Impurity behavior during improved confinement modes

In deuterium discharges, the intensities of highly-ionized metallic ion lines (FeXV, FeXVIII and TiXV) and CVI line excited by the charge exchange recombination (CXR) increased almost linearly with time during the H-mode phase without ELM's although those of less-ionized species (TiXI, FeX and CIV) decreased in comparison with those during the L-mode phase. The time behavior of the intensity of the CVI line excited by CXR indicates that the C^{6+} ion density near the plasma center increased in this phase[1]. On the other hand, in hydrogen discharges intensities of highly-ionized ion lines were about half of those in deuterium discharges, although intensities of less-ionized ion lines were about the same in both discharges. The spatial profile of Fe^{9+} and Fe^{17+} ion densities indicate that impurity accumulation in deuterium discharges was more enhanced in comparison with that in hydrogen discharges and this was not due to the difference of the influx. All of these data suggest that the enhancement of particle confinement by the H-mode transition in deuterium discharges is larger than that in hydrogen discharges[2].

During the H-mode phase with ELM's, the intensities of the less-ionized ion lines had a burst which was well correlated to the H_α/D_α signals and the intensities of highly-ionized ion lines increased slightly with time compared with those during the H-mode phase without ELM's[2]. The increases of $\bar{n}_e$ and P_{rad} were also less than those in the H-mode without ELM's. These results suggest that the impurity accumulation is suppressed by ELM's.

During the improved L-mode phase[3], $\bar{n}_e$ and P_{rad} were almost constant with time and the energy confinement time was about the same as that during the H-mode phase without ELM's. The intensity of TiXX line emitted near the plasma center (roughly $r < a/3$) increased compared with that during the H-mode phase and intensities of other less ionized ion lines (TiXV and TiXI) were almost constant with time during this phase (Fig. II.1-11). These results and the measured density profile of Ti^{19+}, Ti^{14+} and Ti^{10+} ions indicate that the impurity profile became more centrally-peaked compared with those in the H-mode as a result of the enhancement of the particle confinement near the plasma center.

1.5.2 Two dimensional bolometer array

The bolometer array in horizontal line of sight has already been operated[4]. The bolometer array to observe in the vertical line of sight is newly designed and installed at the bottom part of torus. The sensor heads are the same Thinistor as that used in the horizontal array for keeping the data matching. The viewing chords of vertical array is shown in Fig. II.1-12. The viewing chords of the horizontal array and of the divertor array are also shown.

By the observation in two direction the peaked profile druing H-mode phase can be more clearly observed. In addition, strong enhancement in the outer edge plasma region (channel number 13 & 14) is investigated during NB heating and ICRF heating. Figure II.1-13 shows the case of ICRF heating in which the power of about 500 kW is launched during 0.6-0.9 s. The intensity in the edge chord exceeds that in the central chord. The enhancement in outer region is observed in plasma specie of hydrogen and the toroidal magnetic field in clockwise direction. This due to the charge exchange flux of high energy ions trapped by the toroidal ripple.

References

[1] H. Ogawa, et al., Rev. Sci. Instrum. 59 (1988) 1506.

[2] H. Ogawa, et al., in Controlled Fusion and Plasma Physics (Proc. 16th Europ. Conf. Venice, 1989) Vol. 13B, Part 1, European Physical Society, (1989) 217.

[3] M. Mori, et al., Nucl. Fusion 28 (1988) 433.

[4] H. Tamai, et al., JAERI-M 88-120 (1988).

2. Operation and Maintenance

2.1 Introduction

Facility Operation and Engineering Division has been engaged in operation and maintenance of JFT-2M, neutral beam injection (NBI) system, RF heating devices [lower hybrid heating (LHH), fast wave current drive system (FW), and electron cyclotron heating (ECH)] and flywheel motor-generator (MG), and also in development of auxiliary equipments and instruments. In this fiscal year all the devices have been operated smoothly on schedule, and the careful maintenance have been performed daily and periodically.

The bolometer array in horizontal line of sight has already been operated[4]. The bolometer array to observe in the vertical line of sight is newly designed and installed at the bottom part of torus. The sensor heads are the same Thinistor as that used in the horizontal array for keeping the data matching. The viewing chords of vertical array is shown in Fig. II.1-12. The viewing chords of the horizontal array and of the divertor array are also shown.

By the observation in two direction the peaked profile druing H-mode phase can be more clearly observed. In addition, strong enhancement in the outer edge plasma region (channel number 13 & 14) is investigated during NB heating and ICRF heating. Figure II.1-13 shows the case of ICRF heating in which the power of about 500 kW is launched during 0.6-0.9 s. The intensity in the edge chord exceeds that in the central chord. The enhancement in outer region is observed in plasma specie of hydrogen and the toroidal magnetic field in clockwise direction. This due to the charge exchange flux of high energy ions trapped by the toroidal ripple.

References

[1] H. Ogawa, et al., Rev. Sci. Instrum. 59 (1988) 1506.

[2] H. Ogawa, et al., in Controlled Fusion and Plasma Physics (Proc. 16th Europ. Conf. Venice, 1989) Vol. 13B, Part 1, European Physical Society, (1989) 217.

[3] M. Mori, et al., Nucl. Fusion 28 (1988) 433.

[4] H. Tamai, et al., JAERI-M 88-120 (1988).

2. Operation and Maintenance

2.1 Introduction

Facility Operation and Engineering Division has been engaged in operation and maintenance of JFT-2M, neutral beam injection (NBI) system, RF heating devices [lower hybrid heating (LHH), fast wave current drive system (FW), and electron cyclotron heating (ECH)] and flywheel motor-generator (MG), and also in development of auxiliary equipments and instruments. In this fiscal year all the devices have been operated smoothly on schedule, and the careful maintenance have been performed daily and periodically.

2.2 Operation and maintenance

In this fiscal year, regular inspection of the high voltage metal-enclosed switchgear and of the control system for the JFT-2M MG power supply have been performed. A fast wave antenna for current drive experiments and a movable limiter have been installed in the JFT-2M machine. During the necessary venting of the JFT-2M torus, the performance of the vacuum pumping system was improved. Routine operation and maintenance have continued on the JFT-2M neutral beam injectors. The old calorimeter has been replaced by the new one. Improvement of the JFT-2M ECH system from 0.2 sec operation at 0.4 MW to 0.5 sec at 1 MW has started, and will be completed during the next fiscal year. Testing and tuning of the fast wave system have continued, and power levels of 300 kW for 0.1 sec have been successfully launched into JFT-2M plasmas. A summary of the operation of the MG, JFT-2M, NBI, LHH, and ECH are shown in Table II.2-1.

2.3 Development of pellet injector on JFT-2M

In JFT-2M, both single and 4-pellets injectors, pneumatic-gun type, have been developed since 1982[1]. Monitor systems of the pellet, i.e. pellet mass, shadowgraph, ablation, trajectory, etc., have also been developed as shown in Fig. II.2-1[1]. In the injection experiments, the pellet mass is measured by using a micro-wave cavity, which resonates strongly at about 8.8 GHz. The spatial profile of the pellet ablation can be obtained by using the time evolution of the H_α/D_α intensity measured by the 1-ch photo-diode with an interference-filter and the measured pellet-velocity. Also, the quantity of the local ablation is observed by the 8-ch photo-diode array with the interference-filter. The size of the ablation cloud and the velocity of the pellet ablated in the plasma can be estimated from the local ablation measurement. Figure II.2-2 is the typical ablation profile and the local ablation in the diverted discharge with deuterium pellet injection. The pellet penetrated deeply crossing the plasma center ($R = 1.294$ m). In this case, the cloud radius and pellet velocity in the plasma were about 15 mm and 0.822 km/s, respectively. The trajectory of the ablated pellet is monitored by the commercial video-camera with image fiber-scope. Figure II.2-3 shows the trajectories of 4 pellets. This system is a useful tool to understand the pellet behavior in the plasma, i.e. penetration depth, trajectory, etc. The two pellets were ablated near

the plasma periphery and the other pellets reached the plasma center.

References

[1] Y. Miura, et al., JAERI-M 85-192 (1985) (in Japanese), S. Kasai, et al., JAERI-M 87-161 (1987).

Table II.1-1 Parameter dependences of H-mode confinement

Affecting Factors		Characteristics	Comments
Heating Power (P_{add})	P_{th}	Min. $\sim$200kW at q_s=3	Def; P_{add} or P_t?
	W_{dia}	$\tau_{inc} \times P_{add} + \Delta W_H$	τ_{inc} or τ_E?, P_{add} or P_t?
Average Density ($\bar{n}_e$)	P_{th}	Min. at medium $\bar{n}_e$	n_{th}; $\bar{n}_e$ or n_{edge}?
	W_{dia}	$\sim \bar{n}_e^{0.5}$	$T_e \times \bar{n}_e^{0.5} \sim$ invariant
Plasma Current (I_p)	P_{th}	$\sim I_p^{-1}$ $q_s \geq 3$	q_s dep. P_{add} or P_t?
	W_{dia}	$\sim I_p$ $q_s \geq 3$	$\tau_{inc} \sim 0.06 Ip(H^0 \rightarrow D^+)$
Toroidal Field (B_T)	P_{th}	$\sim B_T$ $q_s \geq 3$	q_s dep. P_{add} or P_t?
	W_{dia}	$\sim B_T^0$ $q_s \geq 3$	$\sim B_T$ $q_s < 3$?
Isotope Effect ($H_{vs}D$)	P_{th}	$P_{th}(H)/P_{th}(D) \sim 2$	$H^0 \rightarrow H^+$ vs $H^0 \rightarrow D^+$
	W_{dia}	$\tau_{inc}(D)/\tau_{inc}(H) \sim 1.4$	$\tau_E(D) \sim \tau_E(H)$ at 0.8 MW
Direction of B_T (∇B_T)	P_{th}	Anti.D/Same D$\sim$2	$n_{th} \uparrow$, Hinton's theory
	W_{dia}	$\sim$same	Impurity; not same
Impurity Effect (Z_{eff})	P_{th}	$Z_{eff} \uparrow \rightarrow P_{th} \uparrow$	without Ti-getter$\sim$2$\uparrow$
	W_{dia}	$Z_{eff} \uparrow \rightarrow W_{dia} \downarrow$	n_i reduction
Outer Clearance (δ_{out})	P_{th}	$\delta_{out} \downarrow \rightarrow P_{th} \uparrow$	H/L trans. at $\delta_{out} \sim 3$ cm
	W_{dia}	$\delta_{out} \downarrow \rightarrow W_{dia} \downarrow$	ΔW_H decrease
Magnetic Configuration (κ, δ)	P_{th}	Div.$\rightarrow$Lim.$\rightarrow P_{th} \uparrow$	I_d dep.(Div), κ dep.(Lim)
	W_{dia}	Div.$\rightarrow$Lim.$\rightarrow \Delta W_{dia} \downarrow$	κ dep.(Lim)
Heating Method (ICRF,ECH)	P_{th}	$\sim$same (NBI,ICRF,ECH)	Ohmic H-mode (DIII-D)
	W_{dia}	$\sim$same	Coupling(ICRF)?, Contr.ELM?

Table II.2-1 Operation of MG, JFT-2M, NBI, LHH, FW and ECH

(Month)	1988 4	5	6	7	8	9	10	11	12	1989 1	2	3
M-G	operation and maintenance											
JFT-2M	operation and maintenance											
NBI	operation and maintenance											
LHH	operation and maintenance											
ECH	operation and maintenance											
FW	operation and maintenance											

Detail of the operation (M-G, JFT-2M, NBI, LHH, FW and ECH)

	(Fiscal year)	1987	1988 APR-JUN	1988 JUL-SEP	1988 OCT-DEC	1989 JAN-MAR	Total
M-G	M-G (#1) (hours)	1124	315	325	239	327	1206
	M-G (#2) (hours)	1123	315	324	239	326	1204
JFT-2M	Total days of operation (days)	131	37	42	29	39	147
	Times of discharge (shots)	8333	2242	2770	1275	2632	8919
	Baking (times)	4	2	1	1	0	4
	Discharge cleaning (hours)	184	62	34	60	31	187
	Pellet injection (days)	46	11	3	2	12	28
NBI	Total days of operation (days)	78	23	16	18	28	85
	Flashing injection Conditioning(shots)	A: 39343 B: 24063	13569 13758	8626 6757	9198 7733	12424 9316	A: 43817 B: 37564
LHH	Total days of operation (days)	17	0	0	0	0	0
	Times of power injection (times)	1559	0	0	0	0	0
FW	Total days of operation (days)	-	27	33	17	17	94
	Times of power injection (times)	-	84	263	178	127	652
ECH	Total days of operation (days)	23	0	22	1	14	37
	Times of power injection (times)	6278	0	16517	37	14708	31262

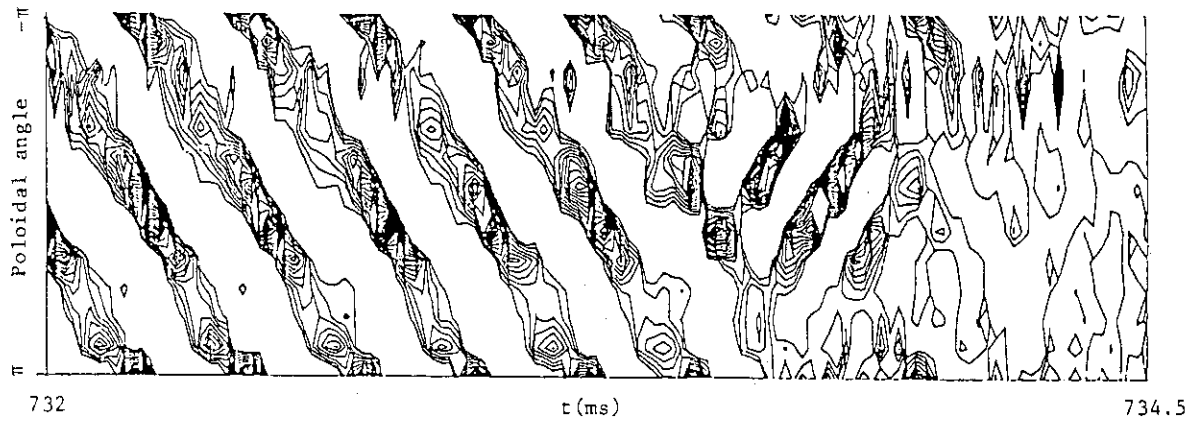

Fig.II.1-1 The contour plot of magnetic probe signal intensity in time and poloidal angle. Vertical axis is the poloidal angle coordinate with 0 at the outer midplane, $-\pi/2$ at the top of the vessel, and $\pi/2$ at the bottom of the vessel. Horizontal axis is time. H-mode transition takes place around 734 ms.

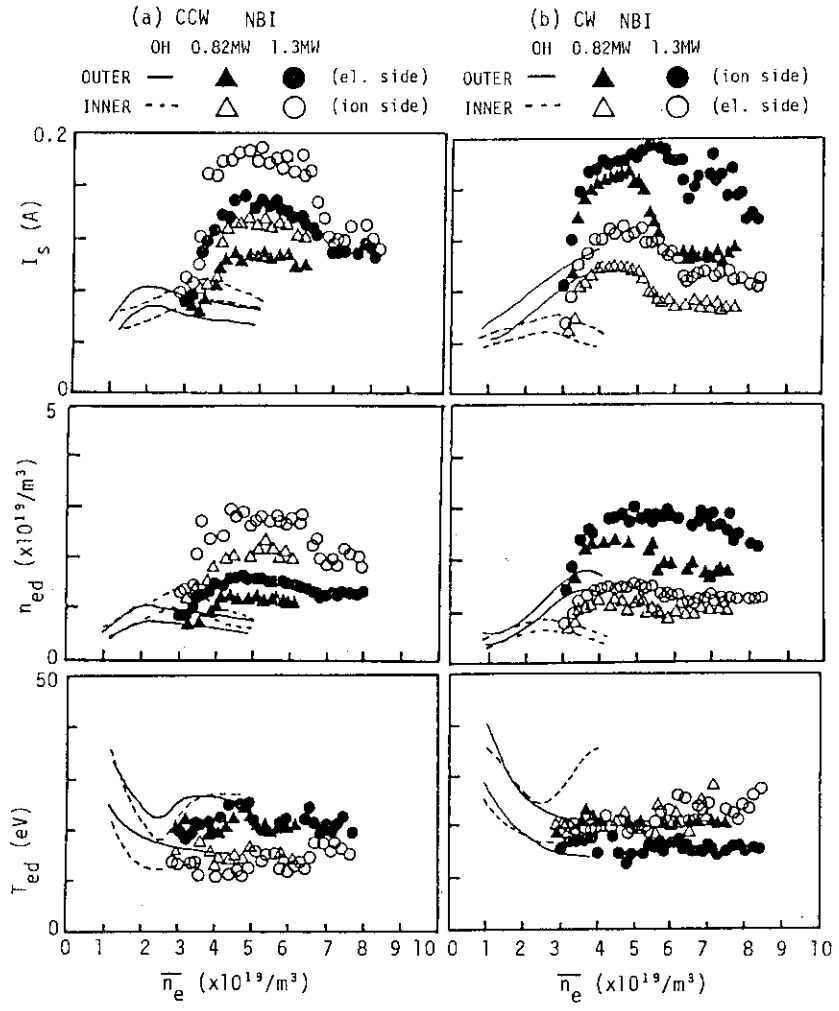

Fig.II.1-2 The peak value of T_{ed} and n_{ed} at the ohmic and the NBI heating phases for two directions of the toroidal field (CCW and CW) versus the main plasma density.

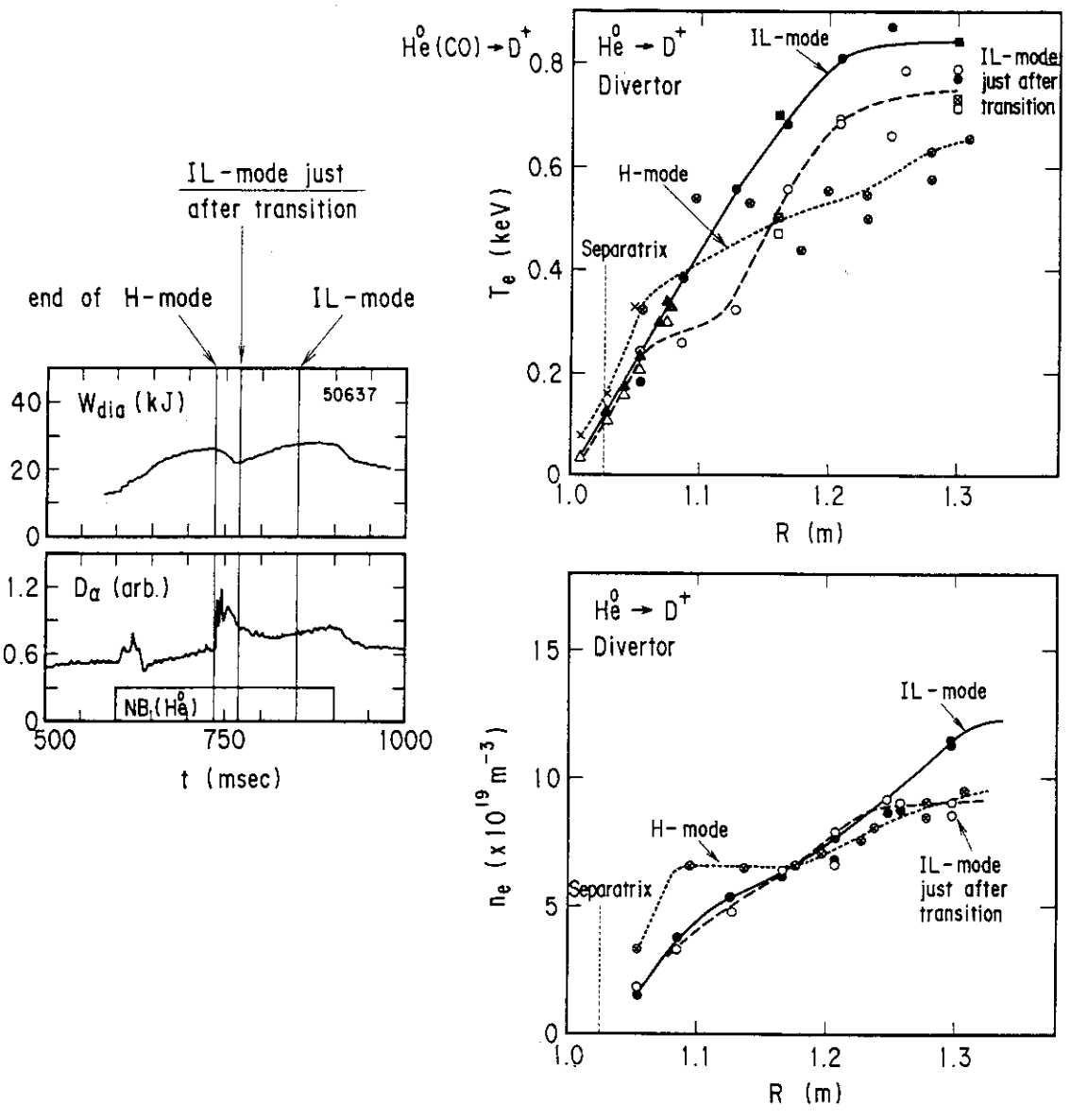

Fig.II.1-3 Profiles of electron density and temperature in H-mode, IL-mode just after the H-L transition, and IL-mode in the stationary state. Helium beam is injected tangentially into a deuterium plasma (I_p=255 kA, B_T=1.25 T) with single null divertor configuration. Each symbol in this figure corresponds to measurement to get profile data, as follows.

	H-mode	IL-mode just after H-L transition	IL-mode
Laser scattering	⊗	○	●
Soft X-ray spectrum	⊠	□	■
EC emission	×	△	▲

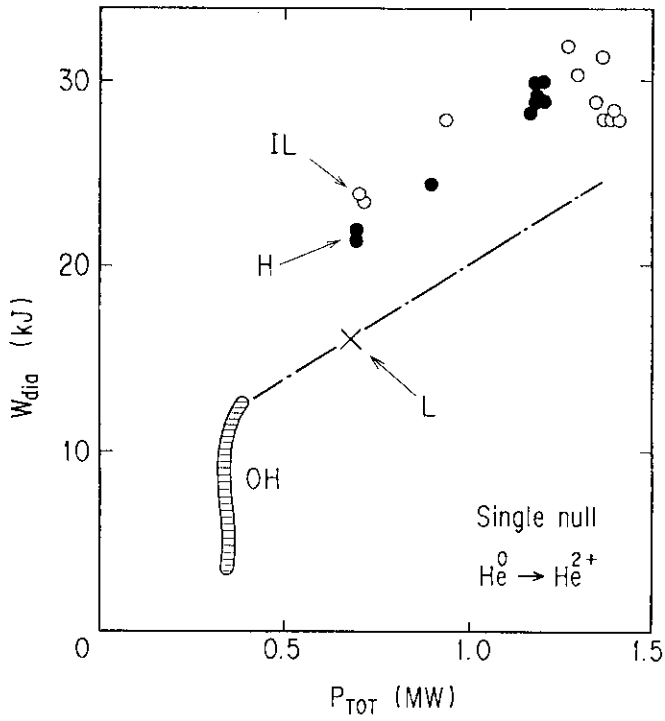

Fig. II.1-4 Power dependence of the stored energy in three modes and ohmic heating case. Helium beam is injected into Helium single null divertor plasmas. Open and closed circles represent the IL-mode and the H-mode, respectively. Cross represents the L-mode.

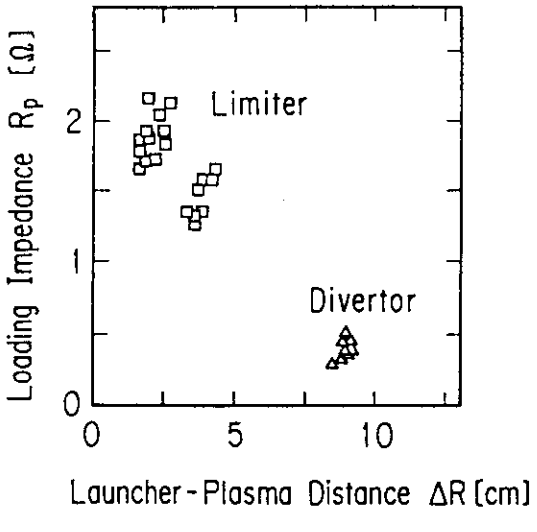

Fig. II.1-5
Dependence of plasma loading impedance on distance between launcher and the separatrix.

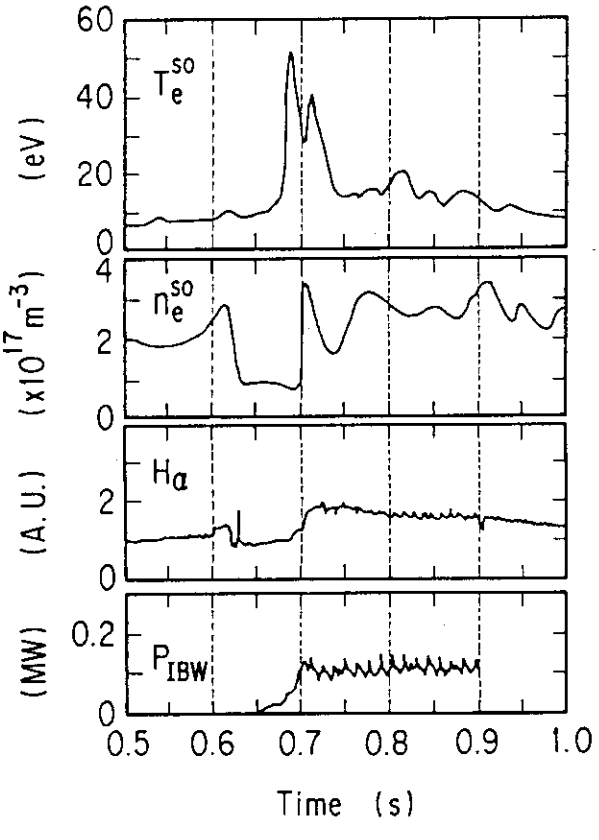

Fig. II.1-6 Temporal behavior during H-mode transition.

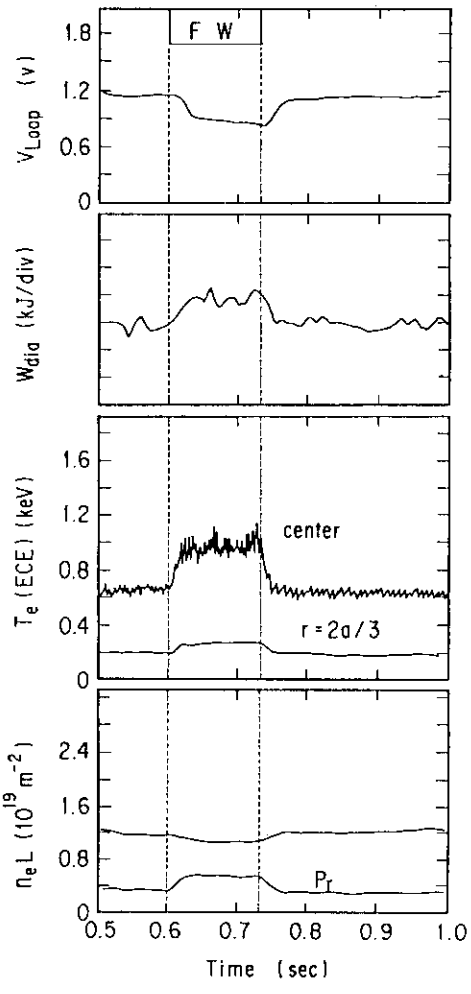

Fig.II.1-7
Time evolution of the plasma parameters in fast wave electron heating experiment. The antenna phasing is 180 degree and the rf power is 450 kW.

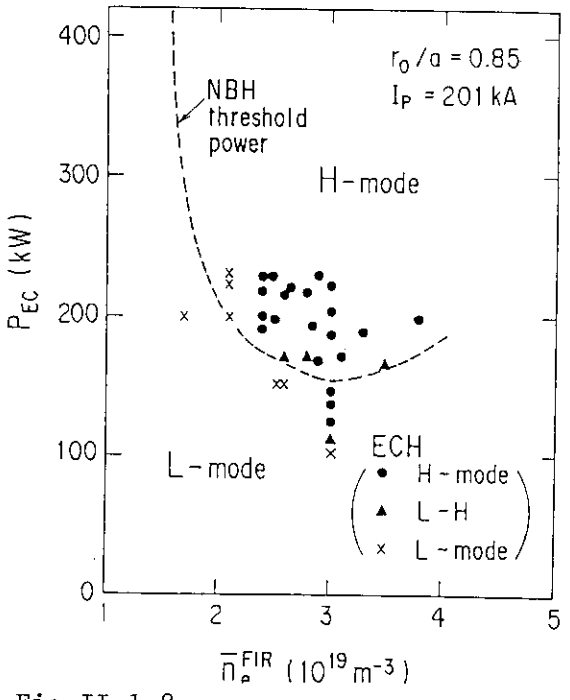

Fig.II.1-8
Density and ECH power plot which shows the parameter region in which H-mode was obtained. The triangle shows the boundary between the H-mode and the L-mode in the parameter space. Broken line shows the threshold power for the H-mode transition by NBI.

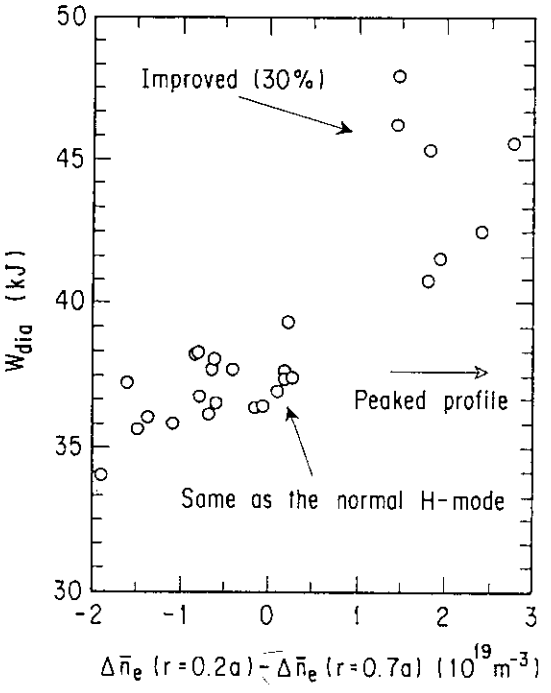

Fig.II.1-9 The peak diamagnetic energy is plotted against [$\Delta\bar{n}_e$(r=0.2a)-$\Delta\bar{n}_e$(r=0.7a)] just after pellets injection.

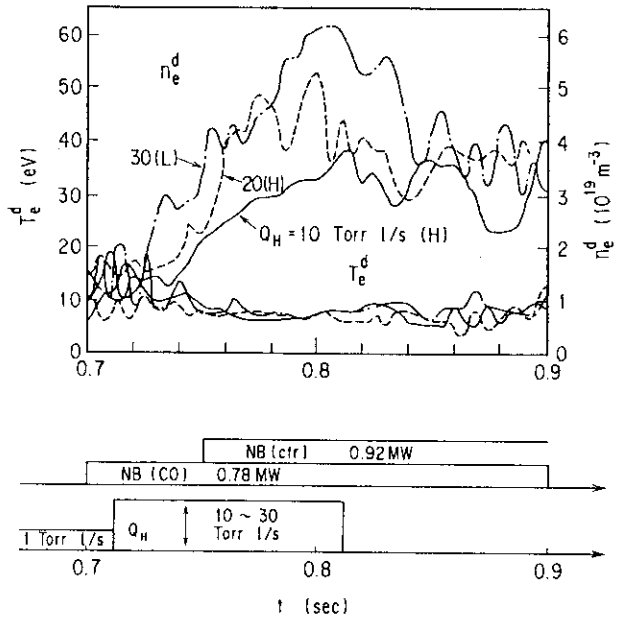

Fig.II.1-10 The dependence of gas-feed rate during 1.7 MW neutral-beam heating, Q_H, on the formation of dense and cold divertor plasma. Discharges got into the H-mode are labeled with (H), other with (L).

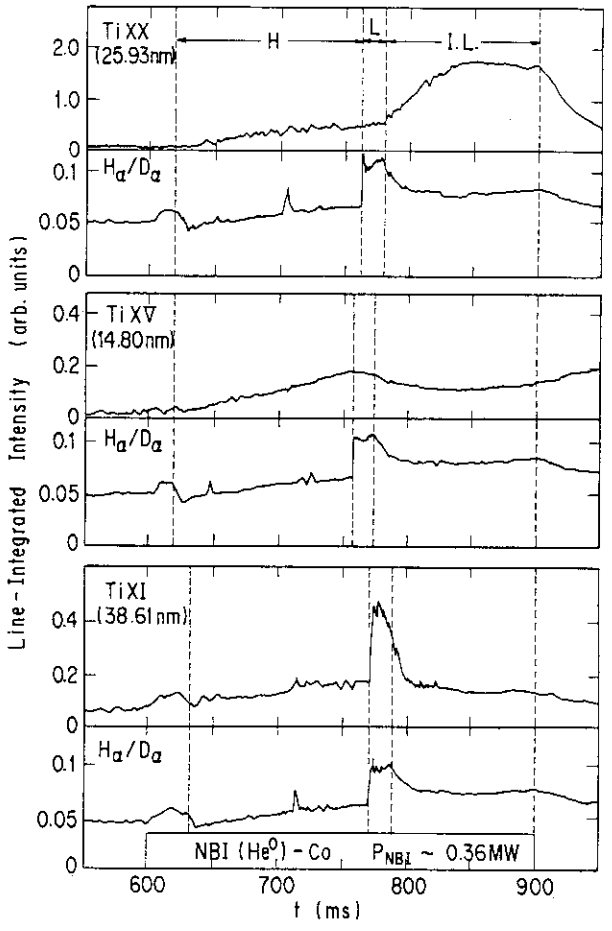

Fig.II.1-11 The typical time evolutions of intensities of the titanium ion lines (TiXX, TiXV and TiXI) in discharges with improved L-mode phase.

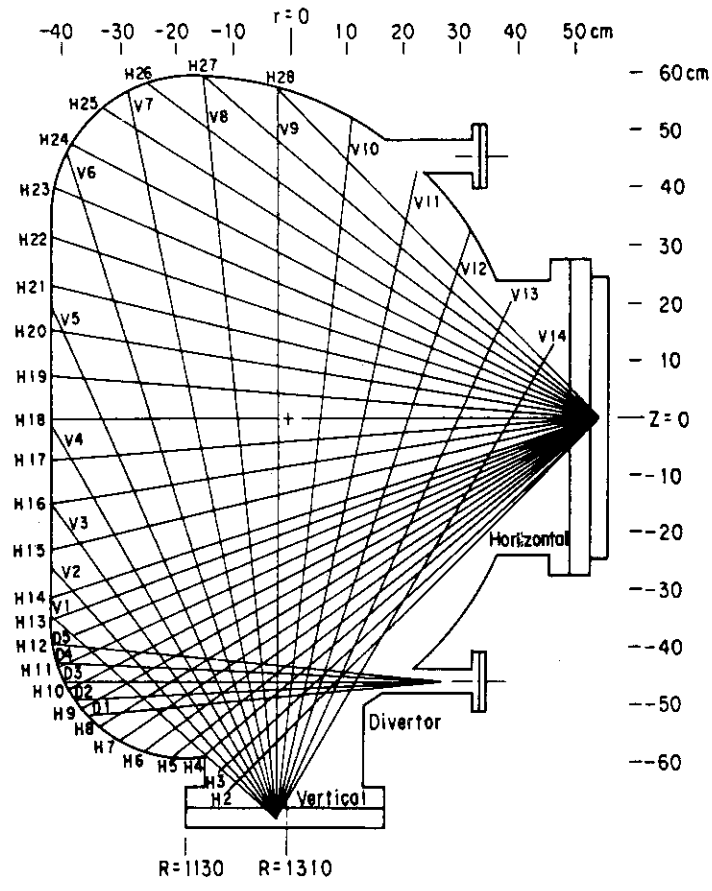

Fig.II.1-12 Viewing chords of bolometer arrays.

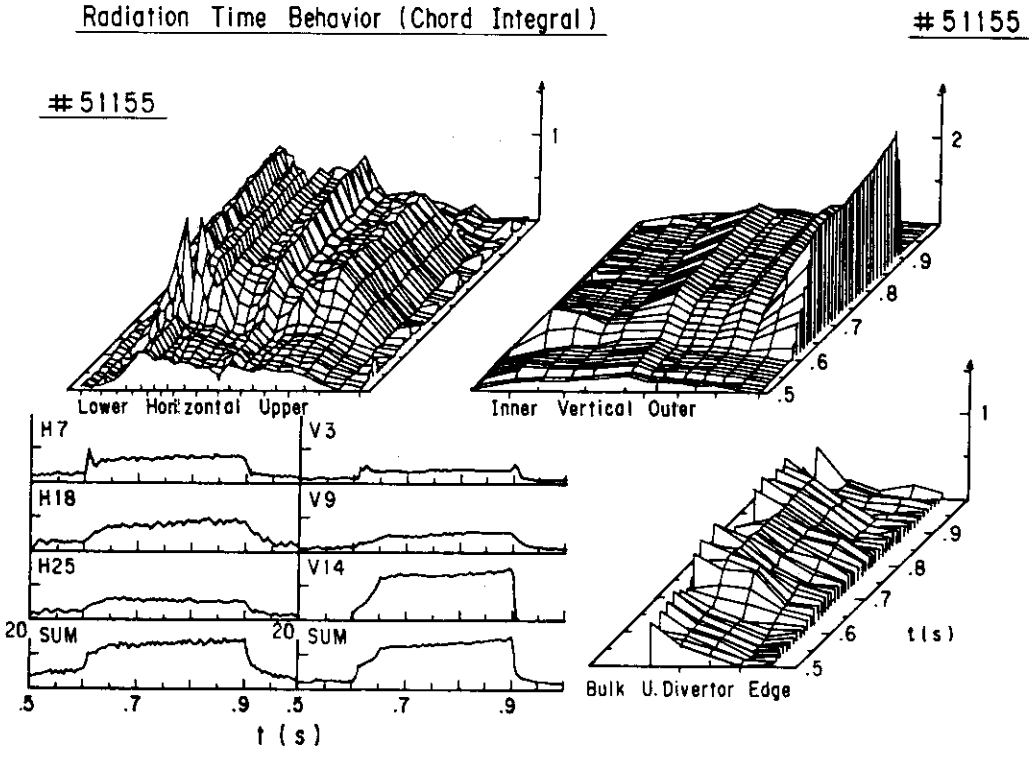

Fig.II.1-13 Temporal behavior of chord integrated radiation profile.

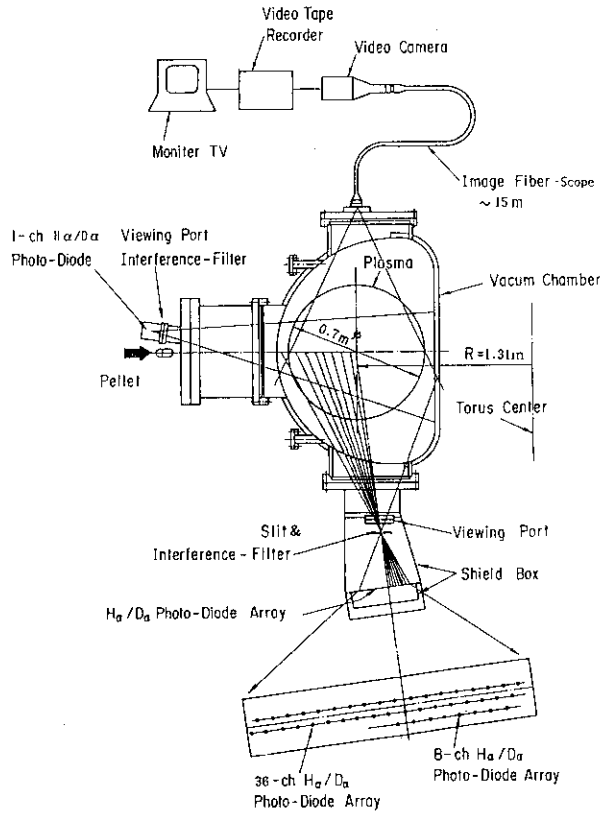

Fig.II.2-1
Schematic diagram of the monitor systems of the pellet ablation, trajectory.

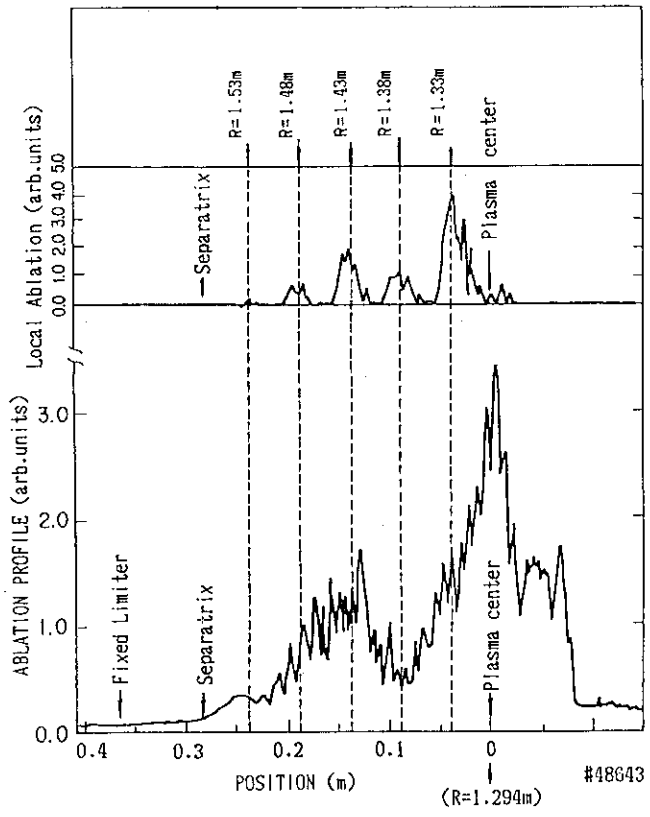

Fig.II.2-2
Lower trace: spatial profile of the pellet ablation measured by 1-ch H_α/D_α photo-diode, upper trace: quantity of local ablation of the deuterium pellet measured by 8-ch H_α/D_α photo-diode array. The pellet velocity measured outside the plasma by the time-of-flight method is about 0.840 km/s.

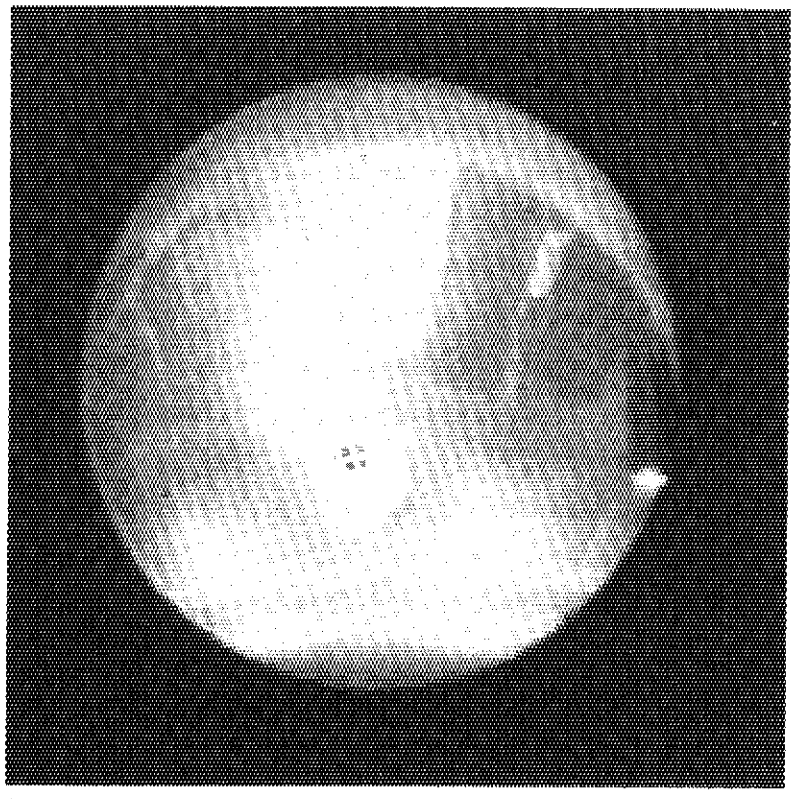

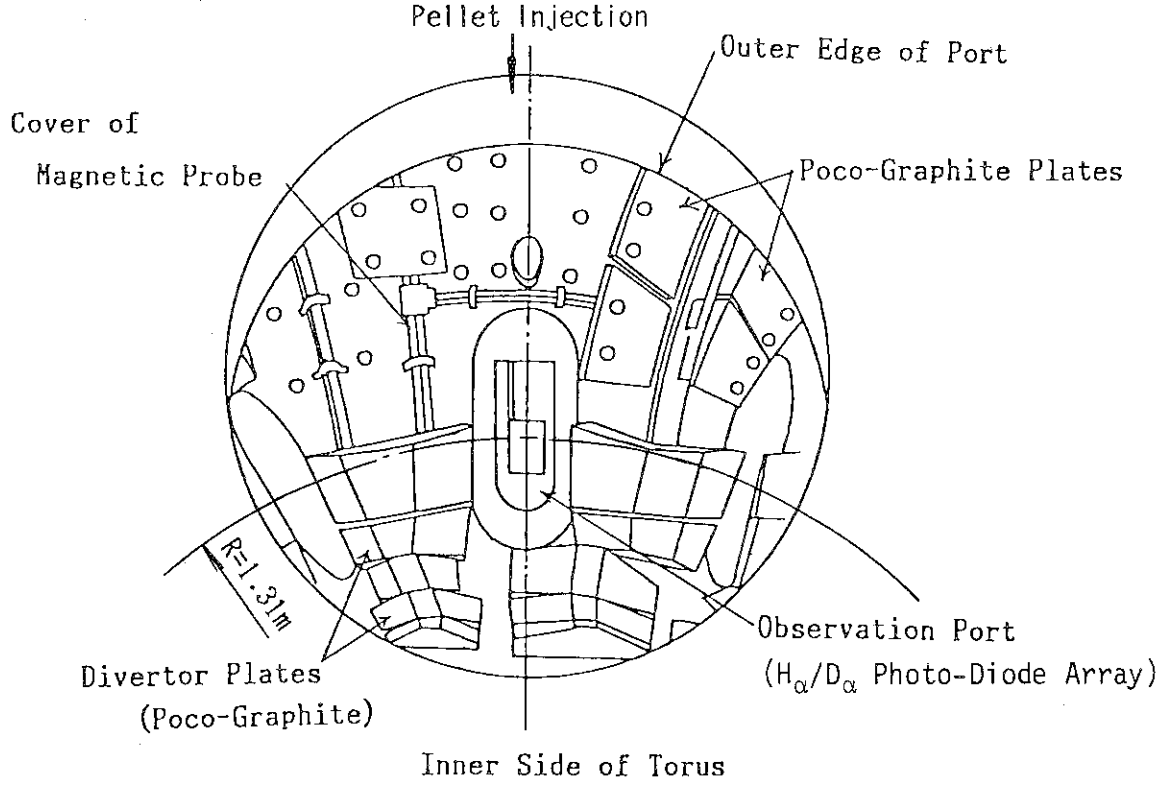

Fig. II.2-3 The trajectories of pellets ablated in the plasma, which were observed by the video camera with image fiber-scope. Lower trace shows the top view of the inside of the vacuum chamber.

III. COOPERATIVE PROGRAM ON TOKAMAK EXPERIMENT

1. DIII-D (Doublet III) Experiment

The U.S./Japan Collaboration in DIII-D continues to be productive and beneficial to both sides. The excellent progress made over the past year which were reported to the world community this fall at the IAEA meeting in Nice, are also contributing to physics R&D activities identified by ITER. The amendment to extend the U.S./Japan Doublet III agreement to August 1992 was signed on March 4, 1988. [The U.S.D.O.E. awarded a five-year contract to General Atomics to continue the operation of the DIII-D Tokamak to November 1993.]

The major accomplishments of the DIII-D program this last year including facility improvements are as follows. A new record beta of 8.0% was obtained with a double null diverted deuterium plasma. Values of beta > 7% were sustained for 0.45 sec. An operational beta limit is found to scale a $\beta(\%) = 3.5\ I(MA)/a(m)B(T)$. As a result of extensive studies on the H-mode, extremely long energy confinement time over 0.3 sec at 2.5 MA H-mode discharges and the sustainment of H-mode discharges for 5 seconds (the duration of neutral beam injection) have been achieved. In an experiment of great significance for next-generation tokamaks, the H-mode both with and without auxiliary heating, has exceeded the saturated ohmic confinement value on DIII-D. DIII-D H-modes have now been achieved also at limiter plasmas. These results, together with earlier NBI and ECH results in divertor configurations, indicate that H-mode is a rather universal confinement regime. A number of diagnostic improvement have occurred this past year. These include a toroidal array of soft X-ray detectors for high beta studies and a UCLA microwave reflectometer for turbulence studies and density measurements. As for the transport analysis, the results show that the improvement in H-mode confinement extends as deep as the half radius, indicating the improvement is more than an edge effect, and that thermal diffusivity decreases at higher plasma current. Neutral beam current drive are now at levels up to 0.5 MA and poloidal betas up to 4.5. Calculations indicate that these experiments are at the entrance to second stability. In May 1988 ten inside launch waveguide systems for ECH heating were tested. Preliminary experiments were carried out, but extensive damage occurred to the waveguides. The problem was identified and corrective measures are underway. On an interim basis, outside launch O-mode experiments have been carried

out, attaining electron temperatures of 5 keV at 1×10^{19} m^{-3}. This last year, an ion Bernstein wave antenna has been installed on DIII-D. And a 2 MW 30-60 MHz RF transmitter was brought into operation. Initial experiments have not indicated central heating. Further experiments and antenna modifications are underway. The installation of a neutron radiation shield around the DIII-D tokamak was completed this year enabling long pulse D-D operations.

The JAERI scientists have continued to make substantial contributions to the productivity and progress of the DIII-D experimental program. Eight JAERI scientists and one engineer were on site at DIII-D since March 1988 with various lengths of stay resulting in 4 full-time equivalents. They worked in the fields of ECH and NBI current drive, stability analysis of ballooning mode, magnetic fluctuation analysis, ECH heating physics and engineering, plasma operations, divertor physics and L-H transition physics. These activities have made significant contributions to the Japanese fusion program. A pioneering work on divertor biasing made by a JAERI scientist with General Atomics collaborators is part of the advanced divertor concept, which is now an important element of the DIII-D program.

During the next calendar year the DIII-D program will give increased emphasis to transport studies at high beta, both with detailed experiments as well as with fluctuation diagnostics. Several new projects are starting in FY89. These include starting a 2 MW 110 GHz ECH system; a fast wave current drive antenna; an advanced divertor program; and a multi pulse Thomson scattering system. Further, a new initiative to begin joint implementation of about 10 MW levels of 110 GHz ECH and 200 MHz ICRF system to emberk on the non-inductive current drive at high β is being proposed.

2. Microwave Tokamak Experiment

2.1 Introduction

The Microwave Tokamak experiment (MTX) has been started at Lawrence Livermore National Laboratory in U.S.A., which heat a plasma using microwave from a free electron laser (FEL). The intense microwave pulses will be injected into the tokamak to establish an application of the free electron laser technology for plasma heating.

Collaboration between JAERI and LLNL under Annex VI to the JAERI-US

out, attaining electron temperatures of 5 keV at 1×10^{19} m^{-3}. This last year, an ion Bernstein wave antenna has been installed on DIII-D. And a 2 MW 30-60 MHz RF transmitter was brought into operation. Initial experiments have not indicated central heating. Further experiments and antenna modifications are underway. The installation of a neutron radiation shield around the DIII-D tokamak was completed this year enabling long pulse D-D operations.

The JAERI scientists have continued to make substantial contributions to the productivity and progress of the DIII-D experimental program. Eight JAERI scientists and one engineer were on site at DIII-D since March 1988 with various lengths of stay resulting in 4 full-time equivalents. They worked in the fields of ECH and NBI current drive, stability analysis of ballooning mode, magnetic fluctuation analysis, ECH heating physics and engineering, plasma operations, divertor physics and L-H transition physics. These activities have made significant contributions to the Japanese fusion program. A pioneering work on divertor biasing made by a JAERI scientist with General Atomics collaborators is part of the advanced divertor concept, which is now an important element of the DIII-D program.

During the next calendar year the DIII-D program will give increased emphasis to transport studies at high beta, both with detailed experiments as well as with fluctuation diagnostics. Several new projects are starting in FY89. These include starting a 2 MW 110 GHz ECH system; a fast wave current drive antenna; an advanced divertor program; and a multi pulse Thomson scattering system. Further, a new initiative to begin joint implementation of about 10 MW levels of 110 GHz ECH and 200 MHz ICRF system to emberk on the non-inductive current drive at high β is being proposed.

2. Microwave Tokamak Experiment

2.1 Introduction

The Microwave Tokamak experiment (MTX) has been started at Lawrence Livermore National Laboratory in U.S.A., which heat a plasma using microwave from a free electron laser (FEL). The intense microwave pulses will be injected into the tokamak to establish an application of the free electron laser technology for plasma heating.

Collaboration between JAERI and LLNL under Annex VI to the JAERI-US

Implementing Arrangement in May 1988. Objectives of this Annex are to conduct and evaluate plasma heating and current drive experiments in MTX and to conduct joint studies of application of FEL microwave technology in follow-on fusion tokamaks to determine the benefits for fusion applications.

The application adds a new tokamak operational regime which could not achieve without FEL including the following:

(1) High power density injection without breakdown from smaller port.
(2) Power deposition profile control using a capability of frequency scan in a short time.
(3) Pulsed power deposition; FEL pulse width, 20-50 ns, is much shorter than electron energy confinement time.

Tokamak operation has begun and target plasmas for 140 GHz signal pulse have been completed. FEL microwave will be injected to MTX this spring.

2.2 Contribution of JAERI

Under this arrangement JAERI has delivered the following equipments during April 1988 to March 1989.

(1) Fast Soft X-ray diagnostic
(2) Neutron diagnostic
(3) Microwave diagnostic box

The fast soft X-ray diagnostic observes electrons which are accelerated by FEL microwave and analyze the energy absorbing filter. In order to follow the FEL pulse whose width is typically 50 ns, very fast response to soft X-ray signal required. Time response reaches now up to 100 ns which is limited by a response of SX detector. We are going to expand the system to multiple spatial and energy channels in Japan fiscal year (JFY) 1989. Neutron diagnostic is consist of two systems, those are fast response and slow response systems. The latter measures an ion temperature in an ohmic and heated plasma. Using BF-3 detector, the time resolution is 10 ms. The former observes an ion response to the FEL pulse, and is required quick response, typically 10 μs. Plastic scintillator is used for the purpose, which has output pulse with 15 ns half width. Microwave Diagnostic Box is installed in an FEL microwave beam line, namely between the last focusing mirror and tokamak port. The box has many small ports seeing a plasma which interact with the FEL microwave. The ports can house several microwave and plasma diag-

nostic to be built partly by JAERI, and partly by LLNL. The box has a diagnostic mirror driving unit and a grid driving unit. A diagnostic mirror is installed on the mirror driving unit which has 3 dimensional adjusting mechanism for aligning the beam to narrow dummy load hole. Grid driving unit is used for alignment of a grid measuring input and reflected power. The dummy load for measurement of absolute power, diagnostic mirror and grid for input and reflected power monitor will be provided in 1989 and 1990 by JAERI. In JFY89, JAERI will also provide three channels of 2nd harmonic ECE heterodyne receivers at separate frequencies around 280 GHz. The following systems are candidates for diagnostics provided by JAERI in the third year of the collaboration; (1) microwave diagnostic component, (2) scattering system based on either FIR or CO_2 laser, (3) rf electric field diagnostic based on Stark coupling to forbidden lines.

IV. JT-60 PROGRAM

1. Overview

Major role of JT-60 is an enhancement of the tokamak plasma performance which is focused on the confinement improvement and exploring the steady state tokamak operation. The experimental program is divided basically into three steps. Advanced Experiment (I), (II) and (III), as shown in Fig.IV.1-1.

The Advanced Experiment (I), the first stage of the advanced experiment has started already in March 1988. After the achievement of the initial JT-60 milestone in October 1987, a new divertor coil was installed to produce divertor plasmas with a lower X-point configuration (R_p ~ 3.1m, a_p ~ 0.7m, κ ~ 1.2) in early 1988. During the shut down period between October and December 1988, new hardwares were installed; they were a new multi-junction type LH launcher for current drive and a new pellet injector with faster velocity pellets.

Experimental emphases on JT-60 in FY 1988 are placed on a) LH current drive characteristics with multi-junction type launcher, b) Confinement study with combination of neutral beam injection, LH current drive and pellet injection. Major experimental results are as follows;

1) The maximum current drive efficiency of 3.4×10^{19} m^{-2} A/W has been achieved with 2.6MW LH injection at 2GHz for discharges with $\bar{n}_e$ ~ 1.5×10^{19} m^{-3} and I_p = 1.74MA.
2) The new multi-junction type launcher provides a sharp $N_{//}$ spectrum with high directivity for $N_{//}$ = 1 ~ 3.4. Low $N_{//}$ (1.3) injection was found to be more effective in order to suppress the sawtooth activity.
3) Improved energy confinement has been obtained with hydrogen pellet injection. Energy confinement time was enhanced up to 40% relative to usual gas fuelled discharges. The discharge has a strongly peaked electron density profile with $n_e(0)/\langle n_e \rangle$ ~ 5 and $n_e(0)$ = 2×10^{20} m^{-3}.
4) A new improved divertor confinement mode IDC (Improved Divertor Confinement) regime have been found.

The future program of JT-60 has been reviewed aiming to advance the Japanese fusion program for the next step ignition device.

1) Advanced Experiment (II)

The second stage of the advanced experiment corresponds to

JT-60 upgrade (JT-60U) program. The design study of this program has already started, in which the vacuum vessel and the poloidal field coil will be replaced completely by the end of 1990 to obtain high current discharges with 6MA in a divertor and 7MA in a limiter configuration (Fig.IV.1-2). Deuterium beams will be injected into deuterium plasmas instead of hydrogen ones in the upgrade experiments. Experiment will start upon the completion of the JT-60U.

2) Advanced Experiment (III)

Development of non-inductive current drive scheme is another important issue of the JT-60 future program, to explore the steady state tokamak operation as well as profile control. In the final stage of the advanced experiment, current build-up and a long pulse operation using current drive will be studied. Physical and technological researches are now going in for a high density current drive system, including negative ion beam injectors and RF system.

2. Operations

2.1 Summary

The operation schedule of the JT-60 in FY 1988 is shown in Fig. IV.2-1. 16-cycle of operations are conducted for advanced experiment after the installation of a new divertor coil and a pellet injector. In November and December, pellet injector had been upgraded on the size and speed. Damaged carbon tiles were replaced by new ones at the same time. For the operation of the new divertor coil the stress of the coil was critical and we operated with care especially after plasma disruption. In this fiscal year, maximum plasma current was 2.9MA and 2.0MA for limiter discharge and divertor discharge, respectively. Main troubles in this fiscal year were as follows. One was leak of cooling water from toroidal field coil at the end of March 1988. Tests of about a month in April were carried out to search the leak position. Another was a break down of the ceramic insulator of LHRF wave guide. We spent five operation days for checking up this trouble. The operation in this fiscal year are summarized in Table IV.2-1. The average number of shots per day by month is shown in Fig.IV.2-2. As shown in this figure, the average number of shots has increased steadily from 1985 to 1988. This result is due to the followings. First, operation time increased from 8:00 - 21:15 to 8:00 - 22:45 from FY 1986. Secondly, daily start up and

JT-60 upgrade (JT-60U) program. The design study of this program has already started, in which the vacuum vessel and the poloidal field coil will be replaced completely by the end of 1990 to obtain high current discharges with 6MA in a divertor and 7MA in a limiter configuration (Fig.IV.1-2). Deuterium beams will be injected into deuterium plasmas instead of hydrogen ones in the upgrade experiments. Experiment will start upon the completion of the JT-60U.

2) Advanced Experiment (III)

Development of non-inductive current drive scheme is another important issue of the JT-60 future program, to explore the steady state tokamak operation as well as profile control. In the final stage of the advanced experiment, current build-up and a long pulse operation using current drive will be studied. Physical and technological researches are now going in for a high density current drive system, including negative ion beam injectors and RF system.

2. Operations

2.1 Summary

The operation schedule of the JT-60 in FY 1988 is shown in Fig. IV.2-1. 16-cycle of operations are conducted for advanced experiment after the installation of a new divertor coil and a pellet injector. In November and December, pellet injector had been upgraded on the size and speed. Damaged carbon tiles were replaced by new ones at the same time. For the operation of the new divertor coil the stress of the coil was critical and we operated with care especially after plasma disruption. In this fiscal year, maximum plasma current was 2.9MA and 2.0MA for limiter discharge and divertor discharge, respectively. Main troubles in this fiscal year were as follows. One was leak of cooling water from toroidal field coil at the end of March 1988. Tests of about a month in April were carried out to search the leak position. Another was a break down of the ceramic insulator of LHRF wave guide. We spent five operation days for checking up this trouble. The operation in this fiscal year are summarized in Table IV.2-1. The average number of shots per day by month is shown in Fig.IV.2-2. As shown in this figure, the average number of shots has increased steadily from 1985 to 1988. This result is due to the followings. First, operation time increased from 8:00 - 21:15 to 8:00 - 22:45 from FY 1986. Secondly, daily start up and

shut-down time was decreased by operational experiences. Thirdly, toubles and time for its repair are greatly reduced by improvement of insulation check system, development of leak test system and improvement of vacuum piping for the vibration caused by electro-magnetic force. The average number of troubles per day were reduced from 4.8 in FY 1987 to 3.3 in FY 1988. In FY 1988, we conducted 2,744 shots. Total discharge number reached 6,691 shots at the end of FY 1988.

2.2 Tokamak

A small amount of water oozed from the pancake winding of the toroidal field coil (TC-5) during the test performance after the installation of the lower divertor coil at the end of March 1988. The inspections were carried out to find the leak channel and the repair work of the brazed joint at the terminal connection of the cooling pipe was finished by the end of May. The leak of water has not been observed to date. The regular inspection of the components and facilities of the tokamak machine was performed from November to December. In the succeeding operation in 1989, the tokamak machine was operated reliably and fulfilled its functions without troubles. The operation of the pellet injection system was started from June and the operational data base was obtained in the initial pellet experiment. The plasma confinement parameters was improved with the pellet-fueled operation. The modification of the pellet injector was carried out during the shutdown from November to December to increase the size and velocity of the pellet. The function of the pressure control was added to the gas injection system to maintain the constant gas pressure in the vacuum chamber during plasma discharges. The observation of the internal components of the vacuum vessel was carried out with a regular interval using the in-vessel inspection system. The damaged first wall tiles were replaced during the shutdown period. The number of the troubles concerning vacuum leak in this FY year was reduced significantly (from 23 to 2), since the gate valve attached to the horizontal ports were removed and the bellows were installed to absorb mechanical shock. In addition, the continuous monitoring of the mass spectrum of the neutral gas in the vacuum vessel was done during operation. The remote leak testing system was used to find the leak around the torus, which served the significant reduction of maintenance work. The low voltage grounding monitoring system was used to check the grounding of the machine

and contributed to the improvement of the operation efficiency. The vacuum leak was observed at the all-metal gate valve of the main pumping system. Stress corrosion cracking was observed at the welded joint between the membrane and the main body of the valve. The same sort of vacuum leak was observed at ten gate valves. The change of the material of the membrane from stainless steel (SUS 304) to Inconel was decided. The repair work is now under way.

2.3 Control system

In April and May 1988, interlock functions have been provided in the JT-60 central control system ZENKEI [1] for protecting the horizontal field coil and the divertor coil from stresses due to electromagnetic force. The interlock functions are optimized with careful analyses [2], which enabled 2MA divertor discharges successfully. Moreover, modification of the control system for the pellet injector was completed in May. The man/machine interface was improved for efficient setting of the preprogrammed waveforms. In the operation of this period, 26 troubles occurred in ZENKEI, corresponds to about 20% of the total number of the troubles in JT-60. Most of the troubles were due to hardware troubles such as CAMAC. Software troubles decreased amazingly due to quality control. ZENKEI is composed of a 7-minicomputer cluster ("HIDIC-80E", Hitachi Ltd.). These computers were originally supposed to be operated under card-base source management ten years ago. To improve the efficiency of making and debugging programs, a new management system with a workstation ("NEWS", SONY Corp.) was built. The scheme and procedure in programming are shown in Fig.IV.2-3. This system is expected to make sure more sophisticated quality assurance of the on-line programs in ZENKEI, because magnetic media such as floppy discs are more reliable than cards.

References

[1] I. Kondo, et al., Fusion Engineering and Design, 5 (1987) 69.
[2] JT-60 Team, JAERI-M 89-033 (1989).

2.4 Power supply system

JT-60 power supplies [1,2] which consist of toroidal field power supply (TFPS), poloidal field power supply (PFPS) and additional heating power supply (H-PS) had been operated on 16 cycle-operations during the

fiscal year 1988. During the period the operation times and troubles in TFPS, PFPS and H-PS were 1591, 1682 and 2055 hours, and 59, 143 and 1 times, respectively. The PFPSs have been remodelled for lower X-point plasmas with an installation of a new thyristor converter (PSEX power supply) and the change of controllers [2,3], and they have been operated successfully.

Some remodellings in the PFPSs have been done to improve the characteristics of JT-60 tokamak plasmas [3]. First, in order to increase the plasma current up to 3.5 MA, the current of F-coils (Ohmic heating coils) delivered by a PSF power supply has been reinforced by stopping the circulation currents between a PSF1 and a PSF2 converters of the PSF power supply by means of changing a DDC (Direct Digital Control) CAMAC controller. Moreover, the PSEX power supply has been connected with the PSF2 converter in parallel. The resultant rate currents of the coils are +92 KA ~ -111.2 kA, and the swingings of the currents correspond to the magnetic flux of 28.5 Volt-sec. Second, in order to reinforce the vertical magnetic field of lower X-point plasmas and also to touch the limiter-plasmas to inner-wall-tiles softly, M1-coils [3] excited by a PSH power supply were connected with a 4.3 mH reactor in series to guard the circuit from over-voltages at the disruptions, and good results as expected were obtained. Annual checks of TFPS, PFPS, H-MG and so on were done in November and December.

References

[1] R. Shimada et al., Fusion Engineering and Design 5(1987) 47.

[2] Annual Report of the Naka Fusion Research Establishment 1988, JAERI-M 88-231.

[3] JT-60 Team, JAERI-M 89-033.

2.5 Neutral beam injection system

The JT-60 neutral beam injection system is originally designed to inject 20MW neutral hydrogen beams at the energy of 75 - 100keV with whole 14 units. Recent JT-60 experiments, however, require a higher beam power rather than a higher beam energy. To increase an acceleration current while keeping an acceleration voltage at a moderate value and thus to increase an injection power, the gap lengths of the acceleration grids were changed. The original first and second gap lengths were 5 mm and 6.5 mm, and now they are 4 mm and 5 mm, respectively. An acceleration

current could be increased from the original standard value 35A to 48A while the acceleration voltage was kept at 75kV. The total injection power increased by 30% and reached 26MW. These high power operations were repeated stably and no defaults were found in the ion sources and the beam lines.

2.6 Radio frequency heating system

Radio frequency heating system in the JT-60 is composed of three units of Lower Hybrid Range of Frequencies (LHRF) heating system with 2 GHz band 24 MW output power and one unit of ion cyclotron range of frequencies (ICRF) heating system with 110 MHz band 6 MW output power[1]. In this period, substantial power of about 11 MW in LHRF and 3 MW in ICRF were injected into plasmas successfully. The aging of the high power amplifier (klystron in LHRF and tetrode in ICRF) could be finished in a relatively quick period, however, the aging of the launcher took much more time. Launcher aging was performed by the rf injection into the vacuum vessel and the TDC (Taylor Discharge Cleaning) plasmas. In ICRF, the launcher baking with 150 degree of centigrade were performed during rf injection. Additional improvements of the aging techniques were performed as follows. The first is the increased notching capability of reflection power in LHRF, and the reflection power limiter and the frequency feed back control to attain good coupling in ICRF. The second is the extension of computer disk for improvement of communication between ZENKEI and data processing, which is planned for the reduction of aging time. The third is concerned with the operational mode which enables many shots in one rf sequence, which is a typical sequence in the rf injection. Furthermore, several fucntions are added to the data processing system. The fourth is concerned with the injection sequence. For the sake of above improvements, the aging period was extremely shorten and the operation became more efficient as shown in Fig.IV.2-4. In LHRF, we have encountered the trouble of the rf leak at waveguide flanges, the deterioration of withstand voltage in the klystron, the breakdown of high voltage cathode cable, the break of detection tool, the break of DC electric isolation and so on. The deterioration of the withstand voltage of klystron was improved by the optimization of electron gun and the high voltage (120 kV DC, 10 min.) spot knocking. The break of DC electric isolation is caused by lack of the choke optimization. In ICRF, we have encountered the trouble of

GCB, the deterioration of withstand voltage in a tetrode, the rf leakage at 131 MHz, the rf breakdown at the dummy load and stub tuner, the break of feed-through to cause vacuum leakage in the JT-60 vacuum vessel. The feed-through was broken due to over energy deposition caused by rf breakdown. However, these troubles can be avoided by performing the fundamental procedure in the rf technology with careful attention.

Reference

[1] T. Nakashima et al., Fusion Eng. & Design 5 (1987) 101.

2.7 Diagnostics system

In the phase of JT-60 shut-down for the installation of a new divertor coil (mid-October 1987 to May 1988), a photo-diode array system (pellet ablation monitor) was newly installed and the charge exchange recombination spectroscopy was improved to measure simultaneously ion temperature at 8 radial points. And several diagnostics apparatuses (Sub-mm and 2-mm interferometers, multipulse Laser scattering, active beam scattering, spectrometers, soft X-ray PHA system, infrared TV and visible TV) and diagnostic support system had been modified for lower X-point divertor experiments. From June 1988 the diagnostic system has been successfully operated and produced large amount of valuable data. And other new diagnostic apparatuses (millimeter wave plasma radar, grating polychromator, Zeeman polarimeter) has been developed. The newly developed ones are described in section IV.4.2. The JT-60 diagnostic system and the status at the end of March 1989 are summarized in Table IV.2-2.

2.8 Auxiliary system

A secondary cooling system, a power distribution system, an emergency power supply system and some utilities [1] have been operated smoothly during the last fiscal year. Annual checks of these systems were performed well as usual year. The operation times and the electric power delivered from these systems were as follows.

(1) Secondary cooling system

Tokamak secondary cooling line :	5649 hours
Power supplies secondary cooling line :	2474 hours
Heating system secondary cooling line :	2620 hours
Auxiliary equipment cooling line :	8157 hours

(2) Power distribution system

11462.2 MWH

(3) Emergency power supply system

6195.6 MWH

Reference

[1] Annual Report of the Naka Fusion Research Establishment 1988, JAERI-M 88-231.

3. Experimental Results

3.1 Lower X-point divertor discharges

Lower X-point divertor configuration has been obtained after reconstructing the poloidal coil system as shown in Fig.IV.3-1. The null point is generated by the divertor coil located below the vacuum vessel, and is stably controlled at a height of < 20 cm. The elongation factor is 1.3 - 1.4. The plasma volume is reduced from ~45 m^{-3} to ~30 m^{-3} compared with old outer X-point divertor plasmas. The maximum plasma current is 2.2 MA, which is limited by the stress of the divertor coil. The vertical positional instability can be well suppressed by introducing a term proportional to the vertical shift of plasma column to the command for the divertor coil. As a result, stable plasma discharges have been obtained up to $n_{index} = -1.99$ (elongation factor of ~ 1.4) [1]. Since there were no magnetic flux loops for plasma position control, we employed a statistical method using only magnetic probes, divertor coil current and plasma current[1,2]. The formulas were derived through regression analysis using an MHD equilibrium database, and were accurate enough to be applicable to the feedback control of non-circular divertor plasmas.

In high power NB heating of lower X-point divertor plasmas, we have obtained two interesting discharge modes, H-mode[1] and IDC-mode[3] (Improved Divertor Confinement). H-mode phases have been obtained in low q discharges of $q < 3.5$ with NB heating power of > 16.5 MW. Figure IV.3-2 shows an example of H-mode discharge. At 5.7 sec, an L-H transition occurs and a quiescent H-mode phase lasts 250 msec. The increment of the stored energy is 160 kJ during the H-mode phase, which corresponds to 8% of improvement in energy confinement time (59 msec -> 63 msec). The increase in stored energy is suppressed due to the occur-

(2) Power distribution system

11462.2 MWH

(3) Emergency power supply system

6195.6 MWH

Reference

[1] Annual Report of the Naka Fusion Research Establishment 1988, JAERI-M 88-231.

3. Experimental Results

3.1 Lower X-point divertor discharges

Lower X-point divertor configuration has been obtained after reconstructing the poloidal coil system as shown in Fig.IV.3-1. The null point is generated by the divertor coil located below the vacuum vessel, and is stably controlled at a height of < 20 cm. The elongation factor is 1.3 - 1.4. The plasma volume is reduced from ~45 m^{-3} to ~30 m^{-3} compared with old outer X-point divertor plasmas. The maximum plasma current is 2.2 MA, which is limited by the stress of the divertor coil. The vertical positional instability can be well suppressed by introducing a term proportional to the vertical shift of plasma column to the command for the divertor coil. As a result, stable plasma discharges have been obtained up to $n_{index} = -1.99$ (elongation factor of ~ 1.4) [1]. Since there were no magnetic flux loops for plasma position control, we employed a statistical method using only magnetic probes, divertor coil current and plasma current[1,2]. The formulas were derived through regression analysis using an MHD equilibrium database, and were accurate enough to be applicable to the feedback control of non-circular divertor plasmas.

In high power NB heating of lower X-point divertor plasmas, we have obtained two interesting discharge modes, H-mode[1] and IDC-mode[3] (Improved Divertor Confinement). H-mode phases have been obtained in low q discharges of $q < 3.5$ with NB heating power of > 16.5 MW. Figure IV.3-2 shows an example of H-mode discharge. At 5.7 sec, an L-H transition occurs and a quiescent H-mode phase lasts 250 msec. The increment of the stored energy is 160 kJ during the H-mode phase, which corresponds to 8% of improvement in energy confinement time (59 msec -> 63 msec). The increase in stored energy is suppressed due to the occur-

rence of grassy ELMs. To improve the energy confinement property of H-mode discharges, attempts were made to reduce particle recycling by the wall conditioning using helium discharges or to heat plasma edge by LHRF power, but were not successful. Other attemps including Ti-gettering will be continued in 1989. The IDC-mode is characterized as high remote radiative cooling in the divertor region and improvement in energy confinement. These properties are very important from a view point of heat control in divertor plasmas. Typical waveforms of an IDC discharge are shown in Fig.IV.3-3. The IDC mode starts at 5.7 sec. The stored energy starts to increase accompanying an increase in electron density. The remote radiative cooling power in the divertor region grows up to 9 MW (about 45% of input power). The heat flux to the divertor plates measured by an IRTV camera decreases due to the remote radiative cooling, which results in the saturation of temperature of the divertor plates at a level of 700°C. The IDC characteristics found so far are; a) There is a threshold in electron density for given heating power, which decreases as the connection length between divertor plates and X-point becomes longer. b) There is also a threshold in NB heating power (about 9 MW). c) Simultaneous decrease in oxygen impurities and increase in carbon impurities plays an important role for an onset of IDC-mode. d) The IDC regime is obtained with the direction of toroidal magnetic field as ion grand B_T-drift is toward the X-point, but not with the reversed direction. e) Energy confinement is improved up to 20%.

References

[1] JT-60 Team, JAERI-M 89-033.

[2] Hosogane N., et al., Nucl. Fusion 26 (1986) 657.

[3] Tsuji S. and JT-60 Team, 12th Intern. Conf. on Plasma Physics and Contr. Nucl. Fusion Research (Nice, 1988), IAEA-CN-50/A-V-1.

3.2 Energy confinement

3.2.1 Global energy confinement scaling study

Figure IV.3-4(a) shows the total stored energy W^* from diamagnetic measurements versus absorbed power P_{abs} for lower X-point discharges. These data seem to obey an offset linear scaling law to fairly low power region (4 ~ 5 times the Joule input). The incremental confinement time τ_E^{inc} is practically independent of the plasma current and has a value

around of 50 msec. A similar for limiter discharges is shown in Fig. IV.3-4(b). Plasma volumes in lower X-point discharges are 20 ~ 40% smaller than that of limiter discharges. The confinement time of limiter discharges increases favorably with plasma current up to 3.1 MA (q_{eff} = 2.2) without any sign of saturation. On the other hands, in diverted discharges, the improvement of τ_E saturates at $I_p \sim 1.8$ MA with lower X-point ($I_p \sim 2.2$ MA with previous outer X-point). These plasma current corresponds to $q_{eff} \sim 3$. The mechanism for this saturation is not yet clear.

As for the dependence of τ_E on the electron density; looking at a time evolution of a single shot, the improvement of τ_E is followed by increasing the electron density, whereas a body of data does not show the explicit density dependence. This difference may be attributed to the way of particle fueling (gas puffing vs. beam fueling).

Size dependence of τ_E shows that a small plasma has poor confinement whereas for a sufficiently large plasma, τ_E is no longer a function of minor radius.

3.2.2 Local energy transport analysis based on ion temperature profiles

Local energy transport analysis has been studied on neutral beam heated plasmas in JT-60, based on the ion temperature profiles measured by the charge exchange recombination spectroscopy. Because of the uncertainty in the data and the paucity of ion temperature profiles, it is difficult to separate the electron and ion heat balances with sufficient accuracy. The effective heat diffusion/conduction coefficients are therefore defined as

$$\chi_{eff}(\rho) = \frac{\frac{3}{2}(T_e\Gamma_e + T_i\Gamma_i) + \frac{1}{\rho < |\rho|^2 >}\int_0^\rho (P_R - P_J - P_{NB})\rho d\rho}{n_e\frac{\partial T_e}{\partial \rho} + n_i\frac{\partial T_i}{\partial \rho}}$$

and $\kappa_{eff}(\rho) = n_e \chi_{eff}(\rho)$.

The heat conduction coefficient represents a weak dependence on a beam heating power such as a power law of $P_{NB}^{0.5}$, although the data points are not large enough. On the other hand, it is found that the effective heat conductivity at a half-radius does not have dependencies on the plasma current. This feature is quite different from the standard L-mode confinement. And also the analysis shows only the explicit density

dependence of the heat diffusivity. The value of heat conductivity is around $1.0 \sim 1.5 \times 10^{20} m^{-1}$ sec^{-1} and is $2 \sim 3$ times as large as the INTOR scaling.

3.2.3 Numerical simulation study by using drift wave turbulence model

Theoretical transport models are examined for two typical shots with limiter and divertor configurations in JT-60. Three models of η_i mode are employed for the test of ion energy transport. Ion temperature profiles are calculated by ion thermal diffusivity models of Lee-Diamond model (T_i^{L-D})[1]. Romanelli model(T_i^R)[2], and Waltz model(T_i^W)[3] for the divertor discharge with high NBI heating power of 14 MW and $I_p = 1.0$ MA. They are in fairly good agreement with experimental data but are rather broader. The broad T_i profiles are results of reduction of χ_i in the outer half region of the plasma, where the temperature is low and the density gradient is large. The theoretical χ_i profiles give underestimated one in the outer region, suggesting that some other mechanisms are required in this region. For simplicity, we add the INTOR type model (χ_i^{INTOR}), which increases the transport in the low density region, to the η_i models. This combined model of χ_i gives the fairly good agreement in the whole plasma region for diverted discharges, although factors of the combination must be properly adjusted. The η_e-model proposed by Guzdar (η_e^G model)[4] is also tested in the electron energy transport for the fixed T_i profile. This model reproduces the electron temperature profile in the limiter and divertor discharges, although it gives the slightly lower electron temperature in the divertor discharge at the plasma center. Simulation results using these models give fairly good agreement with experimental results as shown in Fig.IV.3-5.

3.2.4 Bootstrap current

The neoclassical bootstrap current is calculated directly through the force balance equations between viscous and friction forces according to Hirshman-Sigmar theory[5]. Measured resistive loop voltage is compared with the calculations using the neoclassical resistivity[6] with and without the bootstrap current and the Spitzer resistivity for a wide range of the plasma current ($I_p = 0.5 \sim 2.0$ MA) and the poloidal beta ($\beta_p = 0.1 \sim 2.0$). Figure IV.3-6 shows the comparison of experimental loop voltage with the calculated one using theoretical resistivities. The experimental resistive loop voltage is roughly consistent with the neoclassical one including the bootstrap current, indicating the exis-

tence of both corrections of trapped particles to the electrical resistivity and the bootstrap current. A better analysis of the bootstrap current including the fast ion effect is under development.

References

[1] G.S. Lee, P.H. Diamond, Phys. Fluids, 29 (1986) 3291.
[2] F. Romanelli, JET-P(88) 07.
[3] R.R. Dominguez, R.E. Waltz, Nucl. Fusion, 27 (1987) 65.
[4] P.N. Guzdar et al., Phys. Rev. Lett., 57 (1986) 2818.
[5] S.P. Hirshman, D.J. Sigmar, Nucl. Fusion 21 (1981) 1079.
[6] S.P. Hirshman et al., Nucl. Fusion 17, (1977) 611.

3.3 Pellet injection experiments

A four-barrel pneumatic pellet injector with cylinder-shaped hydrogen pellets (two 2.7 mm and two 3.8 mm pellets, v = 1.6 km/sec) has been installed on JT-60 in March 1988[1], with which improved energy confinement for additionally heated limiter and lower x-point hydrogen discharges was obtained[2-4]. Enhancement in τ_E was up to 40% relative to usual gas fuelled discharges at the medium NB-heating power level of < 15 MW for which the strongly peaked electron density profile with $n_e(0)/\langle n_e \rangle < 5$ and $n_e(0) < 2.0 \times 10^{20} m^{-3}$ was sustained for 0.5 sec following a series of pellets when the stored energy (W^{DIA}) reaches the maximum value. Achieved values of $n_e(0) \times T_e(0) \times \tau_E(a)$ ($< 6.8 \times 10^{19} m^{-3}$ sec keV, $n_e(0) = 1.2 \times 10^{20} m^{-3}$, $\tau_E = 0.2$ sec, $T_e(0) = 2.8$ keV and $P_{abs} = 10$ MW) at $I_p = 2.5$ MA exceeded those previously obtained on JT-60 at $I_p = 3.1$ MA. In 1989, the injector was up-graded to launch larger (3 mm and 4 mm) and faster (< 2.3 km/sec) pellets and the improvable regime was widened to $P_{abs} < 20$ MW. In Fig.IV.3-7, τ_E for the pellet and gas fuelled lower X-point discharges are plotted as a function of the plasma current I_p. The improvement in τ_E for the pellet fuelled 1.8 MA discharges is up to 40% compared to the gas fuelled ones for which the increase in τ_E with I_p is degraded at $q_{eff} < 3$. For the pellet discharges, τ_E increases linearly with I_p even at $q_{eff} < 3$ which is probably due to suppression of the sawtooth activity. Figure IV.3-8 shows the relationship between W^{DIA} and P_{abs} for NB heated 2.1 MA ($q_a \sim 3.4$) and 2.5 MA ($q_a \sim 2.9$) limiter discharges. The pellet data are shown by closed symbols. The increase in W^{DIA} is up to 30% as compared to the base lines of gas fuelled discharges. The enhancement was also observed for pellet injected discharges heated by ICRF or ICRF

+ NBI, for which the improvement was observed only when the ion cyclotron resonant surface was located around the plasma center. Utilizing the highly peaked n_e profile, possibilities of the ion heating with the lower hybrid wave were demonstrated[4].

The improved discharges are characterized by the pressure profile strongly peaked just inside the sawtooth inversion radius[3]. Without the peaking, the confinement can be improved, but the enhancement is smaller (< 20%). The enhanced stage of pellet fuelled plasmas on JT-60 is ended when a large sawtooth recovers or the gradient of the SX emission profile, which is considered to correspond to the pressure profile, reaches a critical value. Figure IV.3-9 shows the dependence of W^{DIA} on the penetration depth from the axis measured with an H_α detector array for 2.1 and 2.5 MA discharges and time evolutions of the SX profiles for the four 2.1 MA discharges. The peaked SX profile corresponding to the distinct improvement in W^{DIA} can be produced only when the pellets penetrate to or beyond the axis. The ablation profiles measured are in good agreement with results calculated based on the Parks-Turnbull's model[4]. The SX profile peaks just inside the sawtooth inversion radius, and the collapse of the peaked portion occurs simultaneously with recovery of the large sawtooth. The improved confinement is observed to be limited by a critical value of the pressure graident. At $P_{abs} > 10$ MW, the gradient is kept almost constant even when P_{abs} is increased.

References

[1] K. Kawasaki, et al., in Proc. 15th Symposium on Fusion Technology (Utrecht, 1988) CO6 and CO7.

[2] R. Yoshino and JT-60 Team, JAERI-M 88-246 (1988).

[3] Y. Kamada, et al., submitted to Nucl. Fusion, see also Y. Kamada, et al., JAERI-M 89-050 (1989).

[4] JT-60 Team, JAERI-M 89-033.

3.4 LHRF experiments

3.4.1 Empirical scaling of LHCD efficiency

Parameter dependence of current drive efficiency in LHCD discharges are investigated with wide parameter $\bar{n}_e = (0.6 - 1.6) \times 10^{19}\ m^{-3}$, $I_p = 0.5 - 1.5$ MA, $B_T = 2.7 - 4.5$ T, $P_{LH} < 2.5$ MW, f = 1.75 and 2.0 GHz, with and without neutral beam (NB) heating ($P_{NB} < 6$ MW), limiter and lower-side single null divertor configurations, and narrow and wide spectra[1].

From the experiments, following evidences were found. 1) The current drive efficiency in the divertor configuration is higher than that in limiter case. 2) The efficiency increases with the electron density. 3) Higher plasma current tends to have a higher efficiency. 4) Combined LHCD and NB heating cases have a higher efficiency. Based on these results, Fig.IV.3-10 shows the empirical scaling of η_{CD} where the horizontal axis is $12 < T_e > / (5 + Z_{eff})$. For the shots where Z_{eff} was not measured, Z_{eff} is estimated from the fitted curve of experimentally obserbed density dependence of Z_{eff}. We assume that Z_{eff} in the limiter case is the same as that in the divertor case. The experimentally observed η_{CD} is fairly well fitted as $12 < T_e > / (5 + Z_{eff})$ for all cases[2]. In conclusion, the empirical scaling $\eta_{CD} \sim 12 < T_e > / (5 + Z_{eff}) \times 10^{19} m^{-2}$ A/W, obtained from JT-60 LHCD data, suggests that higher current drive efficiency can be expected in near future LHCD experiments on high temperature and pure plasmas.

3.4.2 Acceleration of fast ion beam by LH wave

Experiments of ion beam acceleration by LH waves (f = 1.74 HGz) were performed in hydrogen limiter discharges of JT-60 at I_p = 1.5 MA, B_t = 4.5 T. Typical time evolutions of the low power NB ($P_{NB}^{abs} \sim 1.4$ MW) + ($P_{LH} \sim$ 3.4 MW) discharges are shown in Fig.IV.3-11. After LH power injection, NB power was turned on at t = 5.0 s, the stored energy increased largely ($\Delta W^* \sim 220$ kJ) and $\bar{n}_e$ and hard X-ray intensity I_{HX} did not change much. An ion temperature increase by 0.5 ~ 1.0 keV was observed and is the normal or slightly better value of NB heating alone. The τ_E^{INC} due to NB power addition reaches to ~ 110 ms with the correction of the anisotropy of velocity space, which is two and a half times larger than the value of NB alone. It has been observed in the perpendicular charge exchange signal that the fast ions which have more energy than the injected beam energy of NB (E_B = 70 keV) are significantly accelerated by LH wave and the corresponding tail temperature is ~ 60 keV. Decay time of the fast ions at the energy of 84 keV is ~ 190 ms and this value is almost the same as the slowing down time of fast ions at the plasma center. Density dependence of the incremental confinement time has shown that the improvement of τ_E^{INC} is remarkable at lower density than $\bar{n}_e = 2 \times 10^{19} m^{-3}$ in combined NB + LH and the improvement of τ_E^{INC} by ~ 45% at the maximum ($\tau_E^{INC} \sim 73$ ms) is obtained. The accelerated ions are well confined in low density plasmas where the classical slowing down is long.

Therefore, the improved τ_E^{INC} at low density can be explained by the enhancement of the stored energy of the tail ions. It was estimated that the stored energy of the accelerated ion tail is around 79 kJ and the LH power of ~0.56 MW, this is ~16% of the input RF power, is absorbed by beam ions[3].

3.4.3 LH ion heating in pellet fuelled plasmas

Low edge density and high edge temperature are favorable to avoid the occurrence of parametric instabilities at the edge plasma and to heat ions effectively by LH waves. To realize low edge density and high edge temperature at the density regime of $f/f_{LH}(0) \sim 1$, a strongly peaked density profile has been produced by pellet injection for the LH wave heating in JT-60[1]. The wave frequency is set to be 1.74 GHz so that $f \sim f_{LH}$ at $n_e \sim 10^{20}m^{-3}$, $B_T = 4.5$ T in hydrogen plasma. The incremental energy confinement time, the hard X-ray signal and the ion tail temperature suggest that the electron heating by LH occurs in the density regime of $\bar{n}_e < 2.5 \times 10^{19}m^{-3}$ while the ion heating regime is $\bar{n}_e > 4.0 \times 10^{19}m^{-3}$. The incremental energy confinement time of LH waves at $\bar{n}_e > 8.0 \times 10^{19}m^{-3}$ is around 45 - 52 msec, which is almost the same as that of low power NB heating in lower-side X-point divertor discharges.

3.4.4 Current drive experiments by multi-junction launcher

One of three LH launchers in JT-60, which was optimized for heating experiments, has been modified to a multijunction launcher[4]. The new launcher is optimized for current drive experiments and excites waves with the sharp $N_{||}$ spectrum ($\Delta N_{||} \sim 0.5$) and a high directivity (> 80%) for a wide $N_{||}$ range ($N_{||}^{peak} = 1 - 3.4$). Therefore, the high current drive efficiency and a high capability of plasma current profile control can be expected. The phase dependence of the reflection coefficient agree qualitatively with the theoretical prediction and the coupling efficiency of ~90% is obtained. Figure IV.3-12 shows the current drive efficiency η_{CD} as a function of peak $N_{||}$ of excited wave for the hydrogen discharges with $I_p = 1$ MA, $B_T = 4$ T and $\bar{n}_e = (0.8 - 1.3) \times 10^{19}m^{-3}$. Closed and open circles show η_{CD} for the multijunction and the conventional launchers, respectively. For $N_{||}$ more than 1.3, which is very close to the accessibility condition in these parameters, η_{CD} increases with decreasing $N_{||}$. The efficiency η_{CD} for the multijunction launcher is about 1.4 times higher than that for conventional one at low $N_{||}$ regime and high current drive efficiency of $\eta_{CD} = 2.8 \times 10^{19}m^{-2}$ A/W has been ob-

tained. These dependences are well explained by the simple theory[4]. The theory indicates that the improvement of η_{CD} at low $N_{||}$ regime for the multijunction case is due to the sharp spectrum and high directivity. Experiments using the multijunction launcher (the current profile control, the sawtooth stabilization, the current ramp up, the combined heating with LHCD and NB and so on) are in progress.

References

[1] Ushigusa, K., et al., in Plasma Phys. and Contr. Nuclear Fusion Research 1988 (Proc. 12th Int. Conf. Nice, 1988) IAEA-CN-50/E-3-1.

[2] Ushigusa, K., et al., to be published in Nuclear Fusion, 1989, vol.29.

[3] Imai, T., et al., to be submitted in Nuclear Fusion.

[4] Ikeda, Y., et al., to be submitted in Nuclear Fusion.

3.5 ICRF experiments

One of the main objectives of ICRF heating in this period is optimization of the second harmonic ICRF ($2\omega_{cH}$) heating. ICRF power was coupled up to 3.0 MW in the (0,0) phasing mode. Heating characteristics of $2\omega_{cH}$ and H-minority $2\omega_{cH}$ were examined in (0,0) and (π,0) phasing modes [1]. Effective ion heating was observed in both (0,0) and (π,0) phasing modes. In H-minority $2\omega_{cH}$ heating, large sawtooth oscillation in the electron temperature and the ion tail which was further accelerated than in $2\omega_{cH}$ heating were observed in the (0,0) phasing mode. Figure IV.3-13 shows incremental energy confinement time τ_E^{inc}, defined as $\tau_E^{inc} = (\Delta W_s - \Delta W_{OH})/(P_{IC} + \Delta V_L I_P)$ where ΔW_{OH} is the increase in the ohmic stored energy due to the increase in electron density during the ICRF pulse, versus $\bar{n}_e$ obtained in two heating regimes. The data of τ_E^{inc} in $2\omega_{cH}$ heating of the (0,0) phasing mode decreased with $\bar{n}_e$ although the data were scattered from 30 ms to 60 ms. The scattering of the data is due to the difference in the electron stored energy[2], whose reason has not yet been understood. The data of τ_E^{inc} in H-minority $2\omega_{cH}$ were 70 - 80 ms and comparable to those in $2\omega_{cH}$ of the (π,0) phasing mode.

The dependence of τ_E^{inc} on Ip in $2\omega_{cH}$ of the (0,0) phasing mode is shown in Fig.IV.3-14. The data of τ_E^{inc} increased with Ip up to 2 MA ($q_a \approx 3.5$). This result was in contrast with that of the NBI experiments on JT-60 where week dependence on Ip was observed[3]. Lower τ_E^{inc} at Ip = 1 MA seems to be due to the poor ICRF power absorption in the plasma

core because increase in radiation loss during ICRF heating at I_p = 1 MA was much larger than at I_p = 1.5, 2 MA [4]. On the other hand, the data I_p = 2 MA were larger than that of NBI heating by a factor of 1.5. One of the reasons on improved τ_E^{inc} at I_p = 2 MA might be due to efficient ICRF power absorption in the plasma core.

Combination of a centrally-peaked power deposition by ICRF and a centrally-peaked electron density profile by pellet fueling was tried to enhance the energy confinement. Figure IV.3-15 shows the plasma stored energy W^{DIA} against P_{abs} for different heating schemes at I_p = 1.5 MA with and without pellet injection. In any case, τ_E^* was improved with the pellet injection. Especially, the data of ICRF + NBI and NBI alone are improved as well as those at I_p = 2 MA with gas-puffing indicated by the solid line. However, the data were scattered because pellet penetration changed shot by shot. The improvement of τ_E^* for ICRF + NBI is not due to that of τ_E^{inc} which is given by $\Delta W^{DIA}/\Delta P_{abs}$ in the figure but is due to that of τ_E^* of the target ohmic plasma with pellet fueling. For ICRF alone in the (0,0) phasing mode, however, τ_E^{inc} is about 50 ms and seems to be enhanced because τ_E^{inc} of the (0,0) phasing mode decreased with $\bar{n}_e$ as shown in Fig.IV.3-13.

References

[1] T. Fujii, et al., in Proc. of 12th Inter. Conf. on Plasma Physics and Controlled Nuclear Fusion Research, Nice (1988) IAEA-CN-50/E-2-4.

[2] H. Kimura, et al., Section 6.4 of JAERI-M 89-033 (1989).

[3] M. Akiba, et al., to be published in crontrolled Fusion and Plasma Physics.

[4] M. Saigusa, et al., Section 6.1 of JAERI-M 89-033 (1989).

3.6 Other topics

3.6.1 High ion-temperature plasma in JT-60

In June 1988, charge exchange recombination spectroscopy (CXRS) has started ion-temperature measurement[1] and shown that high ion-temperature around 10 keV is obtained by high power NBI heating into low density diverted plasmas (target density $< 1 \times 10^{19} m^{-3}$). Taking into account the Z_{eff} value of ~4 (Discharges with hot carbon wall of 300°C tend to result in high Z_{eff} due to carbon concentration[2]), this can be regarded as the same phenomenon as 'high-Ti mode' previously observed in JT-60 dis-

charges[3], where plasma is limited by TiC-coated molybdenum limiters and high Z_{eff} of 4 - 7 due to oxygen leads to high ion-temperature. In early experiments the duration of high-Ti mode is restricted by short NB-pulse length of < 1 sec[3]. In recent experiments, long-pulse operation of NB has made it possible to study impeding factors for this phenomena, and highly-peaked ion temperature inside q = 1 surface is revealed by CXRS. Some indications of peaked density profile are also obtained. Figure IV.3-16 shows the time evolutions of ion temperature at ~ 0, 0.3a, 0.6a and 0.8a, where 'a' denotes plasma minor radius. NBI is injected during t = 3.5 to 8.2 sec. I_p = 1 MA, B_t = 4.5 T and average n_e (before NB) is $1 \times 10^{19} m^{-3}$. Only the central Ti rises up to 9 keV in the initial phase of NBI, and $T_i(0)$ abruptly decreases at t = 4.8 sec. Even in the peaking phase of T_i, electron temperature profile is rather broad and $T_e(0)$ is about a half of $T_i(0)$. The radius (20 cm), where ion- and electron-temperatures are different is roughly equal to q = 1 surface inferred from the location of m = 1 oscillation observed in PIN signals in the peaking phase. Furthermore, increase in PIN signals inside q = 1 region is recognized irrespective of slight decrease in central T_e, which suggests that electron density (and Z_{eff}) is also peaking. Integration of CXR spectrum (CVI at 5290.5 Å) along wavelength, which is proportional to carbon density, supports this hypothesis.

As shown in Fig.IV.3-16, peaked T_i abruptly crushed into broad profile. This timing is almost simultaneous with the onset of clear sawtooth oscillations. Furthermore, m = 1 oscillation might be partly responsible to low central electron temperature. So the current profile control by varying q(a) or by lower hybrid current drive (LHCD) must be tried for the stabilization of these MHD oscillations as well as the expanding of q < 1 region, to investigate a possibility of better confinement in the central region.

References

[1] Y. Koide, et al., JAERI-M 89-033.

[2] T. Sugie, et al., in IAEA Technical Committee Meeting on Impurity Controll, Naka, Japan, 1989.

[3] N. Hosogane, et al., Nucl. Fusion 28, (1988) 1781.

3.6.2 Measurement of hydrogen beam stopping in a plasma

Evaluation of transmission of a neutral beam in a plasma is of

great importance since multiple collisions such as excitation and the subsequent collisions might enhance stopping cross section of the beams injected into a fusion plasma[1]. In the light of impact of the cross-sectional enhancement due to multistep collisions, it is significant to investigate the enhancement experimentally. This is the prime motive for this subject.

The experiment was carried out measuring the transmission of a 140 keV hydrogen-atomic beam in JT-60 plasmas. From the measurements of Doppler-shifted H_α lines, neutralizing efficiency and beam optics, the fractions of beam energy components were determined: fractions of the first (140 keV), half (70 keV) and third (48 keV) energies were 7%, 32% and 61%, respectively. The transmission was determined from heat loading of a straight-through beam monitor. High density target plasmas were produced by 3 hydrogen pellet injection. Electron line density ($n_e l$) was measured by a mm-wave interferometer for plasmas without pellet injection, and that after pellet injection was determined by numerically integrating a fitted curve for data from Thomson scattering. Error in density measured by Thomson scattering is about 20% at low density of $n_e < 1 \times 10^{13} cm^{-3}$ and less than ±10% at $n_e > 3 \times 10^{13} cm^{-3}$. Effective ionic charge (Z_{eff}) was obtained from bremsstrahlung measurement in visible spectral region (5611 Å). Figure IV.3-17 shows typical radial profiles of electron temperature (T_e), electron density (n_e) and Z_{eff} just after pellet injection. In the central region, the plasma has peaked n_e, flat T_e and Z_{eff} below 2.0.

Figure IV.3-18 shows the experimental results compared to calculations. The data shown by open and closed squares were obtained in Joule-heated plasmas without and with pellet injection, respectively. Error bars of transmission are determined from background noise, temperature rise of the beam monitor due to radiation from the plasma. Central electron temperature (T_{e0}) and Z_{eff} were 1.7 - 2.2 keV and 2.0 - 2.5 at $n_e l \approx (5 - 6) \times 10^{15} cm^{-2}$, and 1.3 keV and 1.8 - 2.0 at $n_e l = 8.6 \times 10^{15} cm^{-2}$, respectively. Crosses stand for transmission calculated from usual cross sections without including multistep collisions. In the calculation, spatial profiles of plasma temperatures, densities and Z_{eff} are given from experimental data. Impurity content is reasonably assumed to be $C^{6+} : O^{8+} = 50\% : 50\%$. As seen in the figure, transmission for the hydrogen beam is smaller than the calculated value from the usual stopping cross sections. A fractional beam stopping increment

(δ), which are defined by $\delta = (\sigma_s - \sigma_s^{(0)})/\sigma_s^{(0)}$ (here σ_s is an experimental stopping cross section and $\sigma_s^{(0)}$ is the cross section not including multistep processes via excited states), was 0.22 ± 0.2 at $\bar{n}_e = (3.1 - 3.5) \times 10^{13}cm^{-3}$ and $Z_{eff} \approx 2.0$, whereas calculation by Boley et al.[1] indicates δ of 0.23 - 0.3 under the present conditions. Their prediction for the beam stopping does not contradict to our experimental result.

Reference

[1] C.D. Boley, et al., Phys. Rev. Lett., 52 (1984) 534.

3.6.3 Acceleration of beam ions accompanying to beam-driven ICRF wave

In the experiment which carried out with $E_b = 60 - 72$ keV in the lower single null divertor configuration, an acceleration of beam ions accompanying beam-driven ICRF wave is observed in CX measurement[1,2]. Production of high energy ion tail during NB injection is detected by analyzers which are viewing plasmas perpendicularly. The responses observed in ion tail can be classified into three cases. The first case is that the tail temperature is decaying just after NB injection. The second one is the growing one, inversely. The third one is that the tail slope is flat just after NB injection and keeps flat until the injection turns off. These responses depend strongly on NB power and B_T as shown in Fig.IV.3-19, but not depend on $\bar{n}_e$, indicating necessary condition for the acceleration as P_{NB} times B_T is greater than 40 MW·T. The acceleration is induced easily with counter-injection rather than co-injection. The ions are accelerated up to 400 keV, however, stored energy measured by the diamagnetic system does not increase clearly. In the discharge accompanied the ion acceleration, excitation of harmonics of ICRF wave from 2 f_{ci} to around 10 f_{ci} are observed. The resonance region of the wave is always in the scrape-off layer at the low magnetic field side of the torus. The relation between wave intensity and the tail temperature is under investigation.

References

[1] K. Kusama, et al., Proc. 15th Eur. conf. on Cont. Fusion and Plasma Physics, Dubrovnik, 1988, 12b(I), EPS (1988) 167.

[2] M. Nemoto, et al., JAERI-M 89-033 215 (1989).

3.6.4 Measurement of power flow to divertor plates by IRTV

A new divertor monitoring system was developed for lower X-point discharges. The system consists of an infrared TV camera and a visible H_α TV camera with identical field of view employing the half mirror which behaves as a mirror for visible wavelength but as a transparency for infrared wavelength. The detector of the IRTV camera is a mercury cadmium telluride mounted on a sapphire substratum and is sensitive to 2 mm to 5 mm. To improve S/N level and time resolution, the IRTV camera is routinely operated in the line scan mode and the temperature data is taken by the data acquisition system controlled by CAMAC and a micro-computer. Heat flux to the divertor is calculated from the history of temperature by applying the Duhamel's theorem to the response of the surface temperature to pulsed heat flux. The radial profile of the power is found to be a function of the plasma density. Figure IV.3-20 shows the profile of the heat flux at the discharges for three cases. As the density increases, the power to the inner leg decreases whereas the power to the outer leg increases. At the highest density regimes shown in the bottom figure, the heat flux to the inner leg is reduced by the radiative cooling of the divertor plasma and broadening of the profile around the inner leg is commonly observed.

4. Related Developments

4.1 RF development

4.1.1 Construction of multi-junction launcher

The JT-60 is the only machine among the four large tokamaks that the LHRF heating is stressed as the first priority of the rf heating. We have already performed 2 MA for 2.5 sec steady current drive and high efficient current drive of $1.7 - 2.8 \times 10^{19} AW^{-1}m^{-2}$ with the conventional 4×8 phased array waveguides launcher. The new multi-junction launcher, originally invented at Grenoble Atomic Energy Institute for PETULA-B tokamak, with the sharp wave spectrum and good directivity to improve the current drive efficiency was installed in the JT-60. Our multi-junction launcher is composed of 4×24 phased array consisted by 8 modules as shown in Fig.IV.4-1. Each waveguide of the conventional launcher was divided into three sections at the top of the launcher in the long length direction to form one module. The geometrical phase shifters with taper type are equipped at the middle position of the

3.6.4 Measurement of power flow to divertor plates by IRTV

A new divertor monitoring system was developed for lower X-point discharges. The system consists of an infrared TV camera and a visible H_α TV camera with identical field of view employing the half mirror which behaves as a mirror for visible wavelength but as a transparency for infrared wavelength. The detector of the IRTV camera is a mercury cadmium telluride mounted on a sapphire substratum and is sensitive to 2 mm to 5 mm. To improve S/N level and time resolution, the IRTV camera is routinely operated in the line scan mode and the temperature data is taken by the data acquisition system controlled by CAMAC and a micro-computer. Heat flux to the divertor is calculated from the history of temperature by applying the Duhamel's theorem to the response of the surface temperature to pulsed heat flux. The radial profile of the power is found to be a function of the plasma density. Figure IV.3-20 shows the profile of the heat flux at the discharges for three cases. As the density increases, the power to the inner leg decreases whereas the power to the outer leg increases. At the highest density regimes shown in the bottom figure, the heat flux to the inner leg is reduced by the radiative cooling of the divertor plasma and broadening of the profile around the inner leg is commonly observed.

4. Related Developments

4.1 RF development

4.1.1 Construction of multi-junction launcher

The JT-60 is the only machine among the four large tokamaks that the LHRF heating is stressed as the first priority of the rf heating. We have already performed 2 MA for 2.5 sec steady current drive and high efficient current drive of $1.7 - 2.8 \times 10^{19} AW^{-1}m^{-2}$ with the conventional 4×8 phased array waveguides launcher. The new multi-junction launcher, originally invented at Grenoble Atomic Energy Institute for PETULA-B tokamak, with the sharp wave spectrum and good directivity to improve the current drive efficiency was installed in the JT-60. Our multi-junction launcher is composed of 4×24 phased array consisted by 8 modules as shown in Fig.IV.4-1. Each waveguide of the conventional launcher was divided into three sections at the top of the launcher in the long length direction to form one module. The geometrical phase shifters with taper type are equipped at the middle position of the

launcher, whereas we have used the variable phase shifters in the conventional launcher. The part of the waveguide piece at the electron cyclotron region due to the leakage of the poloidal field with 2 GHz was carbon coated to get a low secondary electron emission rate and copper was plated inside the waveguide. The most difficult technology during manufacturing the launcher was reduction of deformation due to the welding and the copper plating inside waveguides. The phase difference between adjacent waveguide is set 70 degrees at 2 GHz. Directivity of the multi-junction launcher was improved by 50% compared with the conventional one. By introducing the new multi-junction launcher, we got successful and splended LHCD results on the driving efficiency, the profile control with various refractive index in the toroidal direction (N parallel), the suppression of the instability and so on. The driving efficiency was further enlarged up to $3.4 \times 10^{19} AW^{-1}m^{-2}$.

4.1.2 Performance of high power test of X-2242 tetrode

High power test of X-2242 tetrode was performed for application in CIT and for potential use of JT-60U ICRF program, which is one of the US-Japan exchange programs. The output power of the conventional 8973 tetrode is 750 kW in maximum. New type Varian X-2242 tetrode has been manufactured to increase the output power. This tube has been already used in Doublet III-D in General Atomics for application of Ion Bernstein Wave heating at relatively low frequency (30 - 60 MHz), however, operation at higher frequency like the JT-60 has not experienced. The power test at a higher frequency may be difficult to be performed because the rf loss in the grid is proportional to $f^{2.5}$, where f is the frequency. The material of the grid in 8973 is molibdenum, in which the allowance of the grid dissipation is only 7.5 kW in maximum. In X-2242, the grid material was changed into pyrolitic graphite having excellent thermal and mechanical capability and grids were manufactured by using laser cutting technique. The allowance of grid dissipation increased up to 25 kW in X-2242. We improved some parts of power supply for this test. The output cavity was also doubled for this test. Power test was performed using Spinnar dummy load. The value of load VSWR is from 1.5 to 2.0 during the test and all phases were studied. We have achieved the output power of 1.6 MW, 0.5 sec with 131 MHz, 1.0 MW, 10 sec with 131 MHz and 1.5 MW, 6 sec with 110 MHz. An unexpected results during test was the reverse current in the screen grid. Usually, the screen current

of about 5 A is kept constant, however, when the rf output becomes large and/or the pulse duration is enlarged the screen current decreases to pass zero and follows in the opposite direction. The test will be carried out with new X-2242 improved screen current and anode dissipation.

4.2 Diagnostics developments

4.2.1 20-channel grating polychromator diagnostic system

The grating polychromator utilizes the cross Czerny-Turner type of grating having the advantage of avoiding stray light pickup as compared with the original Czerny-Turner type. A schematic view of the grating polychromator is illustrated in Fig.IV.4-2. A uniqueness of the instrument is to adopt the grating plates grooved in both faces so that each plate can be applied over a wide range of the toroidal field maintaining high grating efficiency more than 70% without change of the plate. The grating efficiency has been surveyed in detail using a grating diffraction code[1,2] for both cases of the electric vector of incident light perpendicular and parallel to the grooves. The grating instrument has been tested using a monochromatic microwave source; the insertion loss is 6 dB, the resolving power, $\lambda/\Delta\lambda$, is 130 ($\Delta R \sim 2.3$ cm) and the grating efficiency is 0.87 (0.91 from calculation) for the use of the d = 2 mm grating at 255 GHz. As for the transmission line, S-band waveguides (WRJ-3) are installed to transport light from the plasma to the grating instrument over the length of ~ 43 m, in which a horn antenna is installed with the viewing sightline of 46.7° to the equatorial plane. Using the microwave source, total transmission losses are also evaluated to be 10.6 dB at 230 GHz, which is compared with a theoretically calculated value of 6.7 dB. A preliminary ECE measurement has been made for the plasma heated by neutral beam injection. The emissions from the plasma is detected by one channel liquid-helium-cooled indium antimonide (InSb) hot electron bolometer in a cryostat. Figure IV.4-3 illustrates the waveform of the spectral line emission from the center of the plasma, in which sawtooth oscillations are clearly observed from t = 5.1 s. The following items in the GPS are in progress. 1) Additional port and transmission line; A horn antenna with the viewing sightline of 7.6° with a new waveguide transmission line. 2) 20-channel detectors in a long hold refrigerator. 3) Data acquisition system; The MDR system is responsible for the data acquisition over the discharge duration with a fixed sampling time of 20 μs for the 20-channel signals. On the other

hand, the CAMAC system using LeCroy 6810 waveform recorders is responsible for flexible data acquisition, providing a quick data processing between shots.

References

[1] Y. Okuno and K. Yasuura, IEEE Trans. Antennas Propagat. Vol.AP-30, pp.580 - 578, 1982.

[2] K. Yasuura and K. Okuno, J. Opt. Soc. Am., 72(1982)847.

4.2.2 Thomson scattering diagnostic with double Ruby lasers

The Thomson scattering system in JT-60 was operated using a single ruby laser (5J/0.5 Hz, 10J/0.25 Hz, 20J/Single) since 1986, In addition to that, another ruby laser (10J/0.25 Hz) and a beam combiner using a Faraday rotator were installed in early 1989. This new Thomson scattering system has the following advantages: (1) Time variable double pulse operation with the minimum time difference less than 10 msec enables to measure the transient phenomena such as H-mode transition or pellet injection, (2) Multi pulse operation can provide the profile data of 4 ~ 6 time slices in one discharge, and (3) Two laser systems could work as the backup system of each other. By double pulse operation, for example, it has been found that the increment of electron stored energy in pellet injected plasma is closely related with the rapid recovery of electron temperature.

4.2.3 Millimeter-wave plasma radar system

A broadband reflectometric system (plasma radar) has been developed on the JT-60 tokamak[1]. For a reflectometer the Abel inversion of the phase information is performed along the line of sight, so only a single viewing chord, and no symmetry assumption, is required. From the dispersion relation of the O-mode wave, the phase delay ϕ of a reflected wave is written in the form:

$$\phi = \frac{2\omega(x)}{c} \int_0^x \sqrt{1 - n(x)/n_c}\, dx - \frac{\pi}{2} ,$$

where n_c and $\omega(x)$ are the cutoff density and frequency, respectively. Position of the reflecting layer x can therefore be determined by the following integral equation[2,3]:

$$x = \frac{c}{\pi} \int_0^{w(x)} \frac{d\phi}{d\omega} [\{\omega(x)\}^2 - \omega^2]^{-\frac{1}{2}}\, d\omega .$$

In its final form for the profile determination, the JT-60 reflectometer system will be composed of fast-sweep (> 20 GHz/ms) YIG/BWO oscillators in a frequency range 2 - 75 GHz (correlating to the electron density of $4 \times 10^{16} - 6 \times 10^{19} m^{-3}$). A novel feature of this system is that the group delay [$(\tau = (1/2\pi)(d\phi/d\omega)$] of the propagating wave to the cut-off layer and back is measured continuously[4,5]. After combined into a single X-band waveguide by a multi-octave combiner/separator network, 23 - 75 GHz radiation is launched into JT-60 through Brewster windows. Ridge-type coupler has been designed for the preliminary experiment with Ka/Q-band BWOs, and it will be replaced with a three-guide hybrid[6] for the full-band operation. The transmitting and receiving horn antennae are separated, and the reflected wave is mixed with the local oscillator generated at a directional coupler for the homodyne detection. The homodyne beat frequency is expected to be around 60 kHz. The system also comprises 24 and 34 GHz Gunn oscillators for fixed frequency reflectometry, which provides informations on the fluctuations and movements of the reflecting layer. Gunn oscillators can also be swept in a narrowband (± 500 MHz) frequency to yield the local value of the group delay, which functions as a reconfirmation of the wideband-sweep data. A schematic of the circuitry for the wideband-sweep and fixed frequency reflectometer is depicted in Fig.IV.4-4.

The first results on the density profile with BWOs (23 to 50 GHz) and the result of fluctuation measurements with 24 and 34 GHz Gunn oscillators will be obtained in mid-1989. The fixed-frequency data is sampled in 5 μs and FFT (Fast Fourier Transform) processed to study the correlations with MHD activities. Informations on the particle diffusion, micro-instabilities, and density pulse propagation can also be obtained.

References

[1] T. Fukuda and T. Matoba, Rev. Sci. Instrum. (to be submitted).

[2] R.J. Colchin, ORMAK Technical Memo No. 93(1973).

[3] F. Simonet, EUR-CEA-FC-1225(1984).

[4] A. Prentice, A.E. Costley, et al., Course and Workshop on Basic and Advanced Diagnostic Technique for Fusion Plasmas, Varenna, Italy, EU19797, Vol. 2,451(1986).

[5] R. Lehecka, E.J. Doyle, et al., GA-A19566(1989).

[6] F. Medeiros and N. Williams, Proc. 12th Int. Conf. on IR and MM waves, Florida, USA(1987).

4.2.4 Tangential charge-exchange neutral particle analyzer with wide energy range

In order to study the ion energy distribution of NB and/or RF heated plasmas, a tangential CX neutral particle analyzer has been developed and installed on JT-60. A wide energy range up to 500 keV for H^0 was required for the analyzer from previous experiments, in which beam ions were perpendicularly accelerated by LHRF up to 400 keV[1]. In addition, a size of that had to be compact in order to install in a limited space for a measurement system. The analyzer is E//B type and using of the acceleration method, wide energy range from 1 keV to 500 keV is available to H^0 energy distribution measurement. An arrangement of MCP detectors was modified in limited space for H^0/D^0 or H^0/He^0 energy distributions measurement. The energy resolution was modified from range of 8.8% - 2.6% in previous detectors to that of 6.5% - 2.0% in spite of a compact size analyzer. The sight-line of the analyzer installed on JT-60 makes an angle of 46° to the magnetic axis and 2.5° to the midplane. The analyzer is successfully operated and has been acquiring useful data for tangential ion energy distributions of NB and/or RF heated plasmas.

Reference

[1] JT-60 Team, JAERI-M 87-113 293(1987).

4.2.5 Time resolved observation of ion temperature from active beam scattering method

A rutherford scattering apparatus was developed and has been routinely used to measure the central ion temperature of JT-60 plasmas [1,2,3]. The maximum energy and the drain current are 200 keV and 3.5 A, respectively. The scattering angle was changed from 7° to 5.3° due to the installation of a new divertor coil in the JT-60 tokamak. The time-resolved measurement of the central ion temperature is important. Since June in 1988 the three pulse injection has become available[4]. The repetition period and the pulse length are restricted to 350 msec and 50 msec, respectively. Time-resolved observation of the central ion temperature was performed in a pellet fuelled plasma having the plasma current of 1 MA and the toroidal field of 4 T as shown in Fig.IV.4-5. The hydrogen pellets were injected at 7.0 sec, 7.02 sec and 7.04 sec and the line density increased. Three active beam pulses were injected

at 7.07 sec, 7.42 sec and 7.77 sec, respectively and the time behavior of the total scattered intensities for three pulses are shown. Each energy spectrum accumulated for 40 msec is shown in Fig.IV.4-5 (a)~(c) for the pulses. The central ion temperatures were obtained to be 0.5 keV, 1.9 keV and 1.9 keV from a theoretically fitted curve for the low energy region scattered by protons and the temporal evolution is shown. Ion temperature measured from the energy analysis of the charge-exchanged neutrals, T_i^{CX}, is also presented for a comparison by a solid line in the figure. The figure shows that the central ion temperature returned to that of before the pellet injection for about 0.4 sec together with the density decrease. The ion source is to be improved to water cooled electrodes in order to inject three beam pulses of 100 msec length with a repetition period of 300 msec. The improvement is expected to measure the temporal evolution of the central ion temperature.

References

[1] T. Itoh, et al., JAERI-M 86-114 (1986) (in Japanese).
[2] K. Tobita, et al., Nucl. Fusion 28(1988) 1719.
[3] H. Takeuchi. et al., Rev. Sci. Instrum., 59(1988)1652.
[4] Y. Kusama, JAERI-M 89-033 (1989), p.247.

4.2.6 Pellet ablation monitor

Pellet injected into the plasma ablates and makes neutral cloud in the plasma. Some fractions of the neutral particles are excited by electrons to emit H_α photons. The ratio of the H_α emission to the ionization is approximately constant over the electron energy range of 50 eV to 1 KeV. The ablation profile can be estimated from the H_α emitting profile of the pellet. H_α emission monitor using fiber optics combined with H_α-filtered multichannel photodiodes has been installed. A schematic view of the ablation monitor is shown in Fig.IV.4-6. Two sets of the fiber optics array consisting of 19 channels are inserted into the diagnostics port and view the injection line. One of the arrays is extracted out of the vacuum and focused on the multichannel photodiodes via H_α-band-passing filter in order to measure the pellet velocity and the ablation profile directly. Another array is combined together and connected to the single channel photodiode to measure the time evolution of the total H_α emissivity. Signals are memorized by the high speed transient recorder with the sampling time of 1 μsec. Spatial resolution

is approximately 6 cm at the central channel on the pellet pass. Figure IV.4-7 shows typical ablation profiles converted from the time evolutions of the total H_α emissivity for successfive two pellets with the interval of 50 msec, former is small (D = L = 2.7 mm) and latter is large (D = L = 3.8 mm), into 2.2 MA ohmically heated plasma with limiter configuration. The 1st and 2nd pellets reach to 60 cm and 90 cm from the plasma surface, respectively. Open square represents ablation profiles calculated from Nakamura's[1] models with self-shielding effect, which agree with experimental results.

Reference

[1] Y. Nakamura, et al., Nucl. Fusion 26 (1986) 907.

4.2.7 Spatial resolved hard X-ray measurement

To study the high energy electron behavior in the lower hybrid current drive (LHCD) discharge, four channel hard X-ray (HX) detectors were installed. The detectors were arranged to view the lower half area of JT-60 cross section perpendicularly with about 10 cm spatial resolution. The 2' by 2' NaI(Tl) scintillator and photo-multiplier tube was used as the HX detector with pulse height analysis system was adopted as the data processing system. The measured energy range of this system is about 50 keV to 1 MeV, which is the most interesting energy region of high energy electron in LHCD discharge. To synthesize the energy spectra measured by this and the soft X-ray system using the Ge detector, we can construct the wide range X-ray energy spectrum of about 3 keV to 1 MeV and these energy spectra well reflect the electron energy distribution of both the thermal and high energy tail components. In LHCD discharges, the measured HX energy spectra have the several characteristic features that 1) the critical energy point (where the thermal component shifts to the high energy tail) is about 15 keV and its value is almost independent of the plasma parameters and the radiated RF power spectrum, indicating that the energy of accelerated electrons don't simply correspond to the energy estimated from the RF spectrum. However, 2) as decreasing the refractive index of radiated power spectrum, the measured high energy tail of hard X-ray shifts to higher energy region, and the HX emission profile becomes more peaking, which corresponds to the decreasing of plasma internal inductance with the increasing of the refractive index. 3) The total HX intensity is decreasing with the

refractive index and its feature is the almost same with the efficiency of current drive. To estimate the more detailed electron distribution induced by LHRF, the parallel HX energy spectrum measurement is necessary and the compact new detectors are now being ready for this.

4.2.8 Zeeman polarimeter

The current density distribution j(r) within a tokamak plasma is a quantity of basic primary interest. On another matter, it has been demonstrated in JT-60 that MHD modes can be influenced by use of non-inductive, lower-hybrid current drive (LHCD). However, it is difficult to measure the current profile directory, in general, we could measure the direction of the magnetic field line in a plasma. A diagnostic technique utilized He^0 beam probe[1] is developed in JT-60. The optical system is installed in JT-60 to measure the light of He beam as shown in Fig.IV.4-8. The He light is gathered by condensing lens, and is focused an image of the beam. The light from an image is collimated by second lens. The direction of polarization of this light is rotated 45° by 1/2 λ plate, and the light passed through the wollastone prism is split into two polarized components. Two 1/4 λ plates are to make the polarization light to circularly polarized light. Each component is focused just on the entrance slit of the spectrometer by condensing lens, relay lens, and an image rotator. The transmittance and the resolution of the spectrometer are important, because He light intensity is very weak and the splitting widths of π component and σ components are small. Therefore, the littrow type spectrometers are used. The echelle grating (Bausch & Lomb) is used in this spectrometer. The exit optical system consists of a prism, a pair of lens and a band-pass filter. The free spectral range of this spectrometer is narrow, therefore, the exit optical system has a band-pass filter. The quantum efficiency of the photomultiplier is usually less than 0.25. Therefore, APD is selected, because the quantum efficiency of APD is large than 0.3 at 500 nm and 0.5 at 670 nm. The total transmittance of this optical system is about 0.2. Therefore, if the adjustment of the optical system is good, it is expected that the count efficiency of this system is about 0.06.

Reference

[1] T. Ito et al; JAERI-M 86-114.

4.2.9 Development of transient Mega data storage system

The transient Mega data storage (TMDS) was developed, and installed in diagnostic data processing system in Aug. 1988, as an alternative system of the former mass data recorder (MDR) system, in order to reduce the discharge interval. The TMDS is the data acquisition system with many transient memory modules. Each module can store 4 MB per channel. And one TMDS can include 48 channel modules which correspond to 192 MB data amount at maximum. The data transfer rate is improved from 300 kB/sec of MDR to 600 kB/sec. Figure IV.4-9 shows an examined performance of TMDS data acquisition capability. Further, there are no mechanical process in TMDS, the total waiting time of data acquisition process is drastically shortened from 7 min - 30 sec to 2 min - 40 sec in case of 100 MB data acquisition.

4.3 Development of pellet injector

The results of pellet injection experiments have suggested that improvement of plasma confinement time depends on the penetration depth of the pellet into plasmas and upgrade of JT-60 pellet injector was needed to obtain higher velocity. At the end of 1988 JT-60 pellet injector was upgraded to obtain the injection velocity over 1.9 km/s. Table IV.4-1 summarizes the specifications of the upgraded JT-60 pellet injector together with those of the original. Newly fabricated components were the pellet gun assembly, fast opening magnetic valve (FMV) and so on. For the pneumatic-type pellet injector higher injection velocity can be obtained by the combination or higher pressure and temperature of propellent gas and shorter response time of valve for the propellent gas line. Especially, the shortening of response time of FMV is essential. Newly developed FMV achieved the working period less than 0.5 ms and the pressure response rate up to 200 $kgf/cm^2/ms$. Leak rates of the body and the seat of FMV are less than 1.0×10^{-3} Pam^3/s and 1.0×10^{-6} Pam^3/s, respectively. Specified velocity has been attained by the combination of a shorter response time of the newly developed FMV from 1.1 ms to 0.5 ms and an increased working pressure from 50 kg/cm^2 to 100 kg/cm^2. Upgraded pellet injector can inject, independently, four pellets, two of which are 3.0 mm in diameter $\times$ 3.0 in length and the other two are 4.0 mm in diameter $\times$ 4.0 mm in length. Main results obtained by the performance tests of the improved JT-60 pellet injector are summarized as follows: Maximum pellet velocity is about 2.3 km/s, which is

the record for the pneumatic-type pellet injector. Operation conditions have been established to make the pellet with the fueling efficiency of 60 - 65%. For the purpose of impurity transport study in plasma, injection tests of specially arranged hydrogen pellets with 5% methan content were carried out. And operation conditions have been established to obtain pellet velocity of around 2.1 km/s and fueling efficiency of 56 - 62% under the propellent gas pressure of 100 kgf/cm^2.

4.4 New partial pressure measurement[1]

In order to realize partial pressure measurement near a plasma we analyzed the light from the Penning discharge in a test stand. The followings are found:

(1) Intensity of spectral lines is proportional to the pressure from 10^{-7} to 10^{-3} Torr for H_2 and He, respectively.

(2) In the gas mixture of H_2 and He, intensity of spectral lines for each gas species is proportional to the partial pressure of each gas species and is independent of the partial pressure ratio (see Fig.IV.4-10).

Reference

[1] N. Ogiwara and M. Maeno, Sinku 32 (1989) 292.

4.5 Code development

Computer codes which have been developed in FY '88 are as follows:

1) LOOK/SCOOP non-circular version
   LOOK (a code to reduce diagnostic data into 1-D profile data) and SCOOP (1-D steady-state transport code) which were originally developed to analyze diagnostic data from a circular tokamak, have been extended to analyze them from a non-circular tokamak.
2) 3-D neutral particle analysis code
3) OFMC vector version
   Orbit-following Monte-Carlo codes to analyze slowing-down process of fast ions produced by NBI and suprathermal fusion products have been tuned up for a super computer with vector processors.
4) OFMC-ICRF analysis code
   The effective collision operator of fast ions in the presence of ICRF waves has been analytically derived and is combined with above mentioned OFMC codes.

5) Interactive data acquisition tool; INDAT

INDAT is a utility code to map diagnostic data on magnetic surfaces and to reduce them into one dimensional profile data. A set of run data for SCOOP/OFMC can be interactively generated with INDAT. Profile data treated are as follows;

Electron temperature --- Thomson, ECE, Filter.
Electron density ------- Thomson, FIR.
Ion temperature -------- CXR, including the toroidal rotation velocity.
Effective Z ------------ Visible Bremsstrahlung.
Radiation power -------- Bolometer.

6) Time-slice data editor; SLICE

SLICE is a utility code to edit time-sliced data from experimental wave forms at specified times. Results can be stored in a user data file.

5. JT-60 Upgrade

5.1 Tokamak[1,2]

The JT-60 tokamak is to be modified wherein the original outer-single null plasma containment vacuum vessel and poloidal field coils, will be exchanged with those of large dee-shaped cross sections (Fig. IV.5-1). The basic dimensions of the new vessel will allow plasma of 3.4 m major radius, and a vertical elongation of 1.4 to 1.7, which are shown in Table IV.5-1. Installation of a large vessel is made possible by demounting all poloidal coils at the cost of low toroidal ripple volume they include and high electromagnetic force acting on the poloidal field coils and on the vessel.

The plasma parameters affecting the design of this tokamak were reviewed including plasma current, power supply capacity, disruption time, error field, impurity control, pulse length, and limiter schemes. The dee vessel is structural designed along a new concept of Inconel 625 all welded continuous chamber in a so-called corrugated construction. Rectangular tubes are employed as fixture instead of waved plates used in other design. The three-dimensionally curved continuous vessel has sufficient strength over the plasma disruption of 7 MA during 10 ms.

While the design work started autumn in 1987, it went into detailed design phase from spring in 1988. Specifications were written meanwhile

5) Interactive data acquisition tool; INDAT

INDAT is a utility code to map diagnostic data on magnetic surfaces and to reduce them into one dimensional profile data. A set of run data for SCOOP/OFMC can be interactively generated with INDAT. Profile data treated are as follows;

Electron temperature --- Thomson, ECE, Filter.
Electron density ------- Thomson, FIR.
Ion temperature -------- CXR, including the toroidal rotation velocity.
Effective Z ------------ Visible Bremsstrahlung.
Radiation power -------- Bolometer.

6) Time-slice data editor; SLICE

SLICE is a utility code to edit time-sliced data from experimental wave forms at specified times. Results can be stored in a user data file.

5. JT-60 Upgrade

5.1 Tokamak[1,2]

The JT-60 tokamak is to be modified wherein the original outer-single null plasma containment vacuum vessel and poloidal field coils, will be exchanged with those of large dee-shaped cross sections (Fig. IV.5-1). The basic dimensions of the new vessel will allow plasma of 3.4 m major radius, and a vertical elongation of 1.4 to 1.7, which are shown in Table IV.5-1. Installation of a large vessel is made possible by demounting all poloidal coils at the cost of low toroidal ripple volume they include and high electromagnetic force acting on the poloidal field coils and on the vessel.

The plasma parameters affecting the design of this tokamak were reviewed including plasma current, power supply capacity, disruption time, error field, impurity control, pulse length, and limiter schemes. The dee vessel is structural designed along a new concept of Inconel 625 all welded continuous chamber in a so-called corrugated construction. Rectangular tubes are employed as fixture instead of waved plates used in other design. The three-dimensionally curved continuous vessel has sufficient strength over the plasma disruption of 7 MA during 10 ms.

While the design work started autumn in 1987, it went into detailed design phase from spring in 1988. Specifications were written meanwhile

and a fabrication contract was signed at the end of 1988 (see Fig. IV. 1-1).

References

[1] M. Kikuchi, et al., Proc. 15th Symp. on Fusion Technology, Utrecht (1988).

[2] M. Matsukawa, et al., ibid.

5.2 Plasma control for the JT-60 upgrade

We have been developing a fast data transfer system and an eddy current model for the advanced plasma control system. An algorithm for calculating the controlled state parameters such as plasma position and shape is under development. Signals of flux loops as well as those of Rogowski coils and magnetic probes are used in the calculations. These developments will be applied to the VME multiprocessor system[1].

Recent experiments showed that dead time in a feedback control loop, in addition to eddy currents, is sensitive to stability of horizontal position control for elongated plasmas. The dead time elements inevitably exist in the thyristor converters (0.7 msec) and in the full digital computation for control (2.0 msec) in real time. The latter is decided by the computer speed. To apply recent hardware development to the JT-60 upgrade control system, the first step was performed where the data transfer rate between a VME (Versa Module Europe, IEEE std. P1014/D1.2) system and a CAMAC system was investigated. Using the fastest linkage with a CAMAC branch driver (CBD8210, Creative Electronic Systems) and an auxiliary controller with branch highway port (ACB, Kokusai Electric Corp.), time required for the data transfer in the plasma control can be reduced to less than a tenth of that in the present system.

It is well known that eddy currents play an important role in the plasma equilibrium control. Not only stabilizing effect on the fluctuation of horizontal and vertical position but also behavior of magnetic field penetration to a vacuum vessel should be precisely analysed, and then an eddy current model should be established. For this purpose, three-dimensional electromagnetic analysis about the vacuum vessel of JT-60U has started.

Improvement of the man/machine interface for the operation such as setting the discharge parameters, executing the discharge sequence, monitoring the plant status and discharge result data, etc. is planned

on the basis of the four-year operational experience. The new man/machine interface will be installed on a network system with workstations.

Reference

[1] T. Kimura, et al., Proceedings of the 6th Conference on Real-Time Computer Application in Nuclear, Particle and Plasma Physics (Williamsburgh 1989) to be published.

5.3 Developments in power supplies for JT-60 upgrade

In order to process instructions in the DDC (Direct Digital Control) CAMAC of thyristor controllers more quickly and also to program the software by a high-level language, a new DDC CAMAC system has been developed. Hardware of the system consists of a work station (AS3260) and VME crates with a 32 bit microprocessor (68030) and I/O modules. Works of the work station are processing the information between power supply and ZENKEI[1] during the on-line processing. Works of the VME crates are processing instructions form the ZENKEI and giving orders to phase controllers of thyristors through CAMAC crates at the real-time processing. Designs of the system were investigated and hardware was set.

In JT-60U the duration time of the plasma current is to be longer of 15 seconds, the heat-load of snubber resistors in thyristors increase approximately 50%. As it is hardly used the existing snubber resistors, ceramic resistors (EREMA resistor) have been developed, manufactured and tested, and the results were well.

Reference

[1] I. Kondo, et al., Fusion Engineering and Design, 5 (1987) 69.

5.4 R&D effort of neutral beam system for JT-60 upgrade

The working gas species of the JT-60 neutral beam injection system will also be changed from present hydrogen to deuterium at the start of deuterium operation of JT-60 Upgrade in 1991. Since a beam atomic mass will be doubled and JT-60 Upgrade plasmas will be fatter than the present JT-60 ones, beam penetrations into plasmas might become insufficient. Therefore, a maximum acceleration voltage is planned to increase from the present 100 kV to 120 kV. This voltage is determined as a highest value with minimum modifications in the acceleration power supplies. The main modifications are 1) the addition of capacitors connected to

the present DC filter in series, and 2) the modification of GTO valves used as fast DC switches. The tap of transformers will be changed to get higher output voltage. Prior to this modification, one power supply will be tested soon. Since significant rippling loss of fast ions produced by neutral beams is expected in the case of quasi-perpendicular injection, four out of fourteen units are planned to be modified to inject tangential beams. Each two units will be combined into one newly-designed beam line box but the present almost all beam line elements including ion sources will be re-used. A negative-ion-based neutral beam injection system is proposed as a current driver in higher density plasmas in JT-60 Upgrade. Conceptual designs of beam lines and auxiliary systems are performed. The main parameters of the system are:

Beam Energy	500 keV
Beam Power	5 MW × 2 beam lines
Beam Species	Deuterium or Hydrogen

Figure IV.5-2 is a horizontal view of the proposed negative-ion-based neutral beam injection system. The tank locations of the present quasi-perpendicular and the planned tangential positive-ion-based neutral beam injection systems are also shown.

5.5 RF system for JT-60 upgrade

Three design studies of the rf heating system aiming to the JT-60U have been performed in this period. The first is concerned with the layout of the coupling system in the torus hall, the second the design study of 3.7 GHz LHRF heating system and the third the 105 - 140 GHz Electron Cyclotron Heating system. First phase in the JT-60U, we planned that two units of LHRF lines will be jointed to form one rf injection with horizontal direction and another with an oblique injection. The horizontal launcher will consist of 4 × 4 module multi-junction with four 18 waveguides at the center and eight 12 waveguides at the top, bottom and side. We also expect further power up of klystrons with some improvements. In ICRF, the present antenna will be replaced by two new antennae, which are also 2 × 2 loop array and have larger width (~ 90 cm) to ensure good coupling for (π,0) mode and H mode. The generator output will be increased up to 10 MW by replacing the present 8973 tetrode with X-2242.

5.6 Diagnostic system

On JT-60 upgrade, diagnostic systems will be improved to measure detailed spatial distributions of plasma parameters (electron temperature, electron density, ion temperature, poloidal field, hard X-ray and so on) and to measure velocity distributions of high energy particles. And new diagnostics systems for fusion products will be installed.

The diagnostic systems of JT-60 shown in Table IV.2-2 will be installed on JT-60 upgrade with rearrangement and improvement. For example, the multipulse laser scattering apparatus will be improved to measure detailed spatial distributions of electron temperature and density with TVTS system. And viewing chords of the other diagnostics systems will be changed and increased for detailed spatial distributions. And CO_2 laser interferometer will be newly installed for higher electron density measurement. For the measurement of high energy particles, the energy ranges of neutral particle energy analysers, of which viewing chords are parallel and tangenial to the magnetic field, will be extended up to 1 MeV. And viewing chords of the hard X-ray monitor will be increased for parallel and perpendicular measurements. For the measurements of fusion products, fission chamber, charged particle fusion product monitor and activation foil will be newly installed. And neutron shield will be also installed on some diagnostics systems to protect neutron flux.

Table IV.2-1 Summarized result of the operation in FY 1988

Operation days	133.5 days
Scheduled days for plasma pulses	105.5 days
Average number of shots per day	26.0
Number of troubles	450
Hours of Taylor discharge cleaning	98Hr36min
Pulses of Taylor discharge cleaning	391,170
Commissioning shots	181

Number of shots	2,744
OH shots	642
NB shots	709
RF shots	803
NB+RF shots	532
Sequence stop	45
No plasma	13

Table IV.2-2 Status of the JT-60 diagnostics systems

Diagnostic System	Subsystem	Specification etc.	Status March,1989
A-1 Electron Density Measuring System	a. Sub-mm Wave Interferometer	CO_2 pumped CH_3 OH LASER, 2 chords $\Delta n_e = 1 \times 10^{17}$ m^{-3}	Operational
	b. 2-mm Wave Interferometer	1 cord, $\Delta n_e = 1 \times 10^{16}$ m^{-3}	Operational
	Millimeter Wave Plasma Radar System	$\tilde{n}_e$, n_e (r) $6 \times 10^{18} < n_e < 3 \times 10^{19}$ m^{-3}	Under Installation
A-2 Electron Temperature Measuring System	a. Fourie Transform Spectrometer	Fourier Spectrometer real time FFT, Δt=10-30ms	Operational
	Grating Polychromator Diagnostic System	20 channels, Δt=20μs (typically), $\lambda / \Delta\lambda \sim 100$	Under Adjusting
	c. Multipulse Laser Scattering Apparatus	Multipulse$\geqq$6, double Ruby Lasers ($\Delta t \geqq$10ms), 8 points for minor radius	Operational
A-3 Ion Temperature Measuring System	a. Neutral Particle Energy Analyser Array	45° Deflection Electro-Static Energy Analyser, E=0.1-110keV, 1 viewing chord E//B Type Mass Energy Analyser (H,D,He) E=1-300keV, 1 viewing chord	Operational
	b. Neutral Particle Mass Energy Analyser	E//B Type Mass Energy Analyser (H,D,He) E=0.1-110keV, 1 viewing chord	Operational
	c. Active Beam Scattering Apparatus	H^0 Beam (200keV, 3.5A, Multi-Pulse), E//B Type Mass Energy Analyser, θ=5.3°	Operational
	d. Neutron Detector	NE 213 Liquid Scintillation Neutron Spectrometer, E=1.5-4MeV	Operational
	Tangential CX Neutral Particle Analyzer	E//B Type Mass Energy Analyser (H,D,He) E=1-500keV, 1 viewing chord	Operational

Table IV.2-2 Status of the JT-60 diagnostics systems (continued)

Diagnostic System	Subsystem	Specification etc.	Status March,1989
A-4 Impurity Measuring System	a. Light Impurity Spectrometer	Flat-Field Grazing Incidence Spectrometer λ= 5-1300Å, 4 viewig chords	Operational
	b. Light Impurity Spectrometer (Doppler)	Normal Incidence Vacuum Spectrometer λ= 600-9000Å,	Operational
	c. Heavy Impurity Spectrometer (Doppler)	2.5m Johann Type Crystal Spectrometer, Ti-Kα, Ni-Kα, Kr-Kα	Operational
	d. Spectrometer for Divertor	Flat-Field Grazing Incidence Spectrometer λ= 5-1300Å, 1 viewig chord	Operational
	e. Visible Monochromator	0.5m Visible Monochromator λ=2000-7000Å,	Operational
	f. Grazing Incidence Monochromator	3m Grazing Incidence Monochromator λ=10-1300Å,	Operational
	Charge Exchange Recombination Spectroscopy	Fiber Optics and 0.5m Visible Spectrometer 8 viewing chords for Heating Beam	Operational
	Visible Spectrometer for Divertor	Fiber Optics and 0.5m Visible Spectrometer λ=2000-7000Å,	Operational
	Visible Monochromator for Z_{eff}	Fiber Optics and 0.25m Visible Spectrometer, λ= 5232Å	Operational
	Zeeman Polarimeter	Polarizer and 1.2m Visible Monocromator, (Plasma Current Distribution Measurement)	Under Adjusting
A-5 Radiation Flux Measuring System	a. High Speed Counting PHA	Ge(I) X-ray Spectrometer E=3-110keV, 1 viewing chord	Operational
	b. Hα Monitor	Filter and Photo Diode, 7 viewing chords for Main Plasma and 1 for Divertor	Operational
	b'. Pellet Ablation Monitor	Hα Filter and Multi-channel Photo Diode 7 for Position and 1 for Total	Operational
	c. PIN Diode Arrays	PIN, 62 viewing chords for Main Plasma	Operational
	d. Bolometer Arrays	Au Bolometer, 31 viewing chords for Main Plasma and 1 for Divertor	Operational
	e. HX Monitor	NaI(Tl), 4 viewing chords	Operational
A-6 Peripheral Plasma & Wall Surface Measuring System	a. Infrared TV	CdHgTe Detector, Temperature Distribution of Divertor Plates, T= 400-1500℃	Operational
	b. Visible TV	CCD Camera with Hα Filter	Operational
	c. Electro Magnetic Probes	15 Channel $\tilde{n}_e$ Probes and a B_N Probe with 25kHz Sampling Rate and a Fast $\tilde{n}_e$ Probe with 200kHZ Sampling Rate	Operational
	d. Spectrometer for Periphery	2 Visible Spectrometers and Rotary Mirror λ=2000-7000Å,	Operational
A-7 Data Processing System	CAMAC, Inter-Shot Processor, Real Time Processor, Timing System, Console Desk, Mass Data Recorder		Operational
A-8 Diagnostic Support System	Vacuum System, Vacuum Control System, Power Supply, Compressed Air Supply, Water Supply, Support Structure		Operational

Table IV.4-1 Specification of pellet injection system

	old type	new type
kind of pellet	hydrogen gas (H_2)	
number of pellet	3 shot (guarantee)	4 shot (mark)
pellet shape	column	
pellet size	ϕ2.7 x 2.7 mm x 2 shot ϕ3.8 x 3.8 mm x 2 shot	ϕ3.0 x 3.0 mm x 2 shot ϕ4.0 x 4.0 mm x 2 shot
pellet velocity	1.3 km/s (guarantee) 1.5 km/s (mark)	1.6 km/s (guarantee) 1.9 km/s (mark)
emit interval of pellet	0 ~ 0.2 s (guarantee)	0 ~ 0.4 s (mark)
operation cycle	15 min (guarantee)	12 min (mark)
pressure	0 ~ 50 kgf/cm^2	0 ~ 100 kgf/cm^2
temperature	normal temperature ~ 80 ℃	normal temperature ~ 200 ℃
fast opening magnetic valve	improvement of market elegance	development elegance

Table IV.5-1 JT-60U parameters

Machine Parameters		
Major Radius (R_P)		3.40 m
Minor Radius (a_P)		1.0 m
Elongation (κ)		1.5
Toroidal Field (RBt)		14.4 T·m
Plasma Current (I_P)	Divertor	6 MA
	Limiter	7 MA
Discharge Duration (τ)		15 sec
Discharge Interval (T)		15 min
Flux Swing		61 V·sec
Heating and Current Drive	NBI (P_{NBI})	40 MW
	LHCD (P_{LH})	15 MW
	IC (P_{IC})	10 MW
Pellet Injection (v_P, D_P)		1.9 km, 4 mm$^\phi$

PFC Parameters		
F coil	Flux Swing	42 V·sec
	A·Turns	120kA x 70 Turns
V coil	Flux Swing	19 V·sec
	Vertical Field	0.5 T
	A·Turns	50kA x 78 Turns 60kA x 58 Turns
H coil	Horizontal Field	0.06 T
	A·Turns	30kA x 26 Turns
D coil	Current	110 kA
	Turns	10 Turns
DCW coil	Sector Turns	3 Turns
	No. of Toroidal Sectors	4
	Current	50 kA

Vacuum Vessel Parameters		
Major Radius (R_v)		3.41 m
Inner Vertical Height (ℓ_z)		3.19 m
Inner Radial Width (ℓ_R)		2.32 m
Thickness (D)		40 mm
One Turn Resistance (Ω_V)		0.2 mΩ
Baking Temperature		300 ℃
First Wall Parameters		
Divertor Armor	Heat Load	2kW/cm^2 x 5sec
	Thickness	50 mm
	Cooling	Water
Limiter	Heat Load	300 W/cm^2 x 5sec
	Thickness	40 mm
	Cooling	Gas

CY	1985	1986	1987	1988	1989	1990	1991	1992	1993	1994
OPERATION SCHEDULE										
MAJOR ATTAINMENT	FIRST PLASMA	20MW NBI	$n_e(0)T_E Ti(0)$ $=6\times10^{19}m^{-3}$ sec·keV	Advanced Ex. (1)			Advanced Ex. (2) → JT-60U		Advanced Ex (3)	
DEVICE Divertor	Outside X-point 1.5MA	2MA	2.7MA	Lower X-point 2.2MA			Lower X-point 6MA			
DEVICE Limiter	1.5MA	2MA	3.2MA	3.2 ~ 3.5MA			7MA			
DEVICE Heating	OH	20MW NBI W_S= 2MJ	Ti(0)=11keV W_S = 3MJ P_{LH} =9.5MW P_{IC} = 2MW				NBI 40MW LH 15MW IC 10MW			
DEVICE Current Drive		1.7MA/1.2MW	2MA	2-LHCD System			LHCD 15MW		High Density CD (NBI/LH/IC)	
DEVICE Others	TiC/Mo Limiter Hydrogen			Graphite Limiter Pellet (1.5km) Pellet (1.9km)			•C/C divertor armor •Local Sector Coil (n=2) •Deuterium			

Fig. IV.1-1 Progress in JT-60 experiments and future program

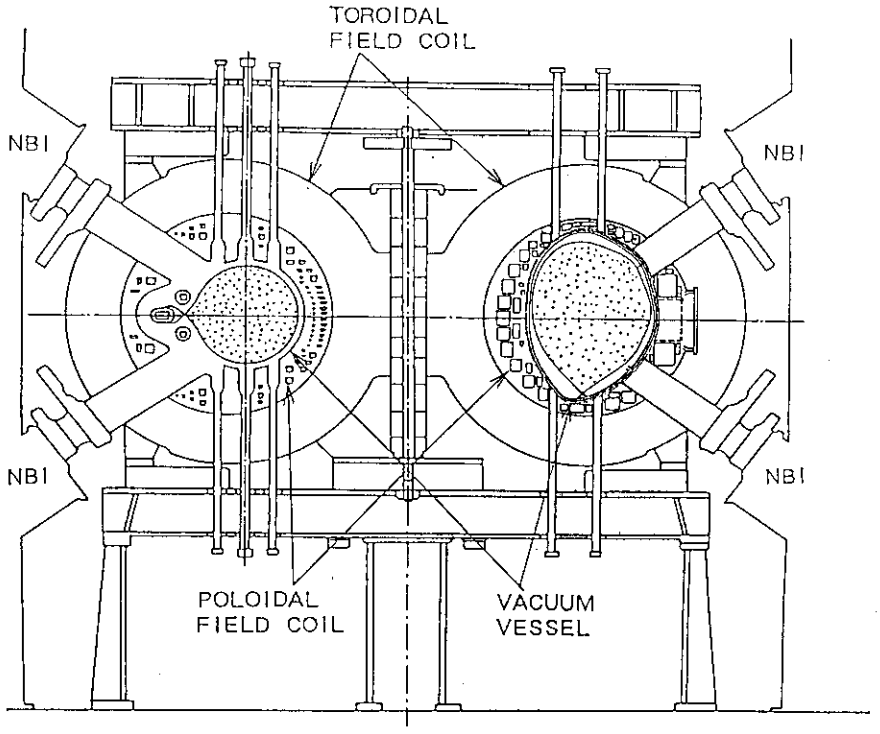

PRESENT DEVICE			UPGRADE DEVICE		
MAJOR RADIUS	3.0	M	MAJOR RADIUS	3.4	M
MINOR RADIUS	0.95	M	MINOR RADIUS	1M×1.5M	
PLASMA CURRENT	2.7	MA	PLASMA CURRENT	6	MA

Fig. IV.1-2 Cross-sectional view of JT-60: Present device (lefthand side) and upgrade one (righthand side)

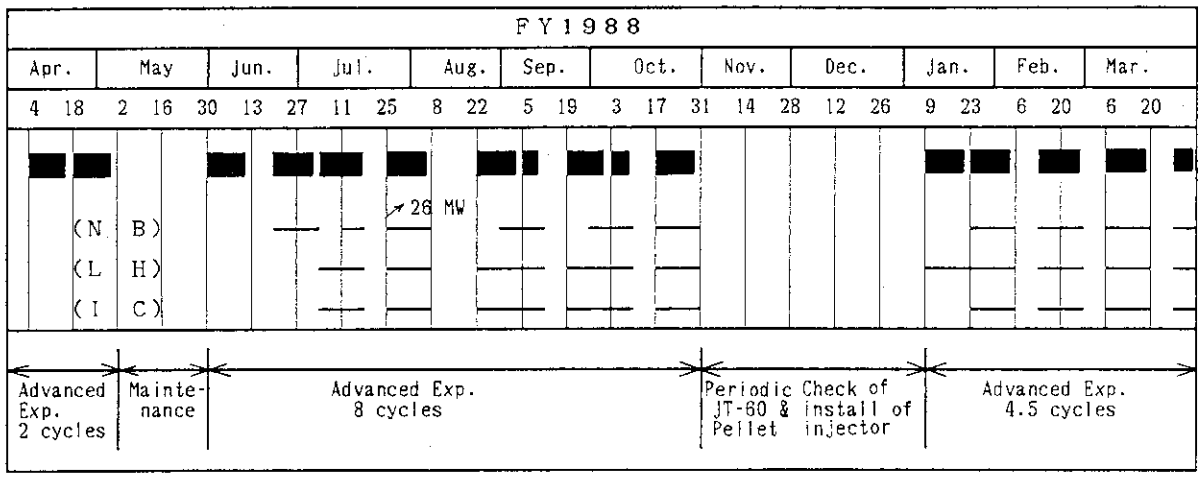

Fig. IV.2-1 JT-60 operation schedule in FY 1988

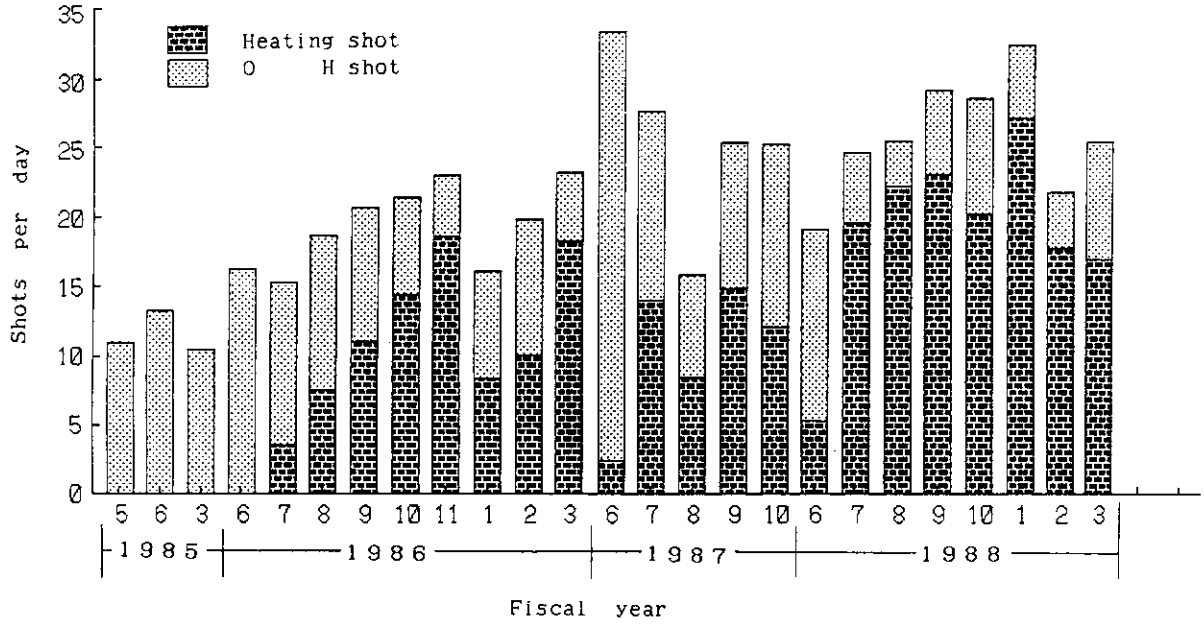

Fig. IV.2-2 Average number of shots per day

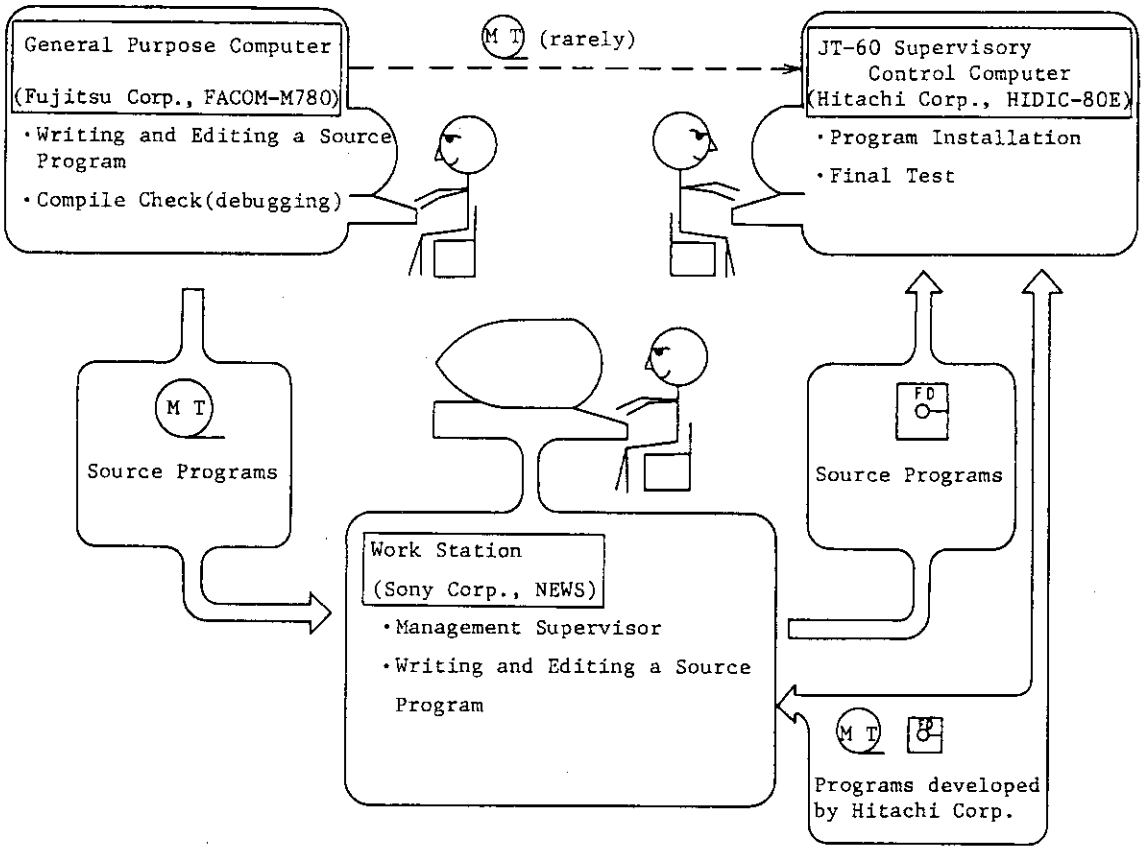

Fig. IV.2-3 Scheme and procedure in developing the ZENKEI computer programs with a new management system

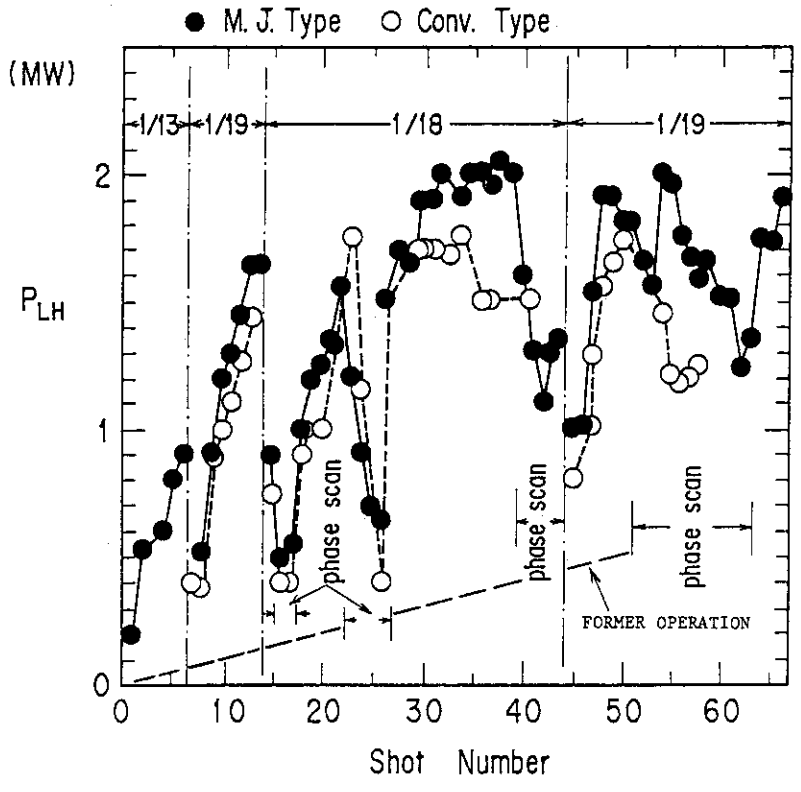

Fig. IV.2-4 Aging history in LHRF conditioning

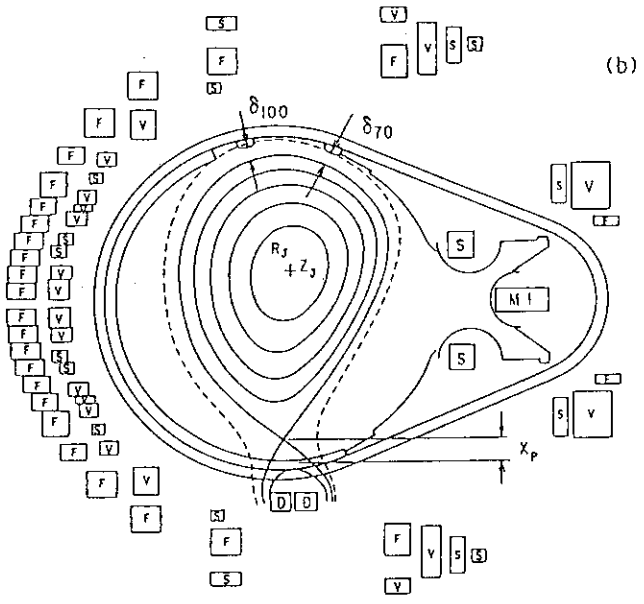

Fig. IV.3-1 Configuration of lower X-point divertor plasma

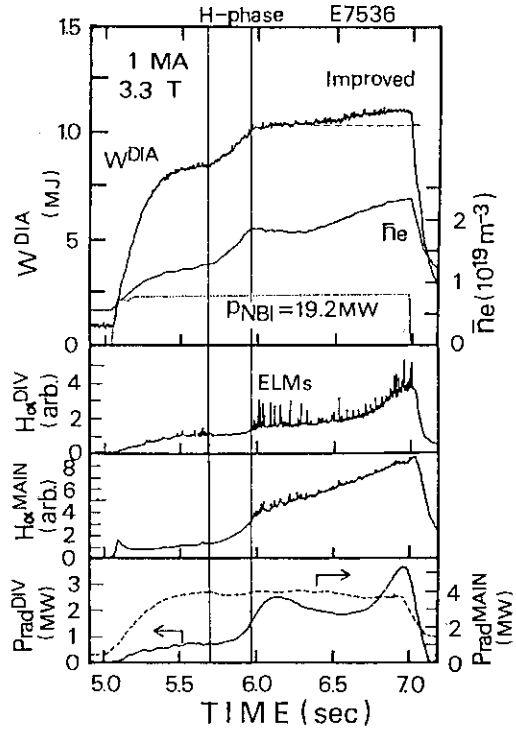

Fig. IV.3-2 Waveforms of an H-mode discharge (shot No.E7536) obtained in lower X-point divertor configuration

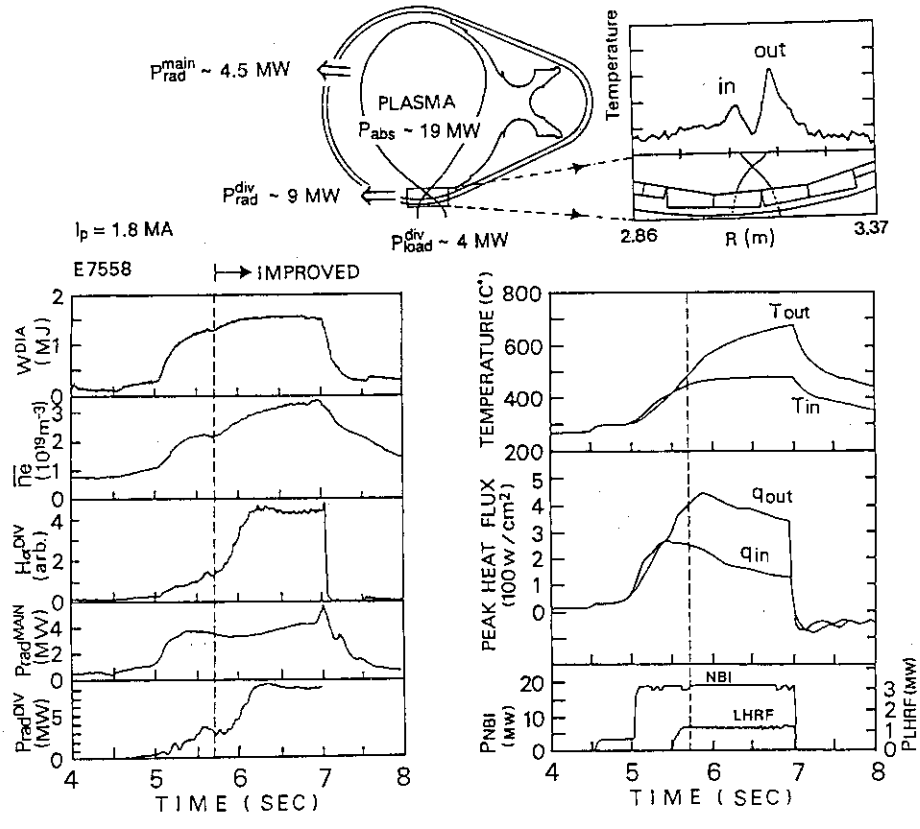

Fig. IV.3-3 Waveforms of a typical IDC discharge and time evolution of the heat flux to the divertor plates and their temperature

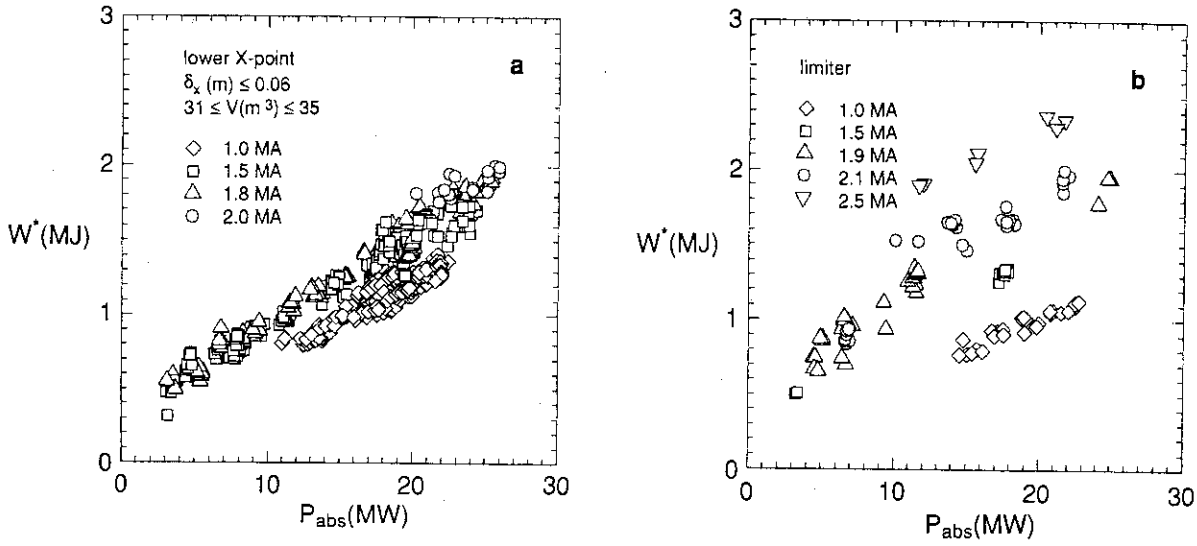

Fig. IV.3-4 Stored energy as a function of absorbed power for lower X-point discharges (a) and for limiter discharges (b)

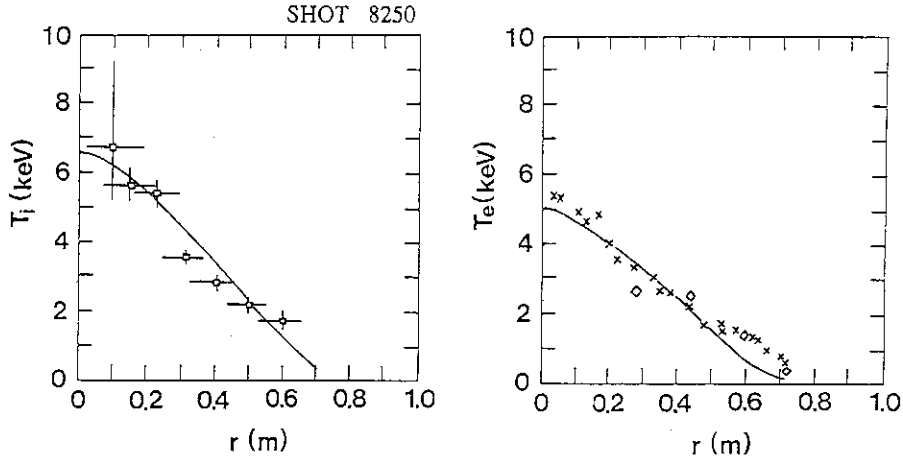

Fig. IV.3-5 Comparison of theoretically evaluated Ti and Te profiles with experimental data for the diverted discharge (Shot No.8250). $\chi_i=0.5\chi_i^{L-D}+\chi_i^{INTOR}$ and $\chi_e=0.5\chi_e^{G}$

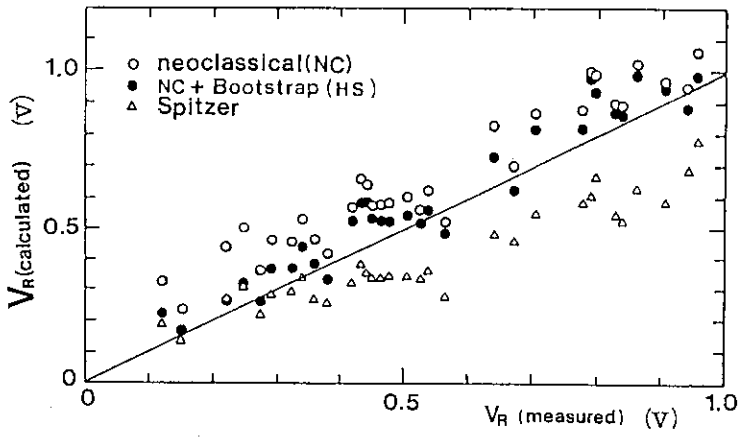

Fig. IV.3-6 Comparison of the measured resistive loop voltage against various calculated resistive loop voltages

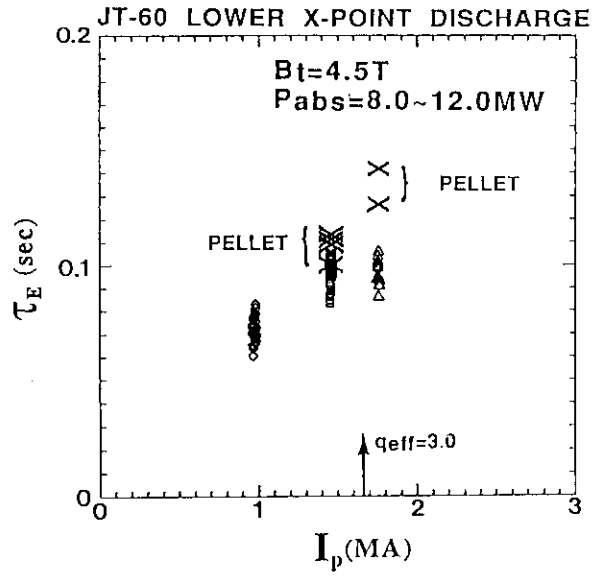

Fig. IV.3-7
τ_E for the pellet and gas fuelled lower x-point discharges with B_t=4.5T are plotted as a function of I_p. The improvement due to the pellet injection is distinct at $q_{eff}<3$.

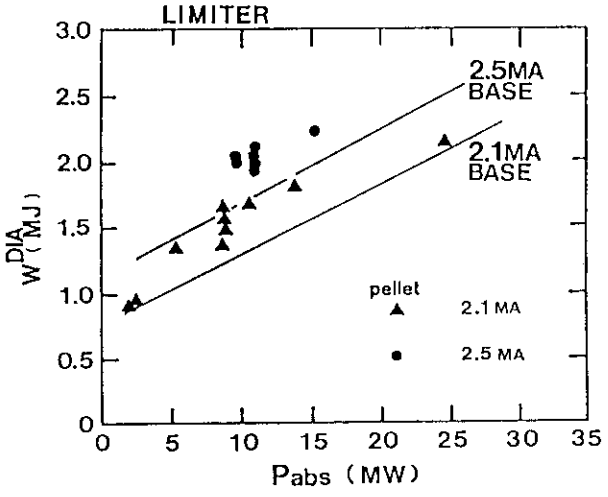

Fig. IV.3-8
The relationship between W^{DIA} and P_{abs} for NB heated limiter discharges. The solid lines correspond to the gas fuelled base lines for which scatter of the data set and the error bar for the measurement are within 80 and 30kJ.

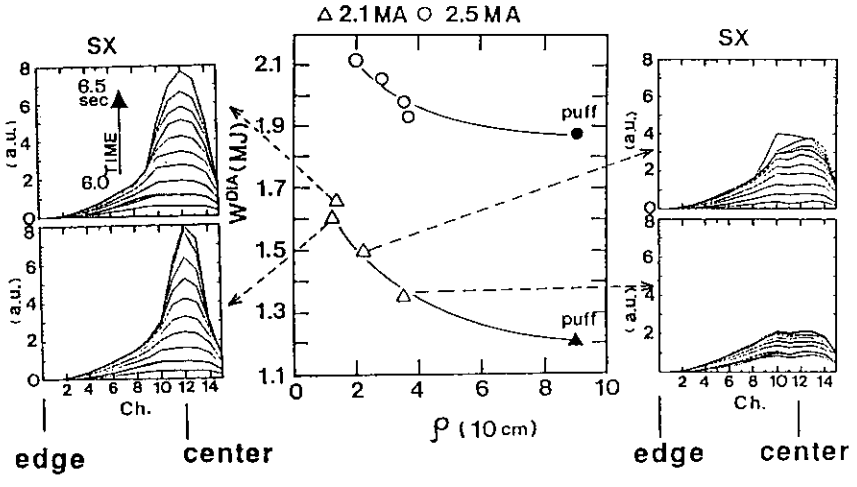

Fig. IV.3-9 Dependence of W^{DIA} on the pellet penetration depth from the magnetic axis. Closed symbols correspond to data for gas fuelled discharges. Time evolutions of the SX profiles for the four 2.1MA pellet injected discharges are also given.

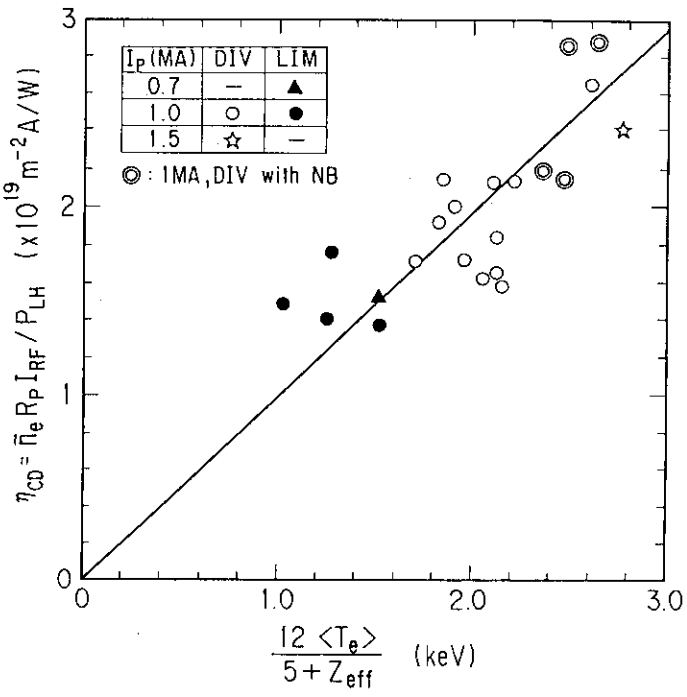

Fig.IV.3-10 The current drive efficiency as a function of $12\langle T_e\rangle/(5+Z_{eff})$.

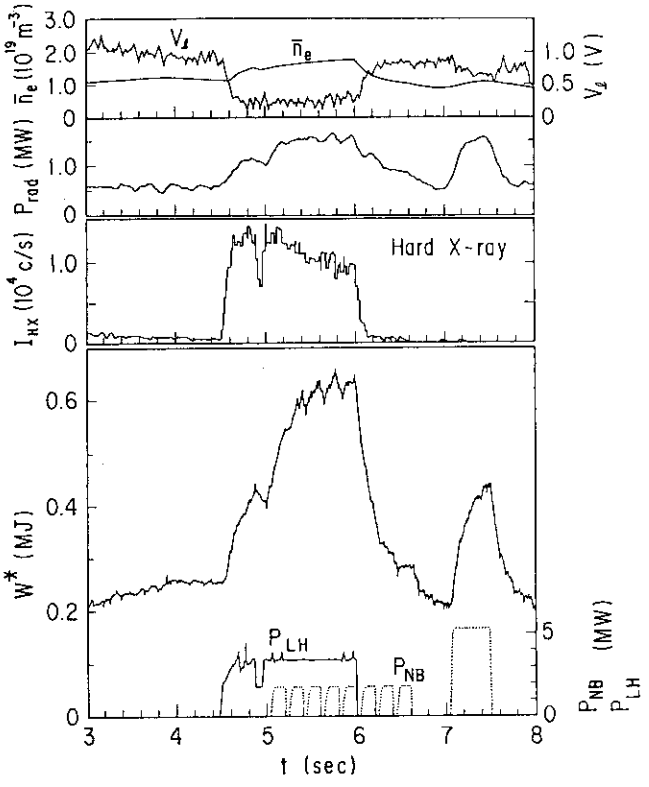

Fig.IV.3-11 Typical time evolution of combined NB+LH discharge. Ip=1.5MA, B_T=4.3T, Limiter.

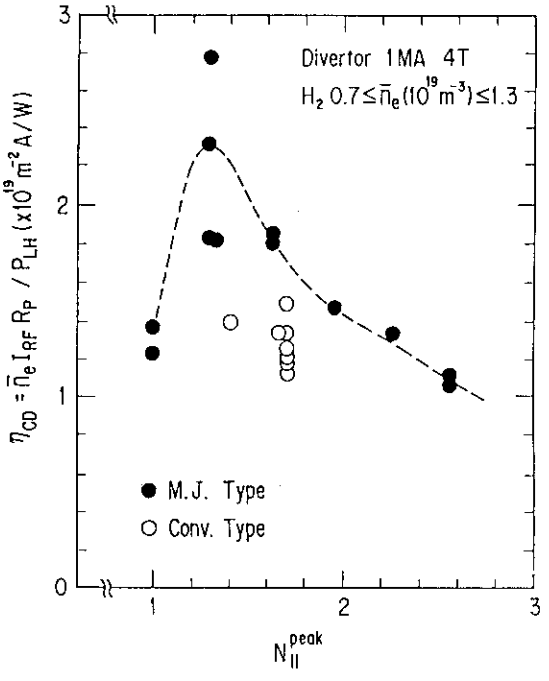

Fig.IV.3-12 The observed current drive efficiency against $N_{\parallel}$.

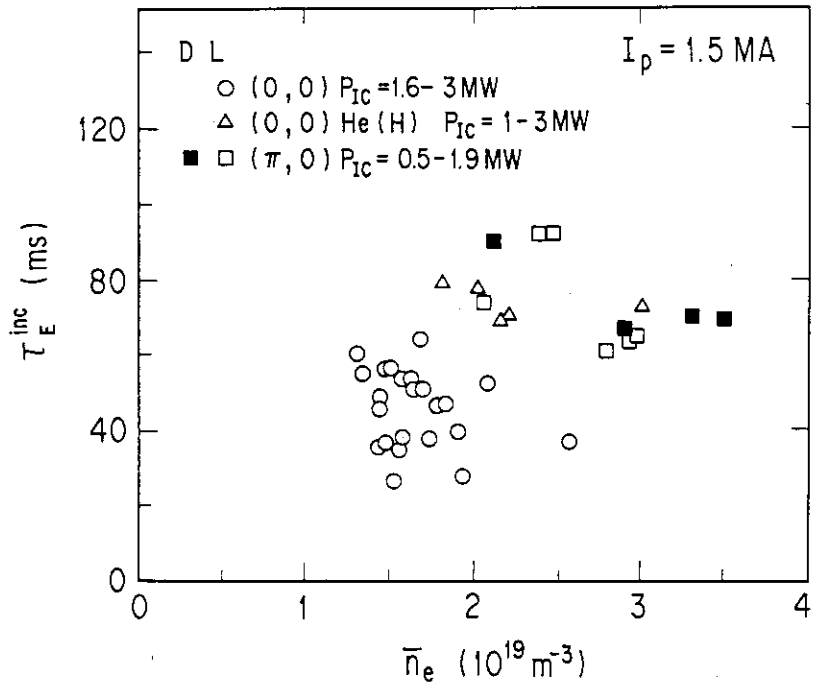

Fig. IV.3-13 Incremental energy confinement time τ_E^{inc} versus $\bar{n}_e$ obtained in $2\omega_{cH}$ and H-minority $2\omega_{cH}$ heating regimes.

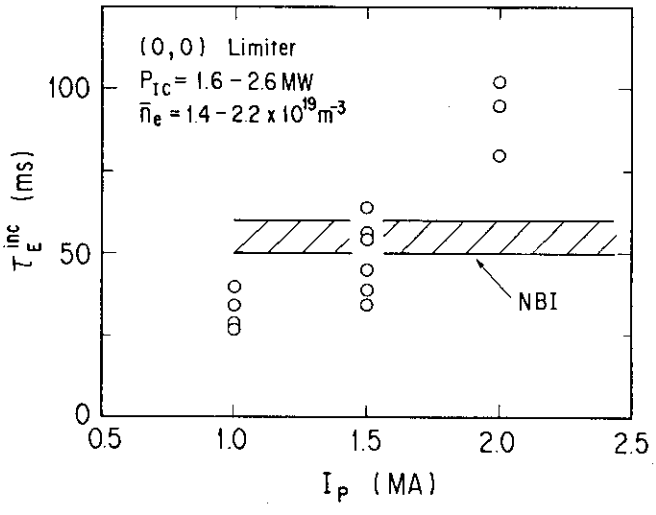

Fig. IV.3-14 I_p dependence of τ_E^{inc} obtained at I_p=1-2MA in $2\omega_{cH}$ heating of the (0,0) phasing mode.

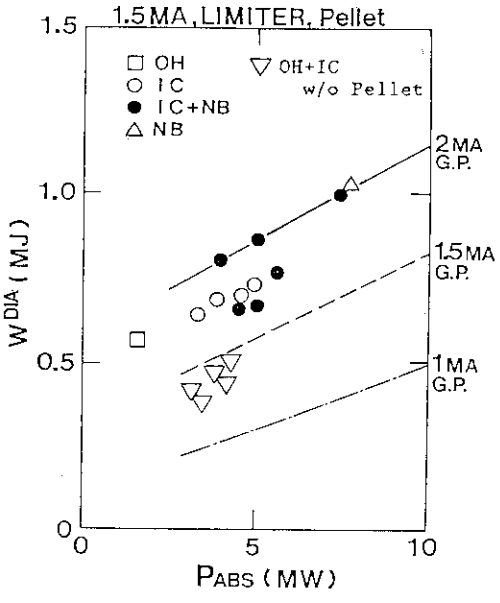

Fig. IV.3-15 The plasma stored energy W^{DIA} measured diamagnetically versus P_{abs} obtained for different heating schemes with and without pellet fueling.

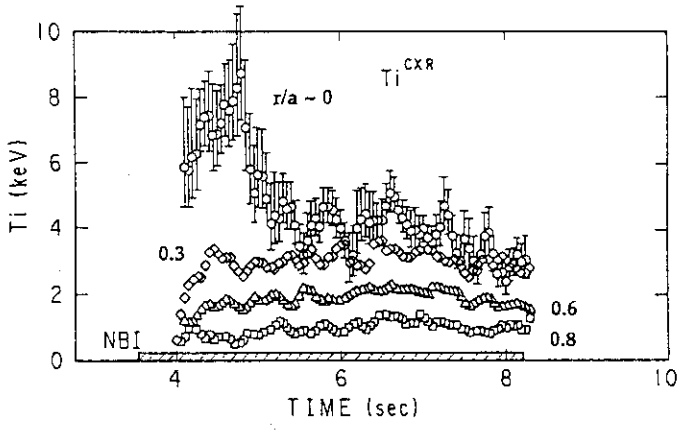

Fig. IV.3-16 Time evolutions of ion temperature from CXRS. NBI is injected during t=3.5-8.2 sec. Central T_i rises up to 9 keV in the initial phase of NBI.

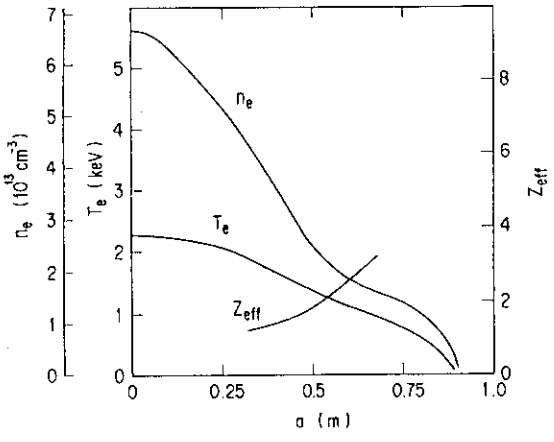

Fig. IV.3-17 Typical profiles of n_e, T_e and Z_{eff} just after hydrogen pellet injection.

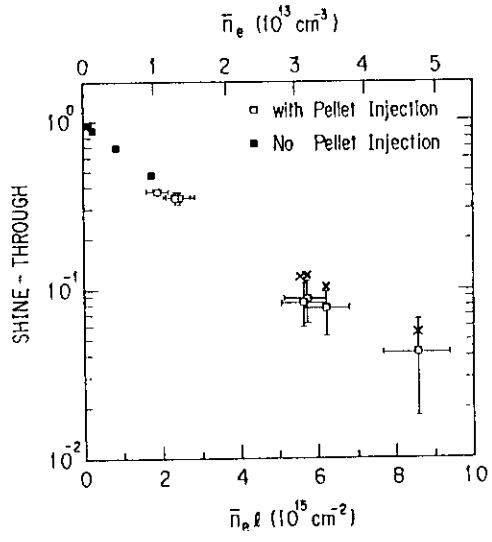

Fig. IV.3-18 Transmission of the hydrogen beam. Crosses stand for transmission calculated from cross sections not including multistep collisions.

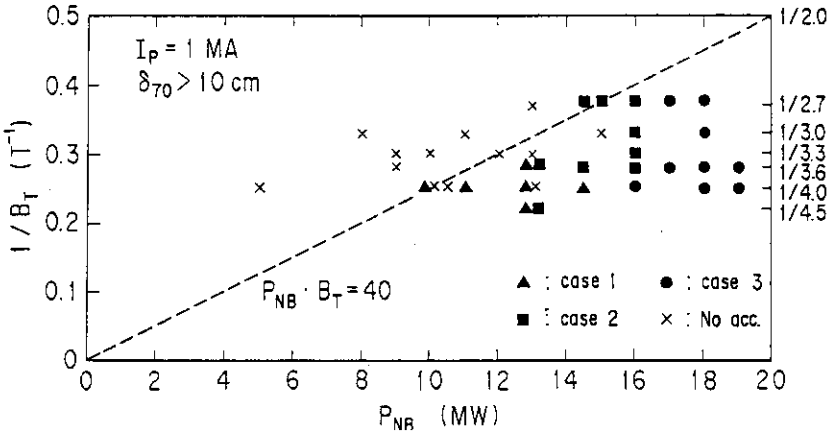

Fig. IV.3-19 The dependences of the tail responses on P_{NB} and B_T. Case 1 is that the tail temperature just after NB injection is decaying.

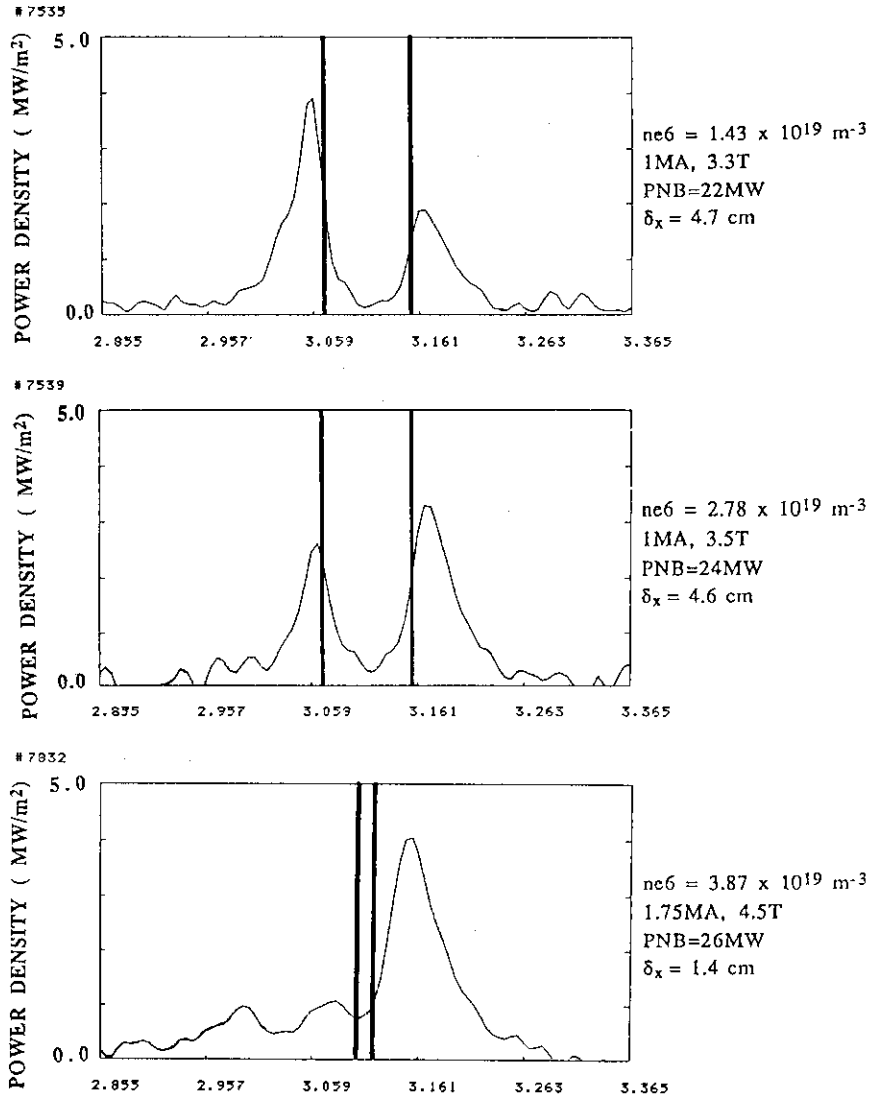

Fig. IV.3-20 The radial profile of the heat flux for discharges with line averaged density (ne6) increasing from 1.43×10^{19} cm^{-3} to 3.87×10^{19} cm^{-3}.

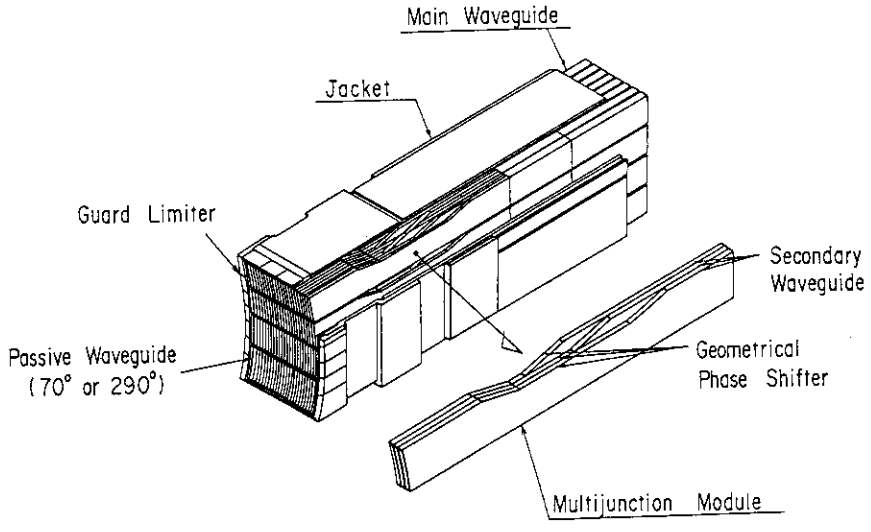

Fig. IV.4-1 Multi-junction launcher in JT-60

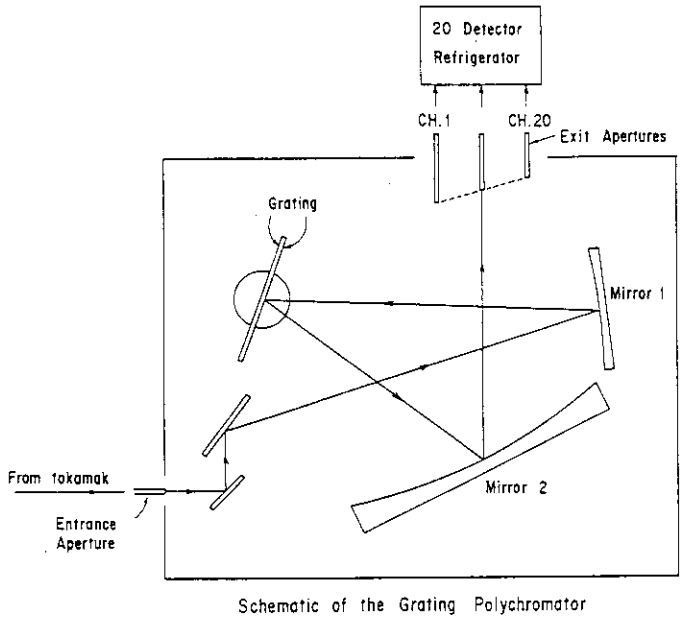

Fig. IV.4-2 Schematic of the JT-60 grating polychromator.

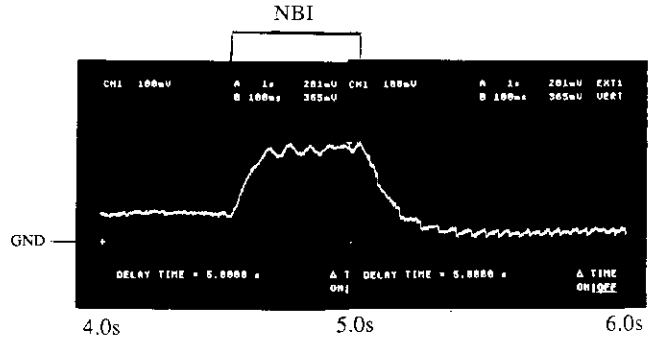

Fig. IV.4-3 Waveform of the spectral line emission from the central plasma in NBI experiments.

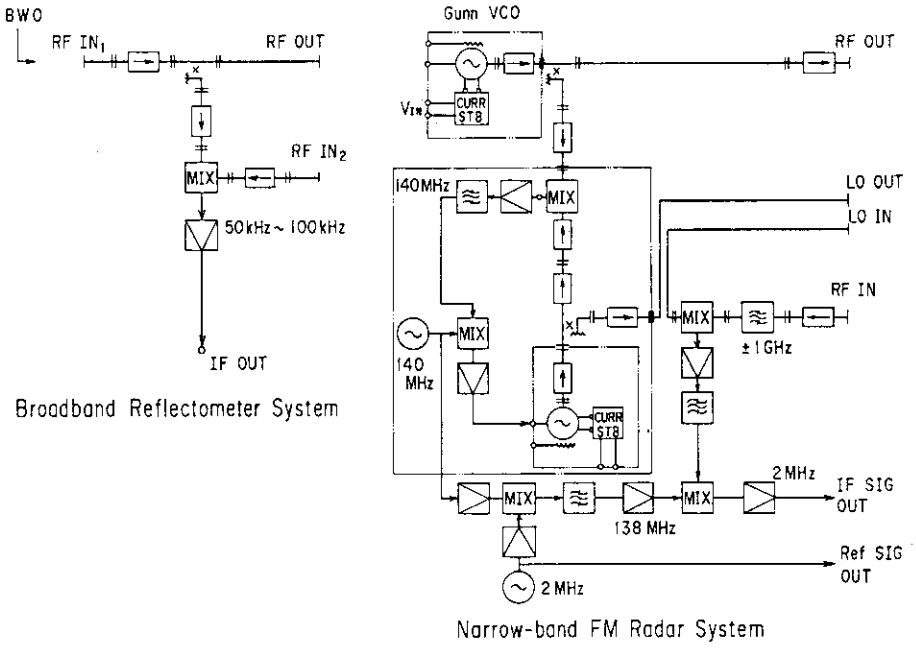

Fig. IV.4-4 A schematic of the circuitry for the wideband-sweep (left) and fixed frequency reflectometer (right).

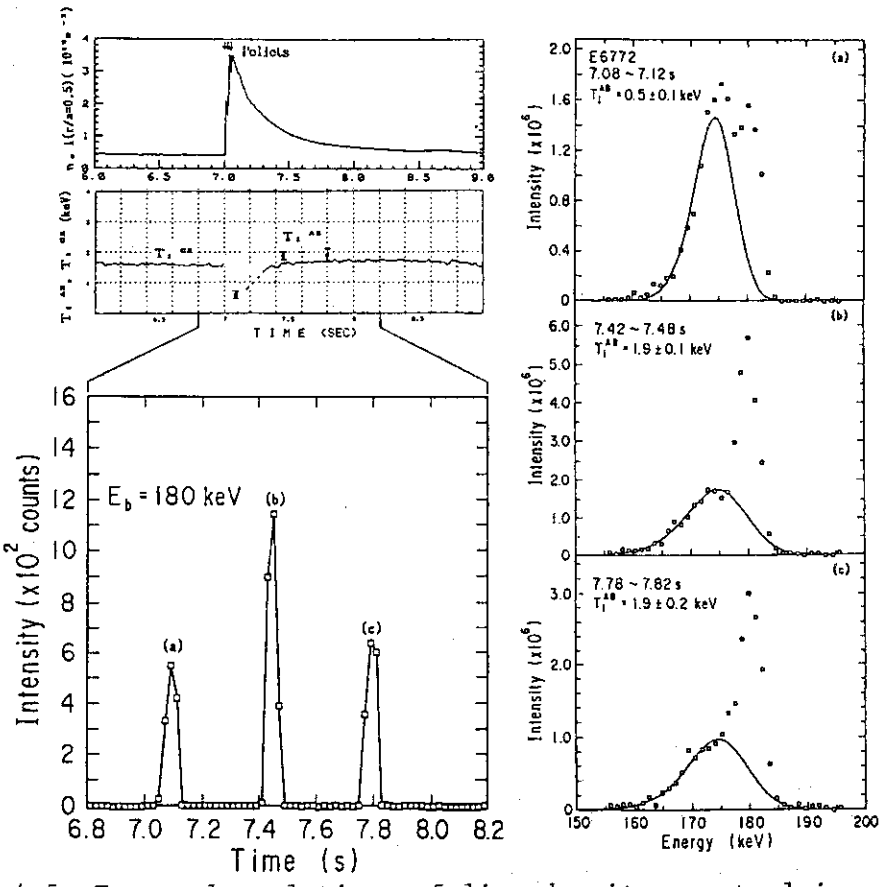

Fig. IV.4-5 Temporal evolutions of line density, central ion temperature measured from the active beam scattering method, T_i^{AB}, and ion temperature deduced from energy analysis of charge-exchange neutral particles, T_i^{CX}, and scattered helium atom intensity for three beam pulses. Energy spectra for three beam pulses are also shown in Fig.(a)∿(c).

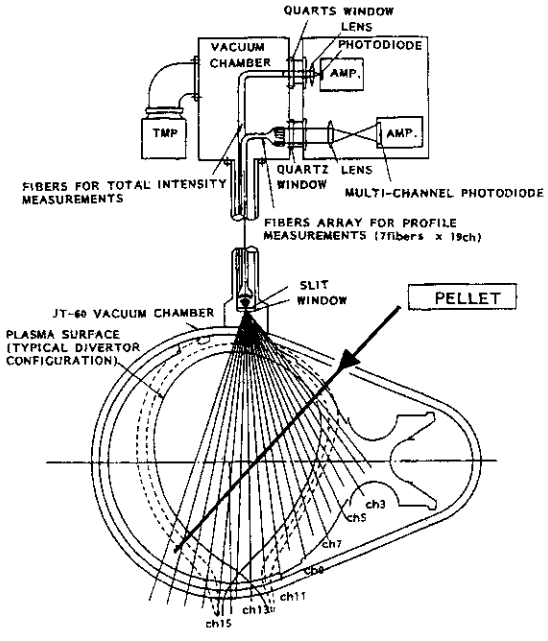

Fig. IV.4-6 Schematic view of the ablation monitor on JT-60.

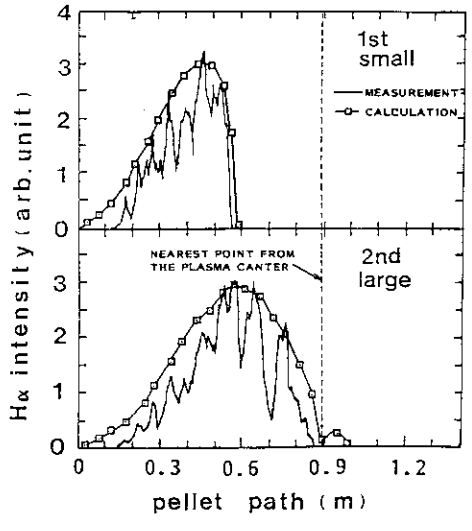

Fig. IV.4-7 Ablation profiles converted from time evolution of the total H_α emissivity comparison with calculations based on Nakamura's model.

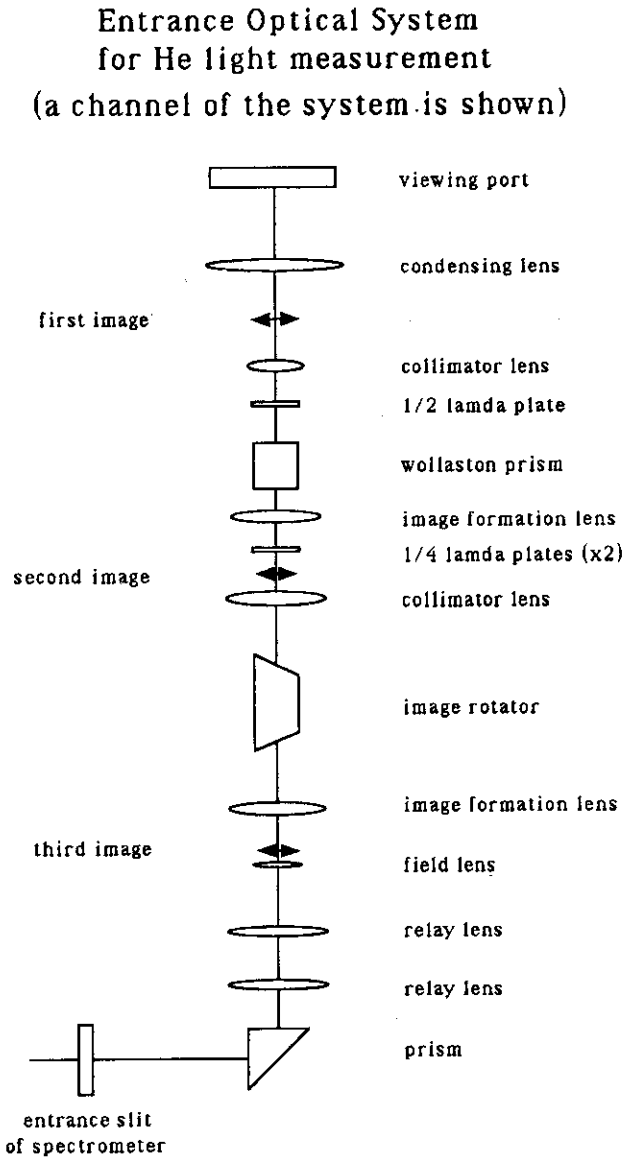

Fig. IV.4-8 Entrance optical system of Zeeman polarimeter.

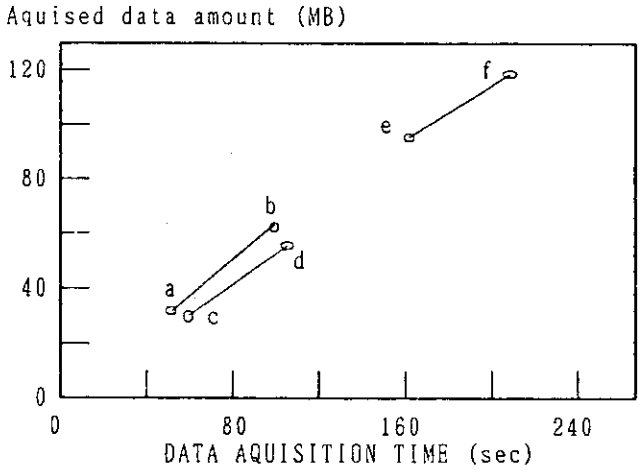

Fig. IV.4-9 Data aquising capability of TMDS.

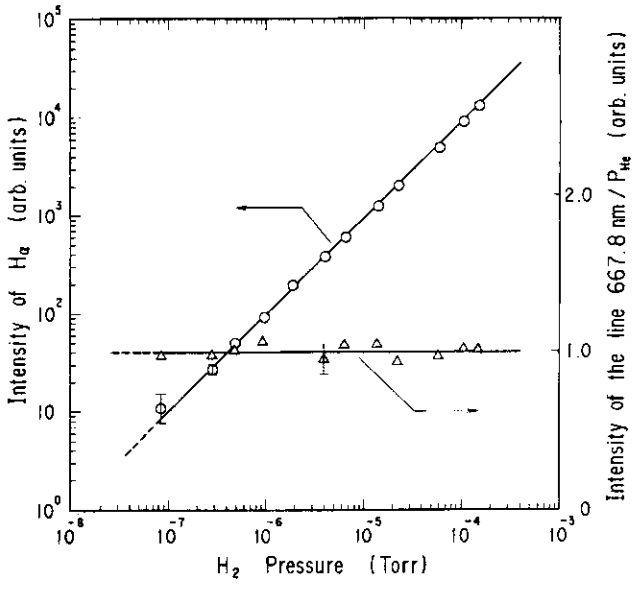

Fig. IV.4-10 The intensity of H_α and line 667.8 nm (from He) as a function of the partial pressure of H_2 and He. The partial pressure of He (P_{He}) is varied from 3×10^{-7} to 1×10^{-6} Torr. The intensity of the line 667.8 nm is normalized with P_{He}.

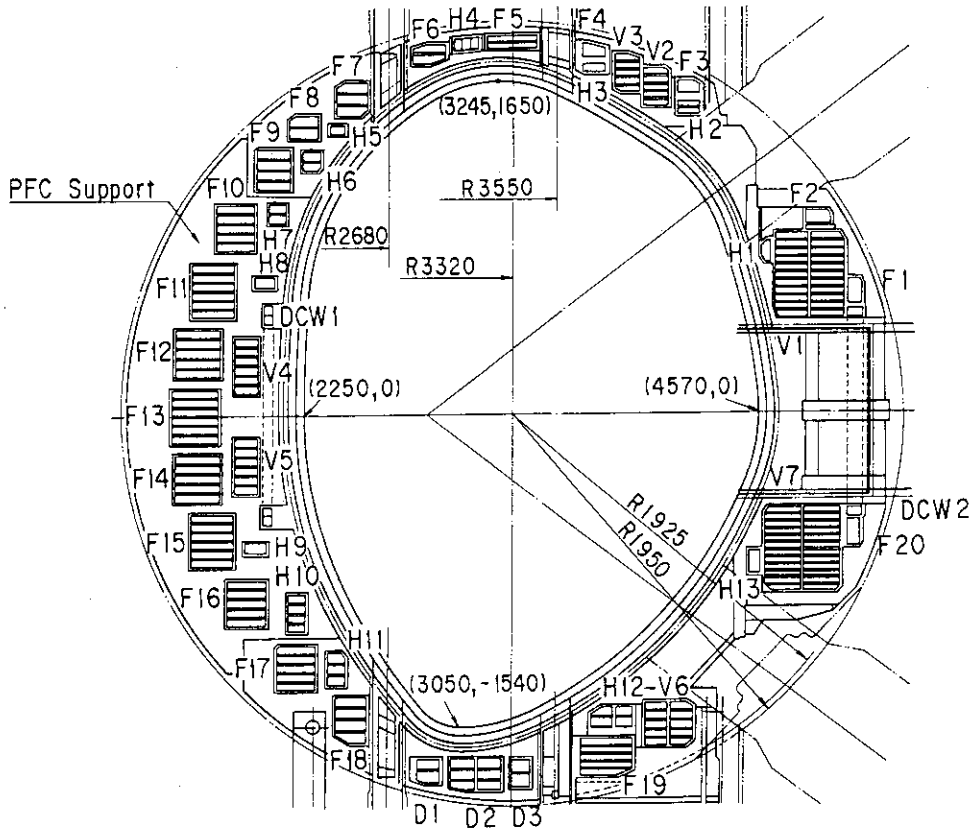

Fig. IV.5-1 Cross sectional view of poloidal field coils.

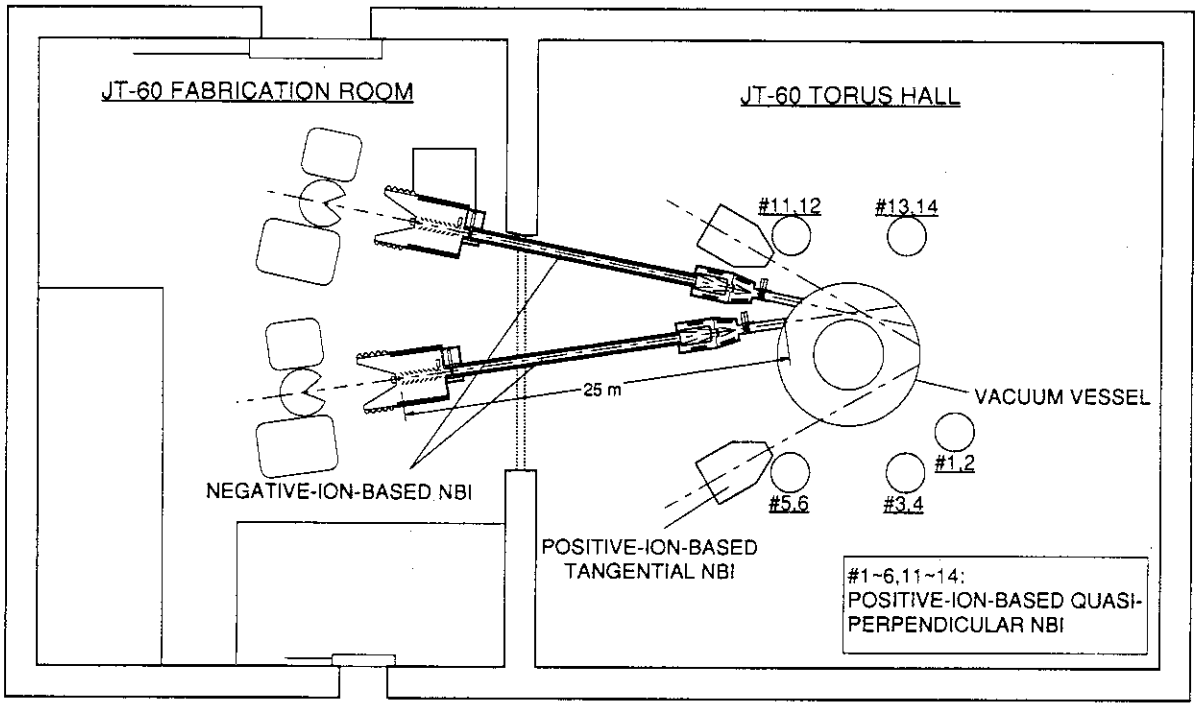

Fig. IV.5-2 A horizontal view of the proposed negative-ion-based neutral beam injection system for JT-60U.

V. TECHNOLOGY DEVELOPMENT

1. Surface Physics and Vacuum Technology

1.1 Introduction

Surface physics studies have been carried out in close connection with the JFT-2M project and JT-60 project, and the design study of next step tokamaks. The primary objective of these studies is to investigate the interaction of plasma with wall and limiter materials using low energy ion accelerators in order to understand surface processes occurring on the surface of wall and limiter, which helps us to find out optimum conditions for minimizing impurity production and controlling hydrogen recycling. On the other hand, vacuum technology is one of the key technologies for the operation and maintenance of current fusion devices and it has been more and more recognized that not only application of conventional techniques but also development of innovative techniques is required for the real design of next step tokamaks. The technology area includes first wall preparation, pumping, gauging, leak hunting, and in-vacuum manipulators.

In this fiscal year, the following progress was obtained with respect to those subjects: $C_xH_yD_z$ formation in graphite due to H^+, D^+ ion irradiation, permeation of deuterium implanted into thin copper plate, performance test of medium size ceramic turbomolecular pump, fabrication and test of modified metal-seal vacuum flanges, and measurement of secondary electron emission coefficient of some wall and window materials.

1.2 $C_xH_yD_z$ formation in graphite due to H^+, D^+ ion irradiation

It is of interest to study whether $C_xH_yD_z$ molecules are formed when carbon materials are exposed to the simultaneous or successive bombardments of H^+ and D^+ ions. For that purpose measurements of signal intensities of QMS ranging from mass 15 to 36 were carried out, using a graphite target that was firstly bombarded with H^+ ions and then secondly with D^+ ions. Figure V.1-1 shows typical results of the successive bombardments of 6 keV H_3^+ and 6 keV D_3^+ ions at 500°C. It can be seen that the signal intensities of mass 17 and mass 19 have a maximum during 6 keV D_3^+ bombardment. These results clearly indicate that the formation of CH_3D, CHD_3 molecules occurs in graphite target.

The other results which are not shown here suggest an important fact that the hydrogen depth profile first implanted into graphite should be overlapped with the deuterium one in order to occurrence of $C_xH_yD_z$ formation.

1.3 Permeation of deuterium implanted into thin copper plate[1,2]

The permeation rates of deuterium through copper foil exposed to a deuterium ion beam of 5 keV D_3^+ were measured as a function of temperature. The permeation flux at a steady state, which was obtained after the 30 min to several hours implantation, had extraordinary temperature dependence shown in Fig. V.1-2. An anomally around 550°C apart from the simple Arrhenius-type dependence cannot be explained in terms of the diffusion constant and recombination of deuterium. The change of surface condition of the sample or some extraordinary deuteron transport to cause the anomaly might happen around the temperature.

1.4 Performance test of a medium size ceramic turbomolecular pump[1,2]

In order to establish a transfer pumping system which is suitable to fusion magnetic/nuclear environment, new ceramic turbomolecular pumps have been developed. The rotor assembly of the pumps is composed of ceramic (Si_3N_4) discs for gas compression, a ceramic shaft with gas turbine blades and a ceramic thrust disc. The rotor assembly is supported by gas bearings and is driven by an impulse gas turbine. A non-contact spiral-groove seal isolates the vacuum side from the high pressure side. After preliminary experiments with an 80 l/s ceramic turbomolecular pump, a medium-size ceramic pump was designed, fabricated and tested in 1988. The major specifications and some measured vacuum characteristics of the pump are as follows:

(1) Outer diameter of Si_3N_4 rotor blades: 210 mm
(2) Number of the rotor blades: 16
(3) Rotation speed: 25,000 rpm
(4) Pumping speed: ca 500 l/s
(5) Ultimate pressure: 4×10^{-7} Pa
(6) Residual gas components at ultimate pressure: H_2, H_2O, and CO

Figure V.1-3 shows the whole view of the medium size ceramic turbomolecular pump.

1.5 Fabrication and test of modified metal-seal vacuum flanges[3,4]

Knife-edge-type metal-seal flanges are widely used in various vacuum

systems. However, the current flanges still present some problems such as heavy weight, high required torque and many bolt holes especially when they are employed as parts of remote maintenance devices. The aim of this study is to reduce the weight, required torque and number of bolt holes of the flanges keeping the leaks free both at room temperature and during high temperature baking. At first, we analyzed the seal mechanisms of the flanges by the finite element method (FEM). Then, we carried out various performance tests including severe heat cycle tests with modified flanges to find out optimum parameter ranges for reliable sealing. Based on the FEM analysis and the experimental results, we decided the flange parameters for different diameter (70, 114, 152, 203 and 253 mm) flanges. With new flanges, the weight, required torque and number of bolts could be reduced by 30%, 40% and 50 - 30% of those of the original knife-edge flanges, respectively. Figure V.1-4 compares the new flanges and the original flanges of the same diameters.

1.6 Measurement of secondary electron emission coefficient of some wall and window materials[5,6]

Secondary electron emission due to energetic electron impact is an important factor for reducing the multipactor discharge which takes place in RF waveguides and on RF windows. In order to study the effect of surface contaminants on the secondary electron emission coefficient of actual materials, we have measured the coefficient of some fusion vacuum materials including OFHC copper and aluminum nitride before and after surface cleaning. Surface composition due to contaminant was analyzed by using an Auger electron spectrometer. From the experiment, it was found that the coefficient of Ar^+ etched OFHC copper is 1.50 at the maximum whereas it changes to 1.86 after an exposure to silicone grease vapor. The coefficient of aluminum nitride was also found to be extremely low, namely, around unity, regardless of the surface condition. Figure V.1-5 shows the secondary electron emission coefficient of aluminum nitride as a function of incident electron energy.

References

[1] T. Abe et al., Vac. Soc. Japan 31 (1988) 334.
[2] K. Ioki*7, et al., Fusion Eng. Design 8 - 10 (1989).
[3] K. Obara et al., J. Vac. Soc. Japan 32 (1989) 2.
[4] K. Obara et al., ibid 165.

[5] S. Hiroki et al., ibid 171.
[6] S. Hiroki et al., Trans. Inst. Electr. Eng. Japan, to be published.

2. Superconducting Magnet

2.1 Introduction

The superconducting magnet development work at JAERI is being carried out for the purpose of engineering establishment on the magnet system in Fusion Experimental Reactor. There are three major developments: toroidal coil, poloidal coil and helium refrigerator. The toroidal coil development has progressed through Cluster Test Program and Large Coil Task (LCT). Cluster Test Program and LCT, producing great achievements, were successfully closed in 1986 and in 1988, respectively. From 1988, the Proto Toroidal Coil Program was started. For the poloidal coil development, the Demo Poloidal Coil (DPC) Program has been progressed. The helium refrigerator technique has advanced in parallel with these developments. The main achievements in FY 1988 are as follows.

1) 7 T/s pulse field operation of the DPC in the first experiment
2) Fabrication of three candidate conductors as trial manufacturing for the Proto Toroidal Coil Program.
3) Transportation of the US-LCT coil to JAERI for the Proto Toroidal Coil Program
4) Development of a Turbo-expander for the 10 kW refrigerator.

2.2 Demo poloidal coil program

2.2.1 Program status

The Demo Poloidal Coil (DPC) program is in progress at JAERI for the purpose of developing technology required for the construction of superconducting poloidal coils in the Fusion Experimental Reactor. In this program two 30-kA NbTi pulsed coils (DPC-U1 and -U2) and a 10-kA Nb_3Sn pulsed coil (DPC-EX) are fabricated and tested. All the coils have forced-flow cooling and winding inner diameters of 1 m. The fabrication of DPC-U1 and -U2 was finished and the first experiment was successfully completed in March, 1989. The achievements in the experiments are summarized in Table V.2-1.

2.2.2 Fabrication of DPC-U1, -U2 and -EX

Fabrication of cables for eight double-pancakes of DPC-U1 and -U2

[5] S. Hiroki et al., ibid 171.
[6] S. Hiroki et al., Trans. Inst. Electr. Eng. Japan, to be published.

2. Superconducting Magnet

2.1 Introduction

The superconducting magnet development work at JAERI is being carried out for the purpose of engineering establishment on the magnet system in Fusion Experimental Reactor. There are three major developments: toroidal coil, poloidal coil and helium refrigerator. The toroidal coil development has progressed through Cluster Test Program and Large Coil Task (LCT). Cluster Test Program and LCT, producing great achievements, were successfully closed in 1986 and in 1988, respectively. From 1988, the Proto Toroidal Coil Program was started. For the poloidal coil development, the Demo Poloidal Coil (DPC) Program has been progressed. The helium refrigerator technique has advanced in parallel with these developments. The main achievements in FY 1988 are as follows.

1) 7 T/s pulse field operation of the DPC in the first experiment
2) Fabrication of three candidate conductors as trial manufacturing for the Proto Toroidal Coil Program.
3) Transportation of the US-LCT coil to JAERI for the Proto Toroidal Coil Program
4) Development of a Turbo-expander for the 10 kW refrigerator.

2.2 Demo poloidal coil program

2.2.1 Program status

The Demo Poloidal Coil (DPC) program is in progress at JAERI for the purpose of developing technology required for the construction of superconducting poloidal coils in the Fusion Experimental Reactor. In this program two 30-kA NbTi pulsed coils (DPC-U1 and -U2) and a 10-kA Nb_3Sn pulsed coil (DPC-EX) are fabricated and tested. All the coils have forced-flow cooling and winding inner diameters of 1 m. The fabrication of DPC-U1 and -U2 was finished and the first experiment was successfully completed in March, 1989. The achievements in the experiments are summarized in Table V.2-1.

2.2.2 Fabrication of DPC-U1, -U2 and -EX

Fabrication of cables for eight double-pancakes of DPC-U1 and -U2

contained continuous welding of stainless steel conduit over 150-m length. TIG welding with filler was employed for this process and non-destructive inspection by eddy current, ultrasonic, and penetrant tests were done in the process. The fabrication was successful and the conductors were confirmed to have no welding defect. The conductors were wound to double-pancakes using overbending method with applying appropriate tensile force. Pre-press technique was employed in order to have sufficient mechanical contact between turns[1]. The fabrication of all the Nb_3Sn strands for DPC-EX was finished and conductor fabrication which also contains the welding of stainless steel conduit is in progress.

2.2.3 Experimental results of DPC-U1 and -U2

Installation and cooldown

DPC-U1 and -U2 were delivered to JAERI in the middle of January, 1989. The coils were installed in the 5-m-dia. vacuum tank and were arranged in coaxial configuration with a gap of about 300 mm (Fig.V.2-1). The DPC facility is composed of cryogenic system which can produce 500-g/s supercritical helium, a 30-kA DC power supply, data acquisition and protection system, and an electrical connection to the JT-60 power supply which can perform pulse operation of the coils up to 7 T/s. Cooldown of the coils started after electrical breakdown test and pressure proof test, and a total weight of about 22 tons was cooled to cryogenic temperature in 125 hours without causing any damage. The cooldown characteristics are shown in Fig.V.2-2.

DC and pulse operations

Both coils of DPC-U1 and -U2 achieved individually the design current of 30 kA in DC operation. The maximum magnetic field and stored energy at this point were 5.2 T and 11 MJ, respectively. During the charge, the coil was cooled by 4.2-K, 0.6-MPa supercritical helium at the mass flow rate of 150 g/s. Pressure drop in the coil was approximately 0.1 MPa, which agrees well with the design. For the pulse operation, one of the coils (DPC-U2) was connected to the JT-60 power supply whose capacity was ±5 kV and +58 kA. It was the first time that the JT-60 power supply was used for a superconducting coil. More than 40 shots were performed in the pulse operation and the design pulsed field of 7 T/s was achieved by ramping up the coil to 30 kA in 0.75 sec. Figure V.2-3 shows this operation, in which coil terminal voltage reached 900 V. In the pulse operation cooling condition was almost the same as in

the DC operation.

Ac losses

Through the pulse operation, ac losses of the coil were investigated. In the 7-T/s operation, the maximum temperature increase of helium at the outlet of the winding was only 0.3 K. Ac losses of the winding were calculated from enthalpy change in helium between the inlet and outlet of the winding. Result indicates that the coil will produce ac losses of 40 - 45 kJ in the designed pulse operation of the bipolar charge to ±7 T (0 to 7 T in 1 sec, 7 to -7 T in 2 sec, then -7 T to 0 in 1 sec). The design calculation using the measured loss-time-constant of the strand indicates 32 kJ. The losses are no more than 0.15% of the stored energy (30 MJ) at the design point of 7 T. Thus the ac losses of the coil was demonstrated to be sufficiently small, but slightly larger than we had expected.

Coil protection

Coil protection is one of the most important issues in this program. Since coil voltage is accompanied by large induced voltage due to a pulsed field, it is difficult to detect small voltage caused by the appearance of normal resistance in the coil. For this purpose co-wound compensation coil method was utilized in the DPC. Signals from the compensation coil and the DPC are led to a quench detector to form bridge circuit. In the 7-T/s operation, the observed maximum balance voltage was 0.2 V, which was 0.02% of the coil terminal voltage (900 V) and was acceptable for quench detection.

2.3 Proto toroidal coil program[2]

The superconducting coil system is requested to have high reliability and the coil performance (maximum field and current density) directly influences the size of the tokamak machine. Therefore, the development program of the proto-type superconducting conductors and coils for the Fusion Experimental Reactor (FER), named "GENTRO" program, is indispensable to realize the superconducting coil system of the FER. The objectives of the GENTRO program are as follows:

(1) Development of high performance superconductor,
(2) Development of manufacturing technique of high rigidity, high voltage and stable coil,
(3) Demonstration of real conductor and real coil fabrication on the proto-type TF coil,

(4) Evaluation of conductor and coil performance required from the FER specifications in the GENTRO test facility.

For the conductor developments, three candidate conductor types have been selected, and their trial manufacturing and the fabrication of test samples are just started. Specifications of the conductor are expected as Table V.2-2. The following three types of conductors are the candidate.

(1) TMC-FF type: Hollow cooling type using Test Module Coil Nb_3Sn conductor techniques (Fig.V.2-4),

(2) Preformed Armor type: Reacted cable-in-conduit in a preformed armor (Fig.V.2-5),

(3) Advanced Disk type: semi-reaction-after-winding technique and disk reinforced (Fig.V.2-6).

2.4 Large coil task

After the LCT (Large Coil Task) coil experiments had been completed, a LCT technical report, which describes design, fabrication, and experiment results for each coil, was being published by the coil participants, JAERI, the US, EURATOM, and Swiss. This report was released as the special issue of the Fusion Engineering and Design (Volume 7, Nos. 1 & 2, September 1988). The executive committee meeting was held at Utrecht in the Netherlands on September 22 in 1988. In this meeting, final check out of the LCT report was completed. And the committee concluded that the LCT symposium would be held on January 24 at Paris in France and that the Annex 1 (the Large Coil Task) of international collaboration under the auspices of the IEA would be completed in this symposium. The LCT symposium was successfully held on schedule and hereby the Annex 1, the Large Coil Task, which had been continued for around ten years, has been completed as the successful international collaboration of the hardware work for fusion energy project. Under agreement between JAERI and US-DOE, one of the US-LCT coil (GE/ORNL LCT Coil) had been transferred from the US to Japan in March of 1989 in order to be used as a buck-up coil for the Prototype toroidal coil development program of Japan.

2.5 High field coil development

Two high field coil systems were developed in this period, and superconductor and superconducting magnet experiments using these coil

systems were started. One is a large superconducting split coil system (Fig.V.2-7) composed of two NbTi coils (SBC) and two Nb_3Sn coil (SP15) for the test of large current superconductors. The SBC coil has an inner diameter of 313 mm, an outer diameter of 675 mm and a height of 197 mm, and was charged up to its nominal state without training. By this system, a full-size superconductor for the toroidal coil of FER can be tested in the magnetic field of more than 10 T. Another is a middle-size high-field superconducting coil system composed of three superconducting coils. 12 T - 140 mm diameter or 14 T - 82 mm diameter are available as the test space in this system.

2.6 Cryogenic system development

2.6.1 Cryogenic component development

A turbo-expander is one of key components for a large, reliable and efficient refrigerator. As a development step, we have fabricated three turbo-expanders with different nozzle and impeller shapes. The major parameters are specified on the basis of the 10-kW refrigerator design[3] for a prototype toroidal coil development, as listed in Table V.2-3.

Using the Superconducting Engineering Test Facility at JAERI, these turbo-expanders were tested in an equivalent condition as listed in Table V.2-3 because of restriction of the present refrigerator capability. The test results show that all turbo-expanders can be operated down to its design temperature of 45 K in stable and a higher efficiency than 73% is obtained in case of the bane-nozzle and shrouded-impeller type. As a whole, the turbo-expander technology for the 10-kW refrigerator is highly advanced.

2.6.2 DPC cryogenic system

The Demonstration Poloidal Coil (DPC) program is being conducted to develop superconducting pulse coils for FER. In this program, three forced-cooled superconducting coils (DPC-U1, U2 and EX) are tested under the cooling conditions of 4 K, 10 bar and 350 g/s by circulating supercritical helium. In order to meet this cooling condition, the cryogenic pump system, which is composed of a circulation pump and cold compressor, was developed[4,5]. The performance test of the whole cryogenic system including the pump system was conducted before the coil testing. We have demonstrated in the performance test that the cryogenic system has

sufficient capability[6,7].

After the performance test, the first coil test with DPC-U1 and U2 was conducted during early of 1989. In this coil test, the whole cryogenic system including the cryogenic pump was continuously operated for around two months in stable and the forced-cooled technology is well established. As a next step, one more test coil will be installed and tested.

2.7 Development of the cryogenic structural materials

The weldment of the Japanese Cryogenic Steels (JCS) has been developed in this year. Mechanical properties of the welded joints made by tungsten inert gas (TIG) welding process and electron beam welding (EBW) process were measured at 4 K. Figure V.2-8 shows the ratio of the fracture toughness of welded joint to that of the base metal. The all of TIG welded joints of the JCS have about 80% of the fracture toughness of the base metal. The fracture toughnesses of EBW joints are larger than those of not only TIG welded joints but also base metals in JN1, JK2.

On the other hand, it is indispensable to establish the standard method of the cryogenic material testing in order to make data base for reliable design of superconducting coils. The standard method of cryogenic tensile test has been established as Japanese Industrial Standard (JIS). This standard will be published next year.

References

[1] H. Tsuji, et al., IEEE Trans. Magn. MAG-25 1484-1487 (1989).
[2] K. Yoshida, IEEE Trans. Magn. MAG-25 1488 (1989).
[3] T. Kato, et al., Proc. of 15th Symposium on Fusion Technology, Utrecht, Sept. 19-23 (1988).
[4] T. Kato, et al., Cryogenic Engineering, 24(1989) p.29.
[5] H. Yamamura, et al., Cryogenic Engineering, 24(1988) p.36.
[6] E. Tada, et al., Cryogenic Engineering, 24(1988) p.21.
[7] E. Tada, et al., ICEC-12, England, July 12-15(1988).

3. Beam Technology

3.1 Negative ion sources

3.1.1 Multi-ampere negative ion source[1]

sufficient capability[6,7].

After the performance test, the first coil test with DPC-U1 and U2 was conducted during early of 1989. In this coil test, the whole cryogenic system including the cryogenic pump was continuously operated for around two months in stable and the forced-cooled technology is well established. As a next step, one more test coil will be installed and tested.

2.7 Development of the cryogenic structural materials

The weldment of the Japanese Cryogenic Steels (JCS) has been developed in this year. Mechanical properties of the welded joints made by tungsten inert gas (TIG) welding process and electron beam welding (EBW) process were measured at 4 K. Figure V.2-8 shows the ratio of the fracture toughness of welded joint to that of the base metal. The all of TIG welded joints of the JCS have about 80% of the fracture toughness of the base metal. The fracture toughnesses of EBW joints are larger than those of not only TIG welded joints but also base metals in JN1, JK2.

On the other hand, it is indispensable to establish the standard method of the cryogenic material testing in order to make data base for reliable design of superconducting coils. The standard method of cryogenic tensile test has been established as Japanese Industrial Standard (JIS). This standard will be published next year.

References

[1] H. Tsuji, et al., IEEE Trans. Magn. MAG-25 1484-1487 (1989).
[2] K. Yoshida, IEEE Trans. Magn. MAG-25 1488 (1989).
[3] T. Kato, et al., Proc. of 15th Symposium on Fusion Technology, Utrecht, Sept. 19-23 (1988).
[4] T. Kato, et al., Cryogenic Engineering, 24(1989) p.29.
[5] H. Yamamura, et al., Cryogenic Engineering, 24(1988) p.36.
[6] E. Tada, et al., Cryogenic Engineering, 24(1988) p.21.
[7] E. Tada, et al., ICEC-12, England, July 12-15(1988).

3. Beam Technology

3.1 Negative ion sources

3.1.1 Multi-ampere negative ion source[1]

A large volume negative ion source called multi-ampere negative ion source was designed and tested. Figure V.3-1 shows the cross sectional view of this ion source. The plasma generator is a magnetically filtered multicusp source, whose dimensions are 24 cm (wide) × 48 cm (long) × 15 cm (deep) volume. The extractor consists of five grids, each of which has 253 apertures of 11.3 mm diameter over a large extraction area of 14 cm × 36 cm. A newly devised filter, called PG filter produces a uniform filter field over the wide extraction area by flowing a high current through the plasma grid itself.

The H^- beam current obtained in the PG filter is shown in Fig.V.3-2 as a function of arc discharge current. The figure also shows the H^- beam currents obtained in a rod filter and an external filter for comparison. The highest H^- beam current of 3.4 A has been obtained in the PG filter with a beam current density of 13 mA/cm^2. The maximum H^- beam currents in the rod filter and in the external filter was 1.6 A and 3.1 A, respectively. It indicates that the PG filter is useful for large ion production.

3.1.2 Small bucket ion source and ECR ion source

A small negative ion source has been developed for two reasons. One is the investigation of an ion source scale size effect, and the other is applications to the ion source for active beam diagnostic system and a high energy accelerator. The plasma generator is a multicusp or a bucket source, whose size is 54 mm in a hexagonal opposite side width and 59 mm in depth. The aperture of the extractor is 20 mm in diameter. A 8mA (2.5 mA/cm^2), 22 keV H^- beam was produced at the arc power density of 12 W/cm^3.

In order to investigate the possibilities of applying the ECR plasma to the negative ion source and to the plasma neutralizer, we have started the experiment on the ECR plasma[2]. Microwave power of up to 5 kW was injected to the mirror confined plasma chamber to produce H_2 and Xe plasma. Measuring the plasma parameters by Langmuire probes, we found that the plasma density was more than 10^{12} cm^{-3} for both cases at the center of the plasma. The degree of ionization was as high as 30% in Xe plasma.

3.1.3 D^- experiment at LBL[3]

As a cooperative research program on fusion between Japan and the U.S., D^- ion production experiment was held at Lawrence Berkeley Labo-

ratory (LBL). In this program, an one ampere volume ion source developed at JAERI was shipped to U.S. and was operated with deuterium gas at TS-IIIA test stand at LBL. The main objective of the experiment is to find out the isotope effect on negative ion production in a volume negative ion source.

By optimizing the magnetic filter strength within the range of 450 - 930 Gauss-cm, we obtained the maximum ion current densities, of 9.1 mA/cm^2 for H^- and 6.6 mA/cm^2 for D^- at the arc discharge power of 40 kW. The ratio of the current was approximately $1\sqrt{2}$, i.e. the square root of the mass ratio, which indicates the same amount of negative ion density can be obtained even in deuterium. It was found, however, higher magnetic filter strength would be required in deuterium operation than in hydrogen. A remarkable difference was observed in the electron currents. The electron current in D^- operation was larger by more than factor of 2 than in H^- operation. The reduction of electron current seems to be the most difficult problem in D^- source.

3.1.4 Beam optics experiment simulating a 500 keV D^- acceleration[4]

In a design of the NBI for ITER or FER, D^- ions are extracted in multi-aperture grids and accelerated to 500 - 1000 keV by single hole electrodes. This extraction/acceleration system is called multi-single type acceleration system.

In order to confirm the beam optics of multi-single type acceleration system, we manufactured a full length 500 keV acclerator and extracted negative hydrogen ion beams up to 50 keV, while the perveance value is equivalent to the 500 keV D^- design value. An e-folding, half-width beam divergence was as low as 9 mrad at the same perveance value as the 500 keV design value, where the deuterium negative ion current density and the electron current density at the sheath boundary are assumed to be 50 mA/cm^2 and 1000 mA/cm^2, respectively. This value is close to the required beam divergence of 5 mrad for the fusion applications. This result indicates that three or more beamlets from the pre-acceleration can be merged in the main-accelerator with good beam optics.

3.2 Positive ion sources

3.2.1 Large ion source with high proton yield[5]

For a joint experiment on an energy recovery system between JAERI and CADARACHE Nuclear Research Center in France, a large positive ion

source has been developed. Required performance is that the proton ratio should be higher than 90%, the plasma spatial uniformity be less than 10% over an area of 8 cm × 120 cm, and the hydrogen ion current density be more than 210 mA/cm^2. Figure V.3-3 shows the proton yield of hydrogen ion as a function of the extraction current at the beam energies of 30 - 46 keV. We confirmed that the required performances were perfectly satisfied at a lower filling pressure of 0.6 Pa.

3.2.2 Steady state discharge cathode

For the next generation tokamaks, steady state operation of the NBI is required. To fulfill this requirement, the NBI ion source should have an ability to endure a continuous discharge. For this purpose, a new cathode was devised. The electron emitter is the barium oxide impregnated porous tungsten cylinders. The emitter is heated by thermal radiation from the ohmically heated tungsten rod in the center of coaxial structure. Non stop 10 hour durability test of this cathode was carried out with success, using a magnetic multipole plasma generator. The discharge conditions were as follows; the gas pressure = 0.76 P_a, the discharge current = 50 to 60 A, and the discharge voltage = 39 to 45 V.

3.3 R&D for future NBI

3.3.1 Design of the negative-ion-based NBI system

We proposed a 1 MeV NBI system for ITER based on a 500 keV, 20 MW FER-NBI design concept. The side views of ITER and NBI beamline are shown in Fig.V.3-4. In each beamline, a single, large ion source which can deliver a 1 MeV, 51 A deuterium negative ion beam is mounted instead of many small ion sources. This will simplify the beamline, and reduce the construction cost. The profile controllability is the major characteristics of the present design. A 1 MV DC power supply utilizes an AC switch coupled with an 500 Hz inverter system, instead of the conventional DC switch. This will improve the reliability of the power supply system. The total system efficiency including the power loss in the power supply system and the auxiliary system is estimated to be 33%. This value will be improved further with aggressive R&D efforts.

3.3.2 Design study on energy recovery system

A beam energy recovery system is an effective method to improve the power efficiency and to reduce the heat flux on the dump surface in

neutral beam injectors. Applicability of this system to the next generation NBI based on negative ions for FER was being studied.

Numerical results indicate that both D^- and D^+ ion beams are perfectly separated and collected on the recovery electrode or the soft-landing beam dump according to their polarities by the stray magnetic field from the tokamak. The total power efficiency can be improved from the 46% to 60% by recovering only negative ion beams.

3.3.3 High energy "inverter" power supply

The high energy negative-ion-based NBI requires 1 MV DC high voltage power supply. Tetrodes or GTO-thyristors have been used as DC switch in the present NBI system for the protection of ion sources. They will not be available for the high energy NBI system, however, because of the increased series number of the elements. Hence, we proposed an "inverter" power supply where the switching is performed in the AC line. The inverter power supply consists of low voltage inverters, a step up transformer and a high voltage rectifier. Inverter controller cuts off the DC output voltage when breakdown occurs in the ion source.

We adopt the inverter power supply in JAERI Electron Beam Irradiation Stand (JEBIS). Characteristics of the inverter power supply will be investigated in detail as a R&D for the future NBI system.

References

[1] Hanada M., et al., Proc. of the International Conference on Ion Sources, Berkeley (1989).

[2] Matsuda Y., et al., Proc. 12th Symp. on Ion Sources and Ion Assisted Technology, Tokyo (1989) p.107.

[3] Inoue, T., et al., Proc. of the International Conference on Ion Sources, Berkeley (1989).

[4] Ohara Y., et al., Proc. 12th Symp. on Ion Sources and Ion Assisted Technology, Tokyo (1989) p143.

[5] Watanabe, K., et al., Proc. 15th Symp. on Fusion Technology, Utrecht (1988).

4. RF Technology

4.1 Development of launcher-related components and their discharge phenomena

New type of ceramic window (pill box) is developed for vacuum

neutral beam injectors. Applicability of this system to the next generation NBI based on negative ions for FER was being studied.

Numerical results indicate that both D^- and D^+ ion beams are perfectly separated and collected on the recovery electrode or the soft-landing beam dump according to their polarities by the stray magnetic field from the tokamak. The total power efficiency can be improved from the 46% to 60% by recovering only negative ion beams.

3.3.3 High energy "inverter" power supply

The high energy negative-ion-based NBI requires 1 MV DC high voltage power supply. Tetrodes or GTO-thyristors have been used as DC switch in the present NBI system for the protection of ion sources. They will not be available for the high energy NBI system, however, because of the increased series number of the elements. Hence, we proposed an "inverter" power supply where the switching is performed in the AC line. The inverter power supply consists of low voltage inverters, a step up transformer and a high voltage rectifier. Inverter controller cuts off the DC output voltage when breakdown occurs in the ion source.

We adopt the inverter power supply in JAERI Electron Beam Irradiation Stand (JEBIS). Characteristics of the inverter power supply will be investigated in detail as a R&D for the future NBI system.

References

[1] Hanada M., et al., Proc. of the International Conference on Ion Sources, Berkeley (1989).

[2] Matsuda Y., et al., Proc. 12th Symp. on Ion Sources and Ion Assisted Technology, Tokyo (1989) p.107.

[3] Inoue, T., et al., Proc. of the International Conference on Ion Sources, Berkeley (1989).

[4] Ohara Y., et al., Proc. 12th Symp. on Ion Sources and Ion Assisted Technology, Tokyo (1989) p143.

[5] Watanabe, K., et al., Proc. 15th Symp. on Fusion Technology, Utrecht (1988).

4. RF Technology

4.1 Development of launcher-related components and their discharge phenomena

New type of ceramic window (pill box) is developed for vacuum

sealing in the high power transmission line of high power. This window is designed to increase a maximum acceptable power which warrant the application to the LHRF system of JT-60U or FER. The good agreement was obtained between the measurement results on RF characteristics, voltage standing wave ratio (VSWR), the electric field in the pill box, and the calculation results[1]. And the ring resonator for the high power transmission experiment are fabricated. As a result, the RF power is confined up to 2 MW with the RF injection of 250 kW, which agrees well with the design value.

The development of LHRF launcher of multijunction type is carried out in cooperation with JT-60 Facility Division III. Using a test waveguide which has one waveguide for power input and three waveguides for output, the phase difference among the three waveguides and a power dividing ratio, etc. are measured with a low power level. It was confirmed the results are acceptable for the specification of the launcher of JT-60. In addition, new method for manufacturing of launcher, Hot Isostatic Pressing (HIP) method, which has a merit on the pressing between the different materials, are tried on the fabrication of the test waveguide. On the high power experiment of this waveguide, transmitted power of 500 kW, for 1 sec was attained.

On the other hand, a line stretcher for ICRF system is developed to obtain a high reliability on the RF circuit for impeadance matching. The equivalent transmitted power of 11.6 MW, 10 sec was obtained.

4.2 Investigation of high power gyrotron at 120 GHz

Development of a high power gyrotron at a frequency of 120 GHz was started in 1987, the projected value of 150 kW level for 10 msec being achieved in 1988[2]. A 500 kW gyrotron with a whispering gallery mode of $TE_{12,2}$ was also tested with preliminary till March, 1988[3].

After the first test of the 500 kW gyrotron, we had continued to evaluate the whispering gallery mode of gyrotron in collaboration with Toshiba Corporation. At first we made some modification of the tube; (1) improvement of thermal isolation in the Magnet Injection Gun to reduce the electron emission from the extra part of the emission belt, (2) decrease in the thickness of the single disc window from 4 mm to 2 mm to increase the frequency bandwidth of the window and overcome the mode competition of the oscillated frequency. After these improvements the maximum power of 517 kW for 1 msec was obtained at the frequency of

120.1 GHz ($TE_{12,2}$) in March, 1989. RF pulse duration is limited by the power supply of the test facility. Efficiency at the peak RF power is 23.5% of the input power of 76 kV-29 A and the maximum efficiency is obtained 27.3% at 450 kW, as shown in Fig.V.4-1.

4.3 Construction of 1 MeV induction linac

As a long term research and development program, we have started a research work utilizing a relativistic high current electron beam for multi-megawatts RF power source such as Free Electron Laser (FEL) and Cyclotron-Auto-Resonance-Peniotron (CARP). The construction of high current accelerator so called as an induction linac was started in 1988 and is completed in July of this year. With 75 cm diameter ferrite core for the inductor, and with three-stage Co-base amorphous cores for the magnetic compression line, the linac is designed to produce 1 MeV, 1 ~ 3 kA, 100 ns pulse with pulse rise time of 10 ns. The beam energy will be increased up to 5 MeV by 1992. FEL and CARP experiment will start in this year. Both FEL and CARP are known by their extremely high conversion efficiency, and in our case, GW level RF power production is expected in the frequency region between 10 GHz ~ 300 GHz. A picture of the induction linac is shown in Fig.V.4-2.

References

[1] Maebara S., et al., to be published in Proc. the 8th Topical Conf. on Radio Frequency Power in Plasmas.

[2] Nagashima T., et al., Proc. 5th Annual Conf. of the Japan Society of Plasma Science and Nuclear Fusion Research, March 1988, p.212 (in Japanese); Okazaki Y.*4, et al., ibid., p.213 (in Japanese); Kikunaga T.*15, et al., ibid., p.214 (in Japanese); Kikunaga T.*15, et al., Proc. 13th Int. Conf. on Infrared and Millimeter Waves, Honolulu, Hawaii, U.S.A., December 1988, p.177.

[3] Okazaki, Y.*4, et al., Proc. 1988 IEEE International Electron Devices Meeting, San Francisco, CA, U.S.A., December 1988.

5. Tritium Technology

5.1 Development of tritium processing technology

5.1.1 JAERI-LANL (DOE) fusion technology collaboration

The original research program under "ANNEX III to the Implementing

120.1 GHz ($TE_{12,2}$) in March, 1989. RF pulse duration is limited by the power supply of the test facility. Efficiency at the peak RF power is 23.5% of the input power of 76 kV-29 A and the maximum efficiency is obtained 27.3% at 450 kW, as shown in Fig.V.4-1.

4.3 Construction of 1 MeV induction linac

As a long term research and development program, we have started a research work utilizing a relativistic high current electron beam for multi-megawatts RF power source such as Free Electron Laser (FEL) and Cyclotron-Auto-Resonance-Peniotron (CARP). The construction of high current accelerator so called as an induction linac was started in 1988 and is completed in July of this year. With 75 cm diameter ferrite core for the inductor, and with three-stage Co-base amorphous cores for the magnetic compression line, the linac is designed to produce 1 MeV, 1 ~ 3 kA, 100 ns pulse with pulse rise time of 10 ns. The beam energy will be increased up to 5 MeV by 1992. FEL and CARP experiment will start in this year. Both FEL and CARP are known by their extremely high conversion efficiency, and in our case, GW level RF power production is expected in the frequency region between 10 GHz ~ 300 GHz. A picture of the induction linac is shown in Fig.V.4-2.

References

[1] Maebara S., et al., to be published in Proc. the 8th Topical Conf. on Radio Frequency Power in Plasmas.

[2] Nagashima T., et al., Proc. 5th Annual Conf. of the Japan Society of Plasma Science and Nuclear Fusion Research, March 1988, p.212 (in Japanese); Okazaki Y.*4, et al., ibid., p.213 (in Japanese); Kikunaga T.*15, et al., ibid., p.214 (in Japanese); Kikunaga T.*15, et al., Proc. 13th Int. Conf. on Infrared and Millimeter Waves, Honolulu, Hawaii, U.S.A., December 1988, p.177.

[3] Okazaki, Y.*4, et al., Proc. 1988 IEEE International Electron Devices Meeting, San Francisco, CA, U.S.A., December 1988.

5. Tritium Technology

5.1 Development of tritium processing technology

5.1.1 JAERI-LANL (DOE) fusion technology collaboration

The original research program under "ANNEX III to the Implementing

Arrangement between the Japan Atomic Energy Research Institute and the United States Department of Energy on Cooperation in Fusion Research and Development for the DOE-JAERI Collaborative program in Development of Improved Components for the Fuel Cleanup System of the Tritium Systems Test Assembly" was completed in Nov. 1988. The Annex III was then extended for one year for additional testing that was proposed and agreed in the Sterring Committee meeting.

The paradium diffuser has been tested with methane and carbon monoxide as assumed impurities in the plasma exhaust. Tritium permeation through the primary containment of the diffuser to the vacuum jacket was measured as a function of temperature. The diffuser has been operated at 150°C with a tritium-impurity mixture. This test will give long-term effect of ^{3}He that generates in the metal.

The electrolysis cell has been tested with tritiated water in the presence of impurities such as carbon dioxide. It was proved that the cell can be used with CO_2 impurity. Practical processing of impurity-tritiated water mixture has been tested with the cell. In this test, gaseous mixture was processed in batch operation of the apparatus and tritium was successfully recovered. Long-term operation of the cell was tried.

5.1.2 The experiment of the fuel cleanup system

The experimental apparatus of the Fuel Cleanup System that had been installed in the TPL in 1987 fiscal year was operated with large amount of tritium in July, after a series of non-tritium operations. Nitrogen and methane were continuously supplied in the 3 days operation as simulated impurity in the plasma exhaust. Tritium of approximately 500,000 Ci in total was continuously processed by the catalytic reactor-cold traps-electrolysis cell train and recovered tritium and tritium free species were separated. Figure V.5-1 shows the example of the efficiency of the cold traps and the electrolysis cell. In this run, integrated loop was successfully operated and all the components were proved to work correctly. However, some problems on the pressure and flow control were found to need improvement to optimize and stabilize the system. Minor troubles have also been found.

Late in this fiscal year, the apparatus and then the glove box were decontaminated so that major mechanical and electrical modification on the apparatus can be conducted. Cold traps and flow/pressure controller

were replaced. Improvement of the stability of the loop by these modification will be examined in the 1989 fiscal year.

5.1.3 Hydrogen isotope separation

Preliminary tests of the experimental apparatus for hydrogen isotope separation installed in a glove box of the TPL have been performed with H-D system. The apparatus consists of two columns differing in inner diameters, and separate hydrogen isotope mixture with tritium up to 10^4 ci. Useful information in the operational problems such as control methods of column pressures and liquid levels in the reboilers was obtained by the above-mentioned cold tests. The operational procedure of the apparatus was also established before proceeding to experimental studies using tritium. Tritium run will be performed in the next fiscal year.

5.1.4 Demonstration study of fusion fuel system by the use of large amount of tritium (Japan-US collaboration of TSTA)

Under the frame-work of Annex IV to the US/Japan Implementing Arrangement for the Development of Fusion Energy, the demonstration study of fusion fuel system was continually performed by using the TSTA. The TSTA is composed of LIO (tritium load-in/out system), UTB (uranium tritide storage and supply system), FCU (fuel cleanup system), ISS (hydrogen isotope separation system), TP (gas transfer, mixing and pumping system), and safety systems such as the TWT (tritium waste treatment system)[1]. To demonstrate functions of the above-mentioned major process such as impurity removal in the FCU and H-D-T and ^3He separation in the ISS, full loop operation tests were carried out with 100g-level tritium. Impurities (N_2 and CH_4) injected into the process loops were successfully removed by the FCU, and no cryogenic plugging of the ISS or the FCU was observed during the loop operation. The ISS was operated in a stable mode during the loop operation. Demonstration of enriching tritium and withdrawal of H_2, D_2, T_2, and ^3He was fully achieved as primary objectives of these full loop tests.

Experimental studies using two-column or four-column cascades in the ISS were performed to obtain engineering data of practical scale column cascades. The HETP (height equivalent to theoretical plate) values (5 cm) previously determined for experimental column were substantiated for all the columns in the ISS. Figure V.5-2 shows an example of comparison between the experimental observation for composition distribution

within the lead column of the ISS and the calculational results under the assumption that HETP is constant with the column height. The composition distribution calculated is in agreement with experimental observation, and it is confirmed that the HETP depends little on the column height. The effect of helium on separation characteristics of the column cascades was also studied in detail varying the concentration of helium in the feed stream of the lead column in the ISS.

5.1.5 Tritium-material interactions and analysis

We have developed an apparatus to carry out tritium implantation/permeation experiments for candidate first-wall materials. The apparatus is equipped with an ion source which generates a low energy triton (T^+) beam with high intensity and high atomic ion percentage. The ion source manufactured for the tritium implantation/permeation experiments is modification of the quartz capillary ion source developed by Isoya and Inoue for the injector of the Lamb-shift polarized ion source.

Preliminary tests of the ion source were carried out using deuterium gas. Ion beam current was measured by a target (Faraday cup, 20 mm in diameter). Ions (D^+, D_2^+, D_3^+) were extracted from the exit hole of the quartz capillary tube at an energy of 400 eV introduced to a mass analyzer and detected by a Faraday cup.

Ion beam current: Figure V.5-3 shows the relationship between the ion beam energy and the ion beam current on the Faraday cup placed at the position of 55 mm from the ion beam exit hole. At high ion energy above 400 eV, the ion beam current decreased gradually with the energy decreasing. However, below 400 eV, it decreased steeply. The distinguishing change in the ion beam current is due to the space-charge effect. The ion beam is spread out and the current density on the target would decrease.

Atomic ion percentage: Figure V.5-4 shows the percentage of each deuterium ion species (D^+, D_2^+, D_3^+) in the extracted ion beam as a function of the anode current. The deuteron percentage takes the larger value for the larger arc current and reaches 83%. Figure V.5-5 shows the relationship between the percentage and the deuterium gas pressure in the ion source chamber. The anode current is fixed at 10 A. The deuteron percentage takes a maximum at around 1×10^{-2} Torr where the output intensity takes a maximum.

Development of a system for in-line analysis of plasma exhaust gas

by Raman and IR spectroscopy has undertaken. On the fusion fuel cycle, chemical composition, concentration and isotope ratio of the process gas should be monitored. Spectroscopic technique mentioned above is available for the in-line analysis of the process gas. Raman scattering spectroscopy has been applied to measure the concentration of H_2, HD, D_2 and CH_4 and distinguish the species of the deutrated methanes (CH_3D, CH_2D_2, CHD_3, CD_4), which is made by isotope exchange between D_2 and CH_4 using Pt/Al_2O_3 catalyst. Figure V.5-6 shows a spectrum of the mixed gas of D_2 and CH_4 after equilibrating.

5.2 System analysis

- Blanket Technology -

The aqueous self-cooled blanket concept has been developed in some fusion nuclear reactor designs. This concept is based on dissolving lithium salt in the water coolant. It is expected that the inherent simplicity of this concept will result in a highly reliable, safe, and economically attractive breeding blanket. However, the concept has some problem areas requiring special investigations. Water chemistry, such as radiolysis of the solution and corrosion of the structural materials, etc., is of particular concern.

Preliminary study for the radiolysis was carried out to estimate the formation rates of the gaseous products. The results show that G-value depends on many factors, such as radiation type, temperature and pH etc., and its dependency on them is not so clear. In nitrate solution, which is a candidate solution of lithium salt, products by radiochemical reaction area,

$$H_2O = H_2,\ H_2O_2,\ - - -$$

$$NO_3 = N_2,\ O_2,\ NO_2,\ - - -$$

Figure V.5-7 shows production rate of hydrogen and nitrogen calculated under assumptions, i.e. 1000 MW fusion power, 100% availability, and unity of tritium breeding ratio. G-values were substituted by those of alpha radiation experimentally obtained for hydrogen and nitrogen by various types of radiation source, and other effects on radiolysis mentioned above were not assessed in the estimation. The results show that gas production rates are affected by nitrate ion concentrations, and that these values are so large that the gaseous products should be appropriately treated to prevent a hydrogen explosion as well as rapid reduction of nitrate concentration. To evaluate the feasibility of this

blanket concept, further study including experimental investigations would be needed.

Beryllium is a feasible neutron multiplier to get higher tritium breeding ratio in the blanket. Therefore, various kinds of R&D on the properties of beryllium, such as compatibility with structural materials, reactivity with water, etc., should be studied for fusion reactor application. Also the beryllium handling technology should be established, because some beryllium compounds are very hazardous. Beryllium handling equipment and facility were designed to investigate these issues.

5.3 Tritium handling technology

In 1988 fiscal year, successive three times oversea transports from ORNL to JAERI (each 2.5 g of tritium) have been conducted in April, July and August. To provide the tritium equivalent to the dispersed and decayed amounts, 6 g of additional tritium gas was also purchased from ORNL and the transport of each 3 g has been performed in February and in March 1989. All the tritium has been loaded on the storage beds in the Tritium Storage System (TSS). In the storage operation, TSS worked well and approximately 99.5% of tritium gas was transferred to the beds. Two Zirconium Cobalt beds have been installed in the TSS, and a new strategy for 60 g tritium handling in the TPL in a few years later was built up to be served for the development of basic engineering study on tritium processes.

The Vacuum Pumping System (VPS), Effluent tritium Removal System (ERS), Glovebox gas Purification System (GPS) and Air Cleanup System (ACS) were fully in tritium service in this period. Several hundreds curies tritium exhausted from the TSS and FCU was processed by the ERS. Decontamination factor of the ERS was estimated to be higher than 10^6, although small amount of tritium release caused by the self-radiolysis of tritiated water was observed when large amount of tritium was stored as absorbed water in the ERS molecular sieve beds. Tens of millicuries were processed in the GPS. The ACS was used for the handling of tritiated water and the ventillation for the decontamination and maintenance of the contaminated devices. To date, all the safety systems in the TPL were thus operated with tritium and proved to work correctly and safely. Some modification and maintenance of contaminated components were conducted with little exposure. Procedure for operation of the systems and handling of tritium are being modified to improve and to minimize

tritium release.

Reference

[1] Anderson J.L., et al., Fusion Technology, 14(1988) 412.

6. High Heat Flux Technology

6.1 Introduction

Since 1988, Plasma Heating Laboratory has been organizing the R&D efforts on plasma facing/high heat flux materials and components for FER/ITER. The efforts include design and construction of new electron beam test facility called JEIBS (JAERI Electron Beam Irradiation Stand), high heat flux tests of materials and small-scale models of a first wall using a hydrogen ion beam in PBETF (Particle Beam Engineering Test Facility), high heat flux tests of carbon-based materials using an existing electron beam facility at industries, high heat removal experiments, and also design-oriented analytical studies of divertor plates and first walls for FER/ITER. Due to the good collaboration with the design team and other laboratories, R&D's are being well promoted.

6.2 R&D's on plasma facing materials and components[1]

6.2.1 High heat flux experiments of CFC materials

Carbon-fiber-carbon (CFC) materials have many attractive properties as plasma facing materials for both JT-60 U and next step machines. The plasma facing materials are repeatedly attacked by extremely high heat flux caused by plasma disruption. Since erosion loss and/or fracture due to the high heat flux to the high heat flux limit the lifetime of the materials, durability against the intense thermal shock is one of the essential characteristics required for the plasma facing materials. Hence we have started to perform high heat flux tests on newly developed CFC's such as CX-2002U, JC/C, MFC-1, pcc, 3DC/C. A high heat flux up to 380 MW/m^2 with a duration of 20 - 200 msec is imposed on the test surface using an electron beam facility at KHI. Weight loss of the test pieces is plotted against absorbed energy in Fig.V.6-1. CX-2002U, which has the highest thermal conductivity among the materials tested, is found to have best performance against the thermal shock.

6.2.2 Thermal shock tests of stainless steels

The stainless steel is a structural material of the first wall in

tritium release.

Reference

[1] Anderson J.L., et al., Fusion Technology, 14(1988) 412.

6. High Heat Flux Technology

6.1 Introduction

Since 1988, Plasma Heating Laboratory has been organizing the R&D efforts on plasma facing/high heat flux materials and components for FER/ITER. The efforts include design and construction of new electron beam test facility called JEIBS (JAERI Electron Beam Irradiation Stand), high heat flux tests of materials and small-scale models of a first wall using a hydrogen ion beam in PBETF (Particle Beam Engineering Test Facility), high heat flux tests of carbon-based materials using an existing electron beam facility at industries, high heat removal experiments, and also design-oriented analytical studies of divertor plates and first walls for FER/ITER. Due to the good collaboration with the design team and other laboratories, R&D's are being well promoted.

6.2 R&D's on plasma facing materials and components[1]

6.2.1 High heat flux experiments of CFC materials

Carbon-fiber-carbon (CFC) materials have many attractive properties as plasma facing materials for both JT-60 U and next step machines. The plasma facing materials are repeatedly attacked by extremely high heat flux caused by plasma disruption. Since erosion loss and/or fracture due to the high heat flux to the high heat flux limit the lifetime of the materials, durability against the intense thermal shock is one of the essential characteristics required for the plasma facing materials. Hence we have started to perform high heat flux tests on newly developed CFC's such as CX-2002U, JC/C, MFC-1, pcc, 3DC/C. A high heat flux up to 380 MW/m^2 with a duration of 20 - 200 msec is imposed on the test surface using an electron beam facility at KHI. Weight loss of the test pieces is plotted against absorbed energy in Fig.V.6-1. CX-2002U, which has the highest thermal conductivity among the materials tested, is found to have best performance against the thermal shock.

6.2.2 Thermal shock tests of stainless steels

The stainless steel is a structural material of the first wall in

FER/ITER. A bare first wall without low-z protection tiles is preferred in terms of structural simplicity and low tritium retention. In the bare wall, however, an extremely high heat flux caused by plasma disruption directly hits the metal surface. Impact of the high heat flux on stainless steel is experimentally examined with an intense hydrogen beam. The heat flux is varied from 80 - 220 MW/m^2 with a heating duration ranging from 60 - 250 ms. The sample used is either a circular disk of 120 mm in diameter of a square plate of 95 mm × 95 mm. More than a hundred test pieces have been subjected to a large thermal shock with the beam. Topography of the resolidified surface after heating exhibits two different features; one is rough as seen in Fig.V.6-2(a),(b),(c) (SS316, SS304, PCA) and the other is smooth in Fig.V.6-2(d) (SS316F). Investigations are being continued to identify the cause to bring about the difference.

6.3 JAERI electron beam irradiation stand (JEBIS)

Construction of JEBIS has completed in March 1989. This stand can continuously produce electron beams of 4 A at energy of 100 keV. Major performance of the stand is summarized in Table V.6-1 and the schematic is shown in Fig. V.6-3. Significant features of JEBIS are as follows;

(1) A magnetic multipole ion source is utilized for an electron gun. The dimensions of this ion source are 14 cm in diameter by 30 cm long, and electrons are extracted from multi-aperture acceleration grids. Therefore, a large irradiation area can be easily obtained by changing a number of grid apertures.

(2) High frequency (5 kHz) inverters are utilized for an acceleration power supply for the first time in the world.

(3) A test sample holder provides a capability of easy replacement of test pieces without breaking vacuum of a test chamber.

An overall performance test is just under way, and an electron beam of 0.4 A, 20 keV has been obtained.

6.4 Thermal analysis of plasma facing components

Plasma facing components are exposed to steady state high heat flux from the plasma. Especially, the divertor plate is anticipated to receive a peak heat flux of as high as 17 MW/cm^2. A separatrix sweeping technique is expected to effectively reduce heat flux on the divertor plate. Table V.6-2 shows typical results for the various conditions.

Sweeping with large amplitude is preferred to that with high frequency for the divertor plate. Thermal analysis of the first wall has been made with HEATING-6VP. The first wall with a radiation cooled armor is found to withstand the heat flux of 0.4 MW/m^2.

Reference

[1] Akiba M., et al., Proc. 13th Symp. on Fusion Engineering, to be published.

7. CAD/CAE System

CAD (Computer Aided Design) and CAE (Computer Aided Engineering) systems were introduced for the design work of ITER in August, 1988. The CAD system is a well-known general purpose mechanical CAD system CADDS developed by the Computervision Corp. It has capabilities of wire-frame modeling, advanced surface modeling, solid modeling, three-dimensional graphics, data extraction/merge, interference check, area/volume calculation, architectural application, piping design application, structural design application and electrical instrumentation application. The CAE system is based on a general purpose mechanical CAE system I-DEAS developed by the SDRC Corp. It is composed of a solid modeler (GEOMOD), a finite element pre/post processor (SUPERTAB) and a finite element solver (Model solution). Since the interface programs between I-DEAS and EDDY-J (a finite element eddy current analysis code) and between I-DEAS and ADINA (a finite element temperature and stress analysis code) were developed, large scale computations by EDDY-J, ADINA and MSC/NASTRAN codes can be performed on a main frame computer FACOM M-780 by transferring large data through Ethernet LAN (Local Area Network) system.

Table V.2-1 Achievements in the first experiment of the DPC-U1 and -U2

	Achieved Value	Condition	Final Goal
High Voltage insulation	20 kV	No breakdown Leak current 3 μA	
Pressure-proof	1.3 MPa (at room temp.)	Equivalent to 5 MPa at 4 K	
Leak	2 x 10^{-9} Acc/s	No cold leak	
Cooldown	123 hours	Total weight 22 tons	Reduction of cooldown time is possible
DC operation	30 kA 5.2 T 11 MJ	Achieved individually by DPC-U1 and -U2	30 kA, 7 T and 30 MJ in simultaneous charge
Pulse operation	30 kA / 0.75 s 7 T/s	Achieved by single coil	To 7 T in 1 s in simultaneuos charge.

Table V.2-2 General requirements of the toroidal field coil from the FER

Maximum Field	12	T
Overall Current Density	12-15	A/mm^2
Winding Current Density	30-40	A/mm^2
Rated Current	30	kA
Margin of Critical Current	2	
Maximum Dump Voltage	20	kV
ENVIRONMENT		
Nuclear Heating Rate	1	mW/cc
Dose Limit for Insulator	20	MGy
Pulsed field	20 T/s - 100 ms	
COIL CONFIGURATION		
Supporting Conditions	Wedging	
Insulation System	Epoxy impregnation	
CONDUCTOR		
Pulsed Loss Time Constant	< 100	ms
Stability Margin	50-100	mJ/ccst*
Hot Spot Temperature	100-150	K
SUPERCONDUCTING MATERIAL	$(NbTi)_3Sn$	
Jc at 12T-4.2K	700	A/mm^2
Critical Axial Strain	0.7	%
Critical Transverse Pressure	50	MPa
STRUCTURAL STEEL	JCS	
Yield Strength	1.2	GPa
Tensile Strength	1.6	GPa
Fracture Toughness	200	MPa/m
COOLING		
Helium Inlet Temperature	4.0-4.5	K
Helium Inlet Pressure	6-10	bar
Maximum Inner Pressure at Insulation Break	50	bar

Note : * mJ/ccst means the energy input averaged by the volume of strands.
: This table dose not consider the Advanced Disk type conductor and Nb_3Al superconductor.

Table V.2-3 Major parameters of the tested turbo-expander and the testing condition

ITEMS		PARAMETERS	
Journal bearing		Tilting pad type gas bearing	
Thrust bearing		Spiral grooved gas bearing	
		Design value	Testing condition
Flow rate	(g/s)	355	60
Inlet temperature	(k)	18	45
Inlet pressure	(atm)	6.18	2.04
Pressure ratio		5.81	1.65
Revolution	(rps)	1122	1122

Table V.6-1 Major characteristics of JEBIS

Acceleration Current	max. 4 A
Acceleration Voltage	20 to 100 keV
Pulse Duration	1 ms to continuous
Heat Flux	max. 1000 MW/m^2
Type of Electron Source	Magnetic Multipole Ion Source
Size of Grid Aperture	ϕ 0.7 cm
Number of Apertures	1,2, or 10
Rastering Frequency	10 to 1000 Hz
Rastering angle	max. ± 16 °
Irradiation Direction	Horizontal or Vertical
Irradiation Area	max. 30 cm x 60 cm

Table V.6-2 Temperature on the divertor plate for 2 separatrix sweeping cases

	Separatrix Sweeping			
	Frequency	Amplitude	Frequency	Amplitude
	0.1Hz	±30cm	0.3Hz	±10cm
CFC Surface	820°C		975°C	
CFC/Cu Interface	250°C		290°C	
Cooled Surface	145°C		172°C	

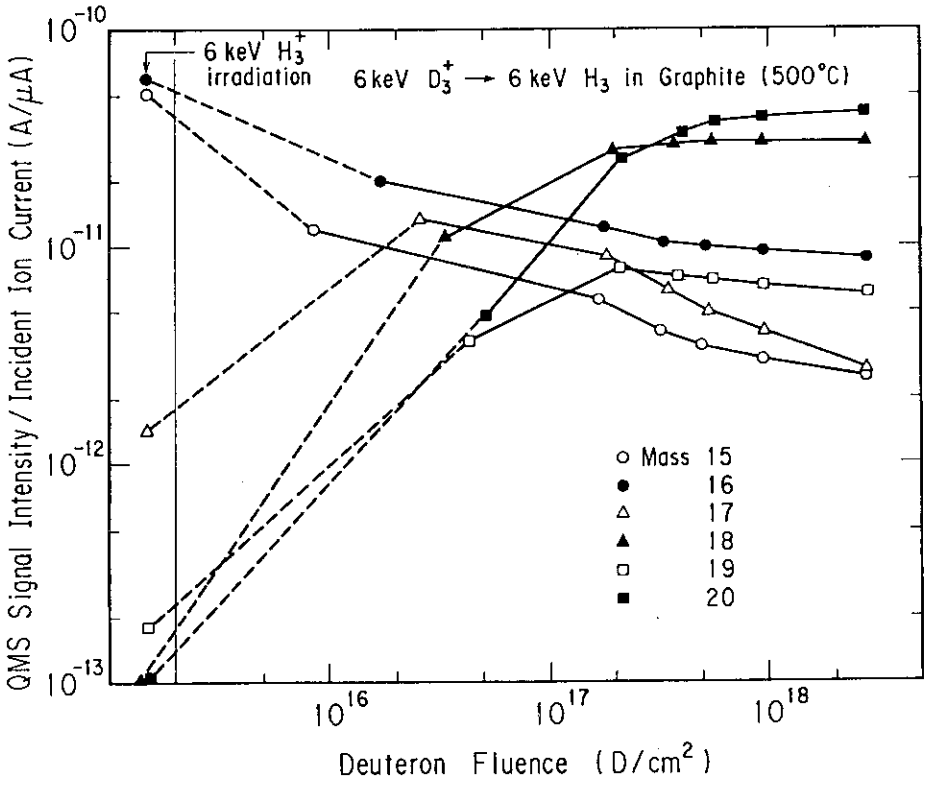

Fig.V.1-1 Deuteron fluence dependence of QMS signal intensities of mass 15 to mass 20 that can be deduced to hydro-dutero methane production from graphite target. The target was first bombarded with 6 keV H_3^+ ions until the steady methane production rate was obtained, and then subsequent bombardment of 6 keV D_3^+ ions was carried out at a target temperature of 500°C.

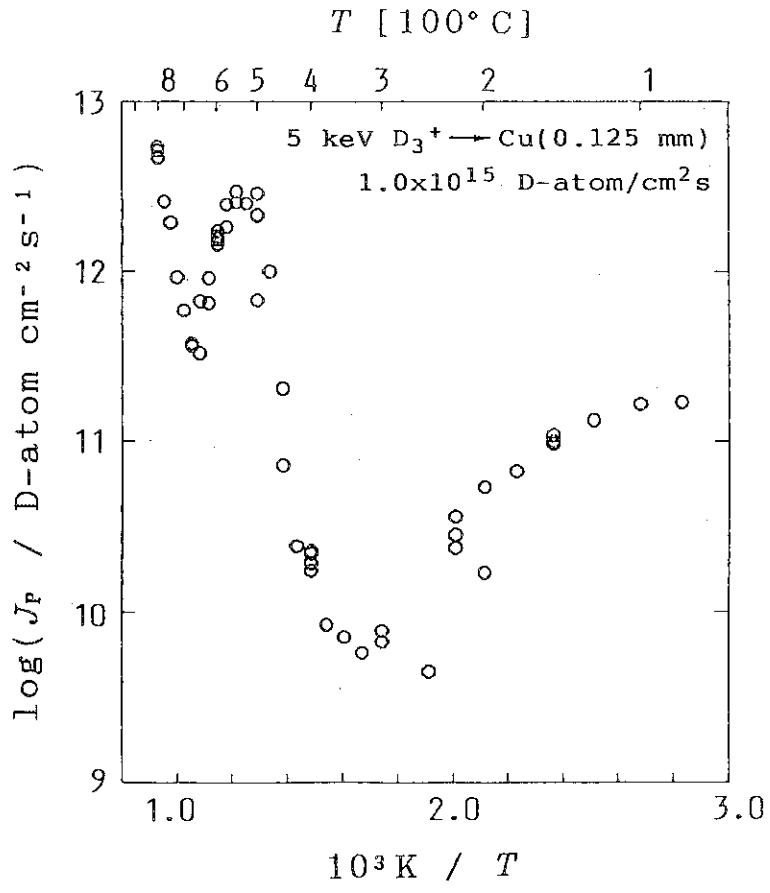

Fig.V.1-2 Temperature dependence of deuterium permeation flux Jp as a function of target temperature. The target was 0.125 mm thick Cu foil and the ion species is 5 keV D_3^+. The ion flux was 1.0×10^{15} D-atom/cm^2s.

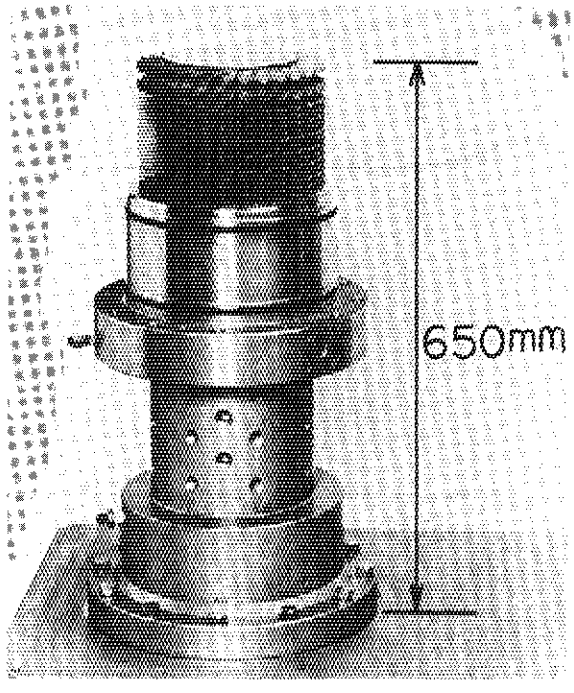

Fig.V.1-3 Whole view of the medium size ceramic turbomolecular pump.

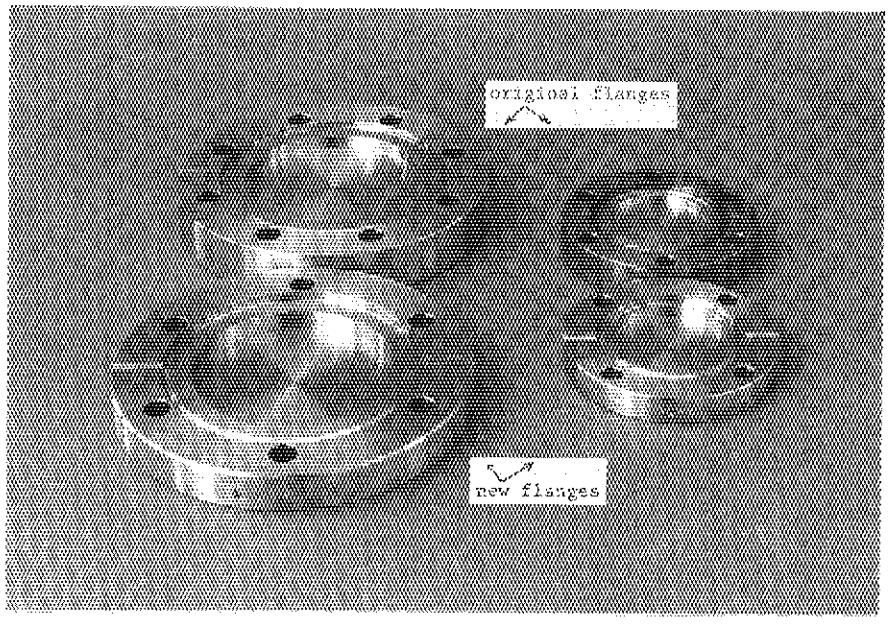

Fig.V.1-4 Comparison of new flanges and the original flanges of the same diameters.

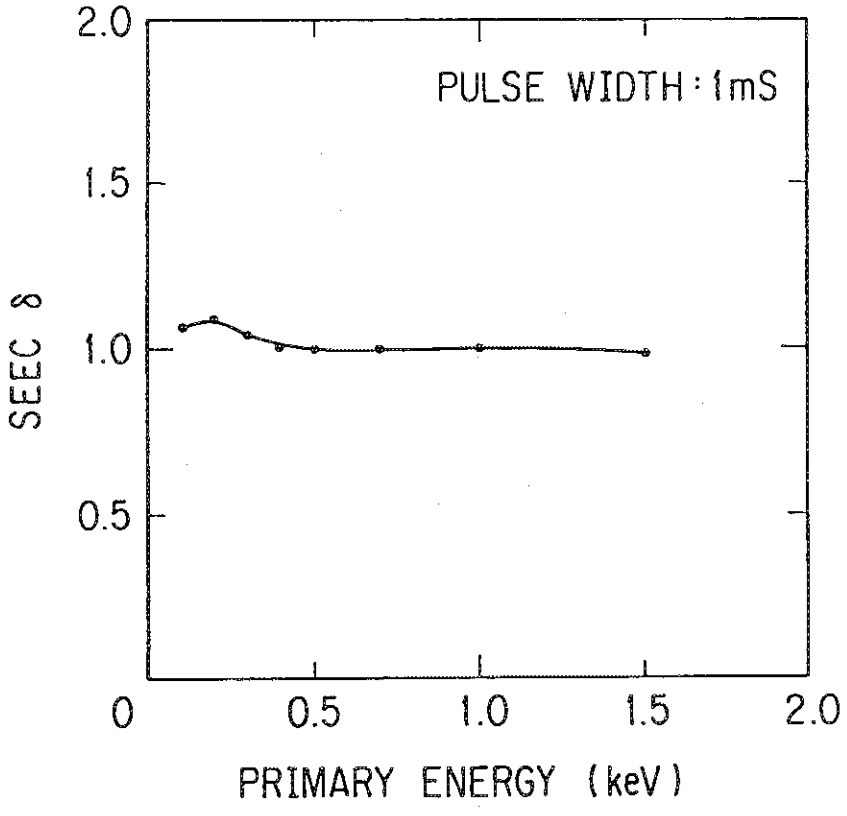

Fig.V.1-5 Secondary electron emission coefficient of aluminum nitride as a function of incident electron energy.

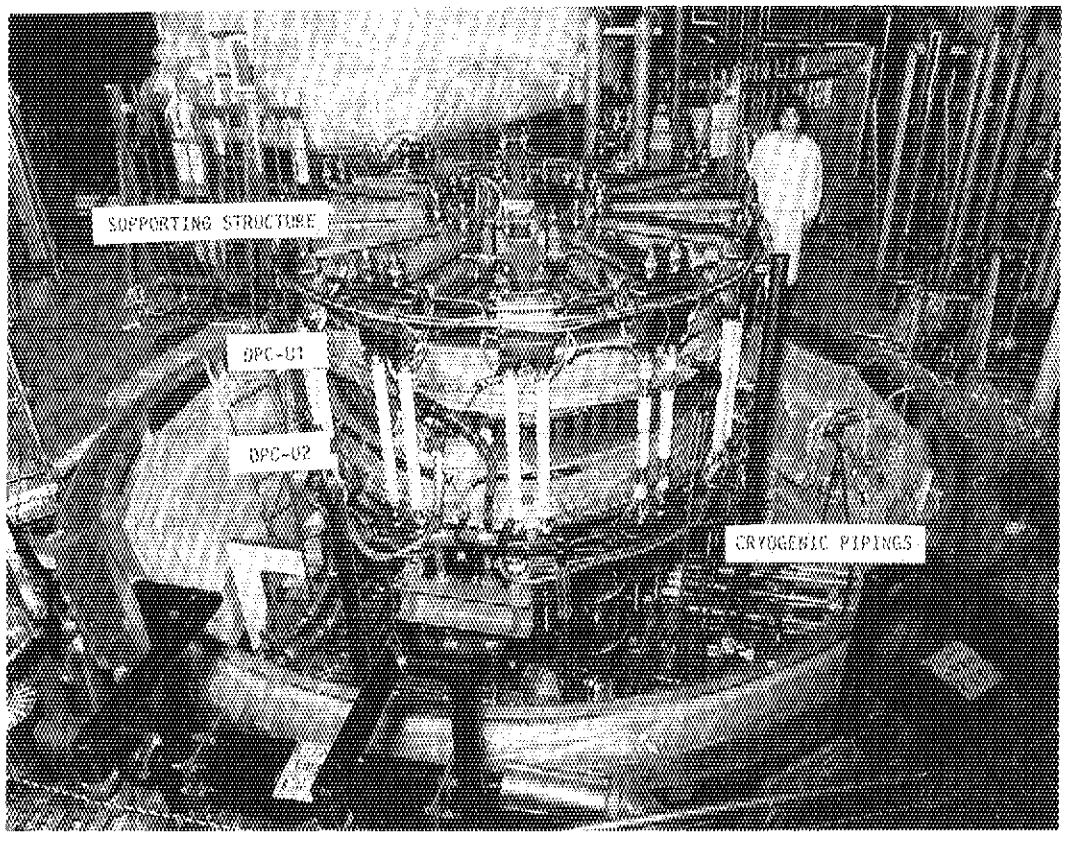

Fig.V.2-1 DPC-U1 and -U2 installed in the DPC facility at JAERI.

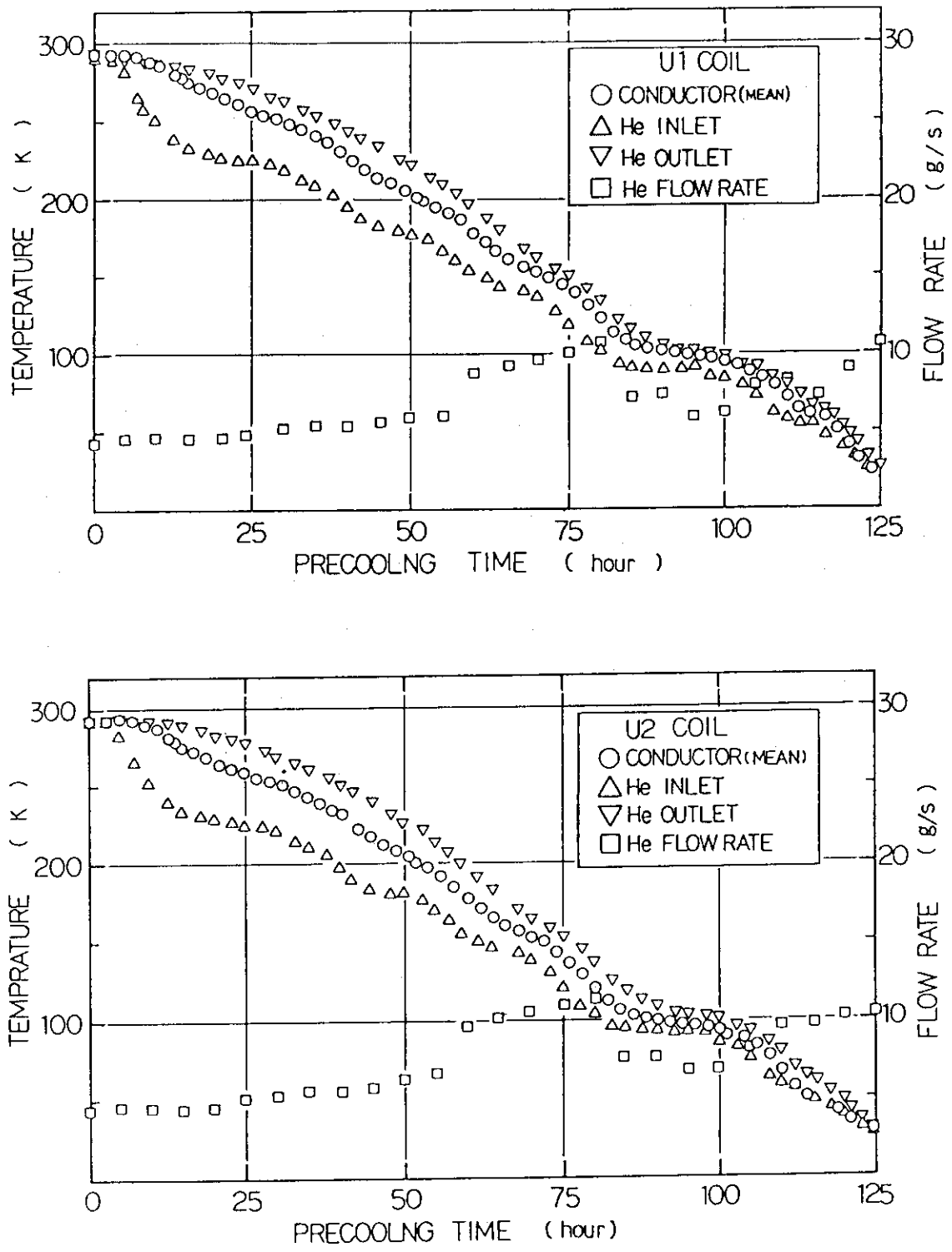

Fig.V.2-2 Cooldown characteristics of the DPC-U1 and -U2.

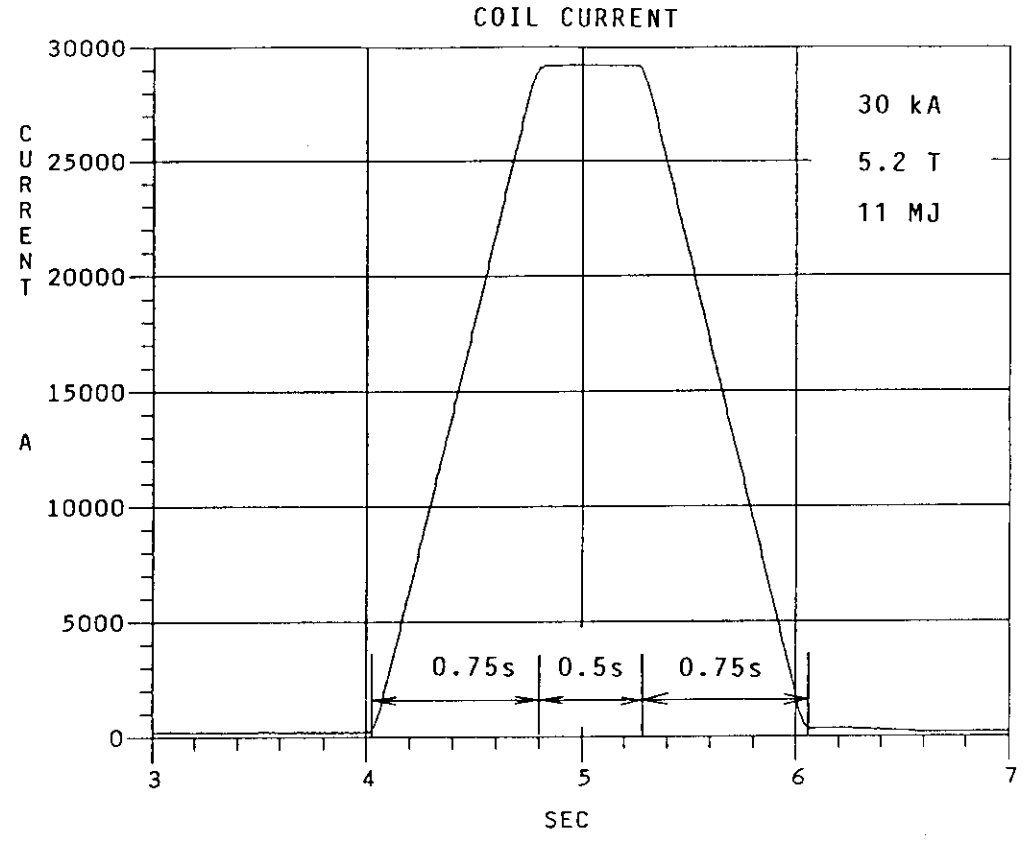

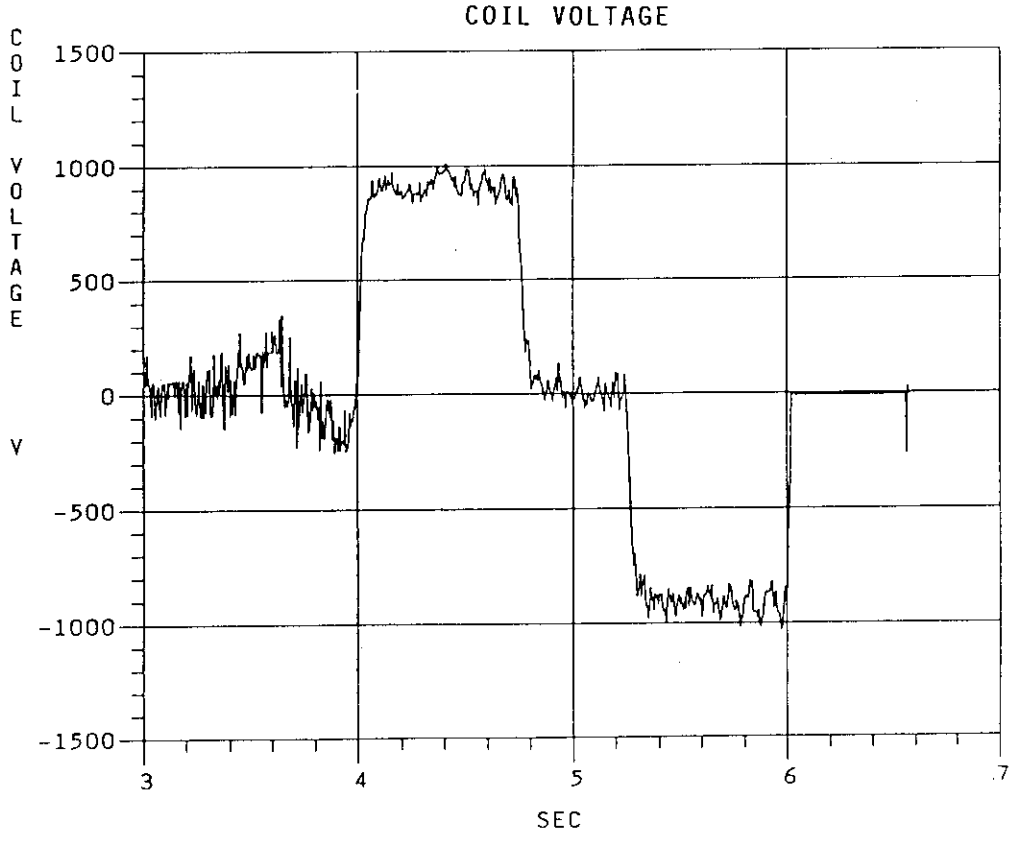

Fig.V.2-3 Pulse operation of the DPC-U2 by the JT-60 power supply. 7T/s was achieved at the coil terminal voltage of 900V.

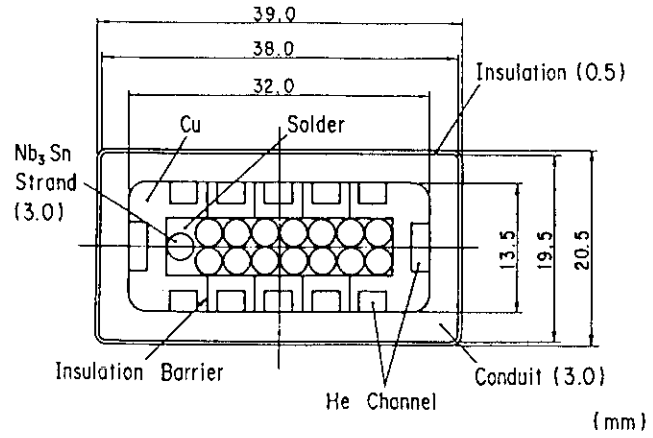

Fig.V.2-4 Cross-sectional view of the TMC-FF conductor.

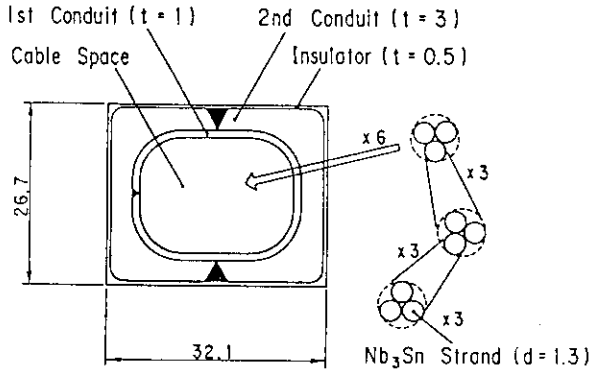

Fig.V.2-5 Cross-sectional view of the Preformed Armor type cable-in conduit conductor.

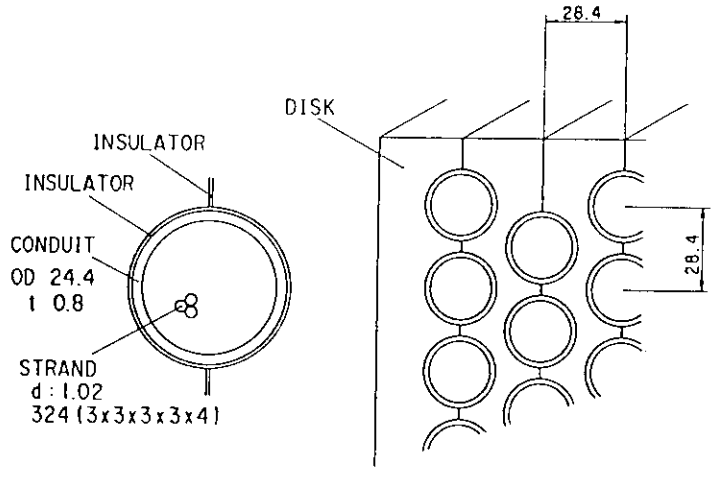

Fig.V.2-6 Cross-sectional view of the Advanced Disk type conductor and winding.

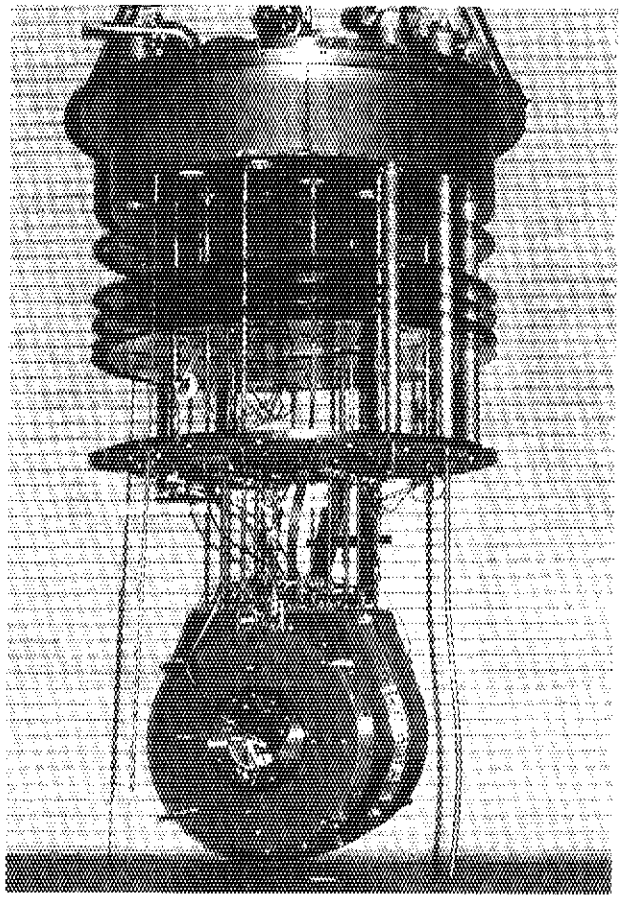

Fig.V.2-7 Developed large superconducting split coil system installed under the 2m-diameter flange.

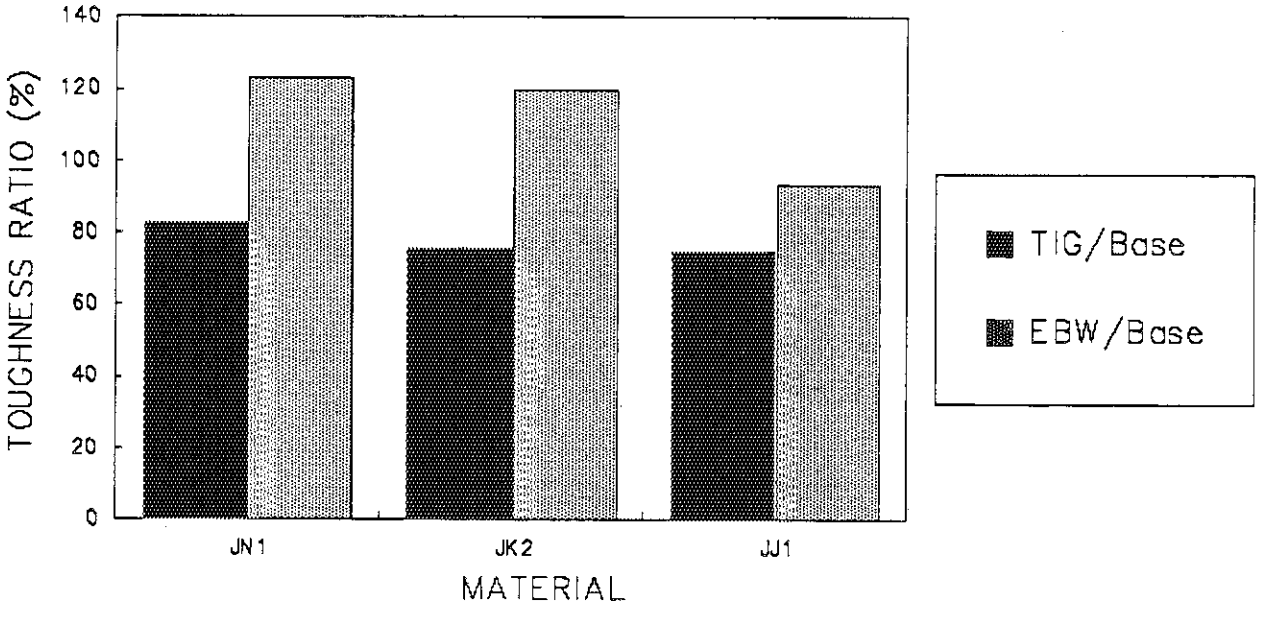

Fig.V.2-8 The ratio of the fracture toughness of welded joint to that of the base metal.

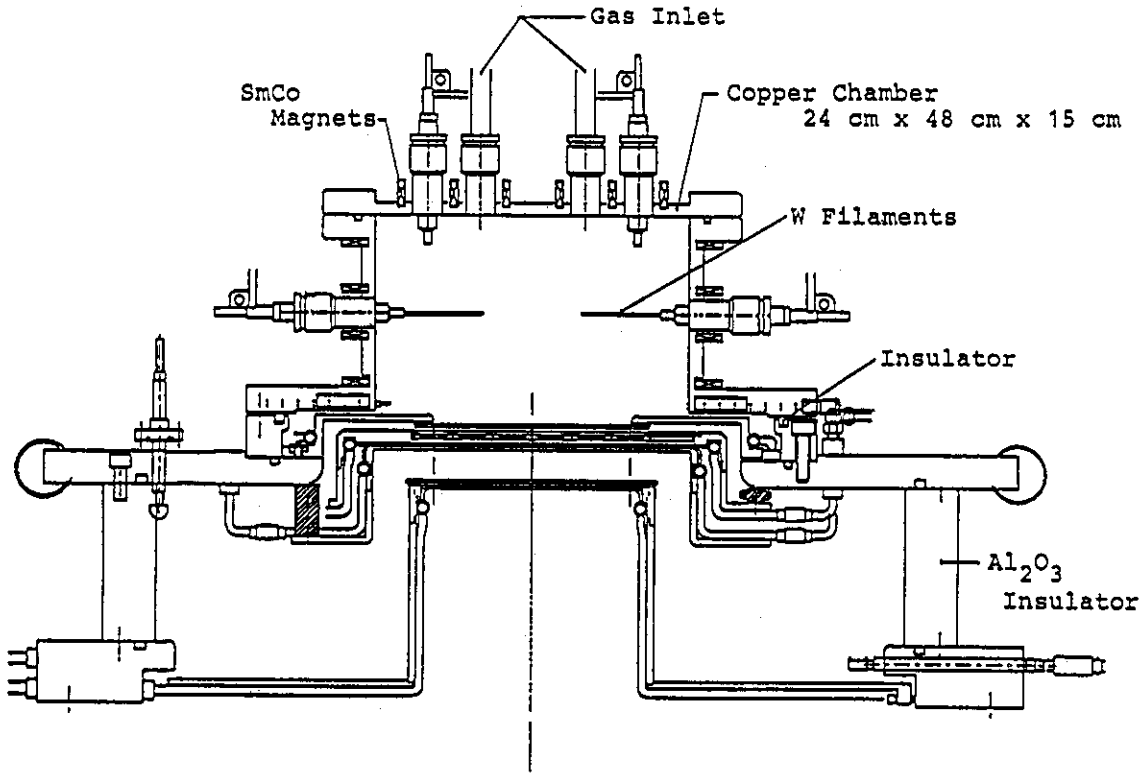

Fig.V.3-1 Cross-sectional view of the multi-ampere ion source.

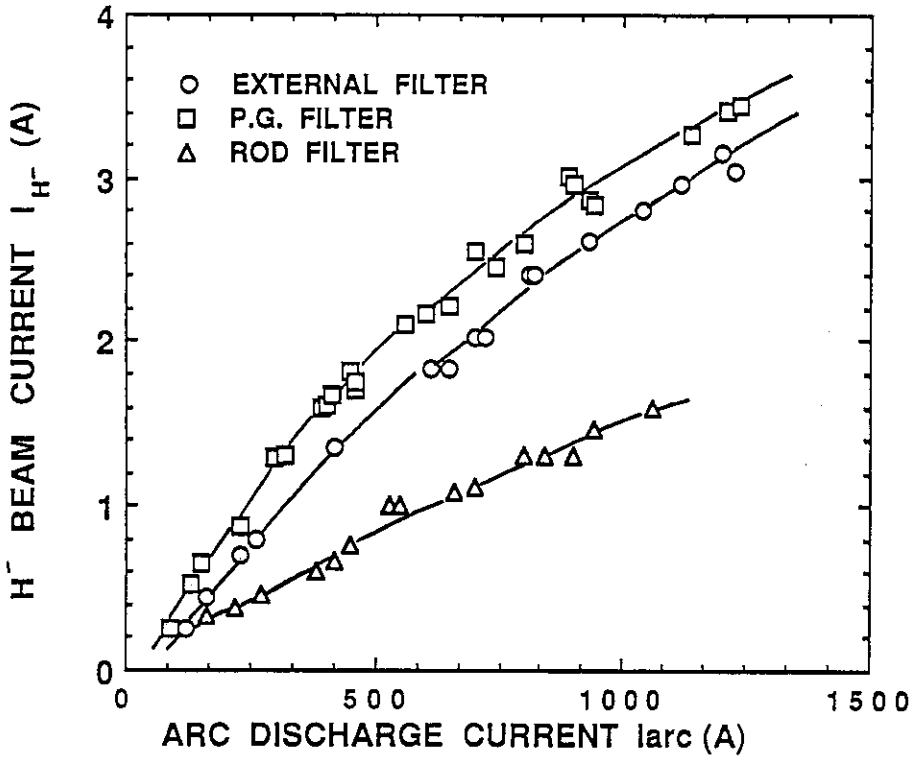

Fig.V.3-2 Dependence of the H^- beam current on the arc discharge current for three different magnetic filters.

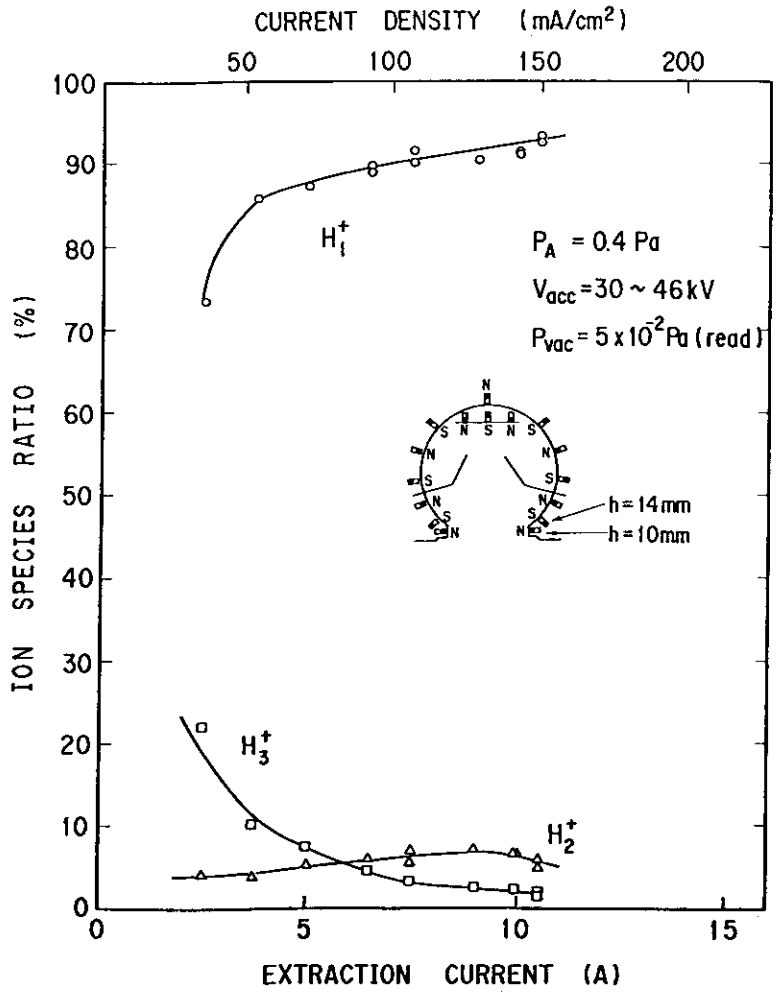

Fig.V.3-3 Proton yield of the hydrogen ion as a function of the extraction current.

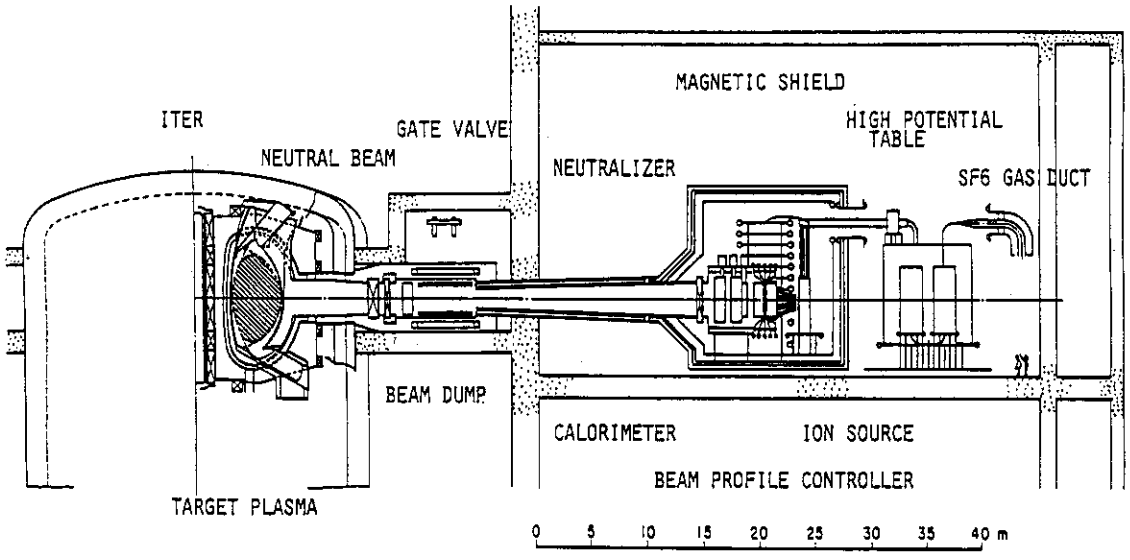

Fig.V.3-4 Conceptual design of 1 MeV/25 MW negative-ion-based neutral beam injector for ITER.

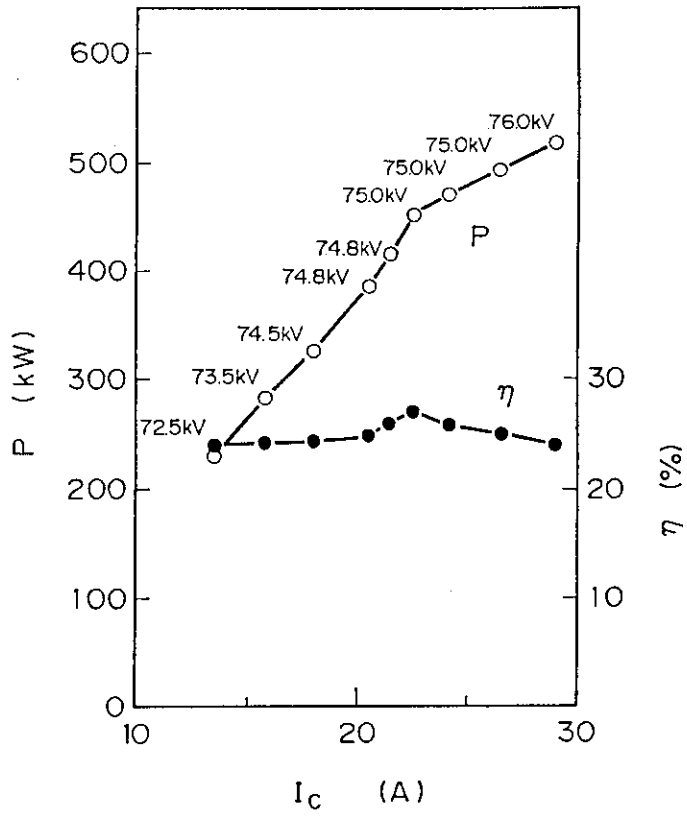

Fig.V.4-1 Output power P and efficiency η vs. collector current I_C of 120 GHz gyrotron.

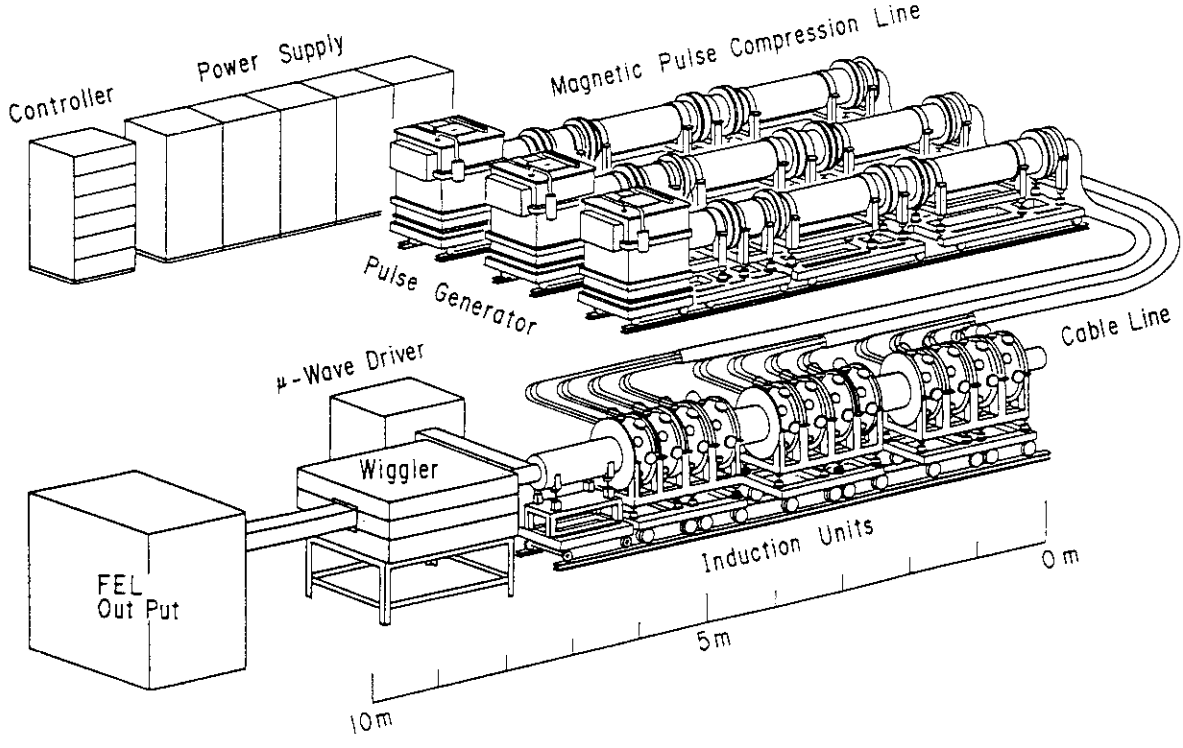

Fig.V.4-2 Picture of induction linac and free electron laser (FEL).

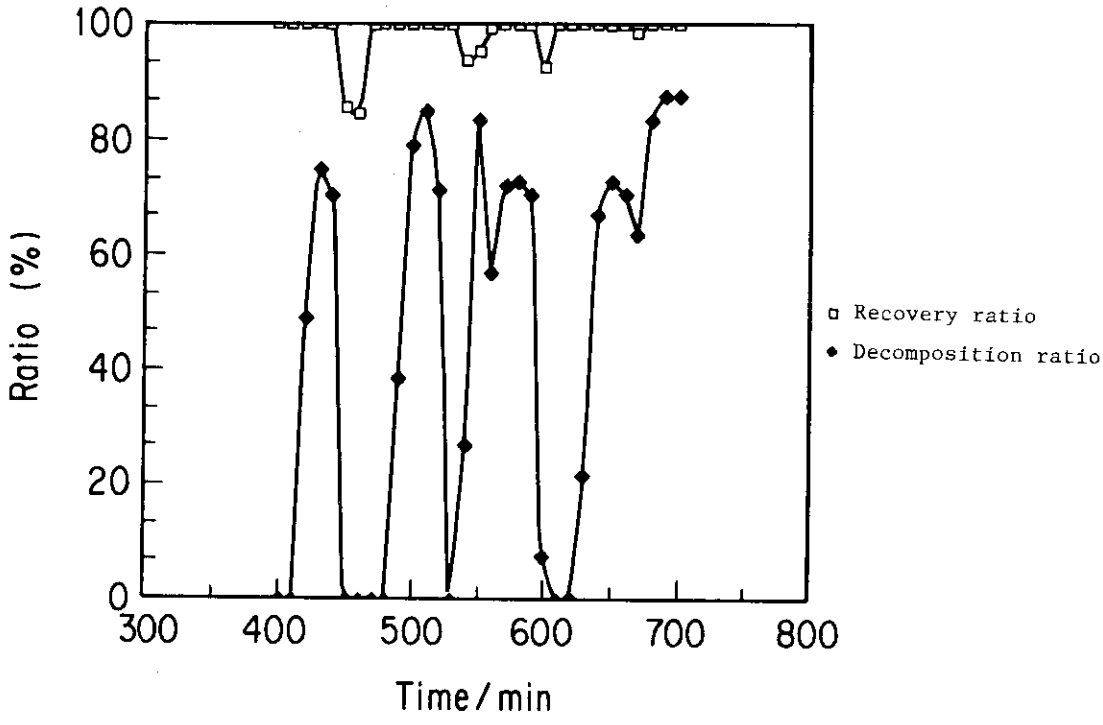

Fig.V.5-1 Water trapping efficiency of cold traps and water vapor decomposition efficiency of electrolysis cell.

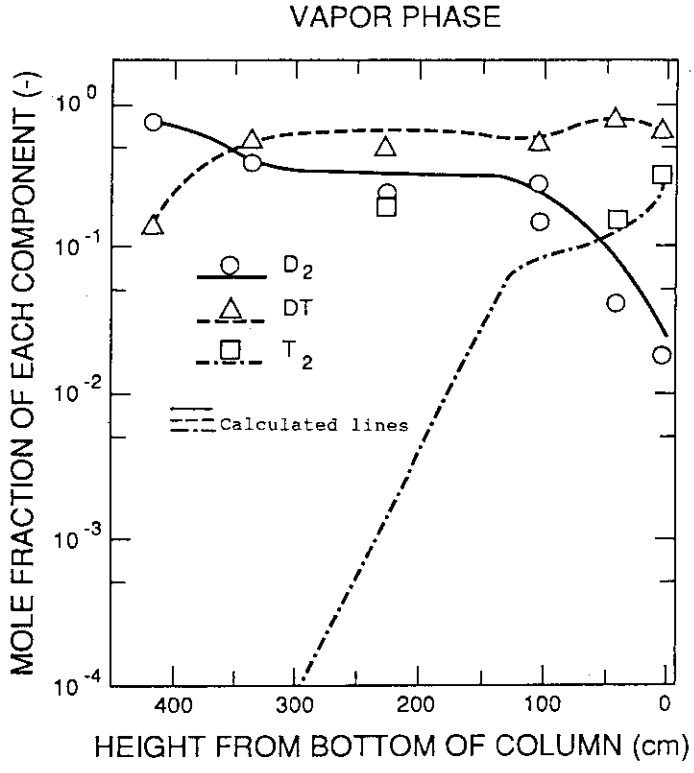

Fig.V.5-2 Comparison between experimental observation and calculational result for composition distribution within column.

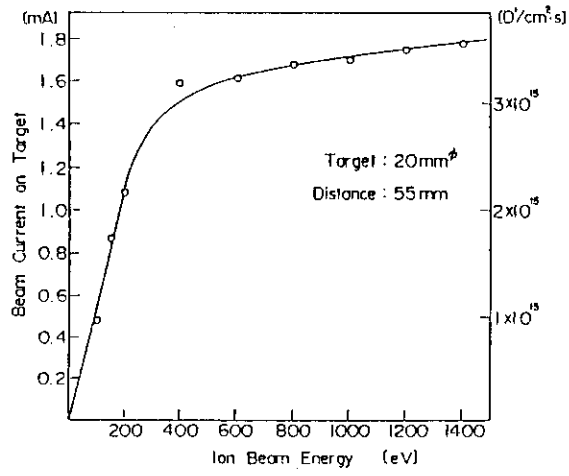

Fig.V.5-3 The relationship between ion beam energy and ion beam current.

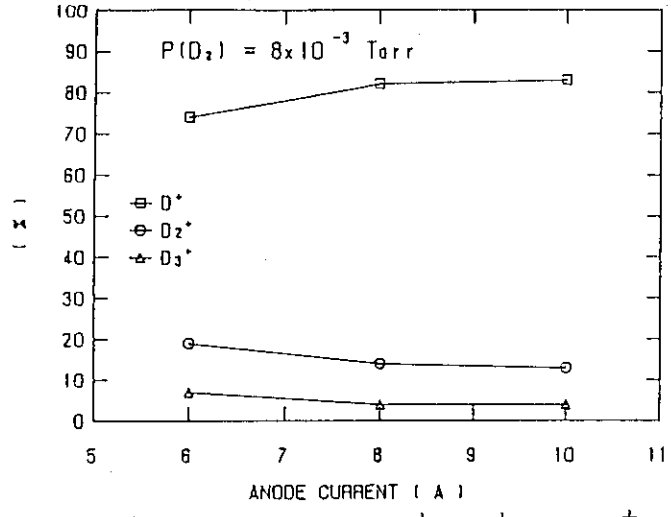

Fig.V.5-4 Percentage of D^+, D_2^+ and D_3^+ ions in extracted ion beam as a function of the anode current.

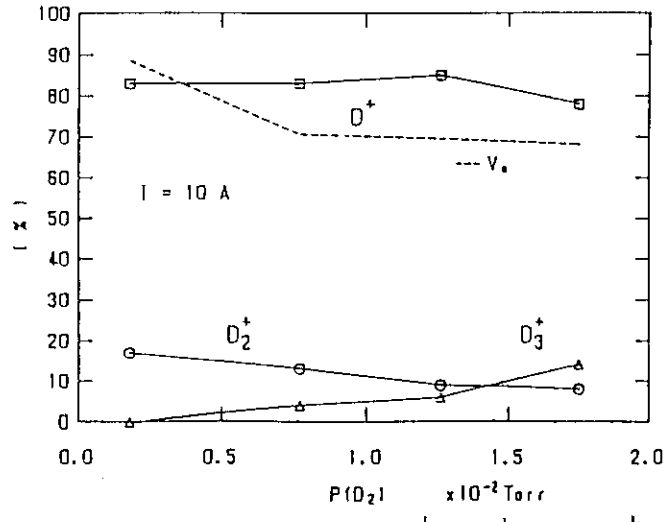

Fig.V.5-5 Percentage of D^+, D_2^+ and D_3^+ ions in extracted ion beam as a function of the deuterium gas pressure in the ion source chamber.

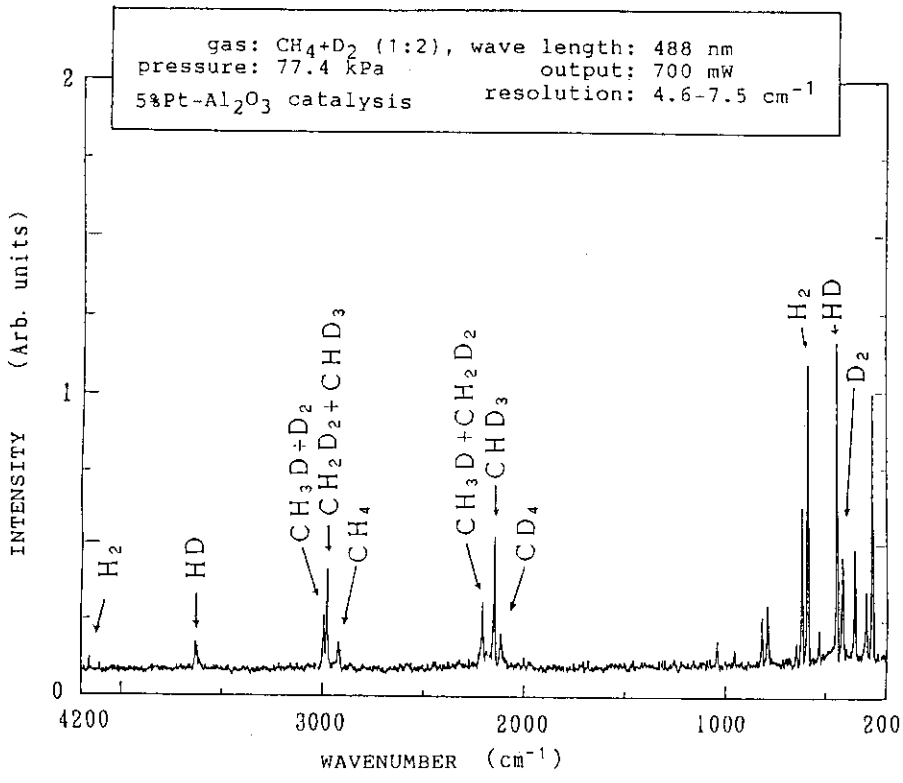

Fig.V.5-6 A spectrum of D_2 and CH_4 mixed gas after quilibrating.

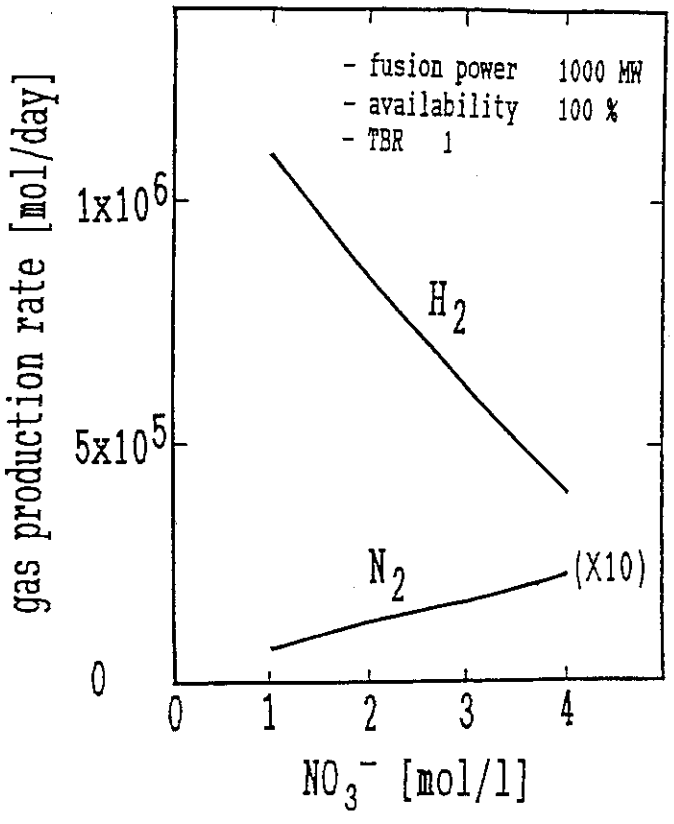

Fig.V.5-7 Gas production rate as a function of lithium nitrate concentration.

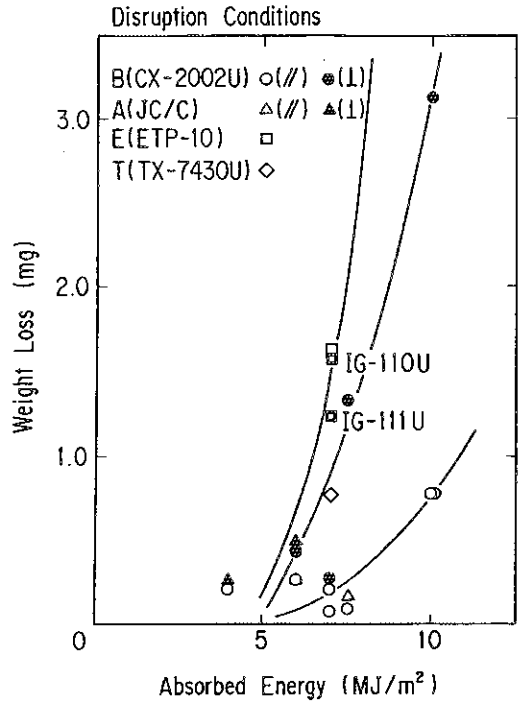

Fig.V.6-1 Relation of weight loss and absorbed energy for 4 test piecies.

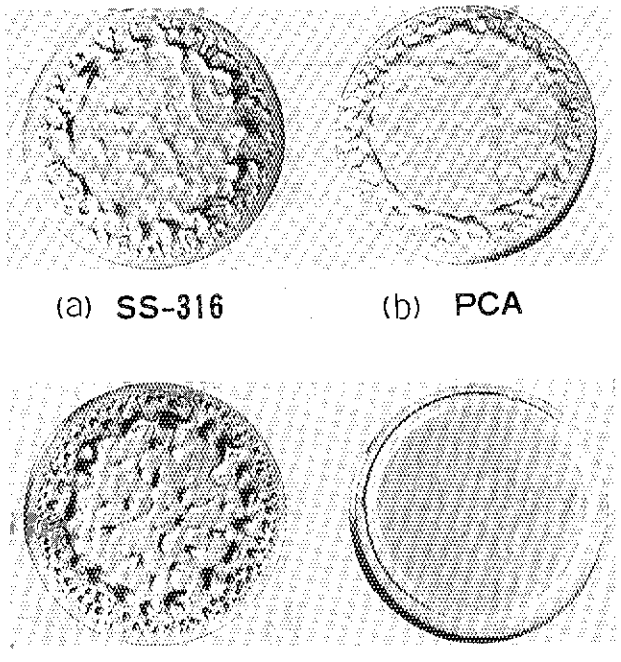

Fig.V.6-2 Features of resolidified surface of stainless steel.

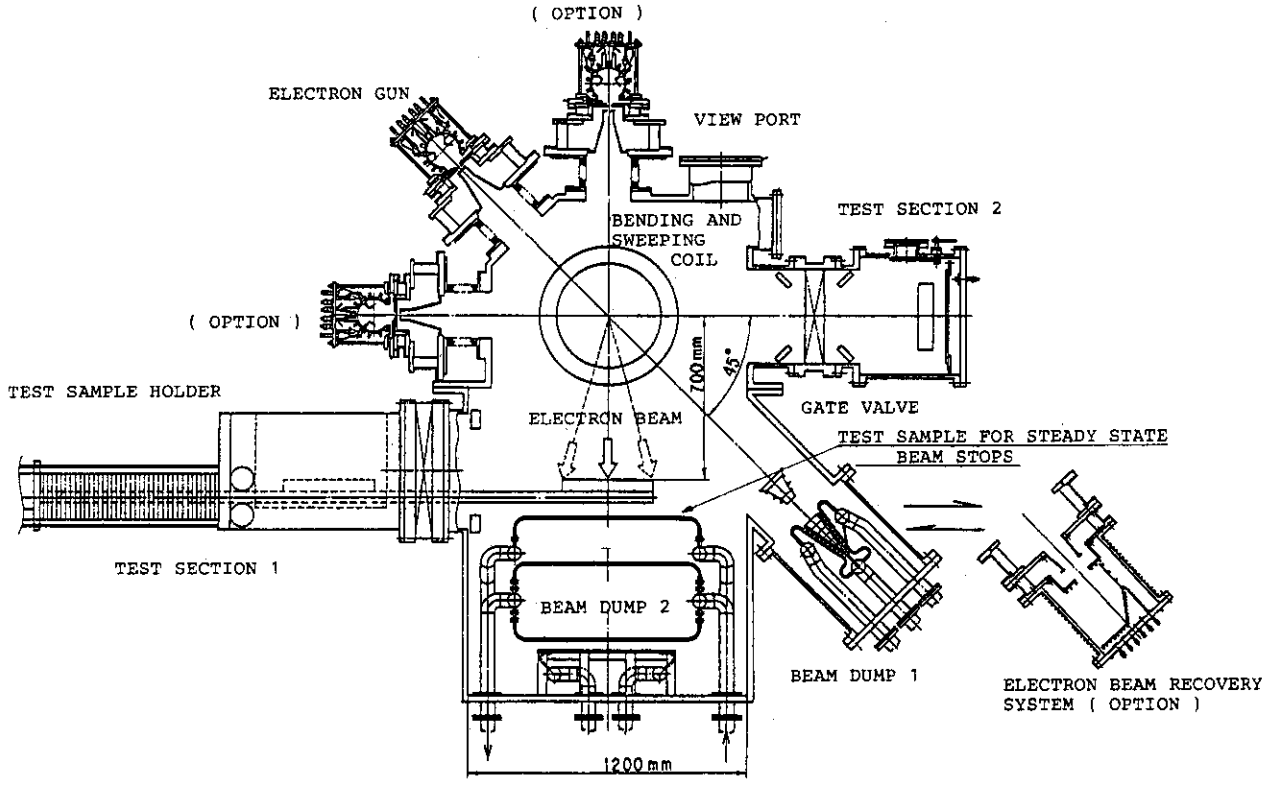

Fig.V.6-3 Cross sectional view of JEBIS.

VI. NEXT STEP FOR JAERI TOKAMAK PROGRAM

1. FER

The Fusion Council of Japan recommended in the National Research and Development Program that the next step fusion device should have a mission of achieving a long ignited and controlled DT burn. In 1987, the design study of FER (Fusion Experimental Reactor) with the above mission was conducted. Because the joint work of the ITER has begun May, 1988, a new organization (Fusion Experimental Reactor Team) was established to support the ITER activities and also to design FER. In order to make the FER and ITER complementary, two concepts of FER were newly proposed. One is the ITER-like machine, and the other is the machine for demonstrating the engineering feasibility of a fusion reactor.

Device parameters and cross section of the engineering-oriented FER are shown in Table VI.1-1 and Fig.VI.1-1, respectively. In order to realize the missions securely and also study the wide range of plasma parameters for DEMO reactor, phased operation and phased construction are proposed. Phased operation consists of cold (D/H discharge) and hot (DT discharge) phases. In the hot phase, maximum plasma current of 15 MA is inductively produced. In the cold phase, the base line plasma is chosen to have a larger size and current up to 20 MA by installing thinner shield. Optimization of PF coil configuration was performed to reduce electric power of PF coil system.

Demonstration of a steady state operation is one of the key issues for DEMO reactor. A 500 keV negative-ion-based injection system is used for both heating and current drive. Realistic current profile control by NBI was presented. An enhancement of energy confinement time of L-mode scaling by 1.5 is required to increase the energy multiplication factor Q up to 5. Plasma profile control by RF waves is employed for this purpose. The concentration of helium ash affects the confinement property. A single null divertor is used for efficient ash exhaust. Short life plasma facing components, such as divertor plate and first wall protection tile, are considered for in-situ repair instead of replacement in order to reduce the radioactive waste disposal. The neutron wall load is about 0.6 MW/m^2. The maximum attainable neutron fluence is relatively low (0.1 $MW \cdot a/m^2$) due to the restricted availability of cooling water at NAKA site. Tritium breeding and recovery are planned

to be tested in blanket test modules.

2. ITER

2.1 Physics

During the concept definition phase (May-September, 1988) and the design workshop (February-March, 1989), physics data base assessment and their extrapolations to ITER were done extensively, and the physics guidelines were prepared to predict the plasma performance and to determine the device and plasma parameters. Several specialist meetings were held for this purpose in the area of power and particle control, confinement, poloidal field design, operation limit, current drive and heating.

Major guidelines thus specified are summarized as follows. Certain improvement of L mode type of confinement is assumed. Four typical L mode scaling are chosen and the improvement factor of 1.5 - 2.0 is assumed, which requires around 20 MA of plasma current to achieve the self-ignition in ITER. Poloidal divertor is assessed to be the most promising way for the power and particle control. However, the present modelling calculations predict large peak power on the divertor plate, and large pumping speed and fuel particle throughput, which increases engineering difficulty. As for the current drive and heating scheme, three candidates are selected depending on the main current driver, i.e., neutral beam, ion cyclotron and electron cyclotron range of frequency wave, respectively. In either options, lower hybrid wave is selected for the peripheral current drive scheme. Bootstrap current is assumed to drive 30% of the total current.

In the reference opeation point of Physics phase, Troyon coefficient is set well below (~ 1.8) the guidelines of the beta limit (2.5 for Physics phase and 3 for Technology phase) due to the heat removal limitation to divertor plate. Very flat current profile is required to attain the target beta value for the specified pressure profile assumed in ITER. It should be the major physics issues in the successive design phase to specify the most desirable density, temperature and current profiles and their active control method.

Thermal quench time during the disruption is predicted as 0.1 - 3 ms and the current quench time is 10 - 20 ms independent of current. Alpha particle loss due to the toroidal field ripple is evaluated by a

to be tested in blanket test modules.

2. ITER

2.1 Physics

During the concept definition phase (May-September, 1988) and the design workshop (February-March, 1989), physics data base assessment and their extrapolations to ITER were done extensively, and the physics guidelines were prepared to predict the plasma performance and to determine the device and plasma parameters. Several specialist meetings were held for this purpose in the area of power and particle control, confinement, poloidal field design, operation limit, current drive and heating.

Major guidelines thus specified are summarized as follows. Certain improvement of L mode type of confinement is assumed. Four typical L mode scaling are chosen and the improvement factor of 1.5 - 2.0 is assumed, which requires around 20 MA of plasma current to achieve the self-ignition in ITER. Poloidal divertor is assessed to be the most promising way for the power and particle control. However, the present modelling calculations predict large peak power on the divertor plate, and large pumping speed and fuel particle throughput, which increases engineering difficulty. As for the current drive and heating scheme, three candidates are selected depending on the main current driver, i.e., neutral beam, ion cyclotron and electron cyclotron range of frequency wave, respectively. In either options, lower hybrid wave is selected for the peripheral current drive scheme. Bootstrap current is assumed to drive 30% of the total current.

In the reference opeation point of Physics phase, Troyon coefficient is set well below (~ 1.8) the guidelines of the beta limit (2.5 for Physics phase and 3 for Technology phase) due to the heat removal limitation to divertor plate. Very flat current profile is required to attain the target beta value for the specified pressure profile assumed in ITER. It should be the major physics issues in the successive design phase to specify the most desirable density, temperature and current profiles and their active control method.

Thermal quench time during the disruption is predicted as 0.1 - 3 ms and the current quench time is 10 - 20 ms independent of current. Alpha particle loss due to the toroidal field ripple is evaluated by a

Monte-Carlo code and is predicted to be less than 1% and the peak power load is about 0.1 MW/m^2, which is sufficiently small owing to the large plasma current and small aspect ratio. Detailed guideline on the related physics issues for the operation scenario is also provided to specify e.g., breakdown voltage, current ramp-up rate, required volt-seconds and so on.

2.2 Engineering

The reference ITER configuration and plasma parameters based on the results of the design efforts to data are shown in Table VI.2-1 and Fig. VI.2-1, respectively. The configuration of the technology phase was designed by substituting breeding blankets inside the vacuum vessel.

Preliminary initial assembly scheme and procedure were studied in conjunction with the vacuum vessel structure and its segmentation. The number of segmentation of in-vessel components, such as divertor, inboard and outboard blankets, is related to the maintenance procedure, port size, pipe penetration, attachment system and electromagnetic forces acting on these components. Both two and three segmentation concepts between two neighboring TF coils are under investigation. The short life components such as divertor plate are planned to be replaced by in-vessel manipulator for minimizing the waste and contaminated space. An ex-vessel access to the divertor module is assumed as a back up replacement system.

PF coil optimization was carried out to maximize available flux within reasonable stored energy and ampere-turns of the coils. For 12 T maximum field experience and plasma burn of $\beta_p = 1$, the maximum available fluxes are around 275 and 250 Vs for the physics and technology phases, respectively. A 290 - 300 Vs is required for the physics phase plasma operation, so an improvement of the solenoid coil by graded layer winding or an expansion of the bore is an important issue. Vertical instability control study has clarified the requirements for the structure of the stabilizing shell and the vacuum vessel, i.e., distance between plasma surface and the shell, outboard blanket segmentation, gap between the neighboring blankets, one-turn resistance of the vacuum vessel, etc.

Reduction of the electromagnetic forces acting on in-vessel components during plasma disruption by segmentation and electrical insulation is under investigation. Peak heat flux to the divertor plate

exceed 10 MW/m^2 which cannot be removed stationary. Separatrix sweep is a hopeful candidate to reduce the peak heat flux effectively, but an increase of the AC loss in the SC magnets and the required electric power is a trade-off problem. Cooperative separatrix sweep by in-vessel and SC coil seems to be an only method to mitigate the problem. Carbon-based materials, such as graphite and c/c composite, was selected as an armor of the plasma facing surface, at least, in initial phase of the operation. Engineering feasibility of these materials concerning to tritium inventory, outgassing, dust production, attaching method and maintenance procedure is under investigation.

2.3 System analysis

A scoping study was done to see the possible parameter space for ITER which should have a self-ignition and extended burn as design targets and non-inductive steady state operation as an ultimate design goal. Results of the study can be discussed in terms of the plasma current and aspect ratio as shown in Fig.VI.2-2. Preferable region for ITER is surrounded by the lines of required enhancement factor H of energy confinement for self-ignition, radial build constraints coming from volt-second capability for extended burn, and required current drive power for steady state operation. In the area of safety and environments, world-wide input was obtained on radiation protection and design dose targets are established. Benchmark calculations for radioactive exposure due to tritium and other radioactivity release have been conducted. Comprehensive cost-center breakdown was developed for future systematic cost estimate of ITER device. In the area of reliability and availability, a first plant evaluation was performed to develop a priority ranking of the key components.

3. Fusion Reactor Design

3.1 Blanket R&D facilities

Design studies of R&D facilities were carried out to provide data base for tritium breeding blanket which employs solid breeder materials. The R&D facilities studied this year are those for hot tests with neutron and tritium handling and some cold facilities which were not covered last year. The following facilities were studied and their concepts were provided; a) Neutron Irradiation Test Facilities, b)

exceed 10 MW/m^2 which cannot be removed stationary. Separatrix sweep is a hopeful candidate to reduce the peak heat flux effectively, but an increase of the AC loss in the SC magnets and the required electric power is a trade-off problem. Cooperative separatrix sweep by in-vessel and SC coil seems to be an only method to mitigate the problem. Carbon-based materials, such as graphite and c/c composite, was selected as an armor of the plasma facing surface, at least, in initial phase of the operation. Engineering feasibility of these materials concerning to tritium inventory, outgassing, dust production, attaching method and maintenance procedure is under investigation.

2.3 System analysis

A scoping study was done to see the possible parameter space for ITER which should have a self-ignition and extended burn as design targets and non-inductive steady state operation as an ultimate design goal. Results of the study can be discussed in terms of the plasma current and aspect ratio as shown in Fig.VI.2-2. Preferable region for ITER is surrounded by the lines of required enhancement factor H of energy confinement for self-ignition, radial build constraints coming from volt-second capability for extended burn, and required current drive power for steady state operation. In the area of safety and environments, world-wide input was obtained on radiation protection and design dose targets are established. Benchmark calculations for radioactive exposure due to tritium and other radioactivity release have been conducted. Comprehensive cost-center breakdown was developed for future systematic cost estimate of ITER device. In the area of reliability and availability, a first plant evaluation was performed to develop a priority ranking of the key components.

3. Fusion Reactor Design

3.1 Blanket R&D facilities

Design studies of R&D facilities were carried out to provide data base for tritium breeding blanket which employs solid breeder materials. The R&D facilities studied this year are those for hot tests with neutron and tritium handling and some cold facilities which were not covered last year. The following facilities were studied and their concepts were provided; a) Neutron Irradiation Test Facilities, b)

Safety and Reliability Test Facilities, c) Remote Handling Device Test Facilities. As an example, the test section of a coolant rupture test facility is shown in Fig.VI.3-1.

3.2 System study of fusion reactors

Using the Tokamak Reactor Automated Design Code "TRADE", a conceptual study of power reactors was carried out based on the current physics database. A long-burn concept with a fully inductive current drive, a steady state reactor concept utilizing a bootstrap current and D-^{3}He and D-D reactors were studied. Costs are evaluated for these concepts.

3.3 Safety analyses

The development of a methodology has been initiated for a comprehensive safety evaluation of a fusion reactor. The structure and the procedure have been made clear for the code system which evaluates the radioactive inventory, the radioactive release probability and the eventual risk to the public and worker by normal and accidental release and by radioactive waste. Along with the methodology development, the following improvements were implemented to the induced activation calculation code system, THIDA-2. a) Speed-up of induced activation calculation, b) updating of activation cross section data based on measurements at the Fusion Neutronics Source Facility and improved calculational procedures, c) improvement in graphical presentation of the time evolution of induced activity and decay heat.

Table VI.1-1 FER major plasma parameters

Plasma current	(MA)	15	-	20
Major radius	(m)	4.5	-	4.7
Minor radius	(m)	1.6	-	1.8
Elongation		1.6	-	2.0
Plasma volume	(m^3)	400	-	600
Field on axis	(T)	5.2	-	5.4
OH coil flux	(Vs)	160	-	170
Fusion power	(MW)	200	-	500
Burn time	(s)	100	-	1000
Heating/CD power	(MW)	80		

Table VI.2-1 ITER major plasma parameters

		Physics phase	Technology phase
Plasma current	(MA)	22	18
Major radius	(m)	5.8	5.5
Minor radius	(m)	2.2	1.8
Elongation		1.9	2.0
Triangularity		~0.3	~0.35
Field on axis	(T)	5	5.3
OH coil flux	(Vs)	280	250
Fusion power	(MW)	~1000	~750
Burn time	(s)	~200	600 s - 2 weeks
Heating/CD power	(MW)	100	100

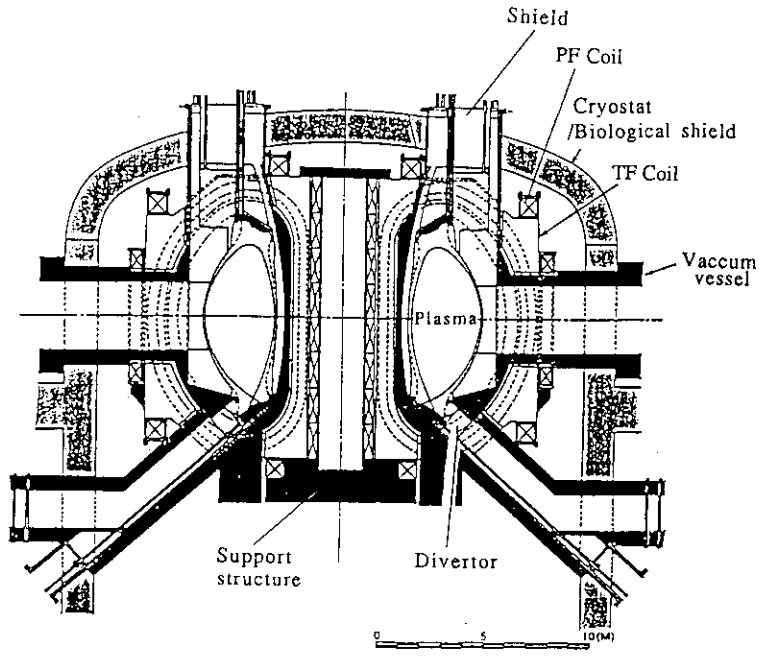

Fig. VI.1-1 Cross sectional view of FER

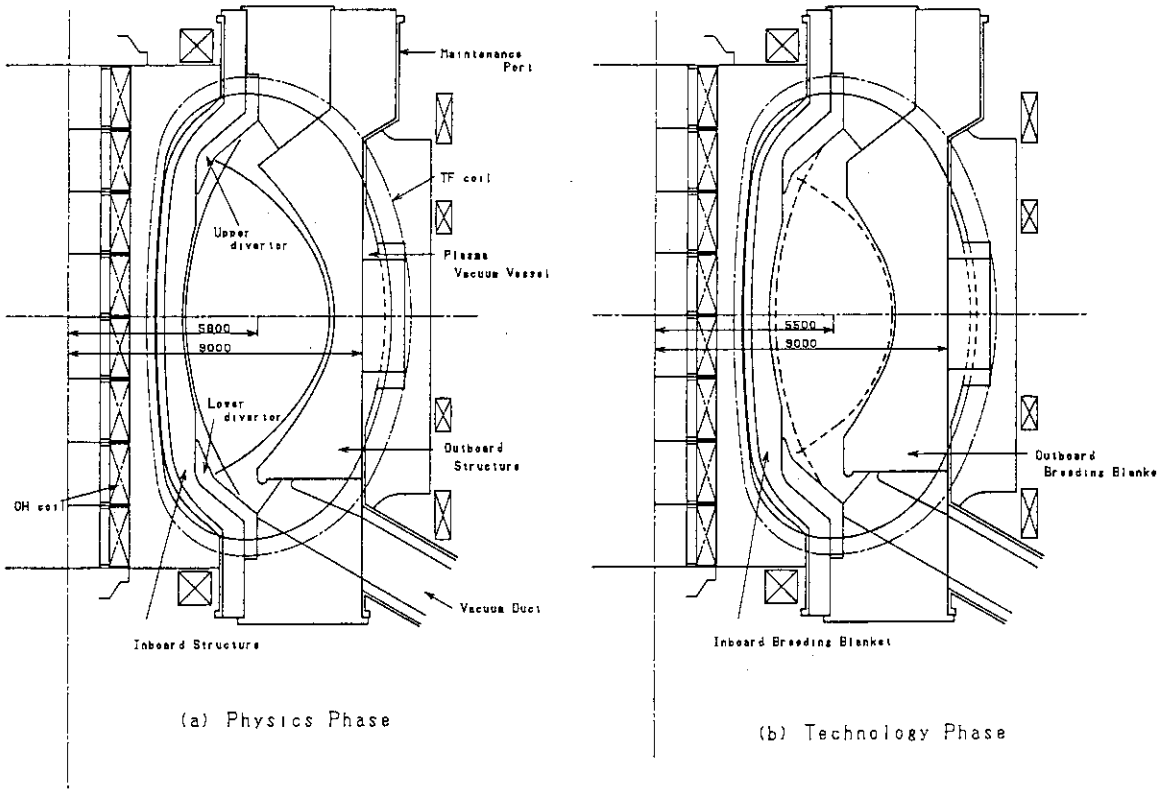

Fig. VI.2-1 Cross sectional view of ITER

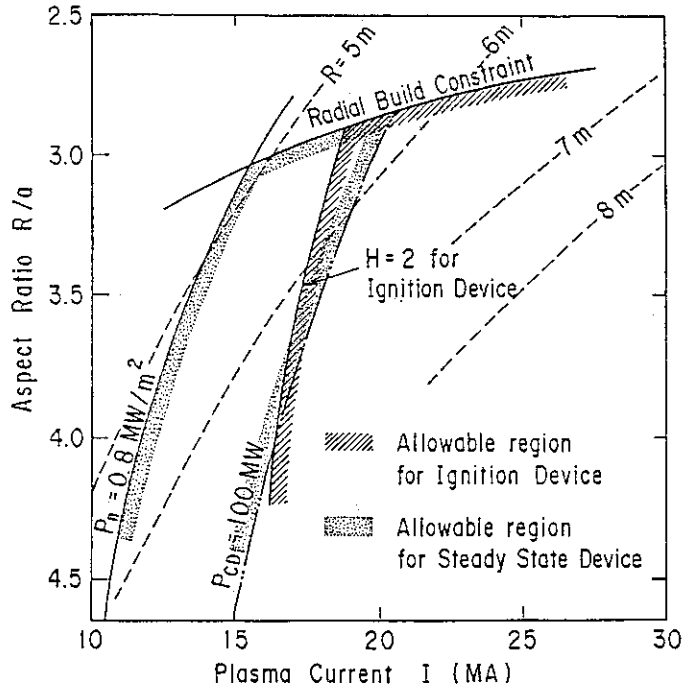

Fig.VI.2-2 Allowable parameter regions for ignition and steady state devices

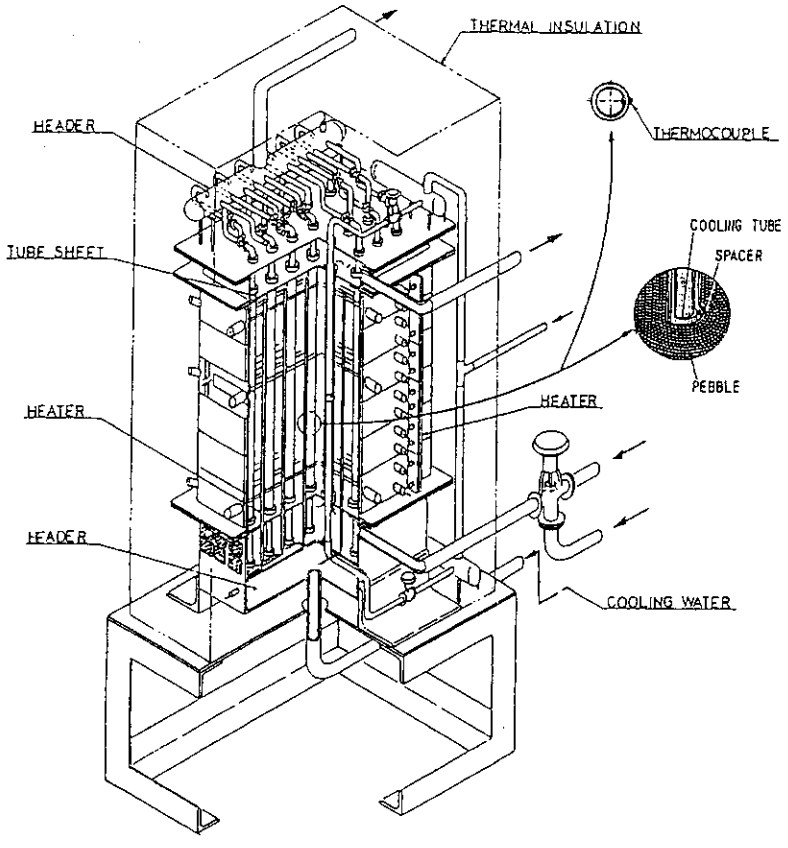

Fig.VI.3-1 Test section of a coolant pipe rupture test facility

APPENDICES

A.1 Publication List
(April 1988 - March 1989)

A.1.1 List of JAERI-M report

1) Watanabe K., Dairaku M., Ebisawa N., Horiike H., Inoue T., Kitamura S., Komata M., Kurashima T., Mizuno M., Ohga T., Oohara H., Okumura Y., Tsuda F., Usami H., Usui K., Yokoyama K., "Development of A Variable Proton Ratio Ion Source", JAERI-M 88-022.

2) Tani K., Suzuki M., Yamamoto S., Azumi M., "On the Analysis of Beam Driven Current in a Tokamak", JAERI-M 88-042.

3) Yamamoto S., Ohara Y., Tani K., Nishio S., Okumura Y., Araki M., Azumi M., Devoto R.S.*3, Fujisawa N., Honda T., Horie T., Horiike H., Inoue T., Kobayashi T.*16, Masuzawa M.*21, Matsuda S., Miki N.*4, Mizuno M., Nakashima K.*15, Okamoto M.*22, Seki Y., Shibanuma K., Shimomura Y., Shinya K., Sugihara M., Tachikawa K., Tanaka S., Tone T., Watanabe K., Iida H., et al., "A Conceptual Design of a Negative-Ion-Grounded Advanced Tokamak Reactor - NAVIGATOR - (FER)", JAERI-M 88-086.

4) Mizuno M., Dairaku M., Horiike H., Kitamura S., Komata M., Kuriyama M., Matsuda S., Matsuoka M., Ohga T., Ohara Y., Oohara H., Tsuda F., Usami H., Usui K. and Yokoyama K., "Low Energy, High Power Injection in JT-60 NBI", JAERI-M 88-088 (in Japanese).

5) FER Design Team, "Conceptual Design Study of Fusion Experimental Reactor (FY 87 FER) -- Summary report --", JAERI-88-090.

6) Haraguchi K.*27, Fukuda T., Takahashi T.*40, Yokomizo H., Yoshida N.*43, "Evaluation of the Optical Efficiency of an 10 μm Band Optical Fiber", JAERI-M 88-091 (in Japanese).

7) Yamagiwa M., Takizuka T., "ICRF Enhancement of Fusion Reactivity in the Presence of Alpha Particles", JAERI-M 88-092.

8) Hosogane N., Akiba M., Kuriyama M., Miya N., Ushigusa K., Yoshino R. and Ninomiya H., "Energy Confinement study in JT-60 Initial Heating Experiment", JAERI-M 88-095.

9) Minato A.*26, "Study of Electromagnetic-Structural Behavior of First Wall Blanket Structure for a Tokamak Fusion Reactor", JAERI-M 88-097.

10) Mori S.*16 and Seki Y., "Accuracy Evaluation of the Current Data and Method Applied to Shielding Design of a Fusion Experimental Reactor

(FER)", JAERI-M 88-103.

11) Yoshino R., Neyatani Y. and JT-60 Team, "Optimization for Getting Stable Plasma Initiation in JT-60", JAERI-M 88-111.

12) Ushigusa, K., Imai T., Ikeda T., Sakamoto K., F. X. Soldner*5, Takase Y.*6, Tsuji S., Shimizu K., Naito O., Uehara K., Akiba M., Araki M., Sato M., Yoshida H., Nagashima K., Kusama K., Kubo H., Nemoto M., Tobita K., "Lower Hybrid Heating into Neutral Beam Heated Plasma in the JT-60 Tokamak", JAERI-M 88-115.

13) Tamai H., Maeno M., Matsuda T., Matoba T., "Multi-Channel Bolometer System on JFT-2M Tokamak", JAERI-M 88-120.

14) Kimura H., Fujii T., Saigusa M., Hamamatsu K., Kusama Y., Tobita K., Nemoto M., Nagashima K., Kobayashi N.*4, Moriyama S., Annoh K., Shinozaki S., Terakado M., et al., "Present Status of JT-60 ICRF Heating Experiment", JAERI-M 88-123.

15) Kubo H., Sugie T., Sakasai A., Koide Y., Nishino N.*2, Akaoka N.*40, "Spectrograms of the JT-60 plasmas in the Vacuum Ultraviolet Region (Wavelength Region 15-1360 Å)", JAERI-M 88-126 (in Japanese).

16) Dimok D.*37, Yamauchi T., "Design Proposal for a JFT-2M TV Thomson Scattering System", JAERI-M 88-137.

17) Saigusa M., Kimura H., Fujii F., Kobayashi N.*4, Moriyama S., Annoh K., Shinozaki S., Terakado M., et al., "Dependence of Coupling Resistance on Toroidal Wave Number Spectrum During H-mode Discharge", JAERI-M 88-153.

18) Yamazaki S.*16, Seki M., Kobayashi T.*16, "Two-dimensional Disruption Thermal Analysis Code DREAM", JAERI-M 88-163.

19) Itoh K.*1, Fukuyama A.*2, Itoh S.*3, Takizuka T., Yamamoto S., Matsuda S., "Steady-State Operation Regime of Tokamak Reactor Plasma - Consistency Analysis (I) -", JAERI-M 88-171 (in Japanese).

20) Koide S.*9, Shimizu K., Sugiyama T.*4, Nishitani T., "A Study of Particle Confinement in the JT-60 Tokamak using Skin Radiative Approximation Model", JAERI-M 88-175 (in Japanese).

21) Nagata H.*44, Shiho M., Sugie T., "Module Type Flat-Field Grazing Incidence Spectrographs for Large Tokamak (JT-60) Plasma Diagnosis: Design and Imaging Properties", JAERI-M 88-179.

22) Ikeda Y., Honda M., Yokokura K., Tsuneoka M., Seki M., Maehara S., Sawahata M., Sato M., Kato T., Imai T., Sakamoto K., Uehara K., "RF Conditioning of LHRF Launcher on JT-60", JAERI-M 88-182 (in Japanese).

23) Yoshida H., Hirata S.*16, Naito T.*7, Yamanishi T., Anderson J. L.*47,

et al., "TSTA Loop Operation with 100 grams-level of Tritium - Milestone Run in June, 1987 -", JAERI-M 88-204.

24) Yoshida H., Hirata S.*16, Naito T.*7, Yamanishi T., Anderson J.L.*47, et al., "TSTA Loop Operation with 100 grams-level of Tritium - Milestone Run in July, 1987 -", JAERI-M 88-205.

25) Tokuda S., Takeda T., Okamoto M.*4, "MHD Equilibrium Calculations Specifying Current Sources," JAERI-M 88-207.

26) Hiratsuka H., Kawasaki K., Takatsu H., Miyo Y., Yoshioka Y.*23, Ohta K., Shimizu M., "Pellet Injector on JT-60", JAERI-M 88-214 (in Japanese).

27) Tokuda S., Takeda T., Okamoto M.*4, "Self-Consistent Calculations of Neoclassical Current Effects in JFT-2M Tokamak Plasma", JAERI-M 88-216.

28) Yoshino R. and JT-60 Team, "Control of the Configuration in JT-60 Lower X-point Divertor Plasma", JAERI-M 88-222.

29) Nishino N.*2, Kubo H., Koide Y., Sakasai A., Sugie T., Takeuchi H., "Measurement of the Current Distribution in JT-60 Plasma by He Beam", JAERI-M 88-229.

30) Seki Y. and Takeyasu Y.*20, "Nuclear and Activation Characteristics of Materials in 14.1-MeV and 2.5-MeV Neutron Field", JAERI-M 88-230.

31) Takizuka T., Yamagiwa M., "Computational Form for DT Fusion Output Power from Toroidal Plasma", JAERI-M 88-234.

32) Yoshida H., Fukui H.*23, Hirata S.*16, Yamanishi T., Naito S.*7, Anderson J.L.*47, et al., "TSTA Loop Operation with 100 grams-level of Tritium - Milestone Run in June, 1988 -", JAERI-M 88-242.

33) Yoshino R. and JT-60 Team, "Results of pellet injection experiments in JT-60", JAERI-M 88-246.

34) Nakamura H., "Studies on First Wall and Plasma Wall Interaction", JAERI-M 88-247 (in Japanese).

35) Yamanishi T., Yoshida H., Naito T.*7, Hirata S.*16, Sherman R.H.*47, et al., "Hydrogen Isotope Separation Study with TSTA Cryogenic Distillation System - Single Column Experiment with D-T system -", JAERI-M 88-253.

36) Yamanishi T., Yoshida H., Fukui H.*23, Naito T.*7, Hirata S.*16, Sherman R.H.*47, "Hydrogen Isotope Separation Study with the TSTA Cryogenic Distillation System - Two-column Experiment with H-D-T -", JAERI-M 88-254.

37) Yamagiwa M., Takizuka T., "ICRF Enhancement of Power Transfer from Alpha Particles", JAERI-M 88-259.

38) Matsumoto H., Goldston R.J.*37, Funahashi A., Hoshino K., Kawashima H., Kawakami T., Maeda H., Matoba T., Matsuda T., Miura Y., Mori M., Nakazawa I.*15, Odajima K., Ogawa H., Ogawa T., Ohasa K., Sengoku S., Shoji T., Suzuki N., Tamai H., Uesugi Y., Yamauchi T., Yamamoto T., Ohtsuka H., "Characteristics of Edge Localized Mode in JFT-2M H-mode", JAERI-M 89-020.

39) Yamamura H.*18, Yoshida J.*2, Hoshino M.*56, Kawano K., Kato T., "Development of Teflon Transfertube", JAERI-M 89-022.

40) Shinya K.*4, Sugihara M., Nishio S., "Study on Poloidal Field Coil Optimization and Equilibrium Control of ITER", JAERI-M 89-028.

41) JT-60 Team*, "Review of JT-60 Experimental Results from June to October, 1988", JAERI-M 89-033.

* Aoki I., Akaoka N., Akasaka H., Akiba M., Akino N., Ando T., Annoh K., Aoyagi T., Arai T., Arakawa K., Araki M., Azumi M., Chiba S. Dairaku M., Ebisawa N., Fujii T., Fukuda T., Funahashi A., Furukawa H., Gunji H., Hamamatsu K., Hanada M., Hara M., Haraguchi K., Hiratsuka H., Hirayama T., Hiroki S., Hiruta K., Honda M., Honda M., Horiike H., Hosoda R., Hosogane N., Iida Y., Iijima T., Ikeda K., Ikeda Y., Imai T., Inoue T., Isaji N., Isaka M., Ishida S., Itami K., Itige N., Itoh T., Kakizaki T., Kamada Y., Kaminaga A., Kaneko T., Kato T., Kawai M., Kawabe M., Kawamata Y., Kawano Y., Kawasaki K., Kikuchi K., Kikuchi M., Kimura H., Kimura T., Kishimoto H., Kitamura S., Kiyono K., Kobayashi N., Kodama K., Kurihata Y., Koide Y., Koike T., Komatsu M., Kondo I., Konoshima S., Kubo H., Kunieda S., Kurihara K., Kuriyama M., Kusaka M., Kusama Y., Kushima T., Mabuti Y., Maehara S., Maeno K., Matoba T., Matsuda S., Matsukawa M., Matsukawa T., Matsuoka M., Matsuzaki Y., Miura Y., Miya N., Miyachi K., Miyo Y., Mizuno M., Mogaki K., Moriyama S., Murakami Y., Muto M., Nagami M., Nagase K., Nagashima A., Nagashima K., Nagashima T., Nagaya S., Naito O., Nakamura H., Nemoto H., Nemoto M., Neyatani Y., Ninomiya H., Nishino N., Nishitani T., Nobusaka H., Nomata N., Obara K., Odajima K., Ogawa Y., Ogiwara N., Ohga T., Ohara Y., Oohara H., Ohshima T., Ohta K., Ohta M., Ohuchi S., Ohuchi Y., Okumura H., Okumura Y., Omori K., Omori S., Omori Y., Ozeki T., Saegusa M., Saitoh N., Sakasai A., Sakata S., Sasajima T., Sato K., Sato M., Sato M., Sawahata M., Sebata T., Seimiya M., Seki M., Seki S., Shibanuma K., Shimada M., Shimada R., Shimizu K., Shimizu M., Shimomura Y., Shinozaki S., Shirai H., Shirakata H., Shitomi M., Suganuma K., Sugawara T., Sugie T.,

Sunaoshi H., Suzuki M., Suzuki M., Suzuki N., Suzuki S., Tachibana H., Takahashi M., Takahashi S., Takahashi T., Takahashi A., Takasaki M., Takatsu H., Takeuchi H., Takeshita A., Takizuka T., Tamura S., Tanaka S., Tanaka T., Tanaka Y., Tani K., Terakado M., Terakado T., Tobita K., Totsuka T., Toyoshima N., Tsuda F., Tsugita T., Tsuji S., Tsukahara Y., Tsuneoka M., Uehara K., Uramoto Y., Usami H., Ushigusa K., Usui K., Yagyu J., Yamagiwa M., Yamamoto M., Yamashita O., Yamazaki T., Yokokura K., Yokoyama K., Yoshikawa K., Yoshida H., Yoshino R., Yoshioka Y., Yonekawa I., Yoneda T., Watanabe K.

42) Tamai H., Ogawa T., Matsumoto H., Odajima K., "Experimental Observation of Ion Bernstein Wave Heating on JFT-2M Tokamak", JAERI-M 89-036.

43) Hoshino K., Yamamoto T., Kawashima H., Suzuki N., Uesugi Y., Aikawa H., Kasai S., Kawakami T., Matsuda T., Miura Y., Mori M., Odajima K., Ogawa H., Ogawa T., Ohtsuka H., Shoji T., Tamai H., Yamauchi T., Kondo T.*46, Nakazawa I.*15, Neufeld C.R.*52, Maeda H., "Observation of H-mode by Edge Heating Solely by Electron Cyclotron Heating in a Divertor Configuration of JFT-2M Tokamak", JAERI-M 89-038.

44) Yamamura H.*18, Kato T., Tada E., Hiyama T., Kawano K., Sato M.*14, Shimamoto S., "Thermal Design of a 10-kW Helium Refrigerator", JAERI-M 89-040.

A.1.2 List of papers published in journals

1) Kishimoto Y., Mima K.*50, Haines H.G.*51, "An Extension of Spitzer-Harm Theory on Thermal Transport to Steep Temperature Case -- II Integral Representation", J. Phys. Soc. Japan 57 (1988) 1972.

2) Yamagiwa M., Takizuka T., Kimura H., Azumi M., "Scaling of Extended-Tail Temperature for Combined NBI and ICRF Heating", Plasma Phys. and Controlled Fusion 30 (1988) 943.

3) Yamagiwa M., Takizuka T., "ICRF Wave Absorption by Alpha Particles", Nucl. Fusion 28 (1988) 2241.

4) Yamauchi T., Shoji T., Yamamoto S., "χ_e at the Temperature Rise Phase and the Internal Disruption Phase during the Sawtooth Oscillation", Plasma Phys. and Controlled Fusion 30 (1988) 133.

5) Yamauchi T., Schweer B.*53, Bay H.L.*53, Hoethker K.*53, Hintz E.*53, Von Neuenhaye R.*53, "Neutral Iron Generation with Sawtooth Oscillation in TEXTOR ICRF Heated Plasmas", Jpn. J. Appl. Phys. 27 (1988) 658.

6) Ogawa H., Miura Y., Kasai S., "Determination on Ion Temperature and Toroidal Rotation Velocity Via Charge-Exchange Recombination Spectroscopy",

Jpn. J. Appl. Phys. 27 (1988) 133.

7) Yamauchi T., JFT-2M Group*, "Steep Gradient and Pedestal of Electron Profiles in H-Mode JFT-2M Plasma", Jpn. J. Appl. Phys. 27 (1988) L924.
* Aikawa H., Hoshino K., Kasai S., Kawakami T., Kawashima H., Kondo T.*46, Matsuda T., Matsumoto H., Miura Y., Mori M., Nakazawa I.*15, Neufeld C.*52, Odajima K., Ogawa H., Ogawa T., Ohasa K., Sengoku S., Shoji T., Suzuki N., Tamai H., Uesugi Y., Yamamoto T., Yamauchi T.

8) Sengoku S., Funahashi A., Hasegawa M., Hoshino K., Kasai S., Kawakami T., Kawashima H., Matoba T., Matsuda T., Matsumoto H., Miura Y., Mori M., Odajima K., Ogawa H., Ogawa T., Suzuki N., Shoji T., Tamai H., Uesugi Y., Yamamoto T., Yamauchi T., "Enhancement of Wall Fueling and Improvement in $n\tau$ of a Beam-Head H-mode Discharge by Electron Cyclotron Wave in the JFT-2M Tokamak", J. Phys. Soc. of Jpn. 57 (1988) 903.

9) Shoji T., Hoshino K., Kasai S., Kawakami T., Kawashima H., Maeda H., Matsuda T., Matsumoto H., Miura Y., Mori M., Nakazawa I.*15, Tamai H., Uesugi Y., Yamamoto T., Yamauchi T., Hasegawa K., Honda A., Ishibori I., Kashiwa Y., Kazawa M., Kikuchi K., Matsuzaki Y., Ohuchi K., Okano H., Sato E., Shibata T., Shibuya T., Shiina T., Suzuki K., Tani T., Uno S., "Confinement Studies of H-mode in Divertor /Limiter Discharges on JFT-2M", in Controlled Fusion and Plasma Heating (Proc. 15th Europ. Conf. Dudrovnik, 1988), Vol.12B, Part 1, European Physical Society (1988) 219.

10) Hoshino K., Yamamoto T., Suzuki N., Kawashima H., Kasai S., Kawakami T., Maeda H., Matoba T., Matsuda T., Matsumoto H., Miura Y., Mori M., Odajima K., Ogawa H., Ogawa, T., Ohasa K., Sengoku S., Shoji T., Tamai H., Uesugi Y., Yamauchi T., Funahashi A., "Transition from the L-mode to the H-mode by Electron Cyclotron Heating of a Tokamak Edge Plasma", Nucl. Fusion 28 (1988) 301.

11) Hoshino K., Yamamoto T., Kawashima H., Kasai S., Matsuda T., Miura Y., Suzuki N., Uesugi Y., Yamauchi T., "Behavior of Peripheral Electron Temperature at the H-Mode Transition Induced by the Peripheral Electron Cyclotron Heating of a Tokamak Plasma", Phys. Letters A130 (1988) 26.

12) Yamauchi T., Odajima K., Uesugi Y., Aikawa H., Dimock D.*37, Kawashima H., Kasai S., Kawakami T., Maeda H., Matsuda T., Matsumoto H., Miura Y., Mori M., Nakazawa I.*15, Ogawa H., Ogawa T., Ohtsuka H., Sengoku S., Shoji T., Suzuki N., Tamai H., Yamamoto T., "Particle Accumulation at the Edge observed in n_e and Te Profiles of H-mode JFT-2M Plasma", Phys. Letters A131 (1988) 301.

13) Mori M., Suzuki N., Uesugi Y., Ogawa T., Ogawa H., Ohtsuka H., Odajima K., Kasai S., Kawashima T., Kawakami T., Shoji T., Sengoku S., Tamai H., Nakazawa I.*15, Hoshino K., Matsumoto H., Matsuda T., Miura Y., Yamauchi T., Yamamoto T., Maeda H., "New Mode of Improved Confinement in Discharges with Stationary Density in JFT-2M", Nucl. Fusion 28 (1988) 1892.

14) Ueda N.*7, Kasai M.*7, Tanaka M.*20, Sugihara M., Sengoku S., "Development of a Two-Dimensional Fluid Code and its Application to the Doublet III Divertor Experiment", Nucl. Fusion 28 (1988) 1183.

15) Matsuzaki Y., "Characteristics of a Magnetically Shielded Cylinder for Vacuum Gauges", J. Vac. Soc. Japan, 31 (1988) 550 (in Japanese).

16) Okano F., Matsuzaki Y., Kashiwa Y., Sato E., "Calibration of nude-type Ionization Gauges by Spinning Rotor Gauge", J. Vac. Soc. Japan, 31 (1988) 413 (in Japanese).

17) Shibata T., Arisawa T., Horiike H., Okumura Y., Tanaka S., "Electron beam extraction from a bucket type plasma generator", J. Vacuum Society Japan 31 (1988) 452 (in Japanese).

18) Yamazaki S., Seki M., "Melting and evaporation behaviors of first wall subjected to high heat flux expected at plasma disruption", J. Atomic Energy Society, 30 (1988) 624.

19) Seki M., "First wall technology", J. Atomic Energy Society, 30 (1988) 730.

20) Miya K.*8, Seki M., "First wall technology", J. Atomic Energy Society, 31 (1988) 117.

21) Okumura Y., "Development of A High Current Negative Ion Source for Fusion Application", The Japan Society of Plasma Science and Nuclear Fusion Research 60 (1988) 329.

22) Nagashima T., "System and Components for RF system for plasma heating", Trans. IEEE of Japan, Vol.108, No.7, p.616-618 (in Japanese).

23) Kinoshita S.*2, Imai T., Kimura H., "RF Coupling System", ibid.

24) Fujii T., Saigusa M., Ikeda Y., Kimura H., Hirashima K., Uehara K., "Joule Loss on a Faraday Shield of JT-60 ICRF Test Antenna", Japan J. Appl. Phys. 27 (1988) P.2378-2382.

25) Saigusa M., Kimura H., Fujii T., Kobayashi N., Moriyama S., Nakamura H., "Coupling properties of the JT-60 ICRF antenna during H-mode discharges", Nuclear Fusion 29, No.1 (1988) p.73-77.

26) Uehara K., "Improvement of Plasma Confinement during RF Current Drive in Tokamaks", J. Phys. Soc. Jpn. 57 (1988) 4169.

27) Saidoh M., Yamada R., "Ion Bombardment Induced Mixing of Oxygen-exposed Solid Surfaces during Sputtering", Nucl. Instrum. Methods B33 (1988) 669.

28) Saidoh M., Yamada R., "On the Surface Modification of Oxygen-exposed Molybdenum during Sputtering", J. Vac. Sci. Technol. A6 (1988) 2410.

29) Abe T., Murakami Y., Takazawa K.*23, Hikida K.*23, "Rotational Test of Ceramic Rotor for Vacuum Pump", J. Vac. Soc. Japan 31 (1988) 334.

30) Obara K., Nakamura K., Murakami Y., Obama M.*4, Kondo M.*4, "In-vacuum Test of a Grease-lubricated Joint-type Actuater", ibid 342.

31) Hiroki S., Abe T., Murakami Y., Iimura Y.*54, "Fabrication and Testing of an Optical Diaphragm Manometer", ibid 540.

32) Nakamura K., Obara K., Murakami Y., "Calculation of Conductance by Monte Carlo Method", ibid 546.

33) Hiroki S., Abe T., Murakami Y., Kinoshita S.*55, Naganuma T.*55, Adachi N.*55, "Experiment on Surface Cleaning by Ultra-violet Ray Irradiation", ibid 850.

34) Obara K., Nakamura K., Murakami Y., Naganuma M.*4, Kitamura K.*4, Uchida T.*4, Kondo M.*4, "A Study for the Improvement on Knife-edge-type Metal-seal Flange", J. Vac. Soc. Japan 32 (1989) 2.

35) Obara K., Nakamura K., Murakami Y., Naganuma M.*4, Kitamura K.*4, Uchida T.*4, Kondo M.*4, "Leak Testing of Modified Knife-edge-type Metal-seal Flanges", ibid 165.

36) Hiroki S., Abe T., Murakami Y., "Secondary Electron Emission Coefficient of Wall Materials and their Change with Surface Contamination", ibid 171.

37) Shimamoto S., Kato T., Okuno K., Takahashi Y., "Experiments on Large Superconducting Toroidal Coil in LCT", Fusion Engineering and Design 7 (1988).

38) Shimamoto S., Okuno K., "Experiments on Large Superconducting Toroidal Coil in LCT", J. Atomic Energy Soc. Jpn. 30 (1988) 488 (in Japanese).

39) Tada E., Kato T., Hiyama T., Kawano K., Yamamura H.*18, Sato M.*14, Hoshino M.*56, Shimamoto S., "Performance Test Results of DPC Cryogenic System", Cryogenic Engineering 24 (1989) 21 (in Japanese).

40) Sato M.*14, Kawano K., Tada E., Hiyama T., Kato T., Yamamura H.*18, Hoshino M.*56, Shimamoto S., et al., "Demonstration Poloidal Coil Test Facility - The Performance Test Results of the Cryogenic Cold Compressor",

Cryogenic Engineering 24 (1989) 29 (in Japanese).

41) Yamamura H.*18, Tada E., Kato T., Hiyama T., Kawano K., Hoshino M.*56, Sato M.*14, Shimamoto S., et al., "Demonstration Poloidal Coil Test Facility - The Performance Test Results of the Cryogenic Circulation Pump", Cryogenic Engineering 24 (1989) 36 (in Japanese).

42) Okamoto M.*62, Yoshida H., Naruse Y., "Fusion Tritium Program in Japan", Fusion Technology, 14 (1988) 412.

43) Anderson J. L.*47, Yoshida H., Yamanishi T., Naito T.*7, Hirata S.*16, Naruse Y., et al., "Experience of TSTA Milestone Runs with 100 Grams-level of Tritium", ibid. 14 (1988) 438.

44) Penzhorn R. D.*63, Yoshida H., Konishi S., et al., "A Catalytic Plasma Exhaust Purification System", ibid. 14 (1988) 450.

45) Yamanishi T., Yoshida H., Hirata S.*16, Naito T.*7, Sherman R. H.*47, et al., "Single Column and Two-Column H-D-T Distillation Experiments at TSTA", ibid. 14 (1988) 489.

46) Yamanishi T., Enoeda M., Yoshida H., Naruse Y., Fukui H.*23, et al., "Experimental Apparatus for Cryogenic Hydrogen Isotope Separation Process in the Tritium Process Laboratory", ibid. 14 (1988) 495.

47) Ashibe K.*4, Yoshida H., Naruse Y., Walthers C. R.*47, et al., "Code Development for Analysis of TSTA Compound Cryopumps", ibid. 14 (1988) 546.

48) Matsuda Y., Yokogawa N.*29, Yoshida H., Konishi S., Naruse Y., et al., "Experimental Apparatus for Thermal Diffusion Process in the Tritium Process Laboratory", ibid. 14 (1988) 585.

49) Konishi S., Inoue M.*23, Yoshida H., Naruse Y., et al., "Experimental Apparatus for the Fuel Cleanup Process in the Tritium Process Laboratory", ibid. 14 (1988) 596.

50) Clemmer R.G.*64, Anderson J. L.*7, Naruse Y., Yoshida H., et al., "The Blanket Interface to TSTA: Requirements for Liquid Lithium Blanket Processing Systems", ibid. 14 (1988) 657.

51) Okuno K., Oohira S., Yoshida H., Naruse Y., Suzuki T.*16, et al., "Experimental Apparatus for Tritium Permeation Studies in Tritium Process Laboratory", ibid. 14 (1988) 713.

52) Ide T.*29, Yoshida H., Naruse Y., et al., "Hydrogen Sorption Properties of $LaNi_3Mn_2$ alloy as a Candidate for the tritium Storage Material", ibid. 14 (1988) 769.

53) Sherman R. H.*47, Yoshida H., Yamanishi T., Naito T.*7, Hirata S.*16,

Naruse Y., et al., "Operation of the TSTA Isotope Separation System with 100 Gram Tritium", ibid. 14 (1988) 1273.

54) Ninomiya H., Itami K., Neyatani Y., Naito O., Yoshino R., "Large m=3/n=1 Locked Mode in JT-60 and its stabilization", Nucl. Fusion 28 (1988) 1275.

55) Miya N., Nakamura H., Tsuji S., Ando T., Hiroki S., Nishitani T., Nagashima K., Koide S., JT-60 Team, "Neutral Pressure in JT-60 Divertor Discharges", J. Nucl. Mater. Vol.162-164 (1989) 618.

56) Simonen T.C.*1, Matsuoka M., et al., "Neutral Beam Current Driven High Poloidal Beta Operation of the DIII-D Tokamak", Phys. Rev. Lett. 61 (1988) 1720.

57) JT-60 Team* presented by Hosogane N., "Characteristics of JT-60 Divertor and Limiter Plasmas with High Power Auxiliary Heating", (8th Int. Conf. on Plasma Surface Interactions in Controlled Fusion Devices, Julich. May, 1988) J. Nucl. Materials Vol.162-164 (1989) 93.
* Aoki I., Akaoka N., Akasaka H., Akiba M., Akino N., Ando T., Annoh K., Aoyagi T., Arai T., Arakawa K., Araki M., Azumi M., Chiba S., Dairaku M., Ebisawa N., Fujii T., Fukuda T., Funahashi A., Furukawa H., Gunji H., Hamamatsu K., Hanada M., Hara M., Haraguchi K., Hiratsuka H., Hirayama T., Hiroki S., Hiruta K., Honda M., Honda M., Horiike H., Hosoda R., Hosogane N., Iida K., Iida Y., Iijima T., Ikeda K., Ikeda Y., Imai T., Inoue T., Isaji N., Isaka M., Ishida S., Itami K., Itige N., Ito T., Kakizaki T., Kamada Y., Kaminaga A., Kaneko T., Kato T., Kawai M., Kawabe M., Kawamata Y., Kawano Y., Kawasaki K., Kikuchi K., Kikuchi M., Kimura H., Kimura T., Kishimoto H., Kitamura S., Kiyono K., Kobayashi N., Kodama K., Kurihata Y., Koide Y., Koike T., Komatsu M., Kondo I., Konoshima S., Kubo H., Kunieda S., Kurihara K., Kuriyama M., Kusaka M., Kusama Y., Kushima T., Mabuti Y., Maehara S., Maeno K., Matoba T., Matsuda S., Matsukawa M., Matsukawa T., Matsuoka M., Matsuzaki Y., Miura Y., Miya N., Miyachi K., Miyo Y., Mizuno M., Mogaki K., Moriyama S., Murakami Y., Muto M., Nagami M., Nagase K., Nagashima A., Nagashima K., Nagashima T., Nagaya S., Naito O., Nakamura H., Nemoto H., Nemoto M., Neyatani Y., Ninomiya H., Nishino N., Nishitani T., Nobusaka H., Nomata H., Obara K., Odajima K., Ogawa Y., Ogiwara N., Ohga T., Ohara Y., Oohara H., Ohshima T., Ohta K., Ohta M., Ohuchi S., Ohuchi Y., Okumura H., Okumura Y., Ohmori K., Ohmori S., Ohmori Y., Ozeki T., Saegusa M., Saitoh N., Sakasai A., Sakata S. Sasajima T., Sato K., Sato M., Sato M., Sawahata M.,

Sebata T., Seimiya M., Seki M., Seki S., Shibanuma K., Shimada M., Shimizu K., Shimizu M., Shimomura Y., Shinozaki S., Shirai H., Shirakata H., Shitomi M., Suganuma K., Sugawara T., Sugie T., Sunaoshi H., Suzuki M., Suzuki M., Suzuki N., Suzuki S., Tachibana H., Takahashi M., Takahashi S., Takahashi T., Takahashi A., Takasaki M., Takatsu H., Takeuchi H., Takeshita A., Takizuka T., Tamura S., Tanaka S., Tanaka T., Tanaka Y., Tani K., Terakado M., Terakado T., Tobita K., Totsuka T., Toyoshima N., Tsuda F., Tsugita T., Tsuji S., Tsukahara Y., Tsuneoka M., Uehara K., Uramoto Y., Usami H., Ushigusa K., Usui K., Yagyuu J., Yamagiwa M., Yamamoto M., Yamashita O., Yamazaki T., Yokokura K., Yokoyama K., Yoshikawa K., Yoshida H., Yoshino R., Yoshioka Y., Yonekawa I., Yoneda T., Watanabe K.

58) Yoshino R., Neyatani Y., Ninomiya H., Hosogane N., Arai T., Itami K., Nishino N., Sato M., Fukuda T. and JT-60 Team, "Density Control for Getting Stable Discharges in JT-60 Graphite Wall Experiment", (8th Int. Conf. on Plasma Surface Interactions in Controlled Fusion Devices, Julich, May, 1988) J. Nucl. Materials Vol. 162-164 (1989) 527.

59) Hosogane N., Shimizu K., Shirai H., Kusama Y., Tobita K., Nemoto M., Sakasai A., Koide Y., Nagashima K., Yoshida H. and JT-60 Team, "High Ion Temperatures and Transport Characteristics of High Z_{eff} Hydrogen Plasmas in JT-60 Limiter Discharges", Nucl. Fusion 28 (1988) 1781.

60) Takase Y.*6, Honda M., Ikeda Y., Imai T., Sakamoto K., Tsuji S., Uehara K., Ushigusa K., "Analysis of Lower hybrid current drive plasma in JT-60", Nucl. Fusion, 28 (1988) 1112.

61) Imai T., Ushigusa K., Sakamoto K., Ikeda Y., Fujii T., Saigusa M., Yoshino R., Uehara K., Nagashima T., Kimura H., "Current Drive and Confinement Studies During LHRF Experiments on JT-60", Nucl. Fusion, 28 (1988) 1341.

62) Niikura S.*7, Nagami M., "Enhancement of Fusion Power Multiplication Factor", Nuclear Engineering and Design No. 6 (1988) 109.

63) Shimizu K., Hirayama T., Shirai H., Azumi M. and JT-60 Team, "Numerical Simulation of JT-60 Divertor Discharge", (8th Int. Conf. on Plasma Surface Interactions in Controlled Fusion Devices, Julich, May, 1988) J. Nucl. Materials Vol. 162-164 (1989).

64) Ozeki T., Azumi M., Ninomiya H., Tokuda S., Tsunematsu T., Seki S., "Divertor Effects on the Stability of Axisymmetric Modes and Kink Modes in a Tokamak", Nucl. Fusion 28 (1988) 1859.

65) Nagayama Y.*8, Tsuji S., Kawahata K.*9, "Soft X-Ray Tomography of Sawtooth Oscillations in the JIPPT-II Tokamak", Phys. Rev. Lett. 61 (1988) 1839.

66) Jackson G.*1, Hass G.*5, Hill D.*3, Nakamura H., Shimada M., "Reduction of Recycling in DIII-D by Degassing and Conditioning of the Graphite Tiles", (8th Inter. Conf. on Plasma Surface Interactions in Controlled Fusion Devices, Julich, May, 1988) J. Nucl. Materials Vol. 162-164 (1989).

67) Imai T., Kimura H., Kinoshita S., "Wave Launching System of RF Heating for Fusion Experiments" (in Japanese), Denki Gakkaishi Vol. 108 (1988) 630.

68) Uehara K., "Comment-Boundary Plasma and Main Plasma" (in Japanese) Kakuyugo Kenkyu 60 (1988) 317 (in Japanese).

69) Madarame A.*8, Kamada Y., Suzuki N.*14, et al., "A Conceptual Design of RFP Fusion Power Core - REPUTER-I", Fusion Engineering and Design, 7 (1989) 389.

70) Ishida S., Shirai H., Nagashima K., Nishitani T., Fukuda T., and JT-60 Team, "Sawtooth Observation in Ohmic Discharge Compared between Hydrogen and Helium Plasmas on JT-60", Plasma Phys. and Cont. Fusion 30 (1988) 1069.

71) Tobita K., Kusama Y., Nemoto M., Takeuchi H., Yoshida H., Sakasai A., Kubo H., Koide Y., Sugie T., Itoh T., Tsukahara Y., Akaoka N.*40, "Ion Temperature Measurements in JT-60 Plasma by Active Beam Scattering", Nucl. Fusion 28 (1988) 1719.

72) Koide Y., Hirayama T., Sugie T., Sakasai A., Kubo H., Akaoka N.*40, Nishitani T., Nagashima K., Shirai H., Takeuchi H., and JT-60 Team, "Study of Impurity Transport in Ohmically and Neutral Beam Heated Divertor Discharges in JT-60", Nucl. Fusion 28 (1988) 1835.

73) Ishida S., Nishitani T., Nagashima K., Matoba T., and JT-60 Team, "Internal Mode Oscillations as a Diagnostic for the Plasma Rotations in JT-60", Nucl. Fusion 28 (1988) 2225.

74) Kubo H., Sugie T., Sakasai A., Koide Y., Nishino N.*2, Yokomizo H., Takeuchi H., Tanaka K.*45, Maezawa H.*45, Yamaguchi N.*46, and JT-60 Team, "Multichordal Spectroscopy on JT-60", Rev. Sci. Instrum. 59 (1988) 1515.

75) Takeuchi H., Tobita K., Kusama Y., Nemoto M., Itoh T., Tsukahara Y. and JT-60 Team, "Ion Temperature Measurements on JT-60 Using He Beam Scattering", Rev. Sci. Instrum. 59 (1988) 1652.

76) Nishitani T., Nagashima K., Sugiyama T.*4, Hara M.*4, Takeuchi H. and JT-60 Team, "Bolometric Measurements in JT-60", Rev. Sci. Instrum. 59 (1988) 1866.

77) Strachan J.D.*37, Nishitani T., Barnes Cris W.*47, "Neutron Spectroscopy on TFTR", Rev. Sci. Instrum. 59 (1988) 1732.

78) Nishitani T., Ishida S., "Radiative Thermal Instability in Peripheral Plasma (marfe)", Kakuyugo Kenkyu 61 (1989) 137.

79) Fukuda T., Yoshida H., Nagashima A., Ishida S., Kikuchi M., Yokomizo H., "Interferometric Density Measurements in the Divertor and Edge Plasma Regions for the Additionally Heated JT-60 Plasmas", J. Nucl. Mater. 162 (1989) 258.

80) Nishino N., Kubo H., Sakasai A., Koide Y., Sugie T., Takeuchi H., and JT-60 Team, "Behavior of Light Impurity from Beam-heated JT-60 Plasmas with Hot Graphite Wall", J. Nucl. Mater. 162 (1989) 386.

81) Hitoki S.*15, Sugihara M., Yamamoto S., "Formation of Cold and Dense Divertor Plasma during Phases of Non-Inductive Current Ramp-up and Recharging in Tokamak Fusion Reactor", Japanese Journal of Applied Physics, 27 (1988) 1291.

82) Ueda K.*15, Nishio S., Sugihara M., Fujisawa N., "Parametric Studies about Vertical Position Control of the INTOR Elongated Plasma", Journal of the Japan Society of Plasma Science and Nuclear Fusion Research 59 (1988) L194.

83) Itoh K.*11, Ueda N.*7, Itoh S-I.*12, Sugihara M., "Simulation of the Ash Exhaust in a Fusion Engineering Reactor", Japanese Journal of Applied Physics, 27 (1988) L1750.

84) Okazaki T.*2, Sugihara M., Fujisawa N., "Effect of Discrete RF Spectrum on Fast Wave Current Drive", Nuclear Fusion 28 (1988) 908.

85) Seki Y., "Conceptual Design of Tokamak Fusion Reactors", J. Nucl. Sci. Technol., 26111 189 (1989).

86) Kimura T., Kondo I., Kumahara T., Kurihara K., Yonekawa I., Murai K.*2, et al., "Development of the CAMAC System in the Multiprocessor Control System for the Large Fusion Experimental Device", The Transactions of the Institute of Electrical Engineers of Japan, Vol. 108-C, No.2 (1988) 111 (in Japanese).

87) Kondo I., Kimura T., Kurihara K., Matsukawa M., Kawamata Y., Murai K.*2, et al., "Development of the Plasma Position and Shape Control System with Multiprocessor System", ibid., Vol. 108-C, No. 6 (1988) 408 (in Japanese).

88) Ogiwara N., Yamashita Y., Yokomizo H., Maeno M., Shimada T.*34, Kimijima F.*34, "Direct Pressure Measurement near a Plasma of JT-60 by using a Penning Discharge Sustained by the Toroidal Magnetic Field", J. Vac. Soc. Jpn. 5 (1988) 407 (in Japanese).

89) Ogiwara N., Maeno M., "A Spherical Ionization Gauge for Use in a High Magnetic Field", J. Vac. Sci. Technol. A6 (1988) 2870.

90) Takatsu H., Ando T., Yamamoto M., Arai T., Kodama K., Ohkubo M., Shimizu M. and the JT-60 Team*, "Present Knowledge about the Material Behavior in JT-60", J. Nucl. Mater. 155 (1988) 286.

* Abe T., Aikawa H., Akaoka N., Akasaka H., Akiba M., Akino N., Akiyama T., Ando T., Annoh K., Aoyagi T., Arai T., Arakawa K., Araki M., Arimoto K., Azumi M., Chiba S., Dairaku M., Ebisawa N., Fujii T., Fukuda T., Funahashi A., Furukawa H., Hamamatsu K., Hanada M., Hara M., Haraguchi K., Hiratsuka H., Hirayama T., Hiroki S., Hiruta K., Honda M., Honda M., Horiike H., Hosoda R., Hosogane N., Iida Y., Iijima T., Ikeda K., Ikeda Y., Imai T., Inoue T., Isaji N., Isaka M., Ishida S., Itami K., Itige N., Ito T., Ito Y., Kakizaki T., Kaminaga A., Kato T., Kawai M., Kawabe M., Kawamata Y., Kawasaki K., Kikuchi K., Kikuchi M., Kimura H., Kimura T., Kishimoto H., Kitahara K., Kitamura S., Kitsunezaki A., Kiyono K., Kobayashi N., Kodama K., Koide S., Koide Y., Koike T., Komata M., Kondo I., Konoshima S., Kubo H., Kunieda S., Kurihara M., Kuriyama M., Kuroda T., Kusaka M., Kusaka Y., Mabuti Y., Maehara S., Maeno M., Matoba T., Matsuda S., Matsukawa M., Matsukawa T., Matsuoka M., Miura Y., Miya N., Miyachi K., Miyo Y., Mizuhashi K., Mizuno M., Mori M., Moriyama S., Murai R., Murakami Y., Muto M., Nagami M., Nagashima A., Nagashima K., Nagashima T., Nagaya S., Naito O., Nakamura H., Nakamura Y., Nemoto M., Neyatani Y., Ninomiya H., Nishino N., Nishitani T., Nomata H., Obara K., Obinata H.*35, Ogawa Y., Ogiwara N., Ohga T., Ohara Y., Ohasa K., Oohara H., Ohshima T., Ohkubo M., Ohsawa S., Ohta K., Ohta M., Ohtaka M., Ohuchi Y., Oikawa A., Okumura H., Okumura Y., Ohmori K., Ohmori S., Ohmori Y., Ozeki T., Saegusa M., Saitou N., Sakamoto K., Sakasai A., Sakata S., Sasajima T., Satou K., Satou M., Satou M., Sakurai A., Sawahata M., Sebata T.*36, Seimiya M., Seki M., Seki S., Shibanuma K., Shimada R., Shimada T.*36, Shimizu K., Shimizu M., Shimomura Y., Shinozaki S., Shirai H., Shirakata H., Shitomi M., Suganuma K., Sugie T., Sugiyama T., Sunaoshi H., Suzuki K., Suzuki M., Suzuki M., Suzuki N., Suzuki N., Suzuki S., Suzuki Y.,

Takahashi M., Takahashi S., Takahashi T., Takasaki M., Takatsu H., Takeuchi H., Takeshita A., Takizuka T., Tamura S., Tanaka S., Tanaka T., Tani K., Terakado M., Terakado T., Tobita K., Tokutake T., Totsuka T., Toyoshima N., Tsuda F., Tsugita T., Tsuji S., Tsukahara Y., Tsuneoka M., Uehara K., Umehara M., Uramoto Y., Usami H., Ushigusa K., Usui K., Yagyu J., Yamagiwa M., Yamaguchi T., Yamamoto M., Yamamoto T., Yamashita O., Yamashita Y., Yamazaki T., Yasukawa T., Yokokura K., Yokomizo H., Yokoyama K., Yoshikawa K., Yoshikawa M., Yoshida H., Yoshinari Y., Yoshino R., Yoshioka Y.*36, Yonekawa I., Yoneda T., Watanabe K., Goldston R.*37, Soldner F.*5, Takase Y.*6, Wong K.*37.

91) Takatsu H., Oku T., "Application of Carbon Materials to Fusion Devices", Tanso 135 (1988) 286 (in Japanese).

92) Ohta M., "Nuclear Fusion" J. Jpn. Soc. Mech. Eng. 91 (1988) 124 (in Japanese).

93) Uehara K. and Yamato H.*4, "Future Prospect in RF Heating Technology" J. Inst. Electr. Eng. Jpn. 108 (1988) 633 (in Japanese).

A.1.3 Papers published in conference proceedings

1) Kurita G., Takizuka T., Azumi M., Takeda T., "Nonlinear Evolution of Free Boundary Mode in a Tokamak", Proceedings of US-Japan Workshop on Advanced Plasma Modelling IPPJ-863 (1988).

2) Kishimoto Y., Takizuka T., Yamagiwa M., Itoh K.*11, Itoh S.*12, "Effect of Electron Spatial Diffusion on Current Drive", 15th European Conference on Controlled Fusion and Plasma Heating (Dubrovnik) Contributed Paper III (May 1988), 1051.

3) Nakamura H., Takizuka T., Tsunematsu T., et al., "Results on Disruption in JT-60", ITER Specialists' Meeting (Garching) (May 1988).

4) Naito O., Takizuka T., et al., "Experimental Results of JT-60 and JFT-2M", ITER Specialists' Meeting (Garching) (May 1988).

5) Natio O., Takizuka T., et al., "Confinement Scaling", ITER Specialists' Meeting (May 1988).

6) Takizuka T., Tani K., Azumi M., "Alpha Particle Confinement", ITER Specialists' Meeting (May 1988).

7) Tsunematsu T., Takizuka T., Nakamura H., Yoshino R., Yonekawa I., "Survey of Disruptions in JT-60", ITER Specialists' Meeting (May 1988).

8) Itoh K.*11, Fukuyama A.*10, Itoh S.*12, Kishimoto Y., Hamamatsu K., Takizuka T., "Comment on ICRF Current Drive in Reactor Grade Tokamak",

US-Japan Workshop on Advanced Current Drive Concept (Kyoto) (December 1988).

9) Kishimoto Y., "Effect of Electron Spatial Diffusion on RF Current Drive", US-Japan Workshop on Advanced Current Drive Concept (Kyoto) (December 1988).

10) Kishimoto Y., "Fast Wave Current Drive in Reactor Size Tokamak", USSR-Japan Workshop on RF Plasma Heating and Current Drive in Tokamak (December 1988).

11) Kishimoto Y., "Effect of Spatial Diffusion on ICRF Heating and RF Current Drive", USSR-Japan Workshop on RF Plasma Heating and Current Drive in Tokamak (December 1988).

12) Yamagiwa M., Takizuka T., Kimura H., "ICRF Wave Absorption by Alpha Particles", US-Japan Workshop on Kinetic Modification of MHD modes, Second Stability and Alpha Particles in Toroidal Systems (Princeton, USA) (January 1989).

13) Kimura H., Fukuyama A.*10, Kishimoto Y., Saegusa M., "ITER ICRF Current Drive and Heating", ITER Specialists' Meeting (Garching) (February 1989).

14) Tsunematsu T., Azumi M., Nakamura H., Ozeki T., "Pressure Profile Effect on Ideal MHD Stability of ITER", ITER Joint Work (Garching) (February 1989).

15) Yoshino R., Kimura H., Yonekawa I., Tsunematsu T., Takizuka T., "Characteristics of Disruption During NB Heating in JT-60", ITER Joint Work (Garching) (February 1989).

16) Takizuka T., "Comments on Sheath Criterion", US-Japan Workshop on Edge Plasma Physics (Hiroshima) (March 1989).

17) Tani K., Takizuka T., Azumi M., "Benchmark Test for Ripple Loss of Particles in ITER", ITER Specialists' Meeting (Garching) (March 1989).

18) Tani K., Takizuka T., Azumi M., "Two-Dimensional Heat Loading on the First Wall", ITER Specialists' Meeting (Garching) (March 1989).

19) Suzuki N., Hoshino K., Kasai S., Kawakami T., Kawashima H., Kondo T., Maeda H., Matsuda T., Matsumoto H., Miura Y., Mori M., Nakazawa I.*15, Odajima K., Ogawa H., Ogawa T., Ohasa K., Ohtsuka H., Sengoku S., Shoji T., Tamai H., Uesugi Y., Yamamoto T., Yamauchi T., Hasegawa K., Honda A., Ishibori I., Kashiwa Y., Kazawa M., Kikuchi K., Okano H., Sato E., Shibata T., Shiina T., Suzuki K., Tani T., Tokutake T., Uno S., "Confinement Studies of the H-mode on JFT-2M', in 12th Int. Conf. on

Plasma Physics and Controlled Nuclear Fusion Research (Nice, 1988) IAEA-CN-50/A-3-5.

20) Yamamoto T., Hoshino K., Kasai S., Kawashima H., Kawakami T., Kondo T., Maeda H., Matsuda T., Matsumoto H., Miura Y., Mori M., Nakazawa I.*15, Odajima K., Ogawa H., Ogawa T., Ohasa K., Ohtsuka H., Sengoku S., Shoji T., Tamai H., Uesugi Y., Yamamoto T., Yamauchi T., Hasegawa K., Honda A., Ishibori I., Kashiwa Y., Kazawa M., Kikuchi K., Okano H., Sato E., Shibata T., Shiina T., Suzuki K., Tani T., Tokutake T., Uno S., "Improvement of the Density Limit of RF Current Drive in the JFT-2M Tokamak", in 12th Int. Conf. on Plasma Physics and Controlled Nuclear Fusion Research (Nice, 1988) IAEA-CN-50/E-4-6.

21) Ogawa H., Kasai S., Aikawa H., Hoshino K., Kawashima H., Kawakami T., Kondoh T., Maeda H., Matsuda T., Matsumoto H., Miura Y., Mori M., Nakazawa I.*15, Odajima K., Ogawa T., Ohasa K., Ohtsuka H., Sengoku S., Shoji T., Suzuki N., Tamai H., Uesugi Y., Yamamoto T., Yamauchi T., "Impurity Behavior during H-mode Phase in JFT-2M", in Controlled Fusion and Plasma Physics (Proc. 16th Europ. Conf. Venice, 1988), Vol.13B, Part 1, European Physical Society (1988) 217.

22) Uesugi Y., Yamamoto T., Aikawa H., Hoshino K., Kasai S., Kawakami T., Kawashima H., Kondoh T., Matsuda T., Matsumoto H., Miura Y., Mori M., Nakazawa I.*15, Neufeld C.R.*52, Odajima K., Ogawa H., Ogawa T., Ohasa K., Ohtsuka H., Sengoku S., Shoji T., Suzuki N., Tamai H., Yamauchi T., Maeda H., "Electron Heating and Current Drive by 200 MHz Fast Wave on JFT-2M Tokamak", in Controlled Fusion and Plasma Physics (Proc. 16th Europ. Conf. Venice, 1988), Vol.13B, Part 4, European Physical Society (1988) 1259.

23) Sengoku S., Aikawa H., Hoshino K., Kawakami T., Kasai S., Kawashima H., Kondoh T., Matsuda T., Matsumoto H., Miura Y., Mori M., Nakazawa I.*15, Neufeld C.R.*52, Odajima K., Ogawa H., Ogawa T., Ohasa K., Ohtsuka H., Shoji T., Suzuki N., Tamai H., Maeda H., Uesugi Y., Yamamoto T., Yamauchi T., Hasegawa K., Honda A., Ishibori I., Kashiwa Y., Kazawa M., Kikuchi K., Okano H., Sato E., Shibata T., Shina T., Suzuki K., Tani T., Tokutake T., Uno S., "Pump Limiter with Gas-Puffing from Divertor Region in JFT-2M Tokamak", in Controlled Fusion and Plasma Physics (Proc. 16th Europ. Conf. Venice, 1988), Vol.13B, Part 3, European Physical Society (1988) 959.

24) Mori M., Aikawa H., Hosahino K., Kawakami T., Kasai S., Kawashima H.,

Kondoh T., Matsuda T., Miura Y., Nakazawa I.*15, Neufeld C.R.*52, Odajima K., Ogawa H., Ogawa T., Ohtsuka H., Sengoku S., Shoji T., Suzuki N., Tamai H., Uesugi Y., Yamamoto T., Yamauchi T., Maeda H., "Improved Confinement in Peaked Density Profile on JFT-2M", in Controlled Fusion and Plasma Physics (Proc. 16th Europ. Conf. Venice, 1988), Vol.13B, Part 1, European Physical Society (1988) 213.

25) Nakazawa I.*15, Shoji T., Aikawa H., Hoshino K., Kasai S., Kawashima T., Kawakami H., Kondoh T., Maeda H., Matsuda T., Matsumoto H., Miura Y., Mori M., Odajima K., Ogawa H., Ogawa T., Ohtsuka H., Sengoku S., Suzuki N., Tamai H., Uesugi Y., Yamamoto T., Yamauchi T., Hasegawa K., Honda A., Ishibori I., Kazawa M., Kikuchi K., Okano H., Sato E., Shibata T., Shiina T., Suzuki K., Tani T., Tokutake T., Uno S., "Divertor Plasma Characteristics during H-mode in JFT-2M Tokamak", in Controlled Fusion and Plasma Physics (Proc. 16th Europ. Conf. Venice, 1988), Vol.13B, Part 3, European Physical Society (1988) 887.

26) Matsuzaki Y. and JFT-2M team, "Probe Measurement of Hydrogen Fluxes during Discharge Cleaning in JFT-2M", 8th Int. Conf. on Plasma-Surface Interactions in Controlled Fusion Devices (Julich, May 1988) to be published in J. Nucl. Materials.

27) JT-60 team presented by Akiba M., "High Power Heating Results on JT-60", Plasma Physics and Controlled Fusion, 30 (1988) 1405.

28) Tanaka S., Akiba M., Araki M., Matsuda S., Matsuda Y.*59, Ohara Y., Okumura Y., Yokoyama K., Watanabe K., "Production of High Current Ion Beams of Various Species from a Magnetic Multipole Source", Proceedings of the 7th International Conference of Ion Implantation Technology, Kyoto, p.128 (1988).

29) Inoue T., Araki M., Hanada M., Kurashima T., Matsuda Y.*59, Ohara Y., Okumura Y., Tanaka S., Watanabe K., "Multi-Ampere negative Hydrogen Ion Source for Fusion Application", Proceedings of 7th International Conference on Ion Implantation Technology, Kyoto, p.111 (1988).

30) Watanabe K., Araki M., Hanada M., Horiike H., Inoue T., Kojima H., Matsuda S., Matsuda Y.*59, Ohara Y., Okumura Y., Tanaka S., Yokoyama K., "Development of a Large Plasma Generator with High Proton Yield", Proceedings of the 15th Symposium on Fusion Technology, Utrecht (1988).

31) Araki M., Dairaku M., Inoue T., Komata M., Kuriyama M., Matsuda S., Ogawa M., Ohara Y., Seki M., Yokoyama K., "Burnout Experiments on the Externally Finned Swirl Tube for Steady-state and High-Heat flux Beam

Stops", Proceedings of the International Symposium on Fusion Nuclear Technology, Tokyo (1988).

32) Seki M., Fukaya K., Takatsu H., Yamamoto M., Horie T., Eto M., Yamasaki S., "High-Heat Flux Experiments on Graphite Materials for Use in High-Heat Flux Components of a Fusion Reactor", Proceedings of the International Symposium on Fusion Nuclear Technology, Tokyo (1988).

33) Bolt H.*53, Miyahara A.*22, Kuroda T.*22, Linke K.*60, Koizlik K.*53, Nickel H.*53, Croessman C.D.*60, Whitley J.*60, Seki M., Fukaya K., Yamasaki S., "Response of Carbon Materials to High Surface Heat Fluxes - Comparison of Experimental Results from Different Laboratories", Proc. of the Int. Symp. on Fusion Nuclear Tech., Tokyo (1988).

34) Ogawa M., Seki M., Fukaya K., Horie T., Araki M., "Thermal Cycling Test of Tungsten-Copper Bonds for Divertor Collector Plate", Proc. of the Int. Symp. on Fusion Nuclear Tech., Tokyo (1988).

35) Kitamura K.*4, Seki M., Horie T., "Thermal Fatigue Tests of W/Cu Duplex Structure for a Divertor Application", Proc. of the Int. Symp. on Fusion Nuclear Tech., Tokyo (1988).

36) Ioki K.*7, Horie T., "Development and Heat Load Experiments of Graphite Brazed to Stainless-Steel for First Wall Structure of FER", Proc. of the Int. Symp. on Fusion Nuclear Tech., Tokyo (1988).

37) Bolt H.*53, Araki M., Seki M., "Structual Response of Tungsten and Molybdenum to High-Heat Fluxes", Proc. of the 15th Symp. on Fusion Tech., Utrecht (1988).

38) Fujii T., Kimura H., Saigusa M., Kusama Y., Annoh K., Tsunematsu T., Kobayashi N., Nagashima K., Nemoto M., Tobita K., Yamagiwa M., JT-60 Team, "Second Harmonic ICRF Experiment with Ohmic and Strong NBI-Heated Plasmas in JT-60", Proc. of 15th European Conference on Controlled Fusion and Plasma Heating II (Dubronik, Yugoslavia, 1988) 766.

39) Ando T., Nishi M., Hoshino M.*56, Oshikiri M.*30, Tada E., Painter T.*6, Shimamoto S., et al., "Experimental Investigation of Pressure Rise of Quenching Cable-in-conduit Superconductor", ICEC 12, (Southampton).

40) Tada E., Kato T., Hiyama T., Kawano K., Hoshino M.*56, Yamamura H.*18, "Performance Test Results of Cryogenic System for Demonstration Poloidal Coil", ibid.

41) Tsuji H., Shimamoto S., Ando T., Hiyama T., Takahashi Y., Nishi M., Tada E., Yoshida K., Okuno K., Koizumi K., Nakajima H., Kato T., Kawano K., Yamamura H.*18, Sato M.*14, et al., "Recent Progress in the

Demo Poloidal Coil Program", IEEE Trans. on Mag., vol.25 (1989) p.1484.

42) Yoshida K., Nishi M., Takahashi Y., Tsuji H., Koizumi K., Okuno K., Ando T., "Design of the Proto-type Conductors for the Fusion Experimental Reactor", ibid. p.1488.

43) Hamajima T.*4, Nishi M., Nakajima H., Koizumi K., Takahashi Y., Ando T., Tsuji H., Shimamoto S., et al., "Development of a Forced-cooled Superconducting Coil with High Average Current Density (DPC-TJ)", ibid. p.1721.

44) Ando T., Nishi M., Shimamoto S., "Measurements of the Stability Margin of a Nb_3Sn Cable-in-conduit Conductor", ibid. p.2386.

45) Koizumi K., Yoshida K., Iida F.*2, Mukai H.*4, Itoh I.*58, Nakajima H., Kato T., Okuno K., Takahashi Y., Tada E., Nishi M., Tsuji H., Hiyama T., Ando T., Shimamoto S., "Design of a Test Coil and the Facility for Proto Toroidal Coil Program", 15th SOFT (Utrecht).

46) Kato T., Tada E., Hiyama T., Kawano K., Yamamura H., Sato M.*14, Hoshino M.*56, Shimamoto S., "Design Concept of the Cryogenics System for Proto Toroidal Coil Program", ibid.

47) Sze D.K.*64, Anderson J.L.*47, Naruse Y., Yoshida H., et al., "The Role of a Blanket Tritium System on the Fusion Fuel Cycle", International Symposium on Fusion Nuclear Technology (ISFNT) Tokyo, Japan, April 10-19, 1988.

48) Enoeda M., Yamanishi T., Yoshida H., Naruse Y., Fukui H.*23, et al., "Hydrogen Isotope Separation Characteristics of Cryogenic Column", ibid.

49) Konishi S., Nagasaki T., Yokogawa N.*29, Naruse Y., "Development of Zirconium-Cobalt Beds for Recovery, Storage and Supply of Tritium", ibid.

50) Anderson J.L.*47, Yoshida H., et al., "Recent Developments and Future Plans at the Tritium Systems Test Assembly", ibid.

51) O'hira S., Hayashi T., Okuno K., Kudo H., "Tritium Dissolution in and Release from Li_2O", ibid.

52) Okuno K., Kudo H., "Tritium Diffusivity in Lithium-Based Ceremic Breeders Irradiated with Neutrons", ibid.

53) Naruse Y., Matsuda Y., Tanaka K., Konishi S., "Commissioning of the Tritium Process Laboratory at the JAERI", ibid.

54) Anderson J.L.*47, Yoshida H., Naruse Y., et al., "The Status of Tritium Technology Development at the Tritium Systems Test Assembly", IAEA 12th International Conference on Plasma Physics & Controlled Nuclear Fusion Research, Nice, France 1988.

55) Iijima T., "Progress in the Japanese Fusion Technology Programme", 15th SOFT Utrecht, Netherlands, Sept., 1988.

56) Kikuchi M., Ando T., Araki M., Horie T., Horiike H., Ikeda Y., Kishimoto H., Koizumi K., Matsukawa M., Neyatani T., Ninomiya H., Nishitani T., Seki S., Takatsu H., Yamamoto M., "JT-60 Upgrade Program", 15th SOFT Utrecht, Netherlands, Sept., 1988.

57) Matsukawa M., Ando T., Araki M., Horie T., Horiike H., Ikeda Y., Kikuchi M., Kishimoto H., Koizumi K., Neyatani T., Ninomiya H., Nishitani T., Seki S., Takatsu H., Yamamoto M., "JT-60U System Design", 15th SOFT Utrecht, Netherlands, Sept., 1988.

58) Ioki K.*7, Matsuoka F.*23, Namiki K.*7, Niikura S.*7, Shimizu K.*7, Tomita M.*7, Nishikawa M.*7, Tsujimura S.*23, Uchikawa T.*23, Ue K.*23, Horie T., Takatsu H., Ninomiya H., Horiike H., "Design of Thin-Double-Wall Vacuum Vessel with D-shape Cross Section for JT-60U", 15th SOFT Utrecht, Netherlands, Sept., 1988.

59) JT-60 Team* presented by Kishimoto H., "Recent Progress in JT-60 Experiments", 12th Int'l Conf. on Plasma and Contr. Nucl. Fusion Research (Nice, IAEA, 1988).

* Aikawa H., Akaoka N., Akasaka H., Akiba M., Akino N., Ando T., Annoh K., Aoki I., Aoyagi T., Arai T., Arakawa K., Araki M., Azumi M., Chiba S., Dairaku M., Ebisawa N., Fujii T., Fukuda T., Funahashi A., Furukawa H., Gunji H., Hamamatsu K., Hanada M., Hara M., Haraguchi K., Hiratsuka H., Hirayama T., Hiroki S., Hiruta K., Honda M., Honda M., Horiike H., Hosoda R., Hosogane N., Iida K., Iijima T., Ikeda Y., Ikeda Y., Imai T., Inoue T., Isaji N., Isaka M., Ishida S., Itami K., Itige N., Ito T., Kakizaki T., Kamada Y., Kaminaga A., Kaneko T., Kato T., Kawai M., Kawabe M., Kawamata Y., Kawano Y., Kawasaki K., Kikuchi K., Kikuchi M., Kimura H., Kimura T., Kishimoto H., Kitamura S., Kitsunezaki A., Kiyono K., Kobayashi N., Kodama K., Koide Y., Koike T., Komata M., Kondo I., Konishi K., Konoshima S., Kubo H., Kunieda S., Kurihara K., Kuriyama M., Kushima T., Kusaka M., Kusama Y., Mabuti Y., Maehara S., Maeno K., Matoba T., Matsuda S., Matsukawa M., Matsukawa T., Matsuoka M., Matsuzaki Y., Miura Y., Miya N., Miyachi K., Miyo Y., Mizuno M., Mogaki K., Mori M., Moriyama S., Muto M., Nagami M., Nagase K., Nagashima A., Nagashima K., Nagashima T., Nagaya S., Naito O., Nakamura H., Nakamura Y., Nemoto M., Neyatani Y., Ninomiya H., Nishino N., Nishitani T., Nobusaka H., Nomoto H., Obara K., Obinata H.*35, Odajima K.,

Ogawa Y., Ogiwara N., Ohga T., Ohara Y., Ohasa K., Oohara H., Ohshima T., Ohkubo M., Ohta K., Ohta M., Ohuchi S., Ohuchi Y., Oikawa A., Okumura Y., Ohmori K., Ohmori S., Ohmori Y., Ozeki T., Saegusa M., Saitoh N., Sakamoto K., Sakasai A., Sakata S., Sasajima T., Satou K., Satou M., Satou M., Sawahata M., Sebata T., Seimiya M., Seki M., Seki S., Shibanuma K., Shimada R., Shimada T., Shimizu K., Shimizu M., Shimomura Y., Shinozaki S., Shirai H., Shirakata H., Shitomi M., Suganuma K., Sugawara T., Sugie T., Sunaoshi H., Suzuki K., Suzuki M., Suzuki N., Suzuki S., Suzuki Y., Tachibana H., Takahashi M., Takahashi S., Takahashi T., Takasaki M., Takatsu H., Takeuchi H., Takeshita A., Takizuka T., Tamura S., Tanaka S., Tanaka T., Tanaka Y., Tani K., Terakado M., Terakado T., Tobita K., Tokutake T., Totsuka T., Toyoshima N., Tsugita T., Tsuji S., Tsukahara Y., Tsuneoka M., Uehara K., Umehara M., Uramoto Y., Usami H., Ushigusa K., Usui K., Yagyu J., Yamamoto M., Yamashita O., Yamazaki T., Yokokura K., Yokomizo H., Yokoyama K., Yoshikawa M., Yoshida H., Yoshino R., Yoshioka Y., Yonekawa I., Yoneda T., Watanabe K., Bell M.G.*37, Bickerton R.J.*41, Engelhardt W.*41, Goldston R.J.*37, Källne E.*41, Källne J.*41, Kugel H.W.*37, Mondino P.L.*41, Söldner F.X.*5, Takase Y.*6, Thomas P.R.*41, Wong K.L.*37.

60) Ninomiya H., Yoshino R., Akiba M., Ando T., Annoh K., Aoyagi T., Arakawa K., Azumi M., Fujii T., Fukuda T., Funahashi A., Hamamatsu K., Hirayama T., Honda M., Horiike H., Hosogane N., Iijima T., Ikeda Y., Imai T., Ishida S., Itami K., Ito T., Kamada Y., Kawano Y., Kikuchi M., Kimura H., Kimura T., Kishimoto H., Koide Y., Koike T., Kondo I., Konoshima S., Kubo H., Kunieda S., Kurihara K., Kuriyama M., Kusama Y., Maehara S., Maeno K., Matoba T., Matsuda S., Matsukawa M., Matsukawa T., Matsuoka M., Matsuzaki Y., Miya N., Miyachi K., Mizuno M., Nagami M., Nagashima A., Nagashima K., Nagashima T., Naito O., Nakamura H., Nemoto M., Neyatani Y., Nishino N., Nishitani T., Odajima K., Ogiwara N., Ohga T., Ohta M., Ohmori K., Ohmori S., Ozeki T., Saigusa M., Sakamoto K., Sakasai A., Sato M., Seimiya M., Seki M., Seki S., Shimizu K., Shimizu M., Shimomura Y., Shirai H., Shirakata H., Sugie T., Takahashi S., Takatsu H., Takeuchi H., Tamura S., Tanaka Y., Tani K., Tobita K., Toyoshima N., Tsuji S., Tsuneoka M., Uehara K., Ushigusa K., Yonekawa I., Yoshida H., "MHD Activities and Related Impurity Behavior in JT-60 Discharges", 12th Int'l Conf. on Plasma and Contr. Nucl. Fusion Research (Nice, IAEA, 1988).

61) Burrell K.H.*1, Fukumoto H.*2, Hosogane N., Kinoshita S.*2, Matsumoto H.,

Neyatani Y., Ozeki T., Sakamoto K., Shimada M., et al., "Energy Confinement in Auxiliary - Heated Divertor and Limiter Discharges in the DIII-D Tokamak", Proc. 12th IAEA Conf. on Plasma Physics and Controlled Nuclear Fusion Research, Nice, 1988, (IAEA-CN-50/AIII-4), (GA-A19443).

62) Strait E.J.*1, Hosogane N., Kinoshita S.*2, Neyatani Y., Ozeki T., Shimada M., et al., "Stability of High Beta Discharges in the DIII-D Tokamak", ibid., (IAEA-CN-50/AII-1), (GA-A19444).

63) Simonen T.C.*1, Matsuoka M., Kinoshita S.*2, et al., "DIII-D Neutral Beam Current Drive Experiments at High Beta Poloidal", ibid., (IAEA-CN-50/EIII-6), (GA-A19447).

64) Prater R. *1, Okazaki T.*2, Ozeki T., Sakamoto K., et al., "Electron Cyclotron Heating Experiments in the DIII-D Tokamak", ibid., (IAEA-CN-50/EI-2), (GA-A19448).

65) Caristrom T.*1, Shimada M., Matsumoto H., et al., "H-mode Transition Studies in DIII-D", Proc. 16th Europ. Conf. on Controlled Fusion and Plasma Physics (Venice, 1989), (GA-A19564).

66) Ali Mahdavi M.*1, Shimada M., et al., "Attainment of Quasi Steady-State H-mode Plasmas in the DIII-D Tokamak", ibid., (GA-A19558).

67) Schissel D.*1, Matsumoto H., et al., "Confinement Scaling Studies in DIII-D", ibid., (GA-A19556).

68) Porter G.*3, Matsuoka M., et al., "Neutral Beam Current Drive Scaling in DIII-D", ibid.

69) Burrell K.H.*1, Matsumoto H., Neyatani Y., Okazaki T.*2, Ozeki T., Shimada M., et al., "Confinement Physics of H-mode Discharges in DIII-D", ibid., (GA-A19609).

70) Ando T., Takatsu H., Nakamura H. and Hosogane N., "Heat Load on the Graphite Divertor Plate of JT-60 in High Power Heating Experiment", Inter. Symp. Fusion Nucl. Technol., Tokyo, April, 1988.

71) Ushigusa K., Imai T., Ikeda Y., Akiba M., Ando T., Annoh K., Aoyagi T., Arakawa K., Azumi M., Fujii T., Fukuda T., Funahashi A., Hamamatsu K., Hirayama T., Honda M., Horiike H., Hosogane N., Iijima T., Ishida S., Itami K., Ito T., Kamada Y., Kawasaki K., Kawano Y., Kikuchi M., Kimura H., Kimura T., Kishimoto H., Koide Y., Koike T., Kondo I., Konoshima S., A, Kubo H., Kunieda S., Kurihara K., Kuriyama M., Kusama Y., Maehara S., Maeno K., Matoba T., Matsuda S., Matsukawa M., Matsukawa T., Matsuoka M., Matsuzaki Y., Miya N., Miyachi K., Mizuno M., Nagami M.,

Nagashima A., Nagashima K., Nagashima T., Naito O., Nakamura H., Nemoto M., Neyatani Y., Ninomiya H., Nishitani T., Odajima K., Ogiwara N., Ohga T., Ohta M., Ohmori K., Ohmori S., Ozeki T., Saigusa N., Sakamoto K., Sakasai A., Sato M., Seimiya M., Seki M., Seki S., Shimizu K., Shimizu M., Shimomura Y., Shirai H., Shirakata H., Sugie T., Takahashi S. Takatsu H., Takeuchi H., Tamura S., Tanaka Y., Tani K., Tobita K., Toyoshima N., Tsuji S., Tsuneoka M., Uehara K., Yonekawa I., Yoshida H. and Yoshino R., "Lower Hybrid Experiments in JT-60", 12th Inter. Conf. on Plasma Physics and Controlled Nuclear Fusion Research, Nice, October, 1988, IAEA-CN-50/E-3-1.

72) Tsuji S., Akiba M., Ando T., Annoh K., Aoyagi T., Arakawa K., Azumi M., Fujii T., Fukuda T., Funahashi A., Hamamatsu K., Hirayama T., Honda M., Horiike H., Hosogane N., Iijima T., Ikeda Y., Imai T., Ishida S., Itami K., Ito T., Kamada Y., Kawasaki K., Kawano Y., Kikuchi M., Kimura H., Kimura T., Kishimoto H., Koide Y., Koike T., Kondo I., K Konoshima S., Kubo H., Kunieda S., Kurihara K., Kuriyama M., Kusama Y., Maehara S., Maeno K., Matoba T., Matsuda S., Matsukawa M., Matsukawa T., Matsuoka M., Matsuzaki Y., Miya N., Miyachi K., Mizuno M., Nagami M., Nagashima A., Nagashima K., Nagashima T., Naito O., Nakamura H., Nemoto M., Neyatani Y., Ninomiya H., Nishitani T., Odajima K., Ogiwara N., Ohga T., Ohta M., Ohmori K., Ohmori S., Ozeki T., Saigusa M., Sakamoto K., Sakasai A., Sato M., Seimiya M., Seki M., Seki S., Shimizu K., Shimizu M., Shimomura Y., Shirai H., Shirakata H., Sugie T., Takahashi S., Takatsu H., Takeuchi H., Tamura S., Tanaka Y., Tani K., Tobita K., Toyoshima N., Tsuneoka M., Uehara K., Ushigusa K., Yonekawa I., Yoshida H. and Yoshino R., "Energy Confinement with Auxiliary Heating in JT-60", 12th Inter. Conf. on Plasma Physics and Controlled Nuclear Fusion Research, Nice, October, 1988, IAEA-CN-50/A-V-1.

73) Fujii T., Kimura H., Saigusa M., Akiba M., Ando T., Annoh K., Aoyagi T., Arakawa K., Azumi M., Fukuda T., Funahashi A., Hamamatsu K., Hirayama T., Honda M., Horiike H., Hosogane N., Iijima T., Ikeda Y., Imai T., Ishida S., Itami K., Ito T., Kamada Y., Kawasaki K., Kawano Y., Kikuchi M., Kimura T., Kishimoto H., Koide Y., Koike T., Kondo I., Konoshima S., Kubo H., Kunieda S., Kurihara K., Kuriyama M., Kusama Y., Maehara S., Maeno K., Matoba T., Matsuda S., Matsukawa M., Matsukawa T., Matsuoka M., Matsuzaki Y., Miya N., Miyachi K., Mizuno M.,

Nagami M., Nagashima A., Nagashima K., Nagashima T., Naito O., Nakamura H., Nemoto M., Neyatani Y., Ninomiya H., Nishitani T., Odajima K., Ogiwara N., Ohga T., Ohta M., Ohmori K., Ohmori S., Ozeki T., Saigusa M., Sakamoto K., Sakasai A., Sato M., Seimiya M., Seki M., Seki S., Shimizu K., Shimizu M., Shimomura Y., Shirai H., Shirakata H., Sugie T., Takahashi S., Takatsu H., Takeuchi H., Tamura S., Tanaka Y., Tani K., Tobita K., Toyoshima N., Tsuji S., Tsuneoka M., Uehara K., Ushigusa K., Yonekawa I., Yoshida H. and Yoshino R., "Second Harmonic ICRF Heating Experiments in JT-60", 12th Inter. Conf. on Plasma Physics and Controlled Nuclear Fusion Research, Nice, October, 1988, IAEA-CN-50/E-2-4.

74) Kikuchi M., Hirayama T., Kubo H., Akiba M., Ando T., Annoh K., Aoyagi T., Arakawa K., Azumi M., Fujii T., Fukuda T., Funahashi A., Hamamatsu K., Hirayama T., Honda M., Horiike H., Hosogane N., Iijima T., Ikeda Y., Imai T., Ishida S., Itami K., Ito T., Kamada Y., Kawasaki K., Kawano Y., Kikuchi M., Kimura H., Kimura T., Kishimoto H., Koide Y., Koike T., Kondo I., Konoshima S., Kubo H., Kunieda S., Kurihara K., Kuriyama M., Kusama Y., Maehara S., Maeno K., Matoba T., Matsuda S., Matsukawa M., Matsukawa T., Matsuoka M., Matsuzaki Y., Miya N., Miyachi K., Mizuno M., Nagami M., Nagashima A., Nagashima K., Nanashima T., Naito O., Nakamura H., Nemoto M., Neyatani Y., Ninomiya H., Nishitani T., Odajima K., Ogiwara N., Ohga T., Ohta M., Ohmori K., Ohmori S., Ozeki T., Saigusa M., Sakamoto K., Sakasai A., Sato M., Seimiya M., Seki M., Seki S., Shimizu K., Shimizu M., Shimomura Y., Shirai H., Shirakata H., Sugie T., Takahashi S., Takatsu H., Takeuchi H., Tamura S., Tanaka Y., Tani K., Tobita K., Toyoshima N., Tsuji S., Tsuneoka M., Uehara K., Ushigusa K., Yonekawa I., Yoshida H. and Yoshino R., "Characteristics of Banana Regime Conductivity in JT-60", 12th Inter. Conf. on Plasma Physics and Controlled Nuclear Fusion Research, Nice, October, 1988, IAEA-CN-50/I-2-4.

75) JT-60 Team* presented by Nagami M., "Recent Results in JT-60 Experiments", 16th Europ. Conf. on Controlled Fusion and Plasma Physics, Venice, March, 1989 (to be published in Plasma Physics).

* Aoki I., Akaoka N., Akasaka H., Akiba M., Akino N., Ando T., Annoh K., Aoyagi T., Arai T., Arakawa K., Araki M., Azumi M., Chiba S., Dairaku M., Ebisawa N., Fujii T., Fukuda T., Funahashi A., Furukawa H., Gunji H., Hamamatsu K., Hanada M., Hara M., Haraguchi K., Hiratsuka H., Hirayama T.,

Hiroki S., Hiruta K., Honda M., Honda M., Horiike H., Hosoda R., Hosogane N., Iida K., Iida Y., Iijima T., Ikeda K., Ikeda Y., Imai T., Inoue T., Isaji N., Isaka M., Ishida S., Itami K., Itige N., Ito T., Kakizaki T., Kamada Y., Kaminaga A., Kaneko T., Kato T., Kawai M., Kawabe M., Kawamata Y., Kawano Y., Kawasaki K., Kikuchi K., Kikuchi M., Kimura H., Kimura T., Kishimoto H., Kitamura S., Kiyono K., Kobayashi N., Kodama K., Koide Y., Koike T., Komatsu M., Kondo I., Konoshima S., Kubo H., Kunieda S., Kurihara K., Kurihata Y., Kuriyama M., Kusaka M., Kusama Y., Kushima T., Mabuti Y., Maehara S., Maeno K., Matoba T., Matsuda S., Matsukawa M., Matsukawa T., Matsuoka M., Matsuzaki Y., Miura Y., Miya N., Miyachi K., Miyo Y., Mizuno M., Mogaki K., Moriyama S., Murakami Y., Muto M., Nagami M., Nagase K., Nagashima A., Nagashima K., Nagashima T., Nagaya S., Naito O., Nakamura H., Nemoto M., Neyatani Y., Ninomiya H., Nishino N., Nishitani T., Nobusaka H., Nomata H., Obara K., Odajima K., Ogawa Y., Ogiwara N., Ohga T., Ohara Y., Oohara H., Ohshima T., Ohta K., Ohta M., Ohuchi S., Ohuchi Y., Okumura H., Okumura Y., Ohmori K., Ohmori S., Ohmori Y., Ozeki T., Saegusa M., Saitoh N., Sakasai A., Sakata S., Sasajima T., Sato K., Sato M., Sato M., Sawahata M., Sebata T., Seimiya M., Seki M., Seki S., Shibanuma K., Shimada M., Shimada R., Shimizu K., Shimizu M., Shimomura Y., Shinozaki S., Shirai H., Shirakata H., Shitomi M., Suganuma K., Sugawara T., Sugie T., Sunaoshi H., Suzuki M., Suzuki M., Suzuki N., Suzuki S., Tachibana H., Takahashi M., Takahashi S., Takahashi T., Takahashi A., Takasaki M., Takatsu H., Takeuchi H., Takeshita A., Takizuka T., Tamura S., Tanaka S., Tanaka T., Tanaka Y., Tani K., Terakado M., Terakado T., Tobita K., Totsuka T., Toyoshima N., Tsuda F., Tsugita T., Tsuji S., Tsukahara Y., Tsuneoka M., Uehara K., Uramoto Y., Usami H., Ushigusa K., Usui K., Yagyuu J., Yamagiwa M., Yamamoto M., Yamashita O., Yamazaki T., Yokokura K., Yokoyama K., Yoshikawa K., Yoshida H., Yoshino R., Yoshioka Y., Yonekawa I., Yoneda T., Watanabe K.

76) Naito O., Hosogane N., Tsuji S., Ushigusa K., Yoshida H. and JT-60 Team, "Operation Regime and Confinement Scaling of Neutral Beam Heated JT-60 Discharges", 15th Europian Conference on Controlled Fusion and Plasma Physics, Dubrovnik Yugoslavia 1988, vol.1, 159.

77) Söldner F.X.*5, Ushigusa K., Imai T., Ikeda Y., Sakamoto K., Takase Y.*6 and JT-60 Team, "LH Power Absorption and Energy Confinement during Combined Lower Hybrid and NBI Heating on JT-60", 15th European

Conference on Controlled Fusion and Plasma Heating (Dubrovnilc) Vol.12B Part III, p.874-877 (1988).

78) Hirayama T., Shimizu K., Shirai H., Kikuchi M., Hosogane N., Yoshida H., Devote R.S.*3, "Transport Studies of High Density Ohmically Heated Plasmas and High Power Neutral Beam Heated Plasmas on JT-60", 15th European Conf. on Controlled Fusion and Plasma Heating (Dubrovnik), 1988, Vol.12B, Part III, 1065.

79) Fukuyama A.*10, Morishita T., Itoh K.*11, Itoh S-I*12, Kishimoto Y., Hamamatsu K. "Feasibility of Ignition by intense ICRF heating", 12th Inter. Conf. on Plasma Physics and Controlled Nuclear Fusion Research, Nice, October, 1988, IAEA-CN-50/G-3-3.

80) Tani K., Takizuka T., Azumi M., Yamagiwa M., Kishimoto Y., Hamamatsu K., Foit J.J.*13, "Burn control of Tokamak Plasma by Toroidal Field Ripple", 12th Inter. Conf. on Plasma Physics and Controlled Nuclear Fusion Research, Nice, October, 1988, IAEA-CN-50/D-2-5.

81) Devote R.S.*3, Tani K., Azumi M., "Computation of Self-Consistent 2-D MHD Neutral-Beam and Bootstrap Currents in Elongated Plasmas", 15th Europ. Conf. on controlled Fusion and Plasma Physics, Vol.12B, Part III, 1055.

82) Imai T. and JT-60 Team, "High Efficiency LHCD Experiments on JT-60", Japan-US Workshop on "Advanced Current Drive Concepts" (1988) Kyoto.

83) Inoue N.*8, Kamada Y., et al., "Results of Ultra-Low-q and Reversed-Field-Pinch Experiments on REPUTE-1 and TORIUT-6", 12th Inter. Conf. on Plasma Physics and Controlled Nuclear Fusion Research, Nice, October, 1988, IAEA-CN-50/C-5-8.

84) Nishino N.*2, Kubo H., Sakasai A., Koide Y., Sugie T., Takeuchi H. and JT-60 Team, "Behavior of Light Impurity from Beam-heated JT-60 Plasmas with Hot Graphite Wall", 8th Int. Con. on Plasma Surface Interactions in Controlled Fusion Devices (Jülich, May 1988) p.91.

85) Fukuda T., Yoshida H., Nagashima A., Ishida S., Kikuchi M., Yokomizo H., "Interferometric Density Measurements in the Divertor and Edge Plasma Regions for the Additionally Heated JT-60 Plasmas", 8th Int. Con. on Plasma Surface Interactions in Controlled Fusion Devices (Jülich, May 1988) p.69.

86) Kusama Y., Nemoto M., Tobita K., Seki M., Saegusa M., "High Energy Ion Tail Formation and its Behavior in Additionally Heated JT-60 Plasma", Proc. 15th Europ. Conf. on Controlled Fusion and Plasma Physics

(Dubrovnik, May 1988) Vol.12B Part I, p.167.

87) Yoshida H., Shimizu K., Shirai H., Tobita K., Kusama Y., Kubo H., Koide Y., Sakasai A., Fukuda T., Nagashima K., Naito O., Tsuji S., Hosogane N. and JT-60 Team, "Energy Confinement Analysis of Neutral Beam Heated JT-60 Discharges", Proc. 15th Europ. Conf. on Controlled Fusion and Plasma Physics (Dubrovnik, May 1988) Vol.12B Part I, p.163.

88) Nishitani T., Itami K., Tsuji S., Hosogane N., Kubo H., Sugie T., "Improved Confinement by Lower Side Divertor in JT-60", US-Japan Workshop on the Role of Edge Physics and Particle Control in Core Plasma Characteristics, (General Atomics, La Jolla, January 1989).

89) Itami K. and JT-60 Team, "Study on Heated Flow to the Divertor Plates in JT-60", US-Japan Workshop on the Role of Edge Physics and Particle Control in Core Plasma Characteristics, (General Atomics, La Jolla, January 1989).

90) Itami K., Nishitani T. and JT-60 Team, "Study on Heat Flow to the Divertor Plates in JT-60 Lower X-point Discharges", IAEA Technical Committee Meeting on Impurity Control, (JAERI, Naka, February 1989).

91) Kubo H., Sugie T., Nishino N.*2, Sakasai A., Koide Y., Akaoka N.*40, Nishitani T., Itami K., Kawano Y., Nagashima K., Tsuji S., Hosogane N., Takeuchi H. and JT-60 Team, "Behavior of Light Impurity in Beam-Heated JT-60 Plasmas with Graphite Walls", IAEA Technical Committee Meeting on Impurity Control, (JAERI, Naka, February 1989).

92) Sugie T., Kubo H., Sakasai A., Koide Y., Nishino N.*2, Akaoka N.*40, Nishitani T., Nagashima K., Hirayama T., Takeuchi H. and JT-60 Team, "Impurity Characteristics in JT-60", IAEA Technical Committee Meeting on Impurity Control, (JAERI, Naka, February 1989).

93) Nishitani T., Itami K., Nagashima K., Tsuji S., Hosogane N., Shimada M., Yoshida H., Ando T. and JT-60 Team, "Radiation Losses and Global Power Balance of JT-60 Plasmas", IAEA Technical Committee Meeting on Impurity Control, (JAERI, Naka, February 1989).

94) Nishitani T., Nishino N.*2, "Experimental Results of Fueling Pellet Injection and Plans for q-profile Measurements on JT-60", US-Japan Workshop on Evaluation of Impurity Pellet Injection for Alpha Diagnostics, (General Atomics, La Jolla, January 1989).

95) Tamura S., "Design Study of Fusion Experimental Reactor of JAERI", International Symposium on Fusion Nuclear Technology, Tokyo.

96) Yamamoto S., Ohara Y., Azumi M., Fujisawa N., Horie T., Iida H.,

Nishio S., Seki Y., Shimomura Y., Sugihara M., Tanaka S., Tachikawa K., Tani K., Okumura Y., Shibata K., Matsuda S. and FER team, "NAVIGATOR (FER) -- Negative-Ion-Grounded Advanced Tokamak Reactor --", 15th Symposium on Fusion Technology, Utrecht.

97) Mori S., Kobayashi T., Seki Y., Iida H., "Neutronics Benchmarking Study of Breeding Shield for the Fusion Experimental Reactor (FER)", 15th Symposium on Fusion Technology, Utrecht.

98) Kobayashi S.*4, Seki Y., "Loss of Coolant Accident of Plasma Vacuum Boundary", 8th Topical Meeting on Technology of Fusion Energy, Salt Lake City.

99) Tomabechi K., "ITER: Concept Definition", 12th International Conference on Plasma Physics and Controlled Nuclear Fusion Research, Nice (1988).

100) Shimomura Y., "ITER: Operational Scenario", 12th International Conference on Plasma Physics and Controlled Nuclear Fusion Research, Nice (1988).

101) Sugihara M., Fujisawa N., Iida H., Nishio S., Seki Y., Yamamoto S., Adachi J.*16, Honda T.*4, Hosobuchi H.*17, Kashihara S.*18, Mizoguchi T.*2, Nakashima K.*15, Riemer B.W.*19, Saito R.*2, Yamada M.*7, "Design Study of Fusion Experimental Reactor", 12th International Conference on Plasma Physics and Controlled Nuclear Fusion Research, Nice (1988).

102) Horie T., Seki M., Yamazaki S.*16, Ohmori J.*4, et al., "Thermal Shock Fracture of Graphite Armor Plate Under the Heat Load of Plasma Disruption", Proc. International Symposium on Fusion Nuclear Technology, April 10-15, Tokyo (1988).

103) Ioki K.*7, Nayama M.*23, Seki M., Horie T., et al., "Development for First Wall Structure of FER", ibid.

104) Kitamura K.*4, Seki M., Horie T., et al., "Thermal Fatigue Tests of W/Cu Duplex Structure for a Divertor Application", ibid.

105) Kobayashi S.*4, Seki Y., Iida H., et al., "Safety Analysis of FER Fuel Circulating System", ibid.

106) Nakahara K.*24, Seki Y., Kobayashi S.*4, "Thermal Effect of Periodical Baking on Tritium Inventory in First Wall and Permeation to Coolant in Reactor Life", ibid.

107) Okazaki S.*16, Seki Y., Yamamoto K.*25, et al., "Review of Fusion Energy Application to Synthetic Fuel Production and Blanket Design Study", International Symposium of Advanced Nuclear Energy Research, February 15, Ooarai (1989).

108) Sugihara M., "Power and Particle Control for ITER", IAEA Technical Committee Meeting on Impurity Control, Naka Japan (1989).

109) Arai T., Takatsu H., Ninomiya H., Yoshino R., Hosogane N., Yamamoto M., Kodama K., Kaminaga A., Shimizu M., Kondo I. and the JT-60 Team*, "Clean-up of Graphite First Walls in JT-60", 8th Int. Conf. on Plasma Surface Interaction, Julich.

* Abe T., Aikawa H., Akaoka N., Akasaka H., Akiba M., Akino N., Akiyama T., Ando T., Annoh K., Aoyagi T., Arai T., Arakawa K., Araki M., Arimoto K., Azumi M., Chiba S., Dairaku M., Ebisawa N., Fujii T., Fukuda T., Funahashi A., Furukawa H., Hamamatsu K., Hanada M., Hara M., Haraguchi K., Hiratsuka H., Hirayama T., Hiroki S., Hiruta K., Honda M., Honda M., Horiike H., Hosoda R., Hosogane N., Iida Y., Iijima T., Ikeda K., Ikeda Y., Imai T., Inoue T., Isaji N., Isaka M., Ishida S., Itami K., Itige N., Ito T., Ito Y., Kakizaki T., Kaminaga A., Kato T., Kawai M., Kawabe M., Kawamata Y., Kawasaki K., Kikuchi K., Kikuchi M., Kimura H., Kimura T., Kishimoto H., Kitahara K., Kitamura S., Kitsunezaki A., Kiyono K., Kobayashi N., Kodama K., Koide S., Koide Y., Koike T., Komata M., Kondo I., Konoshima S., Kubo H., Kunieda S., Kurihara M., Kuriyama M., Kuroda T., Kusaka M., Kusaka Y., Mabuti Y., Maehara S., Maeno M., Matoba T., Matsuda S., Matsukawa M., Matsukawa T., Matsuoka M., Miura Y., Miya N., Miyachi K., Miyo Y., Mizuhashi K., Mizuno M., Mori M., Moriyama S., Murai R., Murakami Y., Muto M., Nagami M., Nagashima A., Nagashima K., Nagashima T., Nagaya S., Naito O., Nakamura H., Nakamura Y., Nemoto M., Neyatani Y., Ninomiya H., Nishino N., Nishitani T., Nomata H., Obara K., Obinata H.*35, Ogawa Y., Ogiwara N., Ohga T., Ohara Y., Ohara K., Oohara H., Ohsima T., Ohkubo M., Ohsawa S., Ohta K., Ohta M., Ohtaka M., Ohuchi Y., Oikawa A., Okumura H., Okumura Y., Ohmori K., Ohmori S., Ohmori Y., Ozeki T., Saegusa M., Saitou N., Sakamoto K., Sakasai A., Sakata S., Sasajima T., Satou K., Satou M., Satou M., Sakurai A., Sawahata M., Sebata T.*36, Seimiya M., Seki M., Seki S., Shibanuma K., Shimada R., Shimada T.*36, Shimizu K., Shimizu M., Shimomura Y., Shinozaki S., Shirai H., Shirakata H., Shitomi M., Suganuma K., Sugie T., Sugiyama T., Sunaoshi H., Suzuki K., Suzuki M., Suzuki M., Suzuki N., Suzuki N., Suzuki S., Suzuki Y., Takahashi M., Takahashi S., Takahashi T., Takasaki M., Takatsu H., Takeuchi H., Takeshita A., Takizuka T., Tamura S., Tanaka S., Tanaka T., Tani K., Terakado M., Terakado T., Tobita K., Tokutake T., Totsuka T.,

Toyoshima N., Tsuda F., Tsugita T., Tsuji S., Tsukahara Y., Tsuneoka M., Uehara K., Umehara M., Uramoto Y., Usami H., Ushigusa K., Usui K., Yagyuu J., Yamagiwa M., Yamaguchi T., Yamamoto M., Yamamoto T., Yamashita O., Yamashita Y., Yamazaki T., Yasukawa T., Yokokura K., Yokomizo H., Yokoyama K., Yoshikawa K., Yoshikawa M., Yoshida H., Yoshinari Y., Yoshino R., Yoshioka Y.*36, Yonekawa I., Yoneda T., Watanabe K., Goldston R.*37, Soldner F.*5, Takase Y.*6, Wong K.*37.

110) Takatsu H., Arai T., Kaminaga A., Yamamoto M., Shimizu M., Iijima T., "In-Vessel Inspection of JT-60 First Walls", 15th Symp. on Fusion Technol., Utrecht.

111) Hiratsuka H., Kawasaki K., Takatsu H., "Development of Fast-Opening Magnetic Valve for JT-60 Pellet Injector", ibid.

112) Kawasaki K., Hiratsuka H., "Development of Pellet Injector for JT-60", ibid.

113) Kikuchi M., Ando T., Araki M., Horie T., Horiike H., Ikeda Y., Kishimoto H., Koizumi K., Matsukawa M., Matsukawa T., Neyatani Y., Ninomiya T., Nishitani H., Seki S., Takatsu H., Yamamoto M., "JT-60U System Design", ibid.

114) Ioki K.*7, Horie T., Takatsu H., Ninomiya H., Horiike H., "Design of Thin-double-wall Vacuum Vessel with D-Shaped Cross Section for JT-60U", ibid.

115) Kuriyama M., Araki M., Horiike H., Matsuda S., Matsuoka M., Ohara Y., Okumura Y., Shibanuma K., Shirakata H. and Tanaka S., "Beam Stops of JT-60 Neutral Beam Injector", Int. Sympo. on Fusion Nucl. Tech. (Tokyo, April 1988).

A.1.4 List of other reports

1) Hamamatsu K., Azumi M., Kishimoto Y., Fukuyama A.*10, Itoh K.*11, Itoh S.*12, "Analysis of Second Harmonic ICRF Waves on NBI-Heated Plasma", HIFT-151 (April 1988).

2) Itoh S.*12, Fukuyama A.*10, Takizuka T., Itoh K.*11, "Steady-State Operation Regime of Tokamak Reactor Plasma - Consistency Analysis -", HIFT-159 (November 1988).

3) Abdou M.A.*65, Imai T., Nagashima T., Tsuneoka M., et al., "ITER Concept Definition", ITER-1, Oct. 1988.

4) Schissel D.P.*1, Shimada M., et al., "Energy Confinement Properties of H-mode Discharges in the DIII-D Tokamak", General Atomics Report GA-A19243 (1988).

5) Ali Mahdavi M.*1, Shimada M., et al., "Modification of the Scrape-off Layer by Edge Plasma Modes", General Atomics Report GA-A19291 (1988).
6) Ozeki T., Lao L.L.*1, Kinoshita S.*2, et al., "Effects of Plasma Shaping on Ballooning Stability near the Separatrix in DIII-D", General Atomics Report GA-A-19495 (1988).
7) Nishitani T., Strachan J.D.*37, "Neutron Spectroscopy on TFTR", PPPL-2512 (May 1988).

A.2 Personnel of the Establishment

A.2.1 Number of the Staff during FY 1988

Department	Regular staff[1)]	Staff on loan[2)]
Dept. of Thermonuclear Fusion Research	110	26
Dept. of Large Tokamak Research	67	34
Dept. of JT-60 Facility	90	11
Dept. of Administrative Services	45	0
Total	312	71

1) Including scientists, technicians and secretaries.
2) From industries.

A.2.2 Scientific Staff and Officers during FY 1988

Naka Fusion Research Establishment

YOSHIKAWA Masaji (Director General, to December 31, 1988)
TANAKA Masatoshi (Director General, from January 1, 1989)
TOMABECHI Ken (Scientific Adviser)
MIYAMOTO Goro*8 (Scientific Adviser)
SEKIGUCHI Tadashi*66 (Scientific Adviser)

(A) Department of Thermonuclear Fusion Research

TANAKA Masatoshi (Director)
SHIMAMOTO Susumu (Deputy Director)
HIRAMATSU Nobuaki (Administrative Manager)

Plasma Theory Laboratory

TAKEDA Tatsuoki (Head)
KISHIMOTO Yasuaki
KURITA Gen-Ichi
NAKAMURA Yukiharu
TAKIZUKA Tomonori
TOKUDA Shinji
TSUNEMATSU Toshihide
TSUDA Takashi
YAMAGIWA Mitsuru
YAMAGUCHI Yuji*49

Experimental Plasma Physics Laboratory

MAEDA Hikosuke (Head)
AIKAWA Hiroshi
HOSHINO Katsumichi
KASAI Satoshi
KAWAKAMI Tomohide
KAWASHIMA Hisato
KONDO Takashi*46
MATSUDA Toshiaki
MATSUMOTO Hiroshi
MIURA Yukitoshi
MORI Masahiro
NAKAZAWA Ichiro*15
NEUFELD Carl*52
ODAJIMA Kazuo
OGAWA Hiroaki
OGAWA Toshihide
OHASA Kazumi
SENGOKU Seio
SHOJI Teruaki
SUZUKI Norio
TAMAI Hiroshi
UESUGI Yoshihiko
YAMAMOTO Takumi
YAMAUCHI Toshihiko

Facility Operation and Engineering Division

SUZUKI Kihachiro (Head)
HASEGAWA Koichi
HONDA Atushi
ISHIBORI Ikuo
KASHIWA Yoshitoshi
KAZAWA Minoru
KIKUCHI Kazuo
OKANO Fuminori
SATOH Eiji
SHIBATA Takatoshi
SHIINA Tomio
TANI Takashi
TOKUTAKE Toshikuni
UNO Sadanori

Plasma Heating Laboratory I

SEKI Masahiro (Head)
AKIBA Masato
ARAKI Masanori
DAIRAKU Masayuki
HANADA Masaya
IIDA Kazuhiro
INOUE Takashi
KOJIMA Hiroaki
MATSUDA Yasuhiro*59
MIZUNO Makoto
OHARA Yoshihiro
OKUMURA Yoshikazu
TANAKA Shigeru
WATANABE Kazuhiro
YOKOYAMA Kenji

Plasma Heating Laboratory II

NAGASHIMA Takashi (Head)
KOBAYASHI Noriyuki*4
MAEBARA Sunao
OHSAWA Satoru*27
OHTOMO Junichi*30
SAIGUSA Mikio
SAKAMOTO Keishi
SHIHO Makoto

Plasma Engineering Laboratory

MARUKAMI Yoshio (Head)
ABE Tetsuya
HIROKI Seiji
NAKAMURA Kazuyuki
OBARA Kenjiro
OHTSUKA Hidewo
TAKEDA Ryuji*33
YAMADA Reiji

Superconducting Magnet Laboratory

SHIMAMOTO Susumu (Head)
ANDO Toshinari
ISONO Takaaki
ITOH Ikuo*58
ITOH Noboru*57
HIYAMA Tadao
KATO Takashi
KAWANO Katsumi
KOIZUMI Koichi
NAKAJIMA Hideo
NISHI Masataka
NISUGI Hikaru*30
OKUNO Kiyoshi
SATOU Masahiko*14
TADA Eisaku
TAKAHASHI Yoshikazu
TSUJI Hiroshi
WACHI Yoshihiro*4
YAMAMURA Hidemasa*18
YOSHIDA Jun*2
YOSHIDA Kiyoshi

Tritium Engineering Laboratory

NARUSE Yuji (Head)
ASHIBE Kusuo*4
IDE Masahiko*29
ITO Hideki*3
ENOEDA Mikio
FUKUI Hiroshi*23
HAYASHI Takumi
HIRATA Shingo*16
HONMA Takashi
INOUE Masahiro*23
KONISHI Satoshi
MATUDA Yuji
MISUMI Masahiro*16
NAITO Taisei*7
OKUNO Kenji
O'HIRA Shigeru
SAKAI Fumio*29
SHIBUYA Mamoru*61
SUZUKI Takumi
TANAKA Kichizo
UDA Tatsuhiko*2
YAMADA Masayuki
YAMANISHI Toshihiko
YOKOGAWA Nobuhisa*29
YOSHIDA Hiroshi

(B) Department of Large Tokamak Research

TAMURA Sanae (Director)
SAITO Ryusei*2 (to May 15, 1988)
KIKUCHI Toshiaki (Administrative Manager)

Large Tokamak Program Division

KISHIMOTO Hiroshi (Head)

*Planning and Coordinating Group

HORIIKE Hiroshi
KIKUCHI Mitsuru
MIYA Naoyuki
NEYATANI Yuzuru
NINOMIYA Hiromasa
SEKI Shogo

*Doublet III Experiment Group

KINOSHITA Shigemi*2
KONOSHIMA Shigeru
MATSUMOTO Hiroshi
MATSUOKA Mamoru
MIYACHI Kengo
NEYATANI Yuzuru
OKAZAKI Takashi*2
OZEKI Takahisa
SAIGUSA Mikio
SAKAMOTO Keishi
SHIMADA Michiya

Large Tokamak Experimental Division I

SHIMOMURA Yasuo (Head)

*Experimental Group

HOSOGANE Nobuyuki
KAMADA Yutaka
KIKUCHI Mitsuru
NAGAMI Masayuki
NAKAMURA Hiroo
TSUJI Shunji
YOSHINO Ryuji

*Analysis Group

AZUMI Masafumi
HAMAMATSU Kiyotaka
HIRAYAMA Toshio
OZEKI Takahisa
SHIMIZU Katsuhiro
SHIRAI Hiroshi
TANI Keiji

Large Tokamak Experimental Division II

SHIMOMURA Yasuo (Head)
FUJII Tsuneyuki
IMAI Tsuyoshi
KIMURA Haruyuki
NAITO Osamu
SHIMADA Michiya
USHIGUSA Kenkichi

Diagnostics Division

FUNAHASHI Akimasa (Head)
KONOSHIMA Shigeru
NAKAMURA Yukiharu
SAITO Naoyuki

*Diagnostics Group I

AKAOKA Noboru*40
HARA Makoto*4
KANEKO Takashi*48
KOIDE Yoshihiko
KUBO Hirotaka
KUSAMA Yoshinori
NAGASHIMA Keisuke
NEMOTO Masahiro
NISHINO Nobuhiro*2
NISHITANI Takeo
SAKASAI Akira
SUGIE Tatsuo
TAKEUCHI Hiroshi
TOBITA Kenji
TSUKAHARA Yoshimitsu
URAMOTO Yasuyuki

*Diagnostics Group II

De KOCK Ber*41
FUKUDA Takeshi
GUNJI Hideho*30
HARAGUCHI Kazumi*27
ISHIDA Shinichi
ITAMI Kiyoshi
KAWANO Yasunori
MABUCHI Yukio*30
MATOBA Tohru
MIURA Yoshikazu*27
SATO Masayasu
SEBATA Tsuyoshi*42
TAKAHASHI Toranosuke*40
YOSHIDA Hidetoshi

*Data Processing Group

AOYAGI Tetsuo
KAKIZAKI Sadayuki*30
NAGASHIMA Akira
OHSHIMA Takayuki
TSUGITA Tomonori

*Operation and Engineering Group

CHIBA Shinichi
ITOH Takao
SAKUMA Takeshi*30
SHITOMI Morimasa
YAMASHITA Osamu

Fusion Reactor System Laboratory

FUJISAWA Noboru (Head)
SEKI Yasushi
TACHIKAWA Katsuhiro

Fusion Experimental Reactor Team

TAMURA Sanae (Team Leader)
HASEGAWA Mitsuru*15
HONDA Tsutomu*4
HORIE Tomoyoshi
HOSOBUCHI Hideo*17
IIDA Hiromasa
KASHIHARA Shin-ichirou*18
KIMURA Haruyuki
KURODA Toshimasa*16
MAKI Koichi*2
MATSUDA Shinzaburo
MIZOGUCHI Tadanori*2
NISHIO Satoshi
SATO Keisuke*16
SHIBANUMA Kiyoshi
SHINYA Kichiro*4
SUGIHARA Masayoshi
TAKATSU Hideyuki
YAMADA Masao*7
YAMAMOTO Shin

(C) Department of JT-60 Facility

IIJIMA Tsutomu (Director)
TANAKA Yuji (Deputy Director)

JT-60 Administration Division

KIKUCHI Toshiaki (General Manager)

JT-60 Facility Division I

SHIRAKATA Hirofumi (Head)
AKASAKA Hiromi
AOYAGI Tetsuo
ARAKAWA Kiyotsugu
FURUKAWA Hiroshi*30
HONDA Mitsuteru*38
HOSODA Ryujiro
ICHIGE Hisashi
IKEDA Yukiharu
ISAJI Nobuaki*39
ISAKA Masayoshi
KAWAMATA Yoichi
KIMURA Toyoaki
KURIHARA Kenichi
MATSUKAWA Makoto
MATSUKAWA Tatsuya
MATSUZAKI Yoshimi
MUTOH Mitsugu
NAGAYA Susumu
NOBUSAKA Hiromichi*28
OHMORI Kenichiro
OHMORI Shunzo
OHMORI Yoshikazu
SAKATA Shinya
SEIMIYA Munetaka
TAKAHASHI Minoru
TAKAHASHI Shunji
TAKESHITA Akira*15
TERAKADO Tunehisa
TOTSUKA Toshiyuki
YAGYUU Junichi
YAMAZAKI Takeshi*28
YONEKAWA Izuru

JT-60 Facility Division II

KONDO Ikuo (Head)
ANDO Toshiro
ARAI Takashi
HIRATSUKA Hajime
HORIIKE Hiroshi
KAMINAGA Atsushi
KAWABE Masaru
KAWASAKI Kozo
KODAMA Kozo
KOIKE Tsuneyuki
KURIHATA Youichi
KUSHIMA Takanori
MAENO Masaki
MIYACHI Kengo
MIYO Yasuyuki
NAGAYAMA Kiyoshi
OGIWARA Norio
OHTA Kazuya
OKUMURA Hiroshi
SASAZIMA Tadayuki
SHIMADA Toru*34
SHIMIZU Masatsugu
SUNAOSHI Hidenori
SUZUKI Michio
SUZUKI Sadaaki
TACHIBANA Hidetoshi
TAKASAKI Manabu
TANAKA Takejiro
TSURUMI Satoshi*2
Yoshioka Yuji*23
YAMAMOTO Masahiro

JT-60 Facility Division III

OHTA Mitsuru (Head)
ANNO Katsuto
AOKI Isao
FUJII Tsuneyuki
FUJISHIRO Kenji*27
HONDA Masao
IKEDA Yoshitaka
KATOH Tsugio*27
KITAI Tatsuya*28
KIYONO Kimihiro
KONISHI Kazumasa*29
MAEBARA Sunao
MORIYAMA Shinichi
OGAWA Yoshiro*4
SEKI Masami
SAWAHATA Masayuki
SUGANUMA Kazuaki
SHINOZAKI Shinichi
SATO Minoru
SATO Kazuya*30
SUZUKI Norio
TERAKADO Masayuki
TOYOSHIMA Noboru
TSUNEOKA Masaki
UEHARA Kazuya
YONEDA Tsuyoshi*27
YOKOKURA Kenji

JT-60 Facility Division IV

KUNIEDA Shunsuke (Head)
HIRUTA Kazuharu (Deputy Head)
AKIBA Masato
AKINO Noboru
EBISAWA Noboru
KAWAI Mikito
KIKUCHI Katsumi*30
KITAMURA Shigeru
KOMATA Masao
KURIYAMA Masaaki
MATSUOKA Mamoru
MIZUNO Makoto
MOGAKI Kazuhiko
NAGASE Katsumoto*4
NOMOTO Hiroki*31
OHGA Tokumichi
OHUCHI Shouju*32
OHUCHI Yutaka
OOHARA Hiroshi
SUGAWARA Tadayoshi*2
TSUDA Fumio*2
USAMI Hiroji*2
USUI Katsutomi

*1 General Atomics, USA
*2 Hitachi Ltd.
*3 Lawrence Livermore National Laboratory, USA
*4 Toshiba Corp.
*5 Max-planck Institute für Plasmaphysik, FRG
*6 Massachusetts Institute of Technology, USA
*7 Mitsubishi Atomic Power Industry Inc.
*8 The University of Tokyo
*9 Nagoya University
*10 Okayama University
*11 Kyoto University
*12 Hiroshima University
*13 Institut für Reaktorbauelements, KfK, FRG
*14 Ishikawajima-Harima Heavy Industries
*15 Mitsubishi Electric Co., Ltd.
*16 Kawasaki Heavy Industry Ltd.
*17 Hazama-gumi Ltd.
*18 Kobe Steel Ltd.
*19 Oak Ridge National Laboratory, USA
*20 Century Research Center Corp.
*21 Northwestern Laboratory
*22 Institute of Plasma Physics, Nagoya University
*23 Mitsubishi Heavy Industry Ltd.
*24 NAIG Nuclear Research Laboratory
*25 Japan Atomic Industrial Forum
*26 Central Research Institute for Electric Power
*27 Nippon Electric Co., Ltd.
*28 Kaihatsu Denki Co.
*29 Sumitomo Heavy Industry Co.
*30 Nuclear Engineering Co., Ltd.
*31 Tomoe Shokai
*32 Ibaraki Kohsan
*33 Tokyo Nuclear Survice Co., Ltd.
*34 ULVAC Co.
*35 Kyushu University
*36 Contract Researcher
*37 Princeton Plasma Physics Laboratory, USA

*38 I.B.S. Data Center Co., Ltd.
*39 Japan Expert Clone Corp.
*40 Nissei Sangyo Co., Ltd.
*41 JET Joint Undertaking, UK
*42 Hodaka Seiki Ltd.
*43 Sumitomo Electric Industry Co.
*44 Nikon Corp.
*45 National Laboratory for High Energy Physics
*46 Tsukuba University
*47 Los Alamos National Laboratory, USA
*48 Japan Radiation Engineering Co.
*49 MEITEC Co., Ltd.
*50 Osaka University
*51 Imperial College, UK
*52 Institute of Research Hydro-Quebec, Varenns, Canada
*53 KFA-IPP, FRG
*54 Ewic Engineering Co., Ltd.
*55 ORC Manufacturing Co., Ltd.
*56 Koike Sanso Kogyo Co., Ltd.
*57 Hitachi Oxygen Co., Ltd.
*58 Fuji Electric Co., Ltd.
*59 Nissin Electric Co., Ltd.
*60 Sandia National Laboratories, USA
*61 JGC Corporation
*62 Tokyo Institute of Technology
*63 Nuclear Research Center Karlsruhe, FRG
*64 Argonne National Laboratory, USA
*65 ITER Team
*66 Yokohama National University

A.3 Budget of the Establishment

	FY1986	FY1987	FY1988
JT-60 Construction	31,412	22,630	17,078
Research & Development	2,810	3,827	3,885
Japan-US Cooperation	507	837	1,107
Site Construction	390	829	73

(Unit: Million ¥)